Spatiotemporal modelling of hormonal crosstalk in the Arabidopsis root.

SIMON PATRICK MEREWETHER MOORE

Spatiotemporal modelling of hormonal crosstalk in the Arabidopsis root.

Simon Patrick Merewether Moore

Submitted in accordance with the requirements
for the degree of Doctor of Philosophy

Department of Biosciences
Durham University

Dec 2017

ABSTRACT

Plant development, growth and response to varying environmental conditions, involves a complex network of overlapping interactions between plant signalling hormones and gene expression, known as 'CROSSTALK', which controls cell proliferation, elongation and differentiation. Hormone response, concentrations and gene expression levels vary through the root tip and display patterning, which ultimately drives development; however, little is known about how this is established. Models have been constructed to explain patterning, including a 'physical' auxin flux model in a simple rectangular 2-D multicellular *Arabidopsis* root which excludes crosstalk (Grieneisen *et al*., 2007), and a single cell 'biological crosstalk' model of multiple hormone and protein interactions in WT and mutants (Liu *et al*., 2010; Liu *et al*., 2013). The project goal was to combine these approaches by embedding the single cell biological crosstalk relationships into a 2-D multicellular root structure to reproduce experimentally observed hormone and gene expression patterning. An initial model was constructed and parameter values calibrated to meet fit criteria and produce a WT parameter set. The model proved robust to parameter variation, indicating that results did not rely on unique parameter value selections. Model results were compared to experimental data to test predictive capability and matched experimentally observed patterning and concentration trends for most species and mutants. A more realistic digital root map was then developed with additional auxin carriers to allow improved comparison between model and experimental images at a cell-scale level. The roles of auxin influx and efflux carriers in regulating auxin patterning were investigated by developing a 'Recovery Principle', where pattern perturbations due to changes in one carrier set could be recovered by adjustments to the other carrier set. Finally, using additional experimental data from the literature, the crosstalk network was revised to produce more representative cytokinin patterning. The model provides an explanation of crosstalk control of gene expression and patterning, and forms a foundation for future expansion of hormonal crosstalk and gene expression modelling in the *Arabidopsis* root. In summary, this project has developed predictive models to further explore hormone and gene expression levels and spatiotemporal pattern formation in the *Arabidopsis thaliana* root tip.

DECLARATION

I confirm that the original research described in this thesis is my own work. In the event that work was carried out by others, appropriate credit has been given within this thesis wherever reference has been made to such work.

The initial version of the model program was written by Dr. Xiaoxian Zhang (Rothamsted Research Institute), the *PLS* expression image in Figure 2.47 and Figure 5.10 was produced by Dr. Anna Mudge (Durham University), and the DII-VENUS response image in Figure 2.59 by Dr. James Rowe (Durham University).

No material contained in this thesis has been submitted elsewhere for the award of a higher degree.

The work in this thesis was supported by funding from Durham University.

STATEMENT OF COPYRIGHT

PUBLICATIONS RESULTING FROM THIS THESIS

Moore S, Zhang X, Mudge A, Rowe JH, Topping JF, Liu J, Lindsey K. 2015a. Spatiotemporal modelling of hormonal crosstalk explains the level and patterning of hormones and gene expression in Arabidopsis thaliana wildtype and mutant roots. *New Phytologist* 207: 1110–1122.

Moore S, Zhang X, Liu J, Lindsey K. 2015b. Some fundamental aspects of modeling auxin patterning in the context of auxin-ethylene-cytokinin crosstalk. *Plant Signaling & Behavior*: 10.

Moore S, Zhang X, Liu J, Lindsey K. 2015c. Modelling Plant Hormone Gradients. *eLS*. DOI: 10.1002/9780470015902.a0023733

Moore S, Liu J, Zhang X, Lindsey K. 2017. A recovery principle provides insight into auxin pattern control in the Arabidopsis root. *Scientific Reports* 7: 430004

Liu J, Moore S, Chen C, Lindsey K. 2017. Crosstalk complexities between auxin, cytokinin and ethylene in *Arabidopsis* root development: from experiments to systems modelling, and back again. *Molecular Plant* 10: 1480-1496.

ACKNOWLEDGMENTS

A special thanks to my supervisors Prof. Keith Lindsey and Dr. Junli Liu, and for the many hours spent in Junli's office talking about the project and drinking mint tea when I am sure he had better things to do! Both Keith and Junli were always available at short notice to discuss issues and plan the next steps in the project – when at times we were never quite sure where it was all going or how to get there.

Dr. Xiaoxian Zhang (Rothhamsted Research Institute) gave us an amazing start by writing the initial model program which would otherwise have delayed the project by many, many months while I tried to resurrect my very rusty programming skills.

Thanks to Dr. Jen Topping who as well as providing extensive technical experience, looks after everyone in the lab. Thanks also to my fellow lab members for their good company (and cake) when I occasionally showed up – thank you Anna, James, Devina, Chunli, Amy, Kat, Heather, Flora, Sam2 and Vinny.

Lastly, a special mention goes to Vinny for the seven very interesting (and sometimes stressful) years we worked together. We both started on the Foundation course at Stockton, then Vinny was my incredibly good and patient lab partner during our undergrad years, and finally we were in the same lab for our PhD.

TABLE OF CONTENTS

Abstract……2
Table of Contents……5
List of Figures……9
List of Tables……13
List of Abbreviations……14

CHAPTER 1: INTRODUCTION 15

1.1 Hormonal crosstalk and patterning……16
1.2 Root structure and developmental zones……18
1.3 Auxin……20
1.4 Cytokinin (CK)……21
1.5 Ethylene (ET)……22
1.6 POLARIS (PLS)……23
1.7 PIN and AUX1/LAX auxin efflux and influx transporter families……23
1.8 Mathematical modelling of hormonal crosstalk and patterning……26
1.9 Research Aims……26

CHAPTER 2: PATTERNING IN A SIMPLE 2-D RECTANGULAR ROOT MODEL 28

2.1 Introduction……29
2.2 Definition of the Rectangular Root Model……33
2.2.1 Generalised root structure……33
2.2.2 Grid point representation of the root……35
2.2.3 The root map……37
2.2.4 Biosynthesis, decay, and receptor activation/inactivation in the cytosol……40
2.2.5 PIN and AUX1 carrier recycling to the plasma membrane……46
2.2.6 Hormonal crosstalk and gene expression network……49
2.2.7 Flux between nearest neighbour (NN) grid points……49
2.2.8 Root/shoot boundary conditions……52
2.3 Running the model and simulation to steady state……52
2.4 Capturing data from experimental images using ImageJ……53
2.5 Definition and calibration of the WT model parameter set……54
2.5.1 Diffusion and permeability constants……54
2.5.2 Average auxin concentration and trends in WT and mutants……55
2.5.3 Auxin reponse images, and concentration colour maps and profiles……57
2.5.4 PIN and AUX1 predominantly locate to the plasma membrane……58
2.5.5 CK concentration patterning and profile……60

2.5.6 Border hormone concentrations 62
2.5.7 Summary results for the WT parameter settings 63
2.6 Model robustness to variation in parameter values 63
2.6.1 Auxin diffusion rates 64
2.6.2 CK diffusion rates 65
2.6.3 ET diffusion rates 67
2.6.4 PIN protein diffusion rates 68
2.6.5 AUX1 protein diffusion rates 71
2.6.6 Auxin decay rates 73
2.6.7 Tissue specific CK biosynthesis 74
2.6.8 *AUX1* gene expression rates 75
2.6.9 *PIN* gene expression rates 78
2.7 Comparison between experimental results and model predictions 82
2.7.1 Shoot to root auxin flux 82
2.7.2 ET concentration profile 83
2.7.3 *POLARIS* (*PLS*) expression pattern 84
2.7.4 PIN concentration trends in WT and mutants 86
2.7.5 PIN concentration profiles 88
2.7.6 Auxin patterning in the *aux1* mutant 91
2.8 Gradual cell growth in the Transition Zone 93
2.8.1 Auxin patterning in the gradual growth (GG) root model. 93
2.8.2 Ethylene and cytokinin concentrations in the *pls* mutant 103
2.8.3 AUX1 patterning 104
2.8.4 PIN profiles in the GG root model 106
2.8.5 PIN and AUX1 permeability and auxin patterning 109
2.9 Summary 111
2.9.1 WT Parameter calibration matched most fit criteria 111
2.9.2 The model proved robust to variations in the WT parameter values 113
2.9.3 Model sensitivity to changes in cell length 115
2.9.4 The model explains most concentration trends and patterning 115

CHAPTER 3: DEVELOPMENT OF AN ANATOMICALLY REALISTIC MODEL ROOT 117

3.1 Introduction 118
3.2 Realistic root cell geometry 119
3.3 Placement of the auxin carriers in the realistic root 124
3.3.1 PIN1 and PIN2 auxin efflux carriers 125
3.3.2 PIN3, PIN4 and PIN7 auxin efflux carriers 127

3.3.3 AUX1, LAX2 and LAX3 auxin influx carriers 129
3.4 Definition of a new model for the realistic root 130
3.5 Results for the wildtype realistic root 133
3.5.1 Auxin patterning 134
3.5.2 PIN1 and PIN2 patterning 136
3.5.3 Ethylene patterning 137
3.5.4 Cytokinin patterning 138
3.5.5 POLARIS (PLS) patterning 139
3.5.6 Auxin biosynthesis rate patterning 140
3.5.7 PIN1 and PIN2 patterning after loss of PINs 3, 4 and 7 141
3.5.8 Auxin patterning with reduced apoplastic auxin diffusion 142
3.5.9 Effects on auxin patterning of changing auxin influx levels 143
3.6 Summary 144

CHAPTER 4: RECOVERY PRINCIPLE GIVES INSIGHTS INTO AUXIN PATTERNING 147

4.1 Introduction 148
4.2 Quantitative recovery of an auxin pattern: 'The Recovery Principle' 150
4.3 Auxin pattern recovery after PIN3,4,7 perturbations 153
4.4 Non-uniform, polar AUX1/LAX required for recovery 161
4.5 Auxin pattern recovery leads to PIN1 and PIN2 pattern recovery 162
4.6 Uniform AUX1/LAX distribution changes the recovered auxin pattern 163
4.7 PIN and AUX1/LAX for a specific auxin pattern are not spatially correlated 165
4.8 Quantitative recovery from AUX1/LAX changes requires modifed PIN polarity 169
4.9 Recovery principle allows searchable relationships for influx and efflux carriers 171
4.10 Summary 173

CHAPTER 5: ALTERNATIVE NETWORK FOR CYTOKININ PATTERNING 176

5.1 Introduction 177
5.2 Crosstalk network revisions 180
5.3 The revised model 183
5.4 Results for the new wildtype root 191
5.5 Summary 197

CHAPTER 6: DISCUSSION 201

6.1 Introduction 202
6.2 The rectangular root model 203
6.3 The realistic root model 206
6.4 The roles of auxin influx and efflux carriers in auxin patterning 207

6.5 Improved cytokinin patterning 210
6.6 Conclusions 212

APPENDIX 1: RUNNING THE REALISTIC ROOT MODEL (WT200) 220

APPENDIX 2: ETHYLENE, CYTOKININ AND AUXIN CROSSTALK 224

App 2.1 Annotated schematic of ethylene, cytokinin and auxin crosstalk. 224
App 2.2 Ethylene receptor complexes..... 236
App 2.3 Ethylene signalling pathways..... 238
App 2.3.1 The Canonical CTR1 dependent pathway: 238
App 2.3.2 The CTR1 independent pathway:..... 239
App 2.3.3 ETR1 phospho-relay ethylene signalling pathway:..... 240

APPENDIX 3: RUNNING THE IMPROVED CYTOKININ MODEL (WT743) 241

BIBLIOGRAPHY 245

LIST OF FIGURES

Figure 1.1: Cell files in the *Arabidopsis* root tip 18
Figure 1.2: *Arabidopsis* root structure and developmental zones 19
Figure 1.3: Auxin response gradient in *Arabidopsis* 4 DAG root 21
Figure 1.4: Auxin 'Reverse fountain flow' in the root tip 25
Figure 2.1: A schematic of the 2-D spatial model components 31
Figure 2.2: Map of root structure and PIN protein placement 34
Figure 2.3: Grid point representation of a cell in the MZ 35
Figure 2.4: Example of flux between nearest neighbour (NN) grid points 36
Figure 2.5: Grid point coding for the proximal EZ cell tier in the root map 38
Figure 2.6: Grid point coding for the standard EZ cell tier in the root map 39
Figure 2.7: Grid point coding for an MZ cell tier in the root map 39
Figure 2.8: Grid point coding for the columella cell tiers 40
Figure 2.9: Hormonal crosstalk and gene expression network 49
Figure 2.10: PIN2 profiles for epidermal and vascular cells using ImageJ 54
Figure 2.11: Relative auxin concentrations in 10 DAG whole seedlings 56
Figure 2.12: Model average auxin concentrations 57
Figure 2.13: Auxin experimental and model results 58
Figure 2.14: Localisation of PIN1, PIN2, PIN3 to the plasma membrane 59
Figure 2.15: Localisation of AUX1 and LAX2 to the plasma membrane 59
Figure 2.16: PIN and AUX1 localisation to the plasma membrane 60
Figure 2.17: CK experimental and model patterning results 62
Figure 2.18: Summary WT model results 63
Figure 2.19: Auxin concentration profiles for varied auxin diffusion 64
Figure 2.20: Average auxin concentration for varied auxin diffusion 65
Figure 2.21: Auxin concentration profiles for varied CK diffusion 66
Figure 2.22: Average auxin concentration for varied CK diffusion 66
Figure 2.23: Auxin concentration profiles for varied ET diffusion 67
Figure 2.24: Average auxin concentration for varied ET diffusion 68
Figure 2.25: Auxin profile for varied PIN protein diffusion 69
Figure 2.26: Auxin concentration maps for varied PIN diffusion 69
Figure 2.27: Average auxin concentration for varied PINp diffusion 70
Figure 2.28: PINp concentration profiles for varied PINp diffusion 70
Figure 2.29: Enlarged PINp profiles for varied PINp diffusion 71
Figure 2.30: AUX1p concentration profile for varied AUX1 diffusion 72
Figure 2.31: Auxin concentration profile for varied AUX1 diffusion 72
Figure 2.32: Auxin concentration maps for varied AUX1 diffusion 73

Figure 2.33: Auxin concentration maps for varied auxin decay 73
Figure 2.34: CK synthesis in central cell files (a) auxin (b) cytokinin results 74
Figure 2.35: CK synthesis in all cells (a) auxin (b) cytokinin results 75
Figure 2.36: Average auxin concentrations for varied *AUX1* expression 76
Figure 2.37: Auxin concentration profiles for varied *AUX1* expression 77
Figure 2.38: Auxin concentration maps for varied *AUX1* expression 77
Figure 2.39: Auxin QC concentration maps for varied *AUX1* expression 78
Figure 2.40: Average auxin concentrations for varied *PIN* expression 79
Figure 2.41: Auxin concentration profiles for varied *PIN* expression 80
Figure 2.42: Auxin concentration maps for varied *PIN* expression 81
Figure 2.43: Auxin concentration maps at QC for varied *PIN* expression 81
Figure 2.44: Relative experimental shoot to root auxin transport 82
Figure 2.45: Relative model shoot to root auxin transport 83
Figure 2.46: ET response and model concentration profiles 84
Figure 2.47: Experimental and model *PLS* gene expression patterning 85
Figure 2.48: *PLS*m transcription patterning in WT 86
Figure 2.49: Relative experimental PIN in WT(c24), 35S(PLSox), *pls, etr1*, *pls etr1* . 87
Figure 2.50: Relative model PIN concentration in WT, PLSox and mutants 87
Figure 2.51: PIN1 images for WT, mutants and PLSox 89
Figure 2.52: PIN1 concentration profiles (A) experimental and (B) model 89
Figure 2.53: PIN2 images for WT, mutants and PLSox 90
Figure 2.54: PIN2 concentration profiles (A) experimental and (B) model 91
Figure 2.55: Auxin patterning in (B) WT (C) *aux1* mutant 92
Figure 2.56: Auxin profiles in WT and *aux1,* (A) experimental (B) model 92
Figure 2.57: Auxin WT colour map and profile (GG model) 94
Figure 2.58: GG Model WT auxin profiles for three different regions 94
Figure 2.59: WT DII-VENUS response and model auxin profiles 96
Figure 2.60: Measures of DII-VENUS levels in different cell types 96
Figure 2.61: The GG model root map. 97
Figure 2.62: Auxin levels relative to QC (A) experimental (B) model. 100
Figure 2.63: Relative auxin trends in different cell types. 102
Figure 2.64: Model cytokinin and ethylene concentrations in WT and *pls*. 103
Figure 2.65: AUX1 patterning 105
Figure 2.66: AUX1 model concentration profiles and image 106
Figure 2.67: PIN1 concentration profiles (A) experimental (B) model 107
Figure 2.68: Model results for *PIN* transcription rate in WT and *pls* 108
Figure 2.69: Model WT pattern of X (downstream ET signalling) and PLSp 109

Figure 2.70: Auxin patterning for different PIN and AUX1 permeabilities 110
Figure 3.1: (a) SimuPlant Image (b) Root structure 120
Figure 3.2: (a) Digital realistic root (b) Root structure (Band *et al*., 2014) 122
Figure 3.3: Example cell-number data for QC cell 100 124
Figure 3.4: PIN12 transfer rates to the plasma membrane 126
Figure 3.5: PIN3, PIN4 and PIN7 level and localisation 128
Figure 3.6: AUX1, LAX2 and LAX3 levels and localisation 129
Figure 3.7: Hormonal crosstalk network for the realistic root 132
Figure 3.8: Model root with (a) cell geometry (b) sample carrier placement 133
Figure 3.9: Auxin patterning in the WT realistic root model 134
Figure 3.10: Auxin levels relative to QC for the WT realistic root 135
Figure 3.11: Relative auxin response and concentration trends 136
Figure 3.12: WT model PIN(1&2) concentration patterning. 137
Figure 3.13: Ethylene concentration patterning in the realistic root 138
Figure 3.14: Cytokinin patterning in the realistic root 139
Figure 3.15: PLS protein patterning in the realistic root 140
Figure 3.16: Auxin biosynthesis rate pattern in the realistic root 141
Figure 3.17: PIN1 and 2 patterning after PIN3, 4 and 7 loss 142
Figure 3.18: Auxin patterning with reduced auxin apoplastic diffusion rates 143
Figure 3.19: Auxin patterning with changed auxin influx levels. 144
Figure 4.1: Auxin pattern recovery after 75% PIN3,4,7 loss 154
Figure 4.2: Auxin pattern recovery after 100% PIN3,4,7 loss 156
Figure 4.3: Auxin pattern recovery after 50% PIN3,4,7 loss 157
Figure 4.4: Auxin pattern recovery after 50% PIN3,4,7 gain 158
Figure 4.5: Auxin pattern recovery after 75% PIN3,4,7 gain 159
Figure 4.6: Auxin pattern recovery after 100% PIN3,4,7 gain 160
Figure 4.7: AUX1/LAX recovery pattern after 75% PIN3,4,7 loss. 161
Figure 4.8: Enlarged AUX1/LAX recovery pattern after 75% PIN3,4,7 loss. 162
Figure 4.9: PIN12 pattern recovery 163
Figure 4.10: Auxin pattern recovery by uniform and non-uniform AUX1/LAX 164
Figure 4.11: PIN and AUX1/LAX pattern combinations giving the same target auxin pattern are not correlated (example 1) 166
Figure 4.12: PIN and AUX1/LAX pattern combinations giving the same target auxin pattern are not correlated (example 2) 167
Figure 4.13: PIN and AUX1/LAX pattern combinations giving the same target auxin pattern are not correlated (example 3) 168

Figure 4.14: PIN3,4,7 polarity after recovery from 50% AUX1/LAX gain compared to WT PIN3,4,7 polarity 170
Figure 4.15: Different PIN and AUX1/LAX combinations can generate the same target pattern 172
Figure 4.16: The recovery principle and auxin carriers and patterning 175
Figure 5.1: Auxin patterning if (a) CK inhibits or (b) CK promotes auxin 179
Figure 5.2: CK patterning if (a) CK inhibits or (b) CK promotes auxin 180
Figure 5.3: Schematic of (a) the original network (b) the revised network 183
Figure 5.4: Auxin and ethylene concentration colour maps 192
Figure 5.5: Relative auxin response and concentration trends 193
Figure 5.6: Average auxin concentration trend 193
Figure 5.7: Experimental cytokinin concentration and response data 194
Figure 5.8: Comparison of experimental and model cytokinin patterning 195
Figure 5.9: Relative model CK and ET concentrations in WT and *pls* 196
Figure 5.10: PLS protein patterning (a) experimental (b) model 196
Figure 5.11: Auxin biosynthesis patterning (a) model (b) experimental 197
Figure 6.1: Iterative process to build the model 212

Figure Ap 2.1: Schematic of Ethylene, cytokinin and auxin crosstalk 224
Figure Ap 2.2: Cytokinin signalling pathway 228

LIST OF TABLES

Table 2.1: Grid Point Codes and Properties 36
Table 2.2: Species codes represented in the model 41
Table 2.3: Rate Equations for hormonal crosstalk 42
Table 2.4: Rate equations for PIN and AUX1 recycling 48
Table 2.5: Species flux 50
Table 2.6: Cell type mapping between experimental and model results 98
Table 2.7: Auxin DII-VENUS response and model data 99
Table 2.8: Matching experimental cell file data to the model 102
Table 3.1: Numbers assigned to each cell in the root map 123
Table 5.1: Hormonal crosstalk rate equations for the cytokinin model 185
Table 5.2: PIN12 cycling rate equations for the cytokinin model 189
Table 5.3: Species flux for the cytokinin model 190

LIST OF ABBREVIATIONS

CK	Cytokinin
CKX	Cytokinin oxidase
DAG	Days (of plant growth) after germination
ER	Endoplasmic reticulum
ET	Ethylene
EZ	Elongation zone
FW	Fresh weight
GFP	Green fluorescent protein
GG	Gradual growth
GP	Grid Point in the root map matrix
LHS	Left hand side
LRC	Lateral root cap
MZ	Meristematic zone
NN	Nearest neighbour
OE	Over-expression
PAT	Polar auxin transport
PLS/*PLS*/*pls*/PLSox	POLARIS peptide/gene/loss of function mutant/over-expressor
PM	Plasma membrane
QC	Quiescent centre
RHS	Right hand side
SCN	Stem cell niche
TZ	Transition zone
WT	Wild-type
X	Downstream ethylene signalling

CHAPTER 1 : INTRODUCTION

INTRODUCTION

1.1 Hormonal crosstalk and patterning

The process of plant development, growth and response to varying environmental conditions, involves a complex network of overlapping interactions between plant signalling hormones and gene expression, known as 'hormonal crosstalk'. The original 'classic' plant hormones are ethylene, cytokinin, auxin, abscisic acid and gibberellins; more recently identified hormones include brassinosteroids, strigolactones, salicylic acid, nitric oxide and jasmonic acid (Santner and Estelle, 2009).

Plant hormones act to control cell proliferation, elongation and differentiation and can act antagonistically or synergistically depending on the context; they can act in a non-linear fashion depending on their concentrations, say to promote or inhibit root length in the case of auxin (Taiz and Zeiger, 2010) and cytokinin (Nishimura *et al*., 2004); they can also act differently in root and shoot development, for example cytokinins have opposite roles in the shoot and root meristems (Werner *et al*., 2003).

Hormone concentrations in the cells are a function of multiple factors such as hormone biosynthesis, long and short range transport, influx and efflux by carrier proteins (such as the AUX1/LAX and PIN auxin carrier families respectively), and hormone activation, inactivation and degradation (Weyers and Paeterson, 2001; Del Bianco *et al*., 2013). Hormones and the associated regulatory and target genes form a network in which relevant genes regulate hormone activities and hormones regulate gene expression (Bargmann *et al*., 2013; Chandler, 2009; Depuydt and Hardke, 2011; Vanstraelen and Benkova, 2012). For example, auxin biosynthesis is stimulated by ethylene and inhibited by cytokinins (Nordstrom *et al*., 2004; Ruzicka *et al*., 2007; Stepanova *et al*., 2007; Eklof *et al*., 1997; Swarup *et al*., 2007), *PIN1* and *PIN2* mRNA and protein levels are promoted by auxin and ethylene (Paciorek *et al*., 2005; Vanneste and Friml, 2009) and inhibited by cytokinin (Ruzicka *et al*., 2009), and cytokinin promotes PIN1 localisation to the lateral plasma membrane in the vascular tissue (Bishopp *et al*., 2011a). Therefore, root development is controlled by an intricate hormonal crosstalk network that integrates gene

expression, signal transduction, transport, and the metabolic conversion complexities associated with hormonal crosstalk activity (Liu *et al*., 2014).

Hormone signalling responses and gene expression display patterning that is essential for regulating correct root development. Cellular patterning in the *Arabidopsis* root is coordinated in part via a localized auxin concentration maximum close to the quiescent centre (QC; Sabatini *et al*., 1999), that regulates the expression of specific genes such as the *PLETHORA* family which acts to define developmental regions in the root (Aida *et al*., 2004; Mahonen *et al*., 2014), *WOX5* which is expressed in the quiescent centre and acts to repress differentiation of the surrounding stem cells (Sarkar *et al*., 2007; Forzani *et al*., 2014), and SHY2 which acts from the cytokinin pathway to inhibit auxin signalling and the expression of the *PIN1, 3*, and *7* genes as well as from the auxin pathway to promote cytokinin biosynthesis (Dello Ioio *et al*., 2008). This auxin gradient has been hypothesized to be sink-driven (Friml *et al*., 2002) and also computational modelling suggests that auxin efflux carrier permeability may be sufficient to generate the gradient in the absence of auxin biosynthesis in the root (Grieneisen *et al*., 2007; Wabnik *et al*., 2010; Clark *et al*., 2014). Genetic studies show that auxin biosynthesis (Ikeda *et al*., 2009; Tivendale *et* al., 2014; Zhao, 2010), the AUX1/LAX influx carriers (Band *et al*., 2014; Jones *et al*., 2008; Krupinski and Jonsson, 2010; Swarup *et al*., 2005; Swarup *et al*., 2008), and the PIN auxin efflux carriers (Grieneisen *et al*., 2007; Krupinski and Jonsson, 2010; Mironova *et al*., 2010; Petrásek *et al*., 2006) all play important roles in the formation of auxin gradients. In addition, it has been proposed that auxin degradation and conjugation could play an important role in auxin homeostasis (Mellor *et al*., 2016b). Recently, it has also been demonstrated that growth and patterning are linked during early vascular tissue formation in *Arabidopsis*, where cell geometry and an integrated network of auxin, cytokinin, auxin transport and cytokinin response, all act to control cell division and pattern formation in vascular tissue growth and development (De Rybel *et al*., 2014). Intercellular movement of mobile transcription factors via the plasmodesmata also appear to be involved in the regulation of plant developmental processes (Helariutta *et al*., 2000; Drisch and Stahl, 2015; Long et al., 2015).

It is not fully understood how hormones interact to coordinate the growth and developmental processes, nevertheless genetic screens, in particular using the *Arabidopsis thaliana* plant model, have extended the knowledge of the action of hormonal signalling systems in the coordination of plant growth and development. While certain hormone response and gene patterning is indicated by experimental analysis, hormone and gene pathways are interlinked, exhibit 'crosstalk' and do not change independently, and little is known about how this gene and hormone interaction network controls patterning.

The *Arabidopsis* primary root is amenable to mutant screening and has a simple radial structure making it a particularly useful system for examining the action of plant hormones in root development and growth. In root development, the root apical meristem is established and is ultimately the source of all root cells. It contains a stem cell niche (SCN) with a quiescent centre (QC) containing 4 cells which divide very slowly, surrounded by initial cells (or stem cells). The initials divide asymmetrically at an intermediate rate to both maintain the stem cell population and generate other faster dividing daughter cells, which eventually elongate and differentiate into different root cell types (Dolan *et al*., 1993).

1.2 Root structure and developmental zones

The structure of the *Arabidopsis* primary root tip and definition of the different cell files is shown in Figure 1.1.

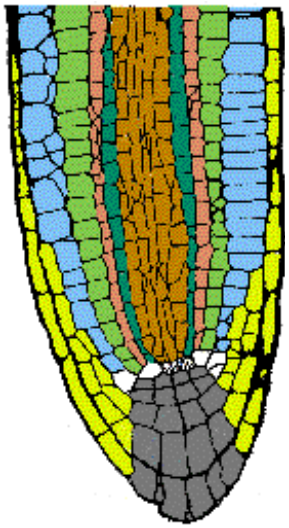

Figure 1.1: Cell files in the *Arabidopsis* root tip
Yellow – Lateral root cap; Blue – Epidermis; Light green – Cortex; Pink – Endodermis; Dark green - Pericycle; Brown – vascular cells; Dark Grey – Columella root cap cells and columella initials; White – Quiescent centre and initials (Dolan *et al*., 1993)

The root tip can be divided into 4 developmental zones (Figure 1.2) consisting of the ‘root cap’ (the most distal zone), the ‘meristematic zone’ containing the quiescent centre and stem cells and where most cell proliferation occurs, the ‘elongation zone’ with reduced cell proliferation and where cell elongation and expansion occurs, and the ‘differentiation or maturation zone’ where cells reach their final developmental stage.

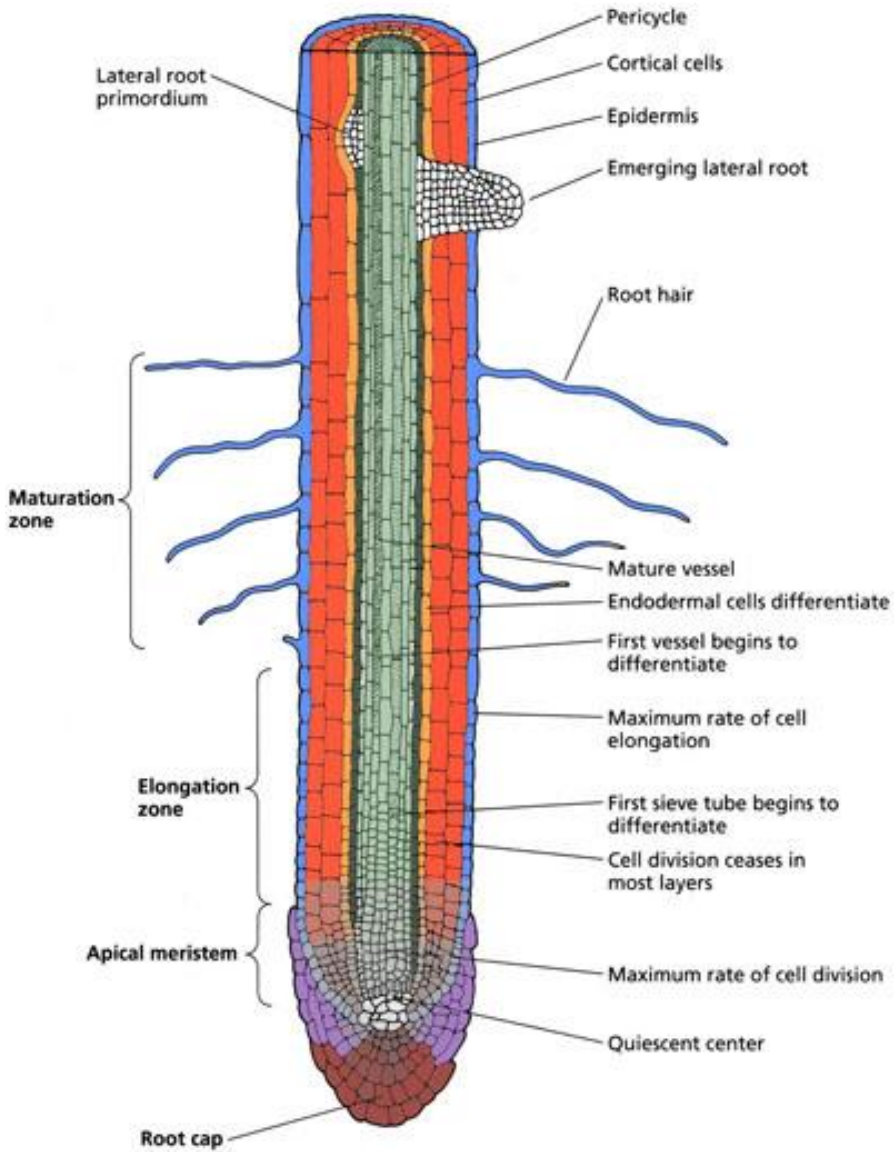

Figure 1.2: *Arabidopsis* root structure and developmental zones
The root cap, meristematic, elongation and differentiation/maturation zones (Taiz and Zeiger, 2010)

1.3 Auxin

While several hormones are involved in the regulation of root development, auxin and cytokinin play central roles in regulating the size of the meristem and root growth (Ruzicka *et al*., 2009). The importance of the interaction between auxin and cytokinin in root and shoot development and the maintenance of cell proliferation was shown in very early experiments on cultured tobacco callus (Skoog and Miller, 1957) where the developmental pathway varied depending on the exogenous auxin to cytokinin ratio in the growth medium.

Auxin is involved in controlling cell identity specification, cell expansion, cell division (Blilou *et al*., 2005; Sabatini *et al*., 1999), in the regulation of the transition from cell proliferation to differentiation (Ishida *et al*., 2010) and in the control of cell elongation and root growth rate (Evans *et al*., 1994). Auxin concentration gradients appear related to cell proliferation, with high auxin concentrations in the QC with a very low proliferation rate, intermediate concentration in the stem cells with intermediate proliferation rates, lower concentrations in the more highly proliferative meristematic zone, and the lowest auxin concentration correlating to cell elongation and differentiation and the cessation of proliferation (Garay-Arroyo *et al*., 2012). The relationship between root growth and exogenously applied auxin is non-linear, following a bell shaped growth response curve (Taiz and Zeiger, 2010).

The maintenance of correct auxin concentrations in the root cells is therefore critical. Auxin is mainly synthesised in young leaves and the shoot apical meristem, with long-range transport from the shoots to the roots via the phloem (Swarup *et al*., 2001). Auxin biosynthesis also occurs locally in the root cells (Ljung *et al*., 2001) and is stimulated by ethylene and inhibited by cytokinins (Nordstrom *et al*., 2004; Ruzicka *et al*., 2007; Stepanova *et al*., 2007; Eklof *et al*., 1997; Swarup *et al*., 2007). Differential auxin distribution in the root cells depends primarily on a combination of shoot to root auxin transport, local auxin biosynthesis and on intercellular short-range influx and efflux transport to and from the cells. Auxin influx is mediated in part by passive diffusion into the cell but mainly by the action of plasma membrane located auxin influx carriers (the AUX1/LAX protein family). The organised asymmetrical placement of the auxin efflux carriers (the PIN protein family) directs polar transport and auxin

distribution through the root cells (Ruzicka *et al*., 2009) to create the classic auxin response patterning (Figure 1.3).

Figure 1.3: Auxin response gradient in *Arabidopsis* 4 DAG root
Auxin response patterning, as demonstrated by expression of the auxin inducible reporter IAA2::GUS and blue staining, indicating a response maximum in the QC region and a proximally decreasing response above the QC (Grieneisen *et al*., 2007)

1.4 Cytokinin (CK)

Together with auxin, cytokinins play an important role in root growth and development. Auxin suppresses total cytokinin biosynthesis in the whole plant (Nordstrom *et al*., 2004). Cytokinins are synthesised in various tissues in the root tip including the columella cells which are located just distal of the QC, the endodermis of the root elongation zone, xylem precursor files, and phloem tissues (Miyawaki *et al*., 2004). While CK transport is not well understood, one mechanism is thought to be transport through the plant in the phloem (Bishopp *et al*., 2011b) and recently cytokinin influx importers have been identified (Zurcher *et al*., 2016). Cytokinin has been found to negatively regulate *PIN1,2 and 3* expression, positively regulate *PIN7* expression, and promote PIN3 and PIN7 localization to the lateral plasma membranes in vascular tissues, so influencing auxin patterning (Ruzicka *et al*., 2009; Bishopp *et al*., 2011a).

Up-regulation of cytokinins results in the reduction of the size of the root meristem and reduction in root length, and plants deficient in cytokinin

biosynthesis have enlarged root meristems. Up-regulation of cytokinin does not affect the rate of cell proliferation in the meristematic zone which suggests that the decrease in size of this zone from increased cytokinin must result from upregulating the rate of differentiation of meristematic cells at the transition zone (TZ), between the meristematic and elongation zones, so affecting the position of the TZ (Dello Ioio *et al*., 2007; Werner *et al*., 2003). It is suggested that cytokinin affects root meristem size by modulating the transcription of auxin efflux PIN proteins, so affecting the auxin to cytokinin ratio in the root cells (Ruzicka *et al*., 2009) and that it also reduces PIN1 by redirecting it for lytic degradation in the vacuoles (Marhavy *et al*., 2011). Cytokinin induces ethylene biosynthesis (Chae *et al*., 2003) and reduces root length via an ethylene dependent pathway which inhibits cell elongation (Ruzicka *et al*., 2009).

1.5 Ethylene (ET)

Ethylene is synthesised in all regions of the plant including the roots and at a high rate in meristematic tissues (Lin *et al*., 2009). Both auxin and cytokinin can stimulate ethylene biosynthesis (Stepanova *et al*., 2007; Vogel *et al*., 1998). Seedlings grown in the presence of ethylene show the 'triple response' with a shortened stem and root, lateral cell expansion and the closure of the apical hook (Taiz and Zeiger, 2010). The ethylene signalling pathway includes ethylene receptors and a molecule CTR1 which, in the absence of ethylene, is active and inhibits downstream signalling pathways. Upon ethylene binding to its receptors, CTR1 is inactivated thus releasing the inhibition of downstream ET signalling.

Ethylene has multiple effects in root development; it promotes root hair differentiation; it inhibits cell elongation through downstream ethylene signalling, by upregulating auxin biosynthesis and PIN2 auxin efflux carriers in the lateral root cap to increase auxin in the elongation zone, so inhibiting cell growth by limiting the ability of the cell walls to elongate (Ruzicka *et al*., 2007; Swarup *et al*., 2007); it promotes QC cell division and possibly root meristem maintenance (Garay-Arroyo *et al*., 2012); and it stimulates auxin biosynthesis.

1.6 POLARIS (PLS)

Another molecule which appears heavily involved in hormonal crosstalk in *Arabidopsis* root development is the short 36 amino acid peptide encoded by the gene *POLARIS (PLS). PLS* is relatively highly expressed in root tips and is required for correct root growth and vascular development and correct auxin and cytokinin-mediated root growth responses (Casson *et al*., 2002). Experimental evidence shows that there is a link between PLS, ethylene signalling, auxin homeostasis and microtubule cytoskeleton dynamics (Chilley *et al*., 2006). *pls* mutant roots are short, with reduced cell elongation, and are hyper-responsive to exogenous cytokinins (Casson *et al*., 2002). Expression of the *PLS* gene of *Arabidopsis* is repressed by ethylene and induced by auxin, and influences PIN protein abundance in roots (Casson *et al*., 2002; Chilley *et al*., 2006; Liu *et al*., 2013). These and other experimental data reveal that interactions between PLS and PINs are important for the crosstalk between auxin, ethylene and cytokinin (Liu *et al*., 2013). *pls* null mutants show increased responsiveness to cytokinins and reduced responsiveness to auxin (Casson *et al*., 2002). *PLS* under-expression in null mutants (*pls*) results in reduced root growth while PLS overexpressing transgenics (PLSox) appear to oppose the root growth inhibitory effects of cytokinins (Casson *et al*., 2002). Experiments indicate that *pls* mutants show enhanced ethylene signalling by measuring the abundance of ethylene induced gene transcripts. Recent experiments indicate that PLS binds copper ions and promotes binding of the copper ions to the ethylene receptor ETR1 to activate the receptor, which in turn activates the downstream CTR1 molecule and inhibits the ethylene signalling pathway (Chilley *et al*., 2006; Mudge *et al*., 2017 (submitted)). ET functions to inactivate the ETR1 receptor and CTR1, so releasing inhibition of downstream ethylene signalling, by both binding and inactivating ETR1 and also by inhibiting *PLS* transcription to further reduce ETR1 and CTR1 activity.

1.7 PIN and AUX1/LAX auxin efflux and influx transporter families

The hormone auxin tends to be protonated in the more acidic cell wall allowing a degree of auxin influx into the cell by diffusion; however, in the more neutral cytosol, auxin tends to become de-protonated which prevents auxin efflux from

the cell by diffusion (Petrásek and Friml, 2009). The AUX1/LAX and PIN protein families act as auxin influx and efflux proteins, respectively, to enhance intercellular auxin transport and also direct auxin flow, facilitating the formation of classic auxin patterning with the auxin maximum in the QC region (Grieneisen *et al*., 2007).

PIN proteins can be apically, basally or laterally targeted to the plasma membrane depending on the PIN protein, the cell type, and the developmental context. For example PIN1 is predominantly located to the basal face of vascular cells but with a weak signal in the epidermis and cortex, PIN2 is located to the apical faces of the lateral root cap and epidermal cells and more homogenously at the boundaries of the cortical cells, and PIN3 is ubiquitously located at all faces in the columella cells and to the inner lateral face of the pericycle cells in the elongation zone (Blilou *et al*., 2005; Friml *et al*., 2003; Muller *et al*., 1998).

The AUX1/LAX protein family members act as auxin influx carriers and can also show polar organisation in the plasma membrane. AUX1 appears to be located on all cell faces but can be enriched at the proximal face of protophloem cells at the opposite face to PIN1, at the upper and lower faces of epidermal cells and with approximately symmetrical distribution in other cell types (Kleine-Vehn *et al*., 2006). It is suggested that PIN1 and AUX1 accumulate at the developing cell plate of dividing cells and are then targeted to the plasma membrane by different vesicle trafficking pathways, accounting for their enrichment at opposite cell faces in the same cell (Kleine-Vehn *et al*., 2006; Geldner *et al*., 2001). The location of the PIN and AUX1/LAX proteins effectively directs auxin from the shoot to the root tip in the vasculature and then back towards the shoot in the root cap and epidermal cells, with some auxin being redirected laterally back towards the vasculature to maintain a ‘reverse fountain flow’ in the root tip (Figure 1.4) to increase accumulation of auxin in the QC (Overvoorde *et al*., 2010; Wisniewska *et al.,* 2006).

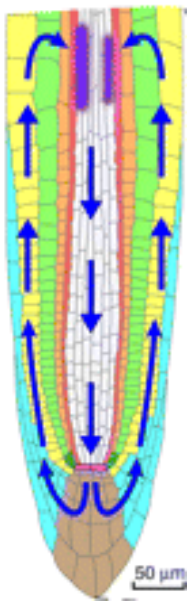

Figure 1.4: Auxin 'Reverse fountain flow' in the root tip
Blue arrows indicate direction of auxin transport-mediated flux from the lateral root cap through the epidermis and then back towards the root tip (Overvoorde *et al*., 2010)

The asymmetrical location of these carrier proteins in the plasma membrane is thought to be based on controlled exocytosis, and then endocytosis and sequestering in endosomal bodies. It has been suggested that the dynamic recycling of these carrier proteins enables the cell to respond quickly to environmental changes by adjusting auxin flow and patterning (Kleine-Vehn *et al*., 2006). Increased cytosolic auxin results in increased *PIN* expression and a reduced rate of endocytosis resulting in increased PIN concentration at the plasma membrane (Paciorek *et al*., 2005). Auxin also promotes the phosphorylation of PIN proteins, resulting in increased activity of the PIN efflux carriers at the plasma membrane by unknown mechanisms (Barbosa *et al*., 2014; Weller *et al*., 2017; Zhang *et al*., 2010; Zourelidou *et al*., 2014). Auxin therefore promotes its own efflux from the cell by multiple mechanisms. As noted previously both ethylene and cytokinin regulate *PIN* expression, and ethylene also promotes *AUX1* expression (Ruzicka *et al*., 2007).

The role of the influx and efflux proteins is critical in organising polar auxin transport and establishing auxin patterning (Grieneisen *et al*., 2007; Band *et al*., 2014).

1.8 Mathematical modelling of hormonal crosstalk and patterning

Mathematical modelling techniques have been used to analyse auxin flux and patterning. Multicellular and predominantly 'physical flow' models of directional auxin flux in a 2-D theoretical *Arabidopsis* root (Grieneisen *et al*., 2007; Mironova *et al*., 2012) suggest that correct PIN protein placement is necessary to establish correct auxin patterning. Rather than representing biological processes of hormone and gene interaction, these models mainly represent auxin synthesis in the root cells, and the physical flux of auxin from the shoot to the root and between cells in the root, with auxin flux being directed by predetermined placement of PIN proteins on selected cell faces to create the classic auxin patterning with a maximum in the QC. Other studies have suggested that auxin patterning and the location of the auxin maximum is due to the action of the influx carriers which effectively act to retain auxin in the cells to create the maxima, while the PIN proteins act to direct auxin flow (Band *et al*., 2014).

Single cell 'biological' models have been built to represent hormonal crosstalk and gene expression. One such model simulates how cytokinins can affect the expression of auxin responsive genes and the *PIN* auxin efflux carriers (Muraro *et al*., 2011). A single cell model (Liu *et al*., 2010; Liu *et al*., 2013) represents hormonal crosstalk and gene expression, including hormone biosynthesis and decay, hormone transport into and out of the cell, and interactions between the hormones auxin, cytokinin and ethylene and gene expression within a single cell. The Liu *et al.* (2010, 2013) models explain experimentally observed relationships, trends in auxin and PIN concentrations in wildtype and a variety of mutants, and the effects of exogenously applied hormones, but are unable to analyse 2-D pattern formation

1.9 Research Aims

The goal of this research project is to attempt to explain the formation of hormone signalling and gene expression patterning in the *Arabidopsis* root tip by using a Systems Biology approach to incorporate experimental data into a mathematical model to simulate experimentally observed patterning in a 2-D

virtual root. This work can be divided into 4 steps as described in each of the following chapters:

- the logical first step from previous work was to embed the single cell biological crosstalk processes from the Liu *et al.* (2010, 2013) models into each cell of the simple rectangular multicellular root framework of the Grieneisen *et al.* (2007) auxin flow model, and also add processes for species flux within and between cells in the root structure. Results from this 2-D spatial model of hormonal crosstalk and gene expression in the *Arabidopsis* root tip could then be compared with experimentally observed hormone concentration and gene expression patterns
- the second step was to replace the simple rectangular root with a much more realistic map, based on experimental imaging, to build a realistic 'wildtype' root which could be used with the model to duplicated experimentally observed hormone and gene expression patterning. This step checks if patterning generated by the initial rectangular root was dependent on the rectangular root architecture. It also allows much more meaningful and detailed comparison between model results and experimental observations.
- the third phase, using the realistic root, was to investigate the relative roles of the AUX1/LAX and PIN influx and efflux carriers in establishing patterning, using a novel recovery principle which enabled the rescue of pattern perturbations (due to changes in either the influx or efflux carriers) by adjusting the cellular distribution and concentrations of the other carrier family.
- the fourth phase involved revising the network (based on additional experimental data from the literature) using alternative relationships between the auxin, cytokinin and ethylene signalling pathways, to correct patterning inconsistencies present in the previous models and so better match experimental results.

The work in Chapters 2 to 4 and Appendix 2 is largely covered in five publications (Moore *et al*., 2015a; Moore *et al*., 2015b; Moore *et al*., 2015c ; Moore *et al.*, 2017; Liu *et al*., 2017).

CHAPTER 2 : PATTERNING IN A SIMPLE 2-D RECTANGULAR ROOT MODEL

PATTERNING IN A SIMPLE 2-D RECTANGULAR ROOT MODEL

2.1 Introduction

Multiple, complex, non-linear hormonal interactions make the understanding and analysis of the hormone crosstalk network and consequent patterning, by laboratory experiments alone, extremely difficult (Band *et al*., 2012). A supplementary approach is the use of mathematical models and simulations based on relationships and parameters observed experimentally, where different theoretical relationships and parameters can be tested to see if they predict results that are consistent with experimental observations. Novel model outcomes can potentially be validated by further experiment.

Auxin concentration is regulated by diverse interacting hormones and gene expression and therefore cannot change independently of the various crosstalk components in space and time; similarly, ethylene and cytokinin concentrations and expression of the associated regulatory and target genes are also interlinked (To *et al*., 2004; Shi *et al*., 2012). Important questions for understanding hormonal crosstalk in root development include how hormone concentrations and expression of the associated regulatory and target genes are mutually related, and then how patterning of both hormones and gene expression emerges under the action of hormonal crosstalk.

In previous work, a hormonal crosstalk network for a single *Arabidopsis* cell was developed by iteratively combining modelling with experimental analysis (Liu *et al*., 2010; Liu *et al*., 2013). This work described how such a network regulates auxin concentration in the *Arabidopsis* root by controlling the relative contributions of auxin influx, biosynthesis and efflux, and by integrating auxin, ethylene and cytokinin signalling as well as PIN function. Mathematical modelling of auxin transport and patterning within a multicellular 2-D root system has also suggested that correct PIN protein placement is necessary to establish correct auxin patterning (Grieneisen *et al*., 2007; Mironova *et al*., 2012). In this project, the work of Liu *et al.* (2010, 2013) and Grieneisen *et al*. (2007) are combined to develop a spatiotemporal model of hormonal crosstalk for the *Arabidopsis* root tip. The model demonstrates that the level and patterning of auxin, PIN localization and *POLARIS* (*PLS*) gene expression in

Arabidopsis wildtype and mutant roots can be elucidated by the action of the spatiotemporal dynamics of hormonal crosstalk, which integrates auxin, ethylene and cytokinin signalling and the function of the auxin transporters AUX1 and PIN.

The proposed 2-D spatial model combines the multi-cellular root structure from Grieneisen *et al*. (2007) with the intracellular relationships, species biosynthesis and decay, and hormone and gene interactions in a single cell from Liu *et al.* (2010, 2013). Additional relationships define species diffusion or permeability within the cytosol and cell walls and across the plasma membrane, and the recycling of PIN and AUX1 auxin transport proteins to and from the plasma membrane. A simplified schematic of the model components is shown in Figure 2.1, consisting of the root structure, hormone flux at the root/shoot border, hormonal biosynthesis, crosstalk and gene expression, the recycling of the auxin carriers to and from the plasma membrane, and species flux within and between cells in the root. All of the model elements are explained in more detail later in this chapter, including details of the root map structure and rate equations.

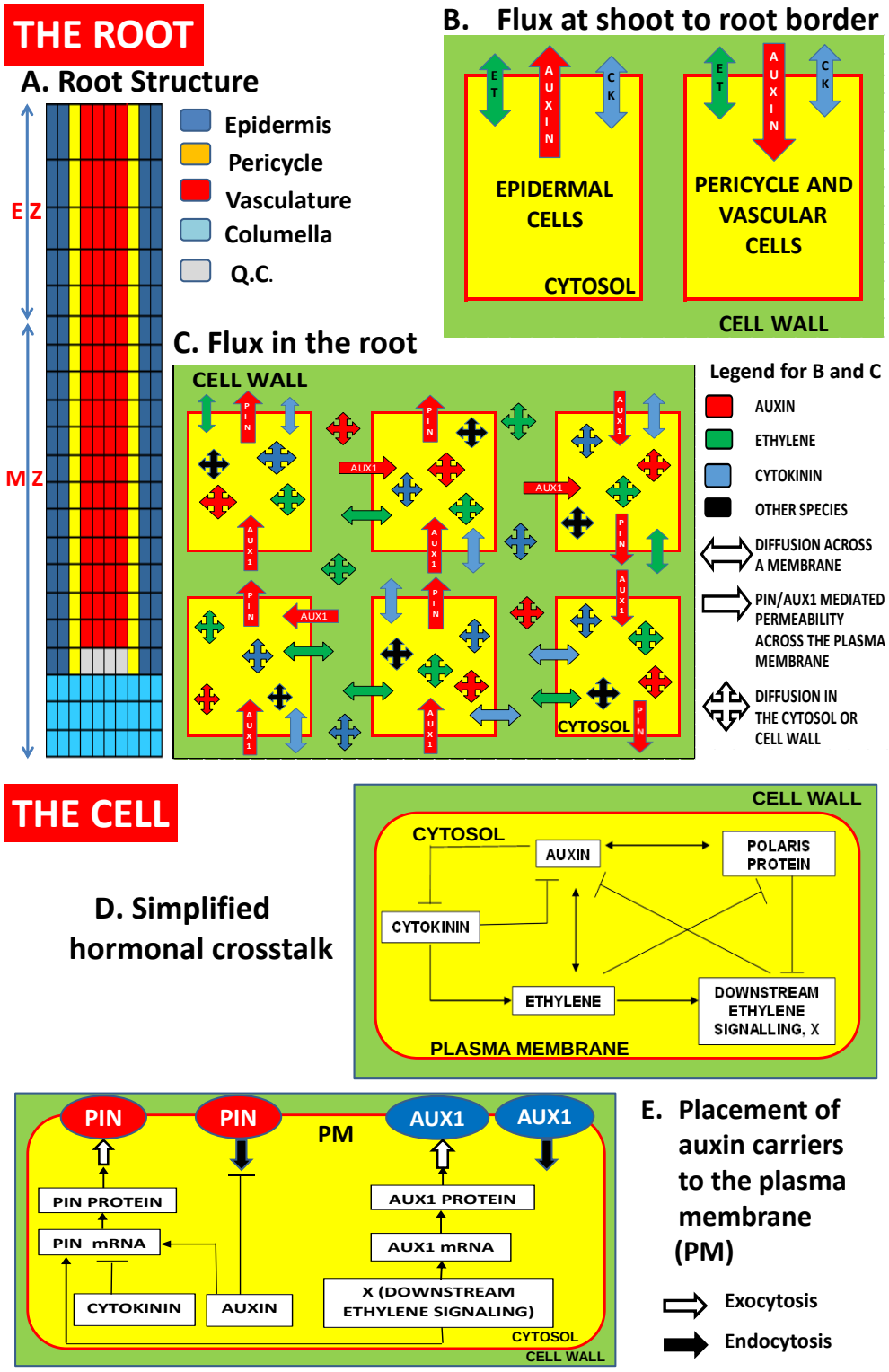

Figure 2.1: A schematic of the 2-D spatial model components

A. Multicellular root structure map, modified from Grieneisen *et al*. (2007), defined by a matrix of grid points (GPs). MZ, meristematic zone; EZ, elongation zone; QC, quiescent centre.
B. Auxin flux by permeability from shoot to root in the pericycle/vascular cells and root to shoot in the epidermal files. Ethylene (ET) and cytokinin (CK) diffuse between shoot and root.
C. Species diffuse between GPs within the cytosol (all species) or cell wall (hormones). Hormone flux across the plasma membrane (PM) by diffusion (for ET and CK) and by permeability (auxin).
D. Simplified Liu *et al.* (2010, 2013) single cell hormonal and gene expression crosstalk.
E. Dynamic recycling of PIN/AUX1 auxin carriers to the PM by exocytosis and endocytosis.

Having constructed the model, the next step was to set up the parameter values. Initial model parameters were set to the values contained in the auxin spatial model by Grieneisen *et al*. (2007) and the single cell model by Liu *et al.* (2010, 2013). Certain parameters in the single-cell hormonal crosstalk network were derived from the literature; for example, parameters relating to ethylene receptors and CTR1 were studied (Diaz and Alvarez-Buylla, 2006), and these values were retained in the 2-D spatial model. Some diffusion and permeability parameters were reset to match known published data, where available (see below).

A model calibration step was then performed where the unknown parameter values were adjusted to produce simulation results, consistent with experimental data and images and meeting the following fit criteria: 1) endogenous average auxin concentration for the WT root is similar to experimental data; 2) changes in average auxin concentration in WT, *pls*, *pls etr1* double mutant, and PLSox transgenic follow experimental trends; 3) auxin concentration patterning in the WT root is similar to experimental observation; 4) the auxin carrier proteins PIN and AUX1 localise predominantly to the plasma membrane; and 5) CK concentration patterning matches experimental results. The goal of model calibration was to produce a 'wildtype' parameter set which could form the basis for future model simulations and predictions.

Once parameter calibration was complete, the model was tested for 'robustness'; in other words how the model responded to variation in WT parameter values. Given that most parameter values are unknown, it is important that the model is relatively insensitive to variation in the parameter settings, otherwise future model results become wholly dependent on certain unknown parameter values that can be very difficult or impossible to verify experimentally. While the modelling equations must be structured in specific forms, many different parameter sets can be fitted against the above criteria since the number of parameters far exceeds the number of results from experimental observations. If a randomly selected 'unknown' parameter value is changed, adjustments to one or more of the other parameters can generate a new set of WT parameters that meets the required fit criteria and makes correct predictions. Also, when a parameter value is reset to be consistent with new

additional experimental data, one or more other parameters can be simultaneously adjusted such the fit criteria are satisfied and the model reproduces experimental results. Therefore, the experimental observations can be reproduced using many different WT parameter sets. In this sense, the model developed here is robust in that it reproduces experimental observations and makes correct predictions with different WT parameter sets and does not rely on a unique set of parameter values that cannot be experimentally verified.

After completion of parameter calibration and robustness testing, model predictions were compared to experimental data, which involved using ImageJ to derive concentration profiles from experimental images. The comparison of model and experimental results gives an indication of whether the model provides a satisfactory explanation of hormonal crosstalk and gene expression interactions in a 2-D spatial context.

2.2 Definition of the Rectangular Root Model

2.2.1 Generalised root structure

The Grieneisen *et al*. (2007) model simulated intercellular auxin flow through a generalised root system (Figure 2.2) based on assumptions on auxin influx from the shoot to the root, local auxin biosynthesis and decay, influx across the plasma membrane from the cell walls into the cytosol mediated by ubiquitous AUX1 protein concentration levels, and auxin efflux from the cells into the cell walls mediated by polar PIN proteins. A generalised PIN protein is represented in the Grieneisen *et al*. (2007) model with assigned ('prescribed') placement and concentration at the plasma membrane depending on the type of cell within the root system, as indicated in the diagrams and supported by the 4 inset cell images in Figure 2.2.

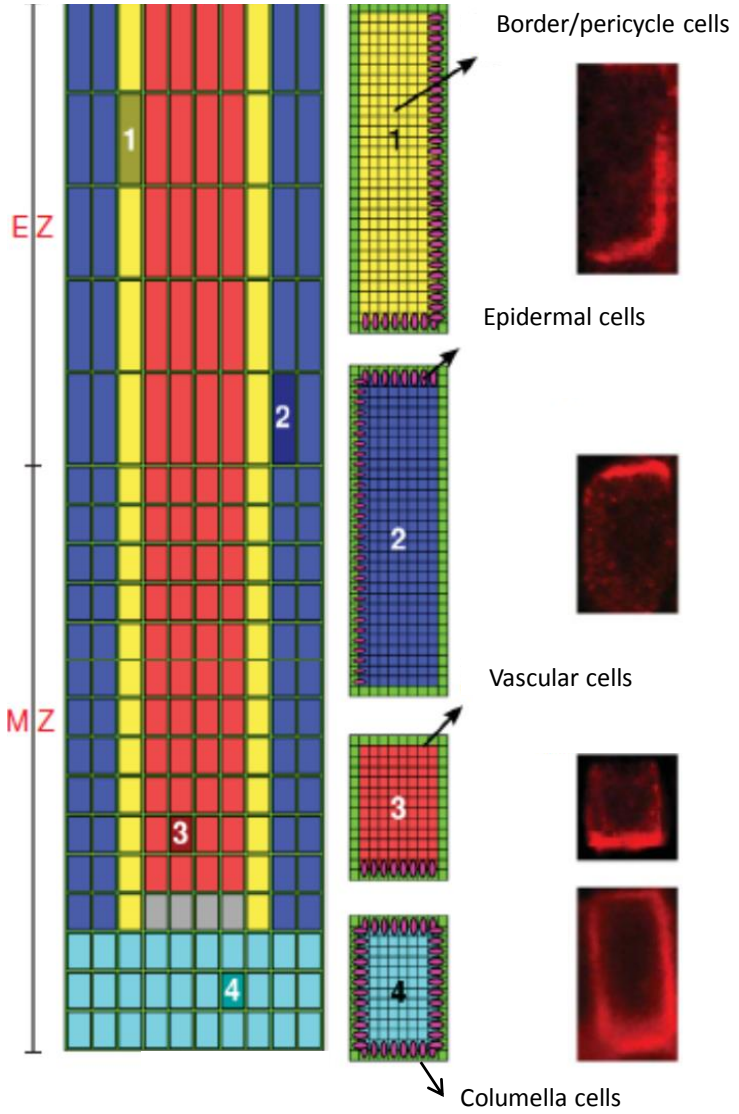

Figure 2.2: Map of root structure and PIN protein placement
Red rectangles – vascular cell files; Yellow – border/pericycle cell files; Blue – epidermal cell files; Grey – quiescent centre (QC) cells; Cyan – columella cells; PIN protein placement: 1 – basal and inner lateral placement in the pericycle cells; 2 – inner lateral and apical placement in the epidermal cells; 3 – basal placement in the vascular and QC cells; 4 – ubiquitous placement in the columella cells. Images show PIN concentrations at the plasma membrane for the different cell types; MZ and EZ - meristematic and elongation zones (Grieneisen *et al*., 2007, modified)

The model root is 10 cells wide with 4 epidermal cell files, 2 border/pericycle files and 4 vascular files, with 3 distal tiers of columella cells (Figure 2.2). The root is 35 cells in length, with 3 tiers of columella cells, 12 tiers in the MZ and 20 tiers in the EZ. Including the cell walls, which are 2 μm thick, all cells are 20 μm wide. Cells vary in length; including the cell walls, cells in the columella and MZ regions are 28 μm long, and cells in the EZ are 64 μm long. The overall root tip

is 200 μm wide and 1700 μm long. In the structure in Figure 2.2, the cell lengths change suddenly from 28 to 64μm from the MZ to the EZ. The effects of a more gradual increase in cell length as cells enter the EZ are investigated later.

2.2.2 Grid point representation of the root

In the model the root is divided up into 2 x 2 μm areas, each of which is represented by a central grid point (Figure 2.3), allowing the root to be modelled by a matrix of 85,000 grid points.

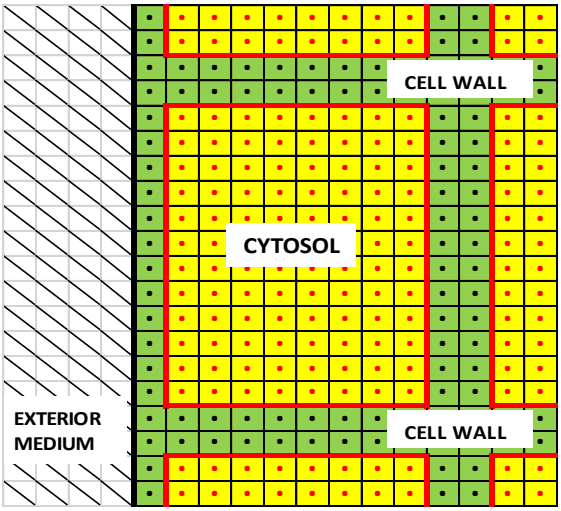

Figure 2.3: Grid point representation of a cell in the MZ
Red/black dots – central grid points each representing a 2 x 2 μm area of the root in the model root matrix; green – cell walls; yellow – cytosol; red line – plasma membrane.

Each grid point (GP) can have different properties depending on its location in the root. For simplicity, adjacent plasma membrane (PM) and cell wall entities are represented by a single model GP identity containing both cell wall and plasma membrane properties. This single identity is referred to as either a cell wall or plasma membrane depending on the context and properties under discussion. Each GP is given a code to represent its properties (Table 2.1).

Table 2.1: Grid Point Codes and Properties

Grid Point Code	Properties
0	Cytosol
1	Plasma membrane with weak background PIN permeability
2	Plasma membrane with medium PIN permeability
3	Plasma membrane with strong PIN permeability
4	Cell wall at the root/shoot boundary of the vascular and border/pericycle cell files, including a plasma membrane with zero PIN permeability
5	Cell wall at the shoot/root boundary of the epidermal cell files, including a plasma membrane with strong PIN permeability

The properties assigned to each GP allow rules to be established governing such processes as species biosynthesis, decay, activation or inactivation at each GP, and flux between neighbouring GPs. Equations are set up to govern the flux between each GP and its 4 nearest neighbours (NN) located to the N, S, E or W (Figure 2.4). For example all species can diffuse within the cytosol but only hormones can cross the plasma membrane (PM) into the cell wall. Cytokinin (CK) and ethylene (ET) can diffuse across the PM while auxin crosses by permeability mediated by PIN and AUX1 carrier proteins. Once within the cell walls, hormones can diffuse between NN grid points. Individual equations for these processes are given later in Table 2.2, Table 2.3 and Table 2.4.

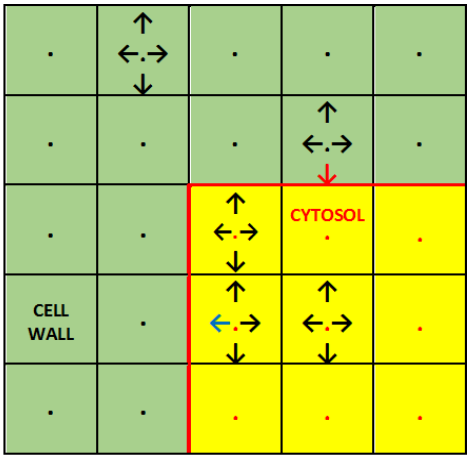

Figure 2.4: Example of flux between nearest neighbour (NN) grid points
Black arrows - diffusion between NN; Red arrow – auxin cell influx mediated by AUX1 carrier proteins; Blue arrow – auxin cell efflux mediated by PIN carrier proteins. Green area – cell wall; yellow area – cytosol; red – plasma membrane.

2.2.3 The root map

The root is represented by a root map containing a matrix of 100 x 850 grid points, each of which has a code 0-5 (Table 2.1). Each grid point is coded as a cytosolic point (GP code 0), or as a plasma membrane/cell wall GP with asymmetrical ‘polar’ PIN efflux permeability and symmetrical ‘non-polar’ AUX1 influx permeability (GP codes 1 to 3), determined by the rate of localisation of the auxin carriers to the plasma membrane as described in more detail in section 2.2.5. The PIN efflux permeability properties result in a relatively high concentration of PIN proteins (at GP code 3) in the apical PM of the epidermal cell files, in the basal PM of the vascular and pericycle/border files, and in the inner lateral PM of the pericycle/border files, and at all faces of the columella cells. There is a relatively medium concentration of PIN proteins (at GP code 2) in the inner lateral PM of the epidermal cells. The remaining PMs have a relatively low background concentration of PIN proteins (at GP code 1) apart from the shoot/root border plasma membrane/cell wall grid points. The GPs at the border of the pericycle and vascular cells (GP code 4) have zero PIN permeability such that auxin is directed into the root from the shoot while the GPs at the border of the epidermal cell files (GP code 5) have high PIN permeability to direct auxin from the root to the shoot.

The root map is made up of 4 different cell tier components each 10 cells wide.

- 1 EZ cell tier at the root/shoot boundary (Figure 2.5)
- 19 standard EZ cell tiers (Figure 2.6)
- 12 MZ cell tiers which includes the QC region (Figure 2.7)
- 3 columella cell tiers (Figure 2.8)

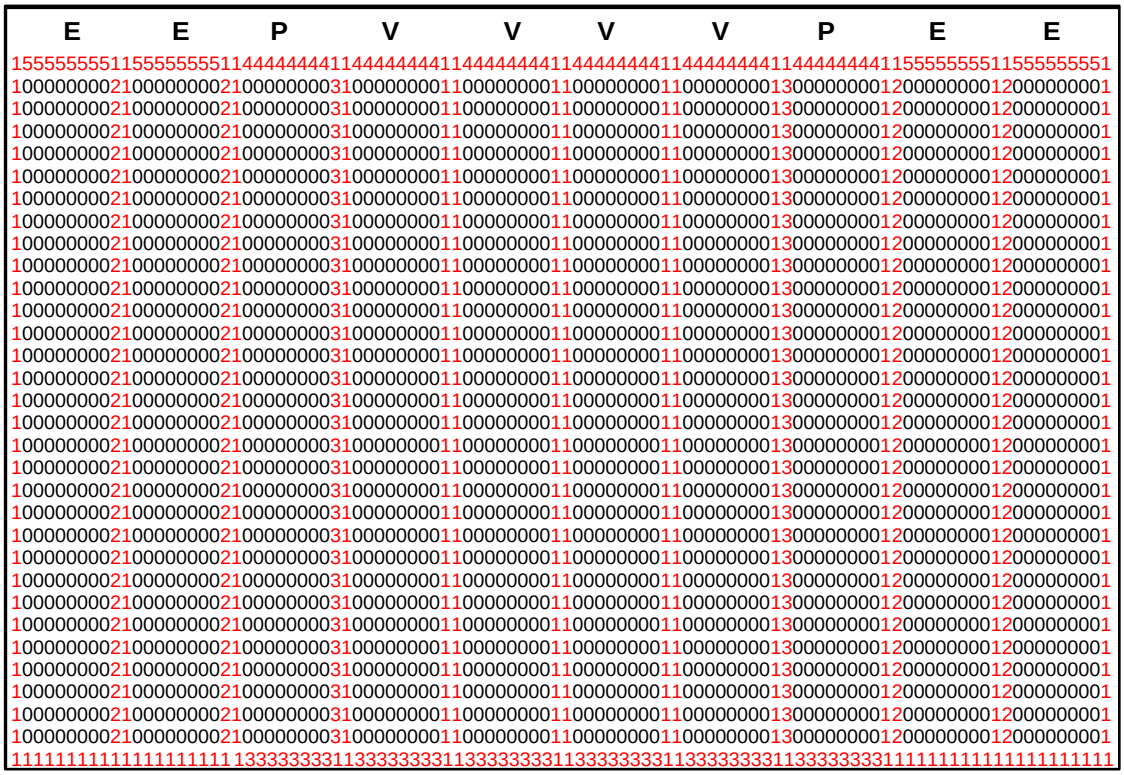

Figure 2.5: Grid point coding for the proximal EZ cell tier in the root map
Cell files: E – epidermal; P – border/pericycle; V – vascular. Grid points: 0 – cytosolic GPs; 1,2,3,4,5 – cell wall/plasma membrane GPs with varying properties.

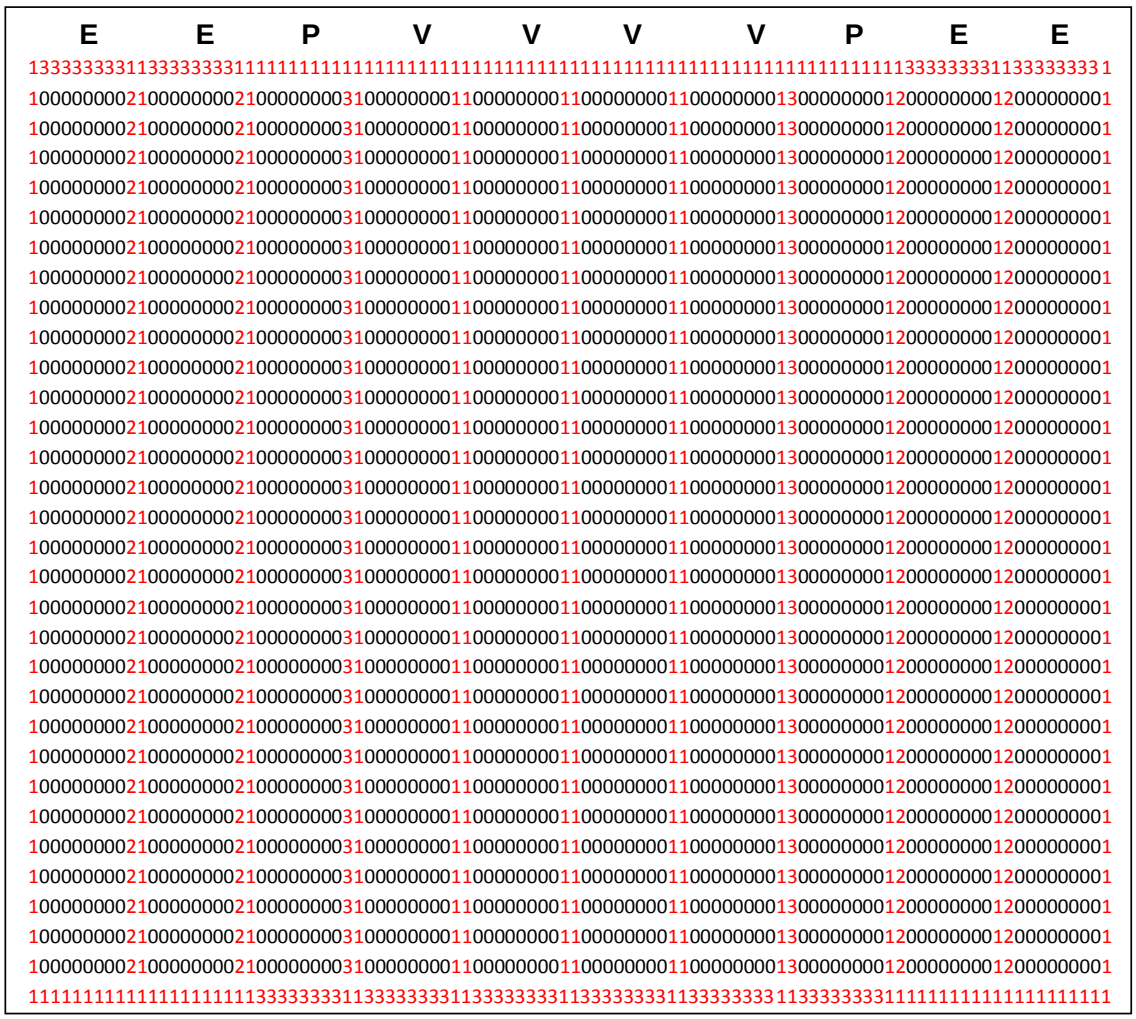

Figure 2.6: Grid point coding for the standard EZ cell tier in the root map
Cell files: E – epidermal; P – border/pericycle; V – vascular. Grid points: 0 – cytosolic GPs; 1,2,3 – cell wall/plasma membrane GPs with varying properties.

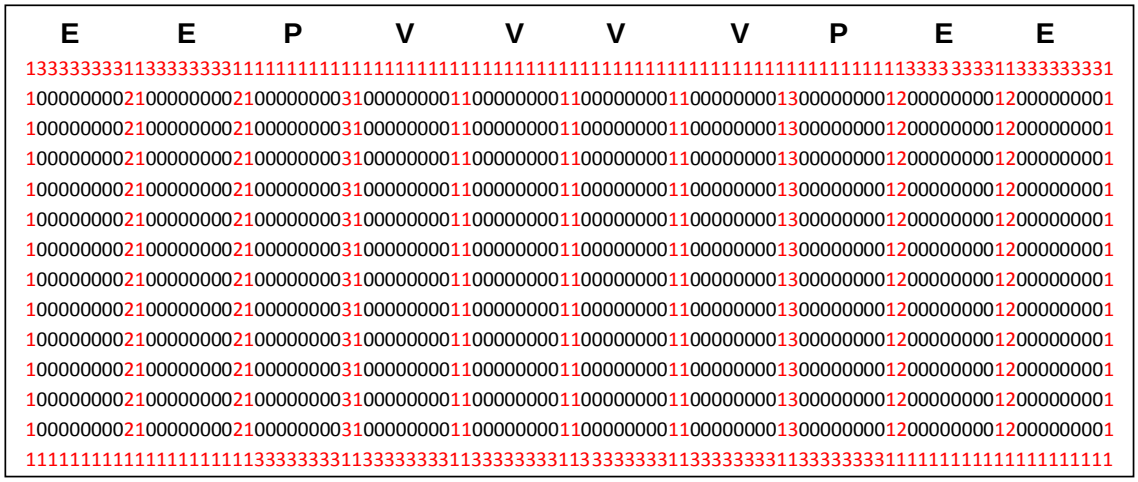

Figure 2.7: Grid point coding for an MZ cell tier in the root map
Cell files: E – epidermal; P – border/pericycle; V – vascular. Grid points: 0 – cytosolic GPs; 1,2,3 – cell wall/plasma membrane GPs with varying properties.

```
    E         E         P         V         V         V         V         P         E         E
1333333331133333333113333333311333333331133333333113333333311333333331133333333113333333311333333331
3000000003300000000330000000033000000003300000000330000000033000000003300000000330000000033000000003
3000000003300000000330000000033000000003300000000330000000033000000003300000000330000000033000000003
3000000003300000000330000000033000000003300000000330000000033000000003300000000330000000033000000003
3000000003300000000330000000033000000003300000000330000000033000000003300000000330000000033000000003
3000000003300000000330000000033000000003300000000330000000033000000003300000000330000000033000000003
3000000003300000000330000000033000000003300000000330000000033000000003300000000330000000033000000003
3000000003300000000330000000033000000003300000000330000000033000000003300000000330000000033000000003
3000000003300000000330000000033000000003300000000330000000033000000003300000000330000000033000000003
3000000003300000000330000000033000000003300000000330000000033000000003300000000330000000033000000003
3000000003300000000330000000033000000003300000000330000000033000000003300000000330000000033000000003
3000000003300000000330000000033000000003300000000330000000033000000003300000000330000000033000000003
3000000003300000000330000000033000000003300000000330000000033000000003300000000330000000033000000003
1333333331133333333113333333311333333331133333333113333333311333333331133333333113333333311333333331
```

Figure 2.8: Grid point coding for the columella cell tiers

Cell files: E – epidermal; P – border/pericycle; V – vascular. Grid points: 0 – cytosolic GPs; 1,2,3 – cell wall/plasma membrane GPs with varying properties.

2.2.4 Biosynthesis, decay, and receptor activation/inactivation in the cytosol

The single cell models (Liu *et al*., 2010; Liu *et al*., 2013) describe hormonal crosstalk and gene expression in a single cell. The interactions in these models are incorporated into all cells of the 2-D spatial root structure. All species are synthesised and decay at all GPs within the cytosol (or in the case of the receptors are activated and inactivated), except CK which is assumed to have tissue specific biosynthesis (Miyawaki *et al*., 2004) predominantly in the central cell files. The rate-limiting step for cytokinin biosynthesis involves a group of isopentenyltransferase (IPT) enzymes. While *IPT* genes are expressed throughout the root, different genes appear to display tissue-specific expression at different levels. In the root, *IPT* genes are predominantly expressed in the xylem precursor cells, the phloem tissue, the columella, and the endodermis of the elongation zone (Miyawaki *et al*., 2004). Therefore, in this version of the model, CK biosynthesis is limited to the central cell files, including the vascular and pericycle/border files, and the central columella files but excluding the epidermal files and the external columella files contiguous to the epidermal files (Figure 2.2). The effects of tissue specific CK biosynthesis on CK spatial distribution are addressed further in the section 2.5.5 on ‘Definition and calibration of the WT model parameter set’.

All species except auxin, CK, ET, PIN and AUX1 proteins are restricted to the cytosol with zero flux across the plasma membrane. Auxin, CK and ET can move across the PM into the cell walls, diffuse and decay within the walls, and move into adjacent cells. PIN and AUX1 proteins are synthesised and decay in the cytosol and are recycled by exocytosis and endocytosis to and from the plasma membrane, where they can also decay but where no diffusion occurs (as noted above the plasma membrane is incorporated into the properties of the cell wall GPs). PIN and AUX1 proteins cannot move between adjacent cells. There are 16 species in the model as listed in Table 2.2 . The rates of gene expression and translation, and species biosynthesis, decay, activation or inactivation are determined by a network of interactions between the hormones and gene products, as summarised in the rate equations in Table 2.3 .

Table 2.2: Species codes represented in the model

Species code	Description
Auxin	Auxin hormone
ET	Ethylene hormone
CK	Cytokinin hormone
PINm	*PIN* mRNA
PINp	PIN protein in the cytosol or plasma membrane (included in cell wall properties)
PLSm	*POLARIS* mRNA
PLSp	POLARIS protein
X	Downstream ethylene signalling
Ra*	Active auxin receptor
RaT	Total of active plus inactive auxin receptors (a constant)
Re*	Active ethylene receptor, ETR1
ReT	Total of active plus inactive ethylene receptors (a constant)
CTR1*	Active CTR1 molecule in ethylene pathway
CTR1T	Total of active plus inactive CTR1 molecules (a constant)
AUX1m	*AUX1* mRNA
AUX1p	AUX1 protein in the cytosol or plasma membrane (included in cell wall properties)

Table 2.3: Rate Equations for hormonal crosstalk

(Rates of species biosynthesis, decay, activation and inactivation at a GP; the V code for each equation is referenced in the network diagram in Figure 2.9)

Species	Rate equations and parameter values	Notes
AUXIN		
V1 Background biosynthesis	k_2	Only in the cytosol
V2 Variable biosynthesis	$\frac{k_{2a}[ET]}{(k_{2d}+k_{2e}[ET])(1+[CK]/k_{2b})}\ \frac{[PLSp]}{(k_{2c}+[PLSp])}$	Only in the cytosol
V3 Decay	$k_3[Auxin]$	In the cytosol and cell walls
Parameters	k2 = 0.001 μM s^{-1}; k2a = 0.025 s^{-1}; k2b=1.0 μM; k2c = 0.01 μM; k2d = 1.0; k2e = 0.0 μM^{-1}; k3 = 0.002 s^{-1}	
References	Eklof *et al*., 1997; Liu *et al*., 2010; Ljung, 2013; Stepanova *et al*., 2007; Swarup *et al*., 2007; Tivendale *et al*., 2014; Zhao, 2010	
Ra*		
V4 Rate of activation	$k_4[Auxin](RaT - Ra^*)$	Only in the cytosol. The receptor switches between active and inactive with the total RaT remaining constant.
V5 Rate of inactivation	$k_5 Ra^*$	Only in the cytosol
Parameters	k4 = 1.0 μM^{-1} s^{-1}; k5 = 1.0 s^{-1}	
References	Liu *et al*., 2010; Ljung, 2013; Mockaitis and Estelle, 2008; Vanneste and Friml, 2009	
PLSm		
V6 Rate of transcription	$\frac{k_6[Ra^*]}{1+\frac{[ET]}{k_{6a}}}$	Only in the cytosol
V7 Rate of decay	$k_7[PLSm]$	Only in the cytosol
Parameters	k6 = 0.03 s^{-1}; k6a = 0.2 μM; k7 = 1.0 s^{-1}; for *pls* null mutant k6 = 0.0 s^{-1}; for PLSox k6 = 0.045 s^{-1}	

References	Casson *et al*., 2002; Chilley *et al*., 2006; Liu *et al*., 2010; Ljung, 2013; Mockaitis and Estelle, 2008; Vanneste and Friml, 2009	
PLSp		
V8 Rate of translation	$k_8[PLSm]$	Only in the cytosol
V9 Rate of decay	$k_9[PLSp]$	Only in the cytosol
Parameters	k8 = 1.0 s^{-1}; k9 = 1.0 s^{-1}	
References	Casson *et al*., 2002; Chilley *et al*., 2006; Liu *et al*., 2010; Ljung, 2013; Mockaitis and Estelle, 2008; Vanneste and Friml, 2009	
Re*		
V10 Rate of activation	$(k_{10} + k_{10a}[PLSp])([\mathrm{Re}T] - [\mathrm{Re}^*])$	Only in the cytosol. The receptor switches between active and inactive with the total ReT remaining constant.
V11 Rate of inactivation	$k_{11}[\mathrm{Re}^*][ET]$	Only in the cytosol
Parameters	k10=0.0003 s^{-1}; k10a=5.0 $\mu M^{-1} s^{-1}$; k11=4.0 $\mu M^{-1} s^{-1}$; for the *etr1-1* gain-of-function mutant k11 = 0.025 $\mu M^{-1} s^{-1}$	
References	Diaz and Alvarez-Buylla, 2006; Liu *et al*., 2010; Wang *et al*., 2002	
ET		
V12 Rate of biosynthesis	$k_{12} + k_{12a}(\frac{[Auxin..]}{(k_{12.b} + k_{12..d1}[Auxin..])} \frac{[CK.]}{(k_{12.c} + k_{12.d2}[CK.])}$	Only in the cytosol. Michaelis Menten kinetics for the rate of biosynthesis regulated by Auxin and CK.
V13 Rate of decay	$k_{13}[ET]$	In the cytosol and cell walls
Parameters	k12 = 0.1 $\mu M\ s^{-1}$; k12a = 0.1 $\mu M^{-1} s^{-1}$; k12b = 0.1; k12c = 0.1; k12d1 = 1.0 μM^{-1}; k12d2 = 1.0; k13 = 1.0 s^{-1}	
References	Liu *et al*., 2010; Vogel *et al*., 1998; Stepanova *et al*., 2007; Tanimoto *et al*., 1995	

CTR1*		
V14 Rate of activation	$k_{14}[\mathrm{Re}^*]([CTR1T]-[CTR1^*])$	Only in the cytosol. The receptor switches between active and inactive with the total CTR1T remaining constant.
V15 Rate of inactivation	$k_{15}[CTR1^*]$	Only in the cytosol
Parameters	k14 = 3.0 μM^{-1} s^{-1}; k15 = 0.085 s^{-1}	
References	Diaz and Alvarez-Buylla, 2006; Liu *et al*., 2010; Wang *et al*., 2002	
X		
V16 Rate of pathway activation	$k_{16}-k_{16a}[CTR1^*]$	Only in the cytosol. Pathway inhibition is regulated by active CTR1.
V17 Rate of pathway inactivation	$k_{17}[X]$	Only in the cytosol
Parameters	k16 = 0.3 μM s^{-1}; k16a = 1.0 s^{-1}; k17 = 0.1 s^{-1}	
References	Diaz and Alvarez-Buylla, 2006; Liu *et al*., 2010	
CK		
V18 Rate of biosynthesis	$\frac{k_{18a}}{1+\frac{[Auxin]}{k_{18}}}$	Only in the cytosol in the central cell files in the MZ and EZ regions, which include the vascular, pericycle/border and central columella cells but exclude the epidermal cell files and external columella files contiguous to the epidermal files.
V19 Rate of decay	$k_{19}[CK]$	In the cytosol and cell walls
Parameters	k18 = 0.1 μM; k18a = 1.0 μM s^{-1}; k19 = 1.0 s^{-1}	
References	Liu *et al*., 2010; Nordstrom *et al*., 2004	

PINm		
V20 Rate of transcription	$\frac{k_{20a}[X][Auxin]}{(k_{20b}+[CK])(k_{20c}+[Auxin])}$	Only in the cytosol
V21 Rate of decay	$k_{21a}[PINm]$	Only in the cytosol
Parameters	k20a = 0.8 μM s^{-1}; k20b = 1.0 μM; k20c = 0.3 μM; k21a = 1.0 s^{-1}	
References	Chandler, 2009; Liu *et al*., 2010; Liu *et al*., 2013; Nordstrom *et al*., 2004; Paciorek *et al*., 2005; Ruzicka *et al*., 2007; Ruzicka *et al*., 2009; Swarup *et al*., 2007; Vanneste and Friml, 2009	
PINp		
V22 Rate of translation	$k_{22a}[PINm]$	Only in the cytosol
V23 Rate of decay	$k_{23a}[PINp]$	In the cytosol and plasma membrane
Parameters	k22a = 1.0 s^{-1}; k23a = 0.75 s^{-1}	
References	Chandler, 2009; Liu *et al*., 2010; Liu *et al*., 2013; Nordstrom *et al*., 2004; Paciorek *et al*., 2005; Ruzicka *et al*., 2007; Ruzicka *et al*., 2009; Swarup *et al*., 2007; Vanneste and Friml, 2009	
AUX1m		
V26 Rate of transcription	$k_{1a}[X]$	Only in the cytosol.
V27 Rate of decay	$k_{26}[Aux1m]$	Only in the cytosol
Parameters	k1a = 0.8 μM s^{-1}; k26=1.0s^{-1}	
References	Ruzicka *et al*., 2007; this work	

AUX1p		
V28 Rate of translation	$k_{27}[Aux1m]$	Only in the cytosol
V29 Rate of decay	$k_{28}[Aux1p]$	In the cytosol and plasma membrane.
Parameters	k27 = 1.0 s^{-1}; k28 = 1.0 s^{-1}	
References	This work	

2.2.5 PIN and AUX1 carrier recycling to the plasma membrane

The basally located PIN proteins in the vascular and pericycle cell files direct auxin from the shoot to the root base where it is redirected laterally by the columella cells and then back up the root by apically located PIN proteins in epidermal cell files, with some auxin being directed back to the vascular cells by laterally placed PIN proteins in the epidermal and border/pericycle cells. This PIN-mediated 'gating' system effectively traps and concentrates auxin within the root tip resulting in a reverse fountain flow which establishes the classic auxin distribution pattern. There are several distinct PIN proteins with different locations in different cell types. In this current model version, these proteins are represented by a generic PIN, regulated by the network, with no distinction between the different types.

Certain PIN proteins show asymmetrical localisation at the plasma membrane of some cell types. While there is also evidence for asymmetrical localisation of AUX1 proteins, in this model it is assumed that AUX1 proteins are located symmetrically in the plasma membranes of all cells, consistent with Grieneisen *et al*. (2007). The recycling of PIN and AUX1 carrier proteins to and from the plasma membrane is represented in this model; however, the actual mechanism of exocytosis and endocytosis and protein transport to and from the membrane is not. The rate of placement of PIN from a cytosolic grid point to a nearest neighbour (NN) plasma membrane GP is dependent on PIN concentration at the cytosolic point and the specific properties of the plasma membrane at that point, as defined in the root map and consistent with Grieneisen *et al*. (2007).

The PIN proteins localise to the plasma membrane at a higher rate for PMs with high permeability (GP code 3), at a medium rate for PMs with medium permeability (GP code 2), and at a lower rate at most other PMs (GP code 1). The PIN protein concentration at the plasma membrane for grid point type 5 (at the root/shoot border in the epidermal cell files where auxin is removed from the root) is high, whereas for GP type 4 at the root/shoot border in the pericycle and vascular cell files (where auxin enters the root) it is 0 (Table 2.4).

The rate of removal of PIN proteins from the plasma membrane is proportional to PIN concentration at the membrane (but is not dependent on the individual properties of the cell face) and is inversely proportional to the concentration of auxin at the NN cytosolic grid point, based on experimental evidence indicating that PIN endocytic internalization is inhibited by auxin (Paciorek *et al*., 2005). In this way auxin promotes its own efflux from a cell by both upregulating *PIN* expression (Table 2.3: V20) and reducing the rate of endocytosis of PIN from the plasma membrane to the cytosol (Table 2.4: V25).

AUX1 moves from a cytosolic GP to the NN plasma membrane GP at a rate proportionate to the concentration of AUX1 at the cytosolic point, and similarly moves from the plasma membrane back to the cytosolic point proportionate to the concentration at the membrane, but at a lower rate (Table 2.4). All cell faces have equal properties regarding the placement and removal of AUX1.

Table 2.4: Rate equations for PIN and AUX1 recycling to and from the plasma membrane

Species	Rate equations and parameter values	Notes
PINp		
V24 Rate of localisation of PINp to the plasma membrane	$k_{24a}(i)[PINpi]$	[PINpi] is the PIN concentration at the cytosolic GP. k24a(i) depends on the property of the NN plasma membrane GP as shown in the parameter values.
V25 Rate of removal of PINp from the plasma membrane	$\frac{k_{25a}[PINpm]}{(1+[Auxin]_0 / k_{25b})}$	[PINpm] is the PIN concentration at the plasma membrane GP. $[Auxin]_0$ is the auxin concentration at the NN cytosolic GP
Parameters	k24a(1)=1.0 s^{-1}; k24a(2) = 5.0 s^{-1}; k24a(3)=20.0 s^{-1}; k24a(4) = 0.0 s^{-1}; k24a(5) = 20.0 s^{-1} K25a = 1.0 s^{-1}; k25b = 1.0 μM	
References	Grieneisen *et al*., 2007; Liu *et al*., 2013; Paciorek *et al*., 2005. This work.	
AUX1p		
V30 Rate of localisation of AUX1p to the plasma membrane	$k_{29}[Aux1pi]$	[AUX1pi] is the AUX1 concentration at a cytosolic GP adjacent to a plasma membrane GP.
V31 Rate of removal of AUX1p from the plasma membrane	$k_{30}[Aux1pm]$	[AUX1pm] is the AUX1 concentration at the plasma membrane GP.
Parameters	k29 = 10.0 s^{-1}; k30 = 1.0 s^{-1}	
References	This work	

2.2.6 Hormonal crosstalk and gene expression network

The equations in Table 2.3 and Table 2.4 contain the hormonal crosstalk and gene expression relationships between the model species, and the regulation of PIN and AUX1 recycling to the plasma membrane. These relationships have been summarised in a crosstalk network (Figure 2.9). For the purposes of clarity PINpi and PINpm have been introduced in the diagram to denote PINp proteins in the cytosol and in the membrane respectively, even though these do not exist as separate species in the model. AUX1pi and AUX1pm are similarly used in the network diagram.

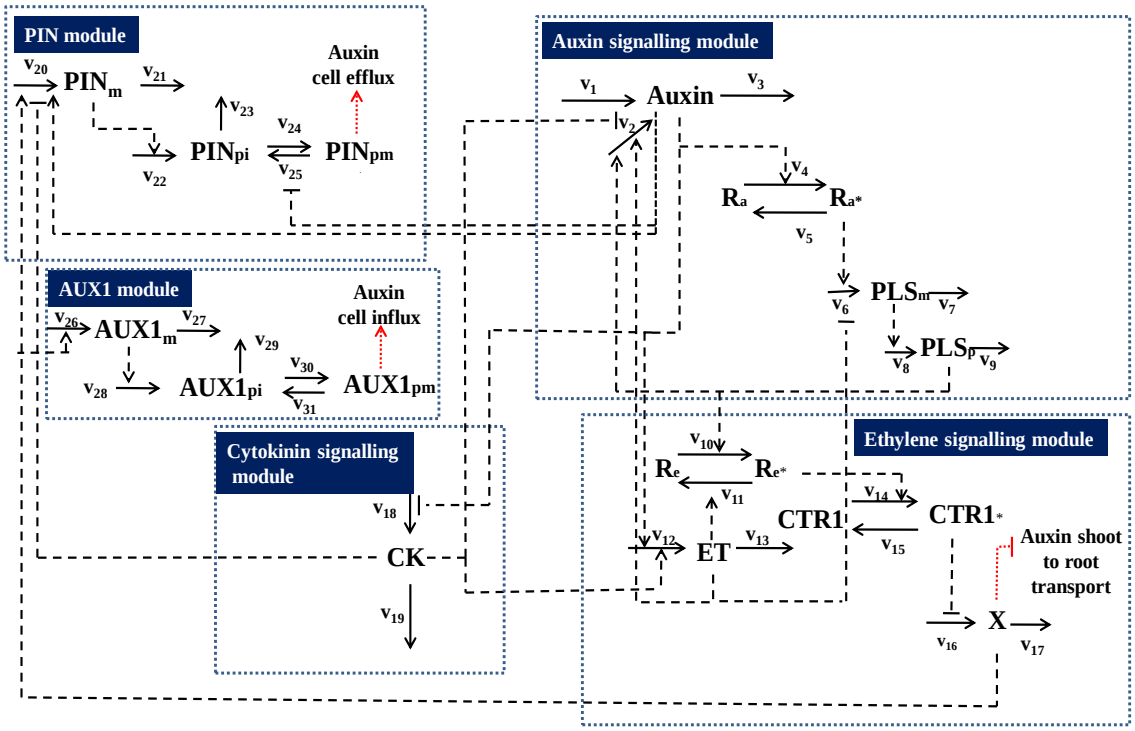

Figure 2.9: Hormonal crosstalk and gene expression network (Liu *et al*., 2013)
for symbols refer to Table 2.2 and for V annotations to equations in Table 2.3 and 2.4
→ mass conversion links; - - · positive and negative regulatory links; ----- auxin transport links

2.2.7 Flux between nearest neighbour (NN) grid points

Species flux between NN grid points depends on the species type and the grid point properties. Since the model does not include structural intracellular resolution and vesicular transport, for modelling purposes flux is assumed to occur by diffusion or permeability, except for the recycling of PIN and AUX1 by exocytosis and endocytosis as discussed separately above. Table 2.5 defines flux equations for each species between each type of grid point.

Table 2.5: Species flux
(between nearest neighbour (NN) grid points A to B)

Species	A → B		Flux equation	Notes
Auxin diffusion	0	0	$Auxindiff\ (cell)\ ([Auxin]_A - [Auxin]_B)/\Delta x$	Diffusion in the cytosol
	1 or 2 or 3	1 or 2 or 3	$Auxindiff\ (wall)\ ([Auxin]_A - [Auxin]_B)/\Delta x$	Diffusion in the cell wall
	4 or 5	Any	No diffusion from GP 4 and 5	Border to cytosol
	any	4 or 5	No diffusion to GP 4 and 5	Cytosol to border
Parameters			Auxindiff(cell) = 220 $\mu m^2\ s^{-1}$ Auxindiff(wall) = 220 $\mu m^2\ s^{-1}$; Δx = 2.0μm	
References			Kramer *et al*., 2011; Rutschow *et al*., 2011; This work.	
Auxin efflux by permeability	0	1,2 or 3	$\frac{1}{\Delta x}\, p(A,B)\, \frac{k_{3b}[PINp]_B[Auxin]_A}{k_{3a} + [Auxin]_A beta}$	Efflux from the cell p(A,B) = 1
	0	4	Above equation but zero flux	p(A,B) = 0
	0	5	Above equation and flux occurs	Efflux from the root to the shoot. p(A,B) = 1
Parameters			p(A,B) is a switch determining if permeability can occur from A to B and is = 0 or 1 Δx = 2.0μm (scaling constant); k3a = 1.0μM; k3b = 0.8 $\mu m^2\ s^{-1}$; beta = 0	Optional Michaelis Menten kinetics depending on the value of beta
References			Kramer *et al*., 2011; This work	
Auxin influx by permeability	1,2 or 3	0	$\frac{1}{\Delta x}\, p(A,B)\, \frac{k_{31}[AUX1p]_A[Auxin]_A}{k_{31a} + [Auxin]_A k_{31b}}$	Influx into the cell p(A,B) = 1
	4	0	$\frac{1}{\Delta x}\, p(A,B)\, \frac{k_{32a}[Auxin]_A}{1 + [X]_B / k_{32b}}$	Influx, shoot to root p(A,B) = 1
	5	0	Same equation as '4 to 0' but zero flux since p(A,B) = 0	Influx, shoot to root. p(A,B) = 0
Parameters			p(A,B) is a switch determining if permeability can occur from A to B and is = 0 or 1 Δx = 2.0μm (scaling constant);	Optional Michaelis Menten kinetics depending on

			k31 = 2.0 $\mu m^2 s^{-1}$; k31a = 1.0μM; k31b = 0; k32a = 10 $\mu m^2 s^{-1}$; k32b = 0.1μM	the value of k31b
References			Chilley *et al*., 2006; Kramer, 2004; Rutschow *et al*., 2014; Suttle, 1988. This work.	
ET diffusion	0, 1, 2, 3, 4 or 5	0, 1, 2, 3, 4 or 5	$ETdiff\ ([ET]_A - [ET]_B)/\Delta x$	ET diffuses between all GPs of the same or different types whether in the cytosol or cell wall with the same diffusion coefficient
Parameters			ETdiff = 600 $\mu m^2 s^{-1}$; Δx = 2.0μm	
References			This work	
CK diffusion	0, 1, 2, 3, 4 or 5	0, 1, 2, 3, 4 or 5	$CKdiff\ ([CK]_A - [CK]_B)/\Delta x$	CK diffuses between all GPs of the same or different types whether in the cytosol or cell wall with the same diffusion coefficient
Parameters			CKdiff = 220 $\mu m^2 s^{-1}$; Δx = 2.0μm	
References			Mellor and Bishopp, 2014. This work	
All other species diffusion	0	0	$Otherdiff\ ([Other]_A - [Other]_B)/\Delta x$	Diffuse within the cytosol only and do not cross the PM and enter the cell wall (for PINp and AUX1p recycling see Table 2.4)
Parameters			Otherdiff = 220 $\mu m^2 s^{-1}$; Δx = 2.0μm	
References			This work	

2.2.8 Root/shoot boundary conditions

From the above equations ET and CK can diffuse in both directions between the cytosol of the proximal cells and the shoot-root boundary cell walls, denoted by grid points 4 proximal to the pericycle and vascular cell files and 5 proximal to the epidermal cell files (Figure 2.5).

At the shoot–root boundary, following previous work (Grieneisen *et al*., 2007), auxin influx from shoot to root occurs only in the pericycle and vascular cell files, from the cell wall grid point 4 into the cytosol (0) of the proximal pericycle and vascular cells, mediated by downstream ethylene signalling, designated X in the model. Auxin efflux in the opposite direction from the root vascular and pericycle cells to the shoot, mediated by PIN proteins, cannot occur. Auxin influx into the root is inhibited by downstream ethylene signalling X, based on experimental evidence which indicates that a relatively high ethylene signalling response inhibits the transport of auxin from the shoot to the root tip (Suttle, 1988; Chilley *et al*., 2006).

Auxin efflux from the root towards the shoot, from the cytosol (0) into the shoot-root border cell wall (5), occurs only in the epidermal cells and is facilitated by PIN proteins. Auxin influx from the shoot to the root epidermal cells, mediated by AUX1 proteins, cannot occur.

The hormone concentrations in the shoot-root border cell wall grid points are set at constants. Auxin concentration is set at a high level in the grid points 4 to encourage shoot to root flux while the auxin concentration in grid points 5 is set to zero to model auxin flux out of the root to the shoot from the border epidermal cells. The concentrations of ET and CK in the border cell wall grid points 4 and 5 are set such that there is a smooth transition of concentration levels from the root to the shoot. The actual border concentration settings are discussed in section 2.5.6 on calibration.

2.3 Running the model and simulation to steady state

The model is both ‘spatial’ and ‘temporal’ since is represents a 2-D multicellular root and simulates changes in hormone concentrations and gene expression over time. At time zero all concentrations within the root are set to 0 (except the

fixed concentrations at the root/shoot border). As time progresses, the concentration levels at each grid point change due to biosynthesis, decay and flux to and from NN grid points, regulated by the hormonal crosstalk and gene expression relationships and the parameter settings. Time is advanced and new concentrations calculated for each species at each grid point using an iterative process called the Conjugative Gradient Method. This process is repeated with time steps of 100 secs until a steady state is reached when there is minimal change in any species concentration between time steps. All simulations were run for 20,000 secs by which time the steady state had been reached.

2.4 Capturing data from experimental images using ImageJ

For both initial parameter calibration and performing in-silico experiments, it is important to be able to compare model predictions with experimental results; however, many experimental results are in the form of fluorescent imaging rather than quantified measurements. Using ImageJ (http://imagej.nih.gov/ij) it is possible to measure and capture relative data from experimental images. The output of ImageJ is the intensity of each pixel in an experimental image. The relative intensity over the image shows the relative hormone response or protein concentration patterning across the whole (or selected part) of the image and this can be used, for example, to create relative response or concentration gradients along the longitudinal axis of the root tip which can then be compared to gradients predicted by the model.

In particular, using the features of ImageJ, it is possible to define regions on an image, such as the vascular cell cylinder, and measure, say, relative concentration profiles along the selected region. Regions were defined by a series of consecutive rectangles which progressively diminished in size towards the distal end of the root tip. Data were collected from each rectangle and concatenated to give a relative concentration profile for the selected cell files derived from an original experimental image. For example, in Figure 2.10, the epidermal and vascular cell files have been defined by rectangles and the relative WT PIN2 concentration profiles for each cell file extracted using ImageJ and then plotted in MATLAB®. This method gives a greater number of data points compared with sampling at intervals, as can be seen from the PIN2 plot

for the epidermal cells (Figure 2.10) which demonstrates the high concentration of PIN2 at the plasma membranes.

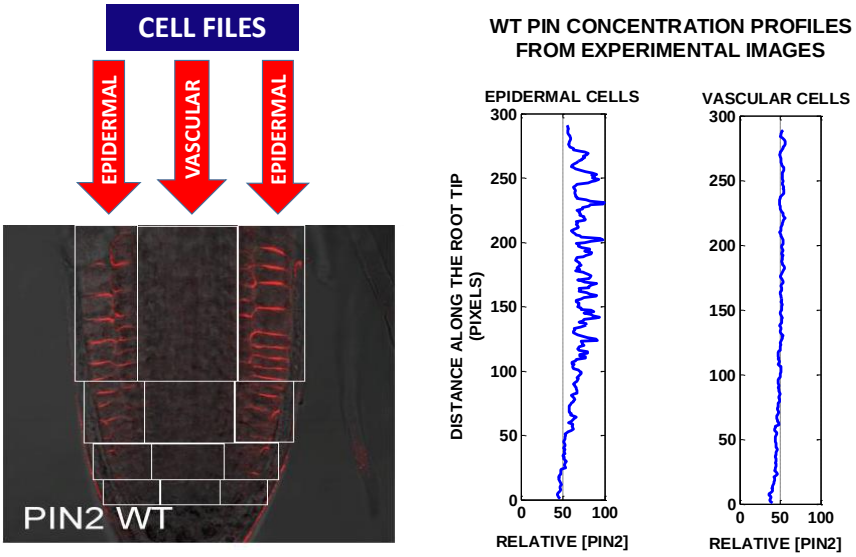

Figure 2.10: PIN2 profiles for epidermal and vascular cells using ImageJ
Using rectangles to define the vascular and epidermal cell files, data for relative PIN2 concentration are extracted from an experimental image (Liu *et al*., 2013) using ImageJ, and longitudinal concentration profiles plotted using MATLAB®

2.5 Definition and calibration of the WT model parameter set

While the modelling equations must be structured in specific forms to describe the kinetics of the processes detailed in Figure 2.9, many different parameter sets can be fitted against the experimental data since the number of parameters exceeds the number of experimental observations. By examining parameters randomly, when a parameter is changed and at least one or more other parameters are allowed to change, then it is possible to find a new set of parameters that meet the criteria for model fitting and also make correct predictions.

2.5.1 Diffusion and permeability constants

Initially the diffusion coefficients for all species were set at 600 μm^2 sec^{-1}, matching the setting for auxin diffusion in Grieneisen *et al*. (2007). The coefficient for auxin was reset to 220 μm^2 sec^{-1} to be consistent with later estimates (Rutschow *et al*., 2014). The molecular weight of CK is approximately

the same as auxin so the diffusion rate of CK was also set at 220 μm^2 sec^{-1}. The diffusion coefficient of ET was left unchanged at the higher value of 600 μm^2 sec^{-1} since ET is a gas. The diffusion coefficients for all other species in the cytosol were also set at 220 μm^2 sec^{-1} in the absence of additional data.

A recent review of published auxin transfer speeds showed a wide range from 0.33 to 5 μm sec^{-1} and mathematical modelling confirmed that PIN efflux permeability rates are comparable with this transfer speed (Kramer *et al*., 2011). The constants for PIN permeability (k3a and k3b) were therefore set to give PIN permeability of 0.9 μm sec^{-1}, based on average PIN concentrations in the plasma membranes, which is well within the required range. It has been suggested that AUX1 influx permeability must be equal to or greater than PIN efflux permeability otherwise cells would be depleted of auxin (Kramer, 2004). Therefore the constants controlling AUX1 permeability (k31, k31a) were adjusted to give an average AUX1 permeability of 3.5 μm sec^{-1}, which is greater than the average PIN permeability.

2.5.2 Average auxin concentration and trends in WT and mutants

Experimental results (Chilley *et al*., 2006) show auxin content in fresh weight (FW) root samples. These were used to calculate values for WT average auxin concentration ranging from 0.23 to 2.3 μM (for water content of 100% or 10% in the FW root samples). The background and variable auxin biosynthesis parameters (k2, k2a) were adjusted to give an average auxin content in the model WT root tip of approximately 0.8 μM which falls within the required range.

Further adjustments were made to parameters for auxin decay (k3), auxin transport from the shoot to root (k32a, k32b), the rate of *PLS* expression (k6), and the rate of ETR1 (or Re*) deactivation (k11) in the ethylene pathway, such that the average auxin root concentrations in WT, *pls,* the *pls etr1* double mutant and the PLSox transgenic matched the trend of changes in experimental concentrations (Chilley *et al*., 2006). The null mutant *pls* was modelled by setting the *PLS* expression parameter k6 = 0. The *etr1-1* mutant (an ethylene insensitive gain-of-function mutant, with high activation, low downstream ethylene signalling and low ethylene response) was only a partial knockout

(induced by drug treatment or Ag application) and was modelled by reducing the parameter (k11) controlling the rate of inactivation of Re* (active ETR1) from the WT value of 4.0 to the *etr1* partial knockout value of 0.025 μM^{-1} sec^{-1}. In the *etr1* partial knockout the level of active ETR1 is increased such that the model is insensitive to ET, resulting in decreased downstream ethylene signalling and increased shoot to root auxin influx.

Figure 2.11 shows the experimental trend in auxin concentrations in WT, mutants and the PLSox transgenic for whole seedlings (Chilley *et al*., 2006). *pls* shows a large decrease in auxin compared to WT, the *pls etr1* double mutant a near recovery to WT levels, and PLSox exceeds WT auxin concentration. Figure 2.12 gives the model results, with *pls* having a similar significant reduction in average auxin concentration, *pls etr1* a slight recovery (but not as significant as in the experimental results) and PLSox an increase over WT similar to experimental results. While the magnitude of auxin changes between the mutants in the model does not exactly match those from experiments, the trends are similar.

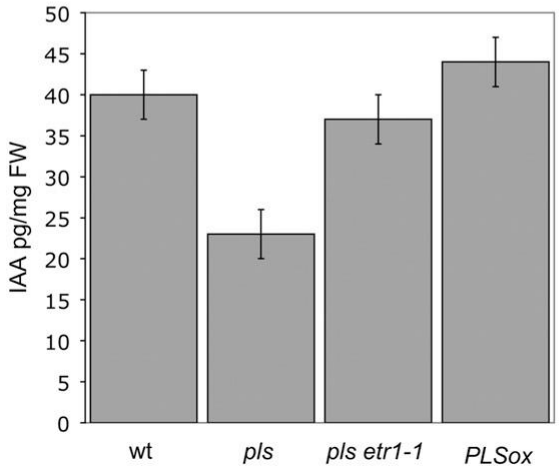

Figure 2.11: Relative auxin concentrations in 10 DAG whole seedlings
Comparison of auxin content in wild-type, *pls and pls etr1-1* mutants, and the PLSox overexpressor in 10 DAG whole seedlings (Chilley *et al*., 2006)

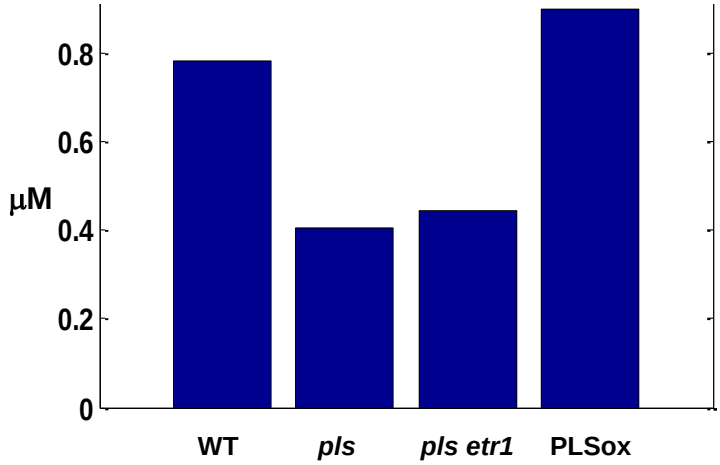

Figure 2.12: Model average auxin concentrations
Comparison of model average auxin concentrations in wild-type, *pls and pls etr1* mutants, and the PLSox overexpressor, showing similar qualitative trends to experimental results in Figure 2.11

2.5.3 Auxin response images, concentration colour maps and profiles

Auxin response has a canonical pattern in the *Arabidopsis* WT root with an auxin response maximum established in the QC region. As part of the calibration process, model auxin concentration colour maps were compared to experimental images. The images were scanned with ImageJ and the data converted into response gradients along the longitudinal axis of the root and compared to concentration profiles from the model. The auxin image (Grieneisen *et al*., 2007) and the ImageJ auxin response profile derived from the image were compared to a concentration colour map and profile from the WT model (Figure 2.13).

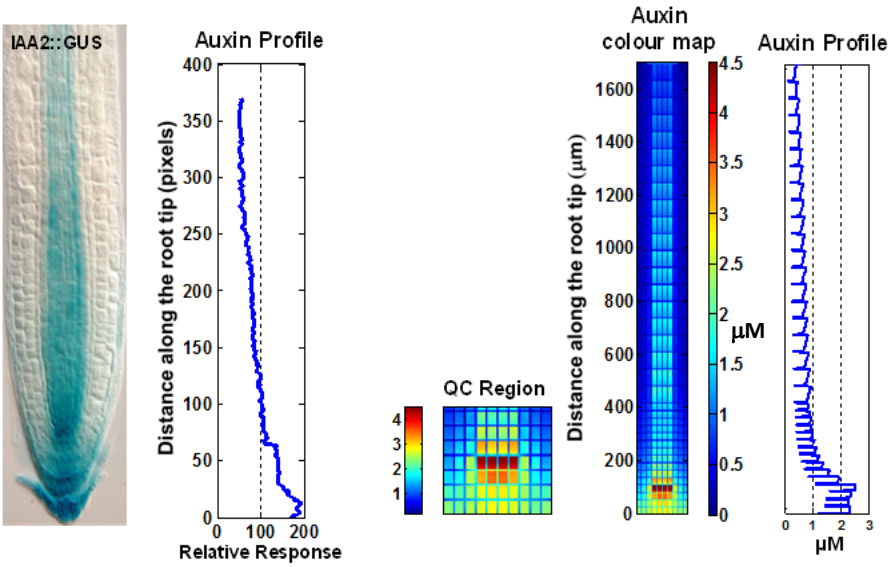

WT auxin image (Grieneisen *et al*., 2007) and the relative response profile.

WT auxin colour map and concentration profile from the model

Figure 2.13: Auxin experimental and model results

The experimental image and model demonstrate similar patterning with an auxin maximum in the QC region and similar trends for the response and concentration profiles (QC, quiescent centre)

2.5.4 PIN and AUX1 predominantly locate to the plasma membrane

The WT images of the PIN1, PIN2 and PIN3 members of the PIN family of auxin carriers clearly show that PIN proteins locate predominantly to the plasma membranes in vascular and root cap cells, the epidermal and cortical cells, and the EZ vascular and columella cells respectively (Figure 2.14). Similarly the AUX1 and LAX2 auxin influx carriers mainly localise to the plasma membrane (Figure 2.15).

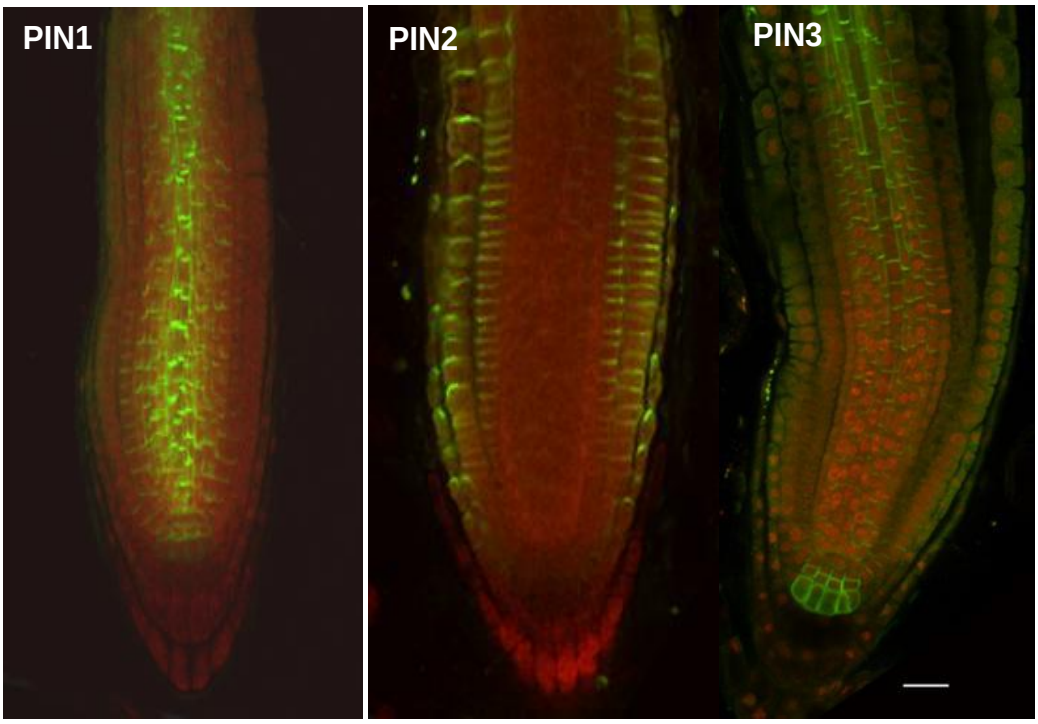

Figure 2.14: Localisation of PIN1, PIN2, PIN3 to the plasma membrane
(Band *et al*., 2014)

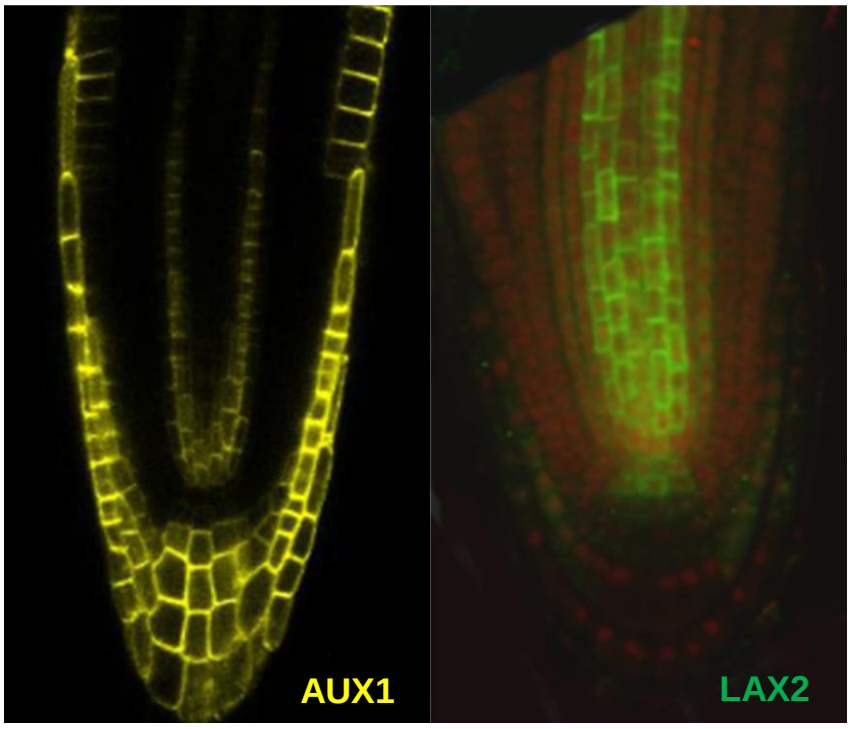

Figure 2.15: Localisation of AUX1 and LAX2 to the plasma membrane
(Band *et al*., 2014)

The localisation of the auxin carrier proteins to the plasma membrane is critical to enable them to function in auxin influx and efflux and therefore the model should exhibit predominant localisation of the carrier proteins to the plasma membrane. Figure 2.16 shows the WT model concentration profiles for PINp and AUX1p with a much higher concentration of these proteins in the plasma membrane than the cytosol. This is also clearly exhibited in the enlarged QC concentration colour maps for these proteins.

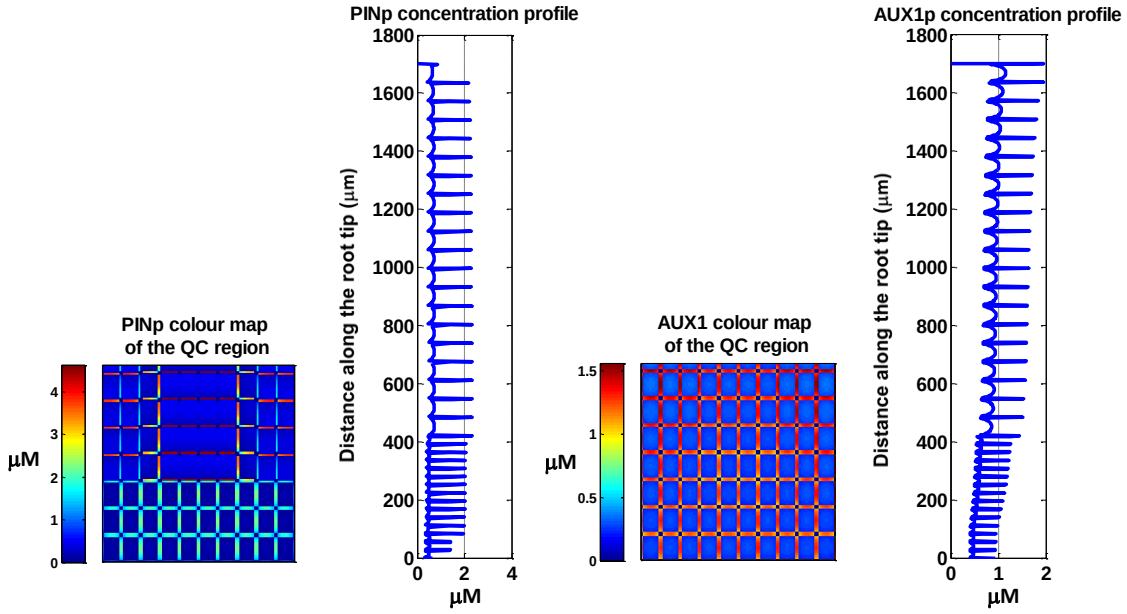

Figure 2.16: PIN and AUX1 localisation to the plasma membrane
The model colour maps of the QC region and peaks at the plasma membrane positions in the concentration profiles indicate auxin carrier localisation to the plasma membrane

2.5.5 CK concentration patterning and profile

Cytokinin biosynthesis in the root is possibly tissue-specific and occurs predominantly in the columella cells, the endodermis of the root elongation zone, xylem precursor files and phloem tissues (Miyawaki *et al*., 2004), as supported by cytokinin response reporter ARR5::GUS imaging (Figure 2.17a). Since CK biosynthesis in the epidermal and cortical cell files appeared to produce a very low CK signal compared to the central cells in this image, CK spatial distribution was tested in two versions of the model, (1) with CK

biosynthesis in all cells and (2) with biosynthesis restricted to the pericycle/border and vascular cell files and the central columella files. The CK experimental image and the CK response profile derived from the image (using ImageJ) were then compared to the CK concentration colour map and profile generated by each version of the model (Figure 2.17).

When CK biosynthesis occurred in all cells, CK patterning in the experimental image differed from the model colour map. However, when CK biosynthesis was restricted to the central cell files, there was a qualitative similarity between lateral patterning in the observed image and the model colour map. The pattern across the root was similar, with apparent maxima occurring in approximately the pericycle/border cell files in both the model colour map and the experimental observation. This initial modelling analysis therefore suggests that CK biosynthesis could be predominantly restricted to the central cell files, although the molecular basis for this is unknown.

The image response profile, showing the CK response gradient along the root axis, did not match the profiles from either model version. Experimental results indicate that CK concentrations decrease proximally along the root axis which is opposite to the gradient exhibited in both versions of the model (Figure 2.17). As demonstrated later, in section 2.6.7 on model robustness to parameter variability, the overall results do not appear to be very sensitive to variations in CK concentration; therefore it was felt that this discrepancy between model and experimental results would not detract significantly from other model results.

The difference in longitudinal cytokinin patterning suggests that additional unknown regulatory factors could influence patterning along the root axis, as investigated later in Chapter 5. However, in this version of the model, cytokinin biosynthesis occurs only in the vascular and pericycle cells and the central columella cell files.

Experimental data (Liu *et al*., 2010) gives the content of different types of cytokinin in 10 days after germination (DAG) WT and *pls* whole seedlings. Using the average WT cytokinin content, the CK seedling concentration was estimated at 0.04 μM (assuming 75% of fresh weight was fluid) which is

consistent with model results where CK biosynthesis is restricted to the vascular and pericycle cell files (Figure 2.17c).

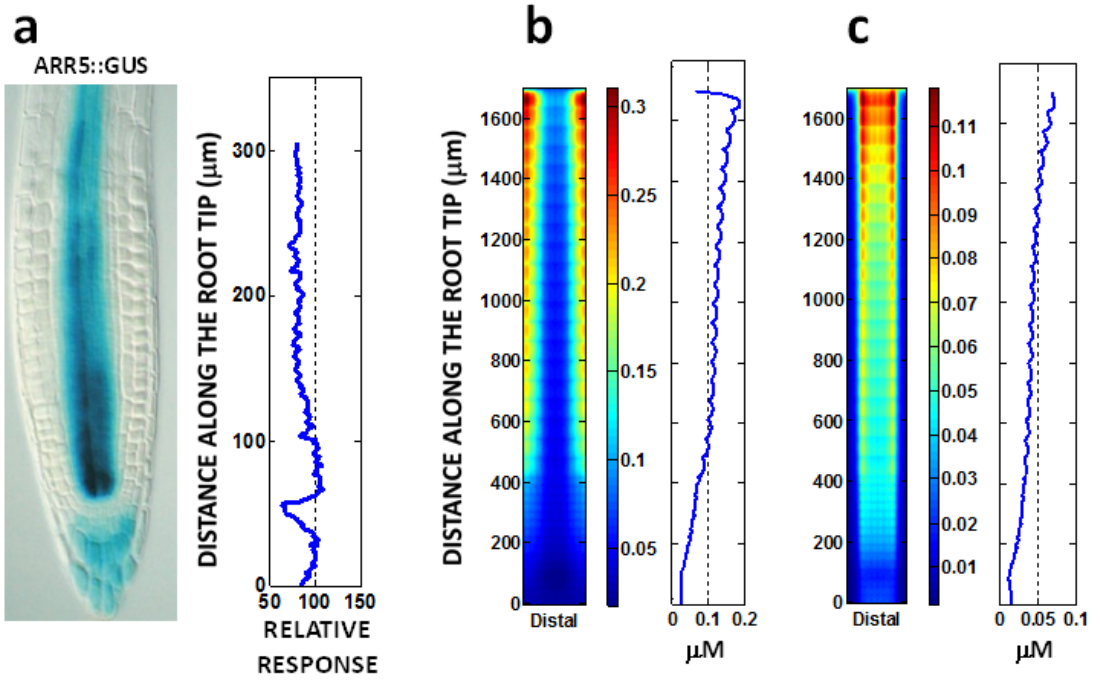

Figure 2.17: CK experimental and model patterning results
(a) CK experimental image (Werner *et al*., 2003) and relative response profile
(b) Model CK concentration image and profile with CK biosynthesis in all cells
(c) Model CK concentration image and profile with CK biosynthesis in pericycle and vascular cells and the central columella cell files. (c) shows similarities in lateral patterning to the experimental image; however profile gradients from both models show a proximally increasing CK gradient while the experimental response gradient shows a proximally decreasing trend (colour bar units μM).

2.5.6 Border hormone concentrations

Hormone concentrations at the root/shoot border were set to give a smooth transition from concentrations in the proximal root cells to the border. ET border concentrations in grid points 4 and 5 were set at a constant 0.1 μM. Auxin was set at a constant 1.0 μM in grid points 4 at the border of the pericycle and vascular cells, which is slightly higher than the average root concentration of approximately 0.8 μM (representing influx from the shoot), and was set at 0.0 μM at grid points 5 at the border of the epidermal cells where there was auxin efflux from the root to the shoot. CK concentrations were set at 0.07 μM in all border grid points 4 and 5.

2.5.7 Summary results for the WT parameter settings

The process for setting the WT parameters described above, started by using the original parameter values in the reference papers (Grieneisen *et al*., 2007; Liu *et al*., 2010), with adjustments based on parameter values from the literature. Additional calibration adjustments were derived by comparing model outcomes to the experimental results for WT average auxin concentration, auxin concentration trends in WT and mutants, WT auxin images and concentration profiles, auxin carrier protein concentrations at the plasma membrane, and WT CK profiles and concentrations. Figure 2.18 summarizes model results for the preferred WT parameter set, showing the concentration colour maps and profiles for Auxin, ET and CK, and charts comparing the average auxin and PIN protein concentrations for WT, *pls, etr1, pls etr1* mutants and the PLSox transgenic.

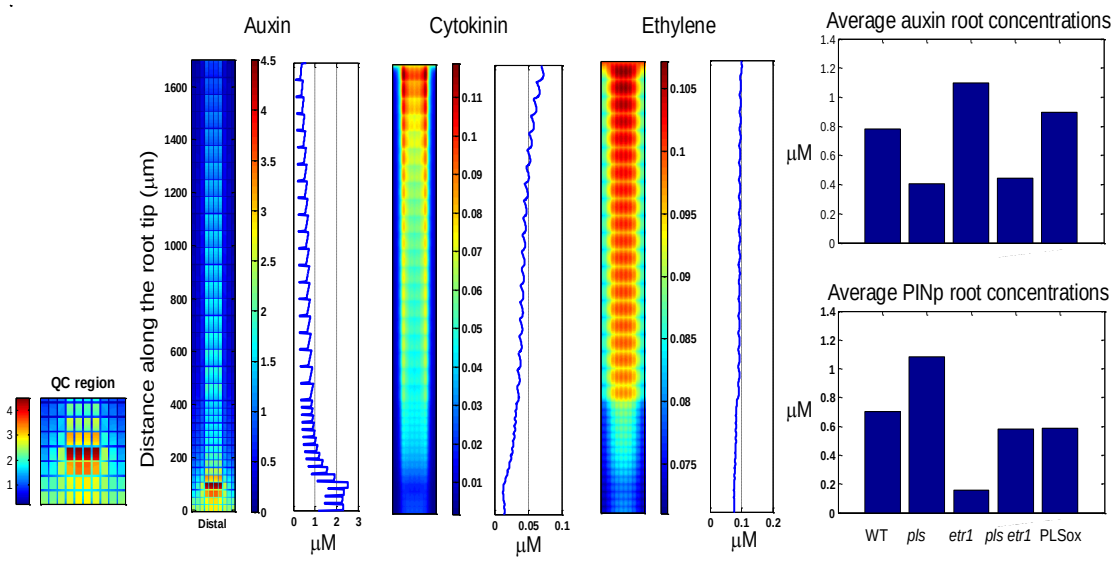

Figure 2.18: Summary WT model results

Auxin, cytokinin and ethylene colour maps and concentration profiles, and WT and mutant average root concentrations for auxin and PIN protein (colour bar units μM)

2.6 Model robustness to variation in parameter values

Most parameter values are unknown and are very difficult to confirm experimentally; it is therefore important that the model is not overly sensitive to small changes in parameter values otherwise model results would depend on specific parameter values that could not be verified. While the sensitivity of the

model was not tested for all parameter values, a variety of tests were performed.

2.6.1 Auxin diffusion rates

The auxin diffusion constants for the cytosol and cell wall were varied from 1 to 1000 μm^2 sec^{-1} and the auxin concentration profiles and average root auxin concentrations compared to the WT parameter setting of 220 μm^2 sec^{-1}. At a very low diffusion constant of 1 μm^2 sec^{-1}, no auxin maximum was observed in the QC. The auxin maximum was well established in the QC region for diffusion constants from 50 to 400 μm^2 sec^{-1} with some minor reduction at the higher values. Thereafter the maximum continued to decrease as the diffusion constant increased to 1000 μm^2 sec^{-1} (Figure 2.19). At the very low diffusion constant of 1 μm^2 sec^{-1}, the average auxin concentration was approximately 0.86 μM. With the constant equal to 50 μm^2 sec^{-1}, the average concentration decreased to approximately 0.79 μM and did not vary significantly for higher auxin diffusion constants between 50 and 1000 μm^2 sec^{-1} (Figure 2.20). From these results the model appears to be relatively insensitive to variations in the auxin diffusion constant from the WT parameter setting (220 μm^2 sec^{-1}).

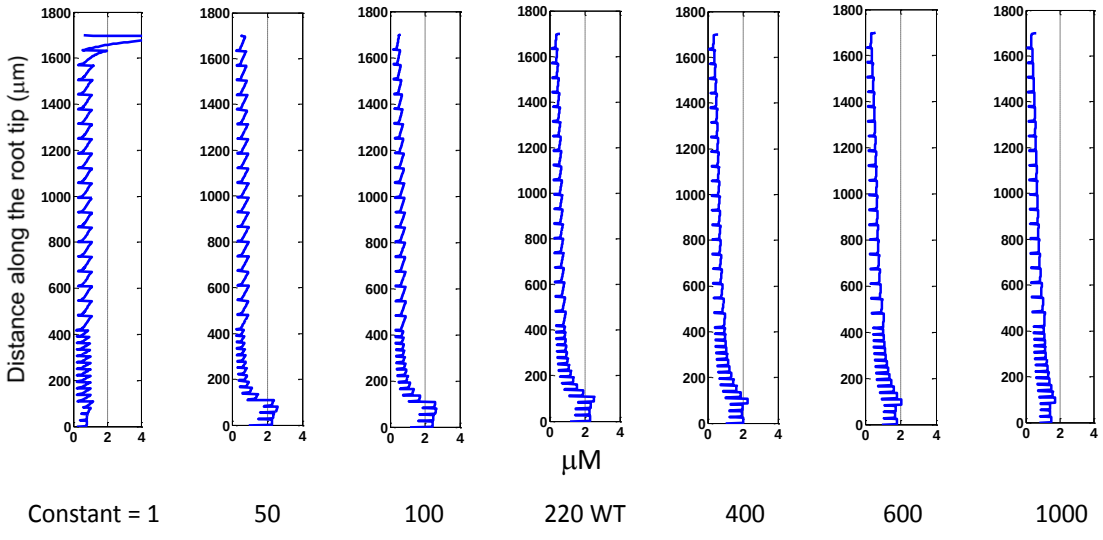

Figure 2.19: Auxin concentration profiles for varied auxin diffusion
The auxin maximum at the QC does not emerge at very low rates and starts to decrease at higher diffusion rates (diffusion constant varies from 1 to 1000 $\mu m^2 sec^{-1}$, WT = 220 $\mu m^2 sec^{-1}$)

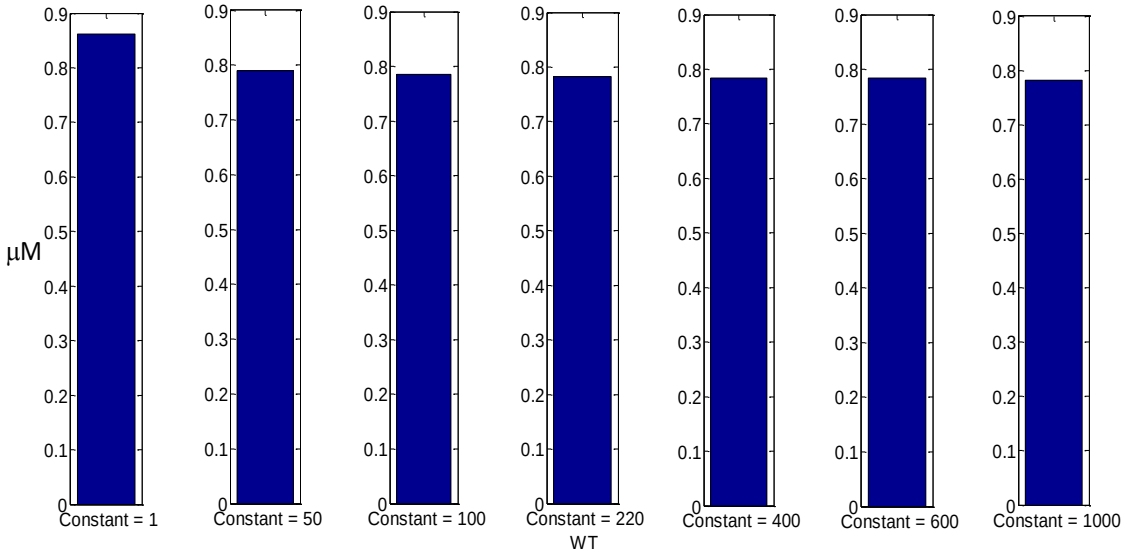

Figure 2.20: Average auxin concentration for varied auxin diffusion
The average auxin concentration is higher than WT at very low diffusion rates but remains fairly constant over a wide range of rates around WT (diffusion constant from 1 to 1000 $\mu m^2 sec^{-1}$, WT = 220 $\mu m^2 sec^{-1}$)

2.6.2 CK diffusion rates

CK diffusion rates in the cytosol and cell wall were varied between 1 and 600 μm^2 sec^{-1} and the results compared to the WT value of 220 μm^2 sec^{-1}. There was minimal apparent difference in either the auxin concentration profile or the root average auxin concentration over this range of CK diffusion constants (Figure 2.21, Figure 2.22). These apparently identical results were tested further and it was found that at extremes of CK diffusion rates there was a change in the CK concentration colour image and average root concentrations in auxin, ET and CK.

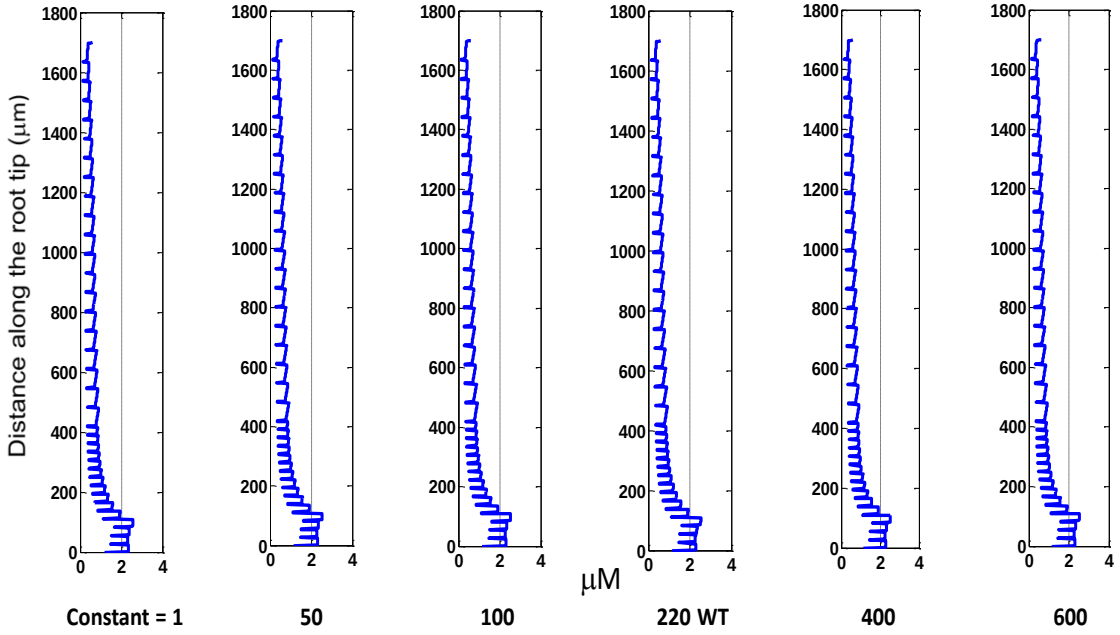

Figure 2.21: Auxin concentration profiles for varied CK diffusion
There was minimal change in the auxin concentration profiles over this range of CK diffusion constants (diffusion constant from 1 to 600 $\mu m^2 sec^{-1}$; WT = 220$\mu m^2 sec^{-1}$)

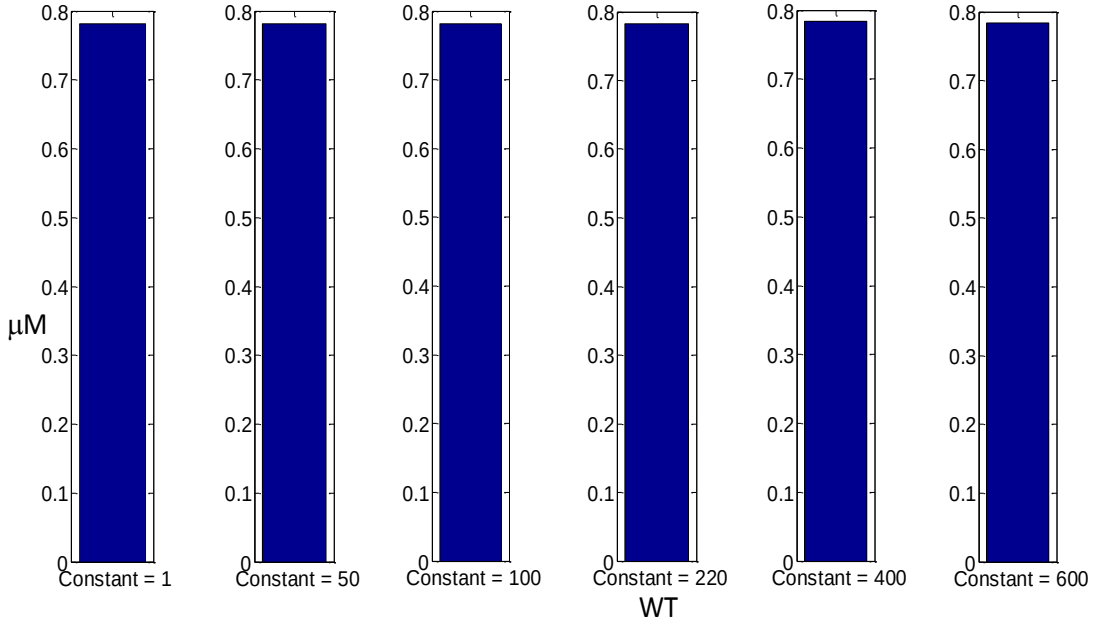

Figure 2.22: Average auxin concentration for varied CK diffusion
There was minimal change in the average auxin concentration over this range of CK diffusion constants (diffusion constant from 1 to 600 μm^2 sec^{-1}; WT = 220 μm^2 sec^{-1})

2.6.3 ET diffusion rates

The constants for ET diffusion within the cytosol and cell wall were varied from 1 to 1000 μm^2 sec^{-1} compared to the WT value of 600 μm^2 sec^{-1}. There was minimal change in either the auxin concentration profile or the average root auxin concentration for values between 100 and 1000 μm^2 sec^{-1} (Figure 2.23, Figure 2.24) indicating that the model is relatively insensitive to the rates of ET diffusion.

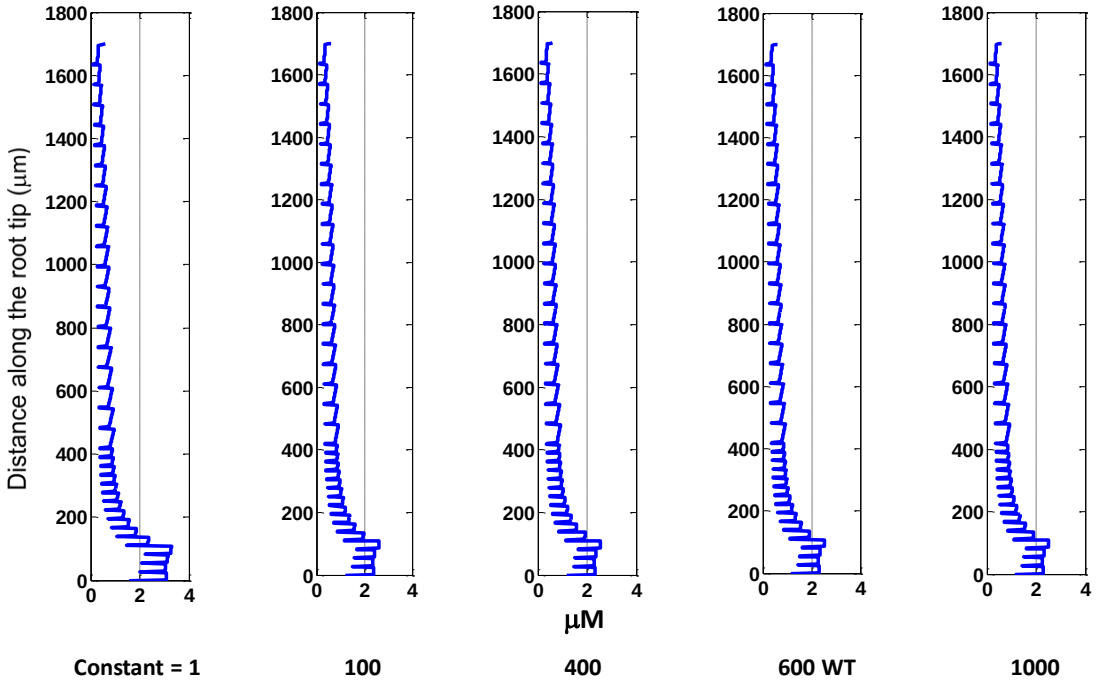

Figure 2.23: Auxin concentration profiles for varied ET diffusion
At very low ET diffusion rates there is an increase in the auxin maximum at the QC, but over the remainder of the range the maximum remained relatively constant (diffusion constant from 1 to 1000 $\mu m^2 sec^{-1}$, WT = 600 $\mu m^2 sec^{-1}$)

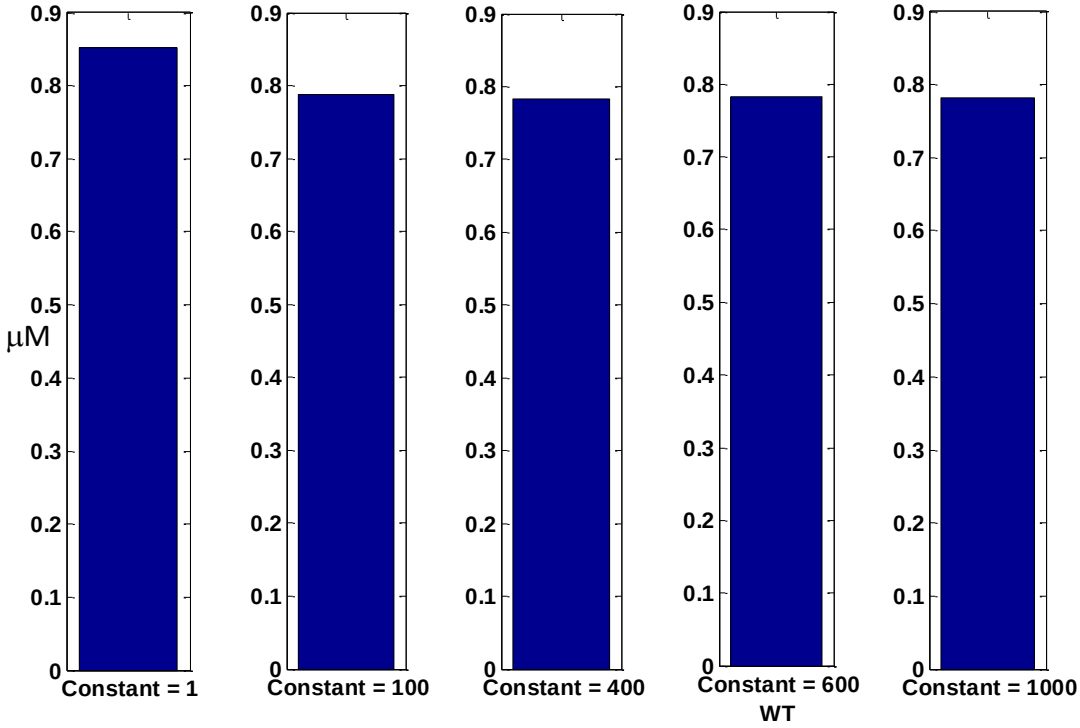

Figure 2.24: Average auxin concentration for varied ET diffusion
At very low diffusion rates there is an increase in average auxin concentration, but over the remainder of the range the average remained relatively constant (diffusion constant from 1 to 1000 $\mu m^2 sec^{-1}$, WT = 600 $\mu m^2 sec^{-1}$)

2.6.4 PIN protein diffusion rates

PIN protein diffusion rates in the cytosol were varied from 1 to 600 μm^2 sec^{-1}, compared to WT of 220 μm^2 sec^{-1}. At effectively zero diffusion (1 μm^2 sec^{-1}) the auxin maximum was not established, while at 50 μm^2 sec^{-1} a weak maximum started to emerge in the QC region. From 100 to 600 μm^2 sec^{-1} the QC maximum progressively strengthened (Figure 2.25). This result is confirmed by the auxin concentration colour maps for each diffusion rate (Figure 2.26) which show weaker maxima at the lower rates of diffusion, with a gradual strengthening in the maxima as diffusion rates increase. Although this indicates a progressive accumulation of auxin at the QC maximum, the average auxin concentration in the root tip decreases gradually (Figure 2.27) as the diffusion rates increase, indicating a reallocation of auxin from the proximal parts of the root to the distal root tip. As diffusion rates increased the concentration of PIN proteins at the plasma membrane also increased (Figure 2.28). An enlarged PIN protein profile (Figure 2.29) shows the PIN protein concentration in the

cytosol and plasma membrane in greater detail. At very low diffusion rates (1 μm^2 sec^{-1}) the concentration of PIN protein in the cytosol was greater than in the plasma membrane. As the diffusion rate increased, this balance was reversed with an increasing ratio of PIN protein at the plasma membrane compared to the cytosol.

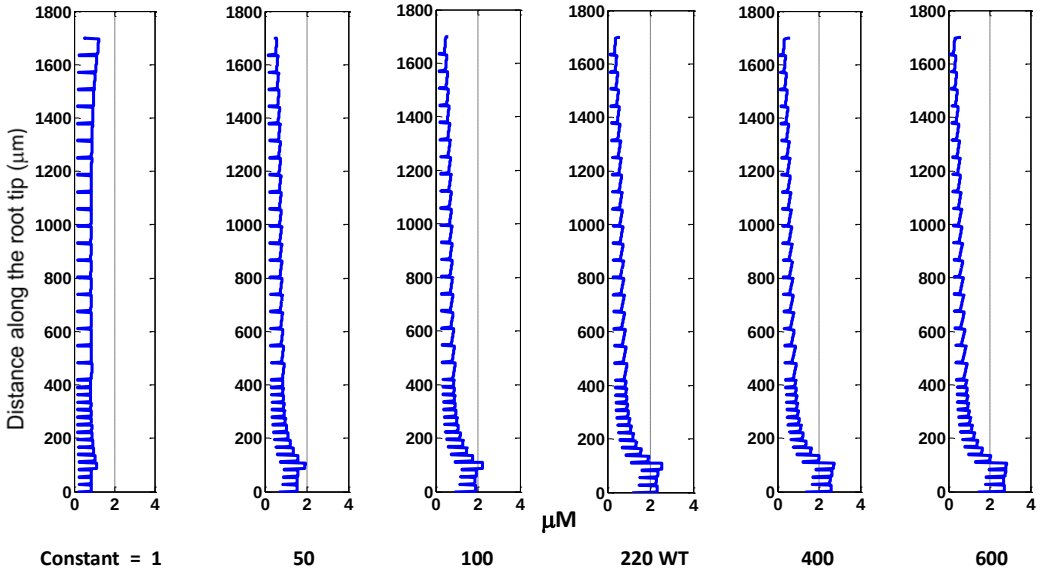

Figure 2.25: Auxin profile for varied PIN protein diffusion

At very low diffusion rates the auxin maximum at the QC was very weak, but progressively strengthened as diffusion rates increased (diffusion constant from 1 to 600 μm^2 sec^{-1}, WT = 220 μm^2 sec^{-1})

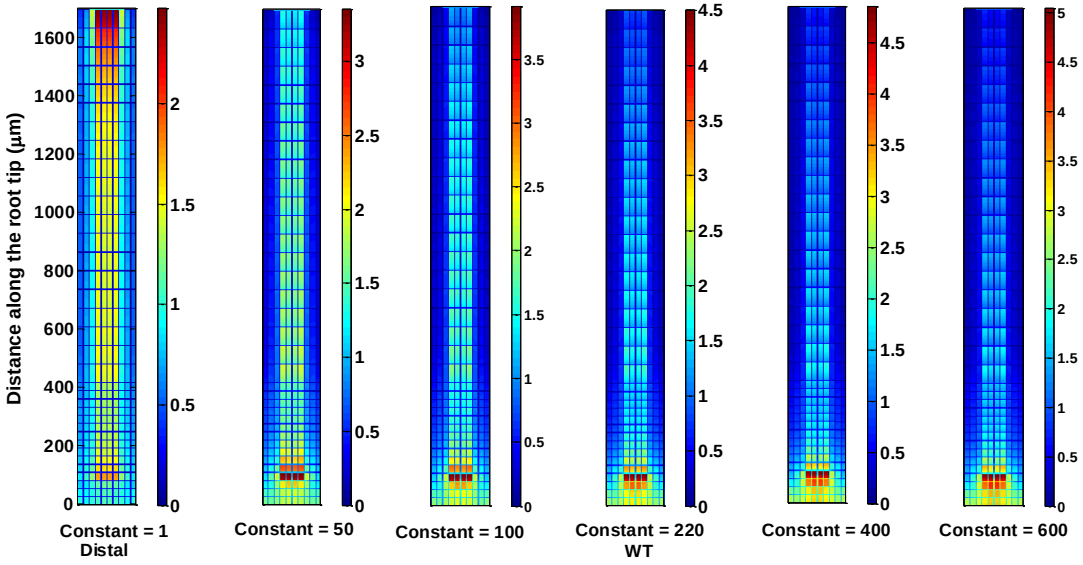

Figure 2.26: Auxin concentration maps for varied PIN diffusion

At very low diffusion rates the auxin maximum at the QC was very weak but progressively strengthened as diffusion rates increased (diffusion constant from 1 to 600 μm^2 sec^{-1}, WT=220 μm^2 sec^{-1}, colour bar units μM)

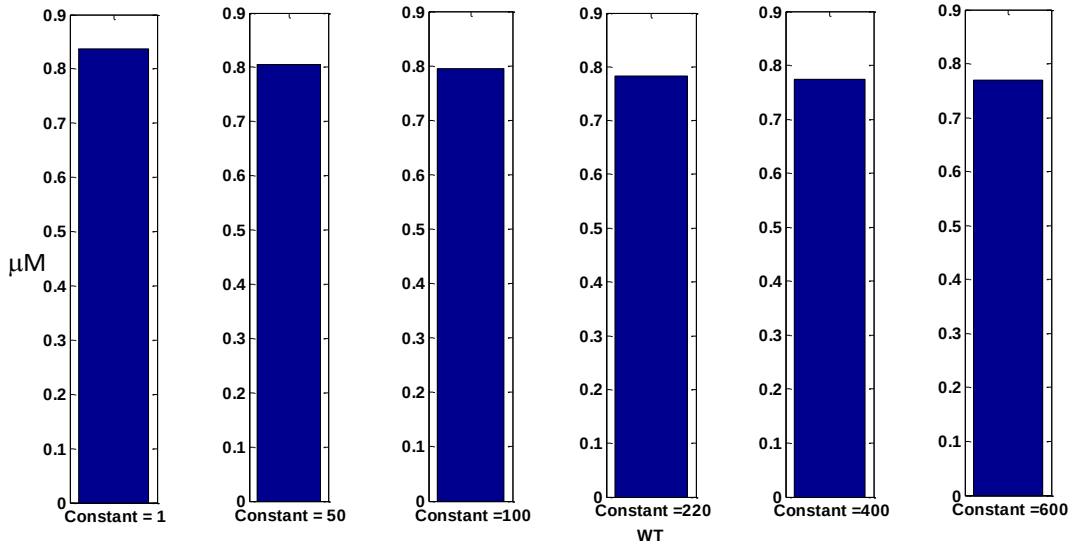

Figure 2.27: Average auxin concentration for varied PINp diffusion
Average root auxin concentration decreases as the diffusion rate increases (diffusion rate from 1 to 600 $\mu m^2 sec^{-1}$, WT = 220 $\mu m^2 sec^{-1}$)

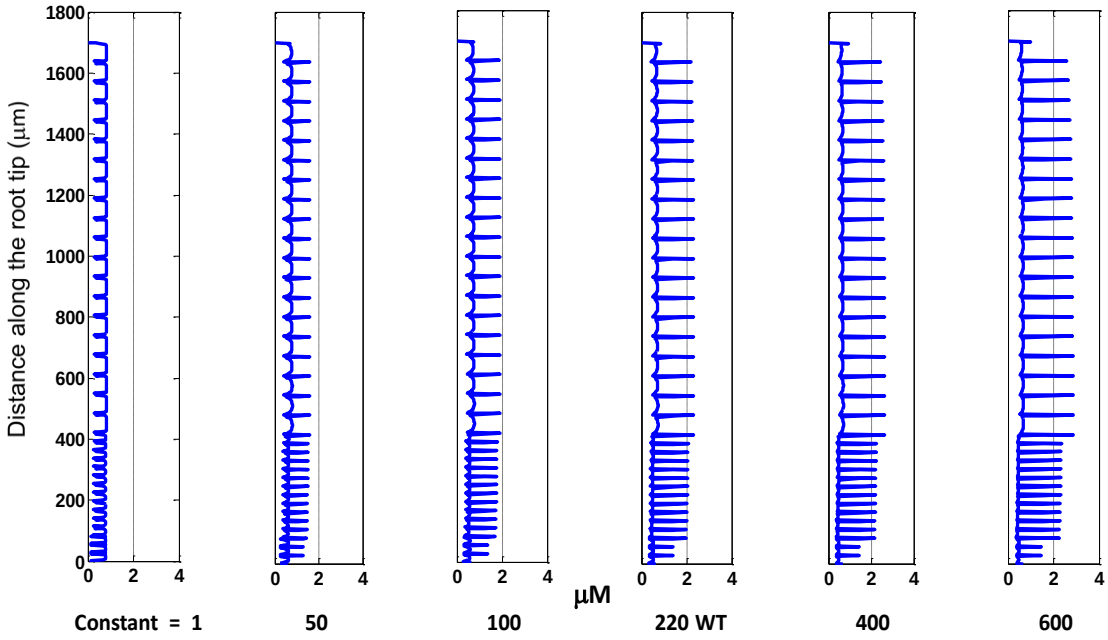

Figure 2.28: PINp concentration profiles for varied PINp diffusion
At low diffusion rates PINp is concentrated mainly in the cytosol but is progressively reallocated to the plasma membrane as diffusion rates increase (diffusion constant from 1 to 600 $\mu m^2 sec^{-1}$, WT = 220 $\mu m^2 sec^{-1}$)

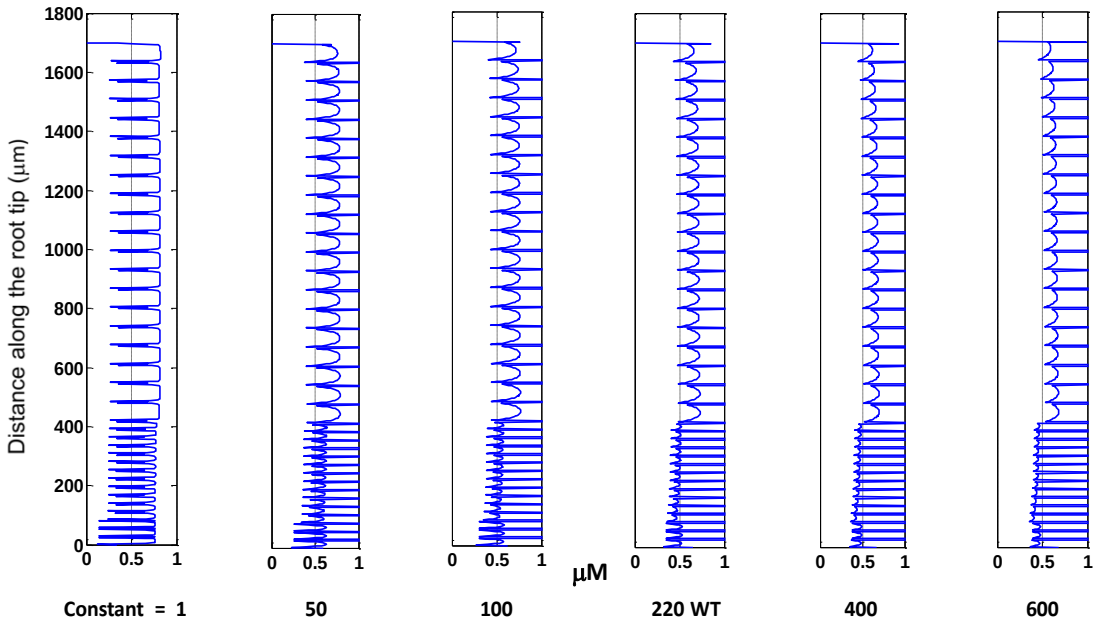

Figure 2.29: Enlarged PINp profiles for varied PINp diffusion
This clearly demonstrates that at low diffusion rates PINp is concentrated mainly in the cytosol but, as diffusion rate increase, PINp is progressively reallocated to the plasma membrane (diffusion constant from 1 to 600 $\mu m^2 sec^{-1}$, WT = 220 $\mu m^2 sec^{-1}$).

2.6.5 AUX1 protein diffusion rates

At very low diffusion rates (1 $\mu m^2 sec^{-1}$), as for PIN proteins, AUX1 concentrates mainly in the cytosol with very low concentrations at the plasma membrane. As the diffusion rate increases, AUX1 is reallocated from the cytosol to the plasma membrane to function as an auxin influx carrier (Figure 2.30).

The auxin concentration maximum exists even at very low diffusion rates (Figure 2.31), is nearly fully established at the diffusion constant of 50 $\mu m^2 sec^{-1}$ and thereafter remains stable. In addition the average auxin concentration in the root tip is very stable throughout the range (not shown). This is confirmed by the auxin concentration colour maps (Figure 2.32) which show the existence of auxin maxima (of varying strengths) at all diffusion constants.

Auxin patterning appears to be fairly insensitive to the AUX1 diffusion rates, even at low values, possibly indicating that the PIN protein and not AUX1 is the limiting factor in auxin transport through the root and for establishing auxin patterning.

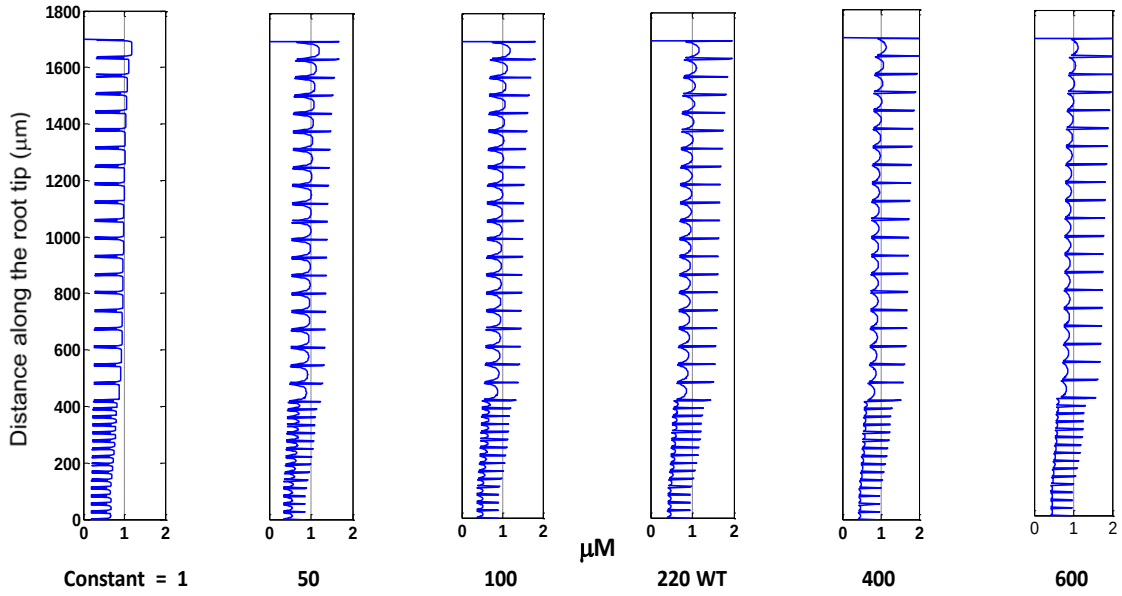

Figure 2.30: AUX1p concentration profile for varied AUX1 diffusion
At low diffusion rates AUX1p is concentrated mainly in the cytosol but is reallocated to the plasma membrane as diffusion rates increase (diffusion constant from 1 to 600 μm^2 sec^{-1}; WT = 220 μm^2 sec^{-1})

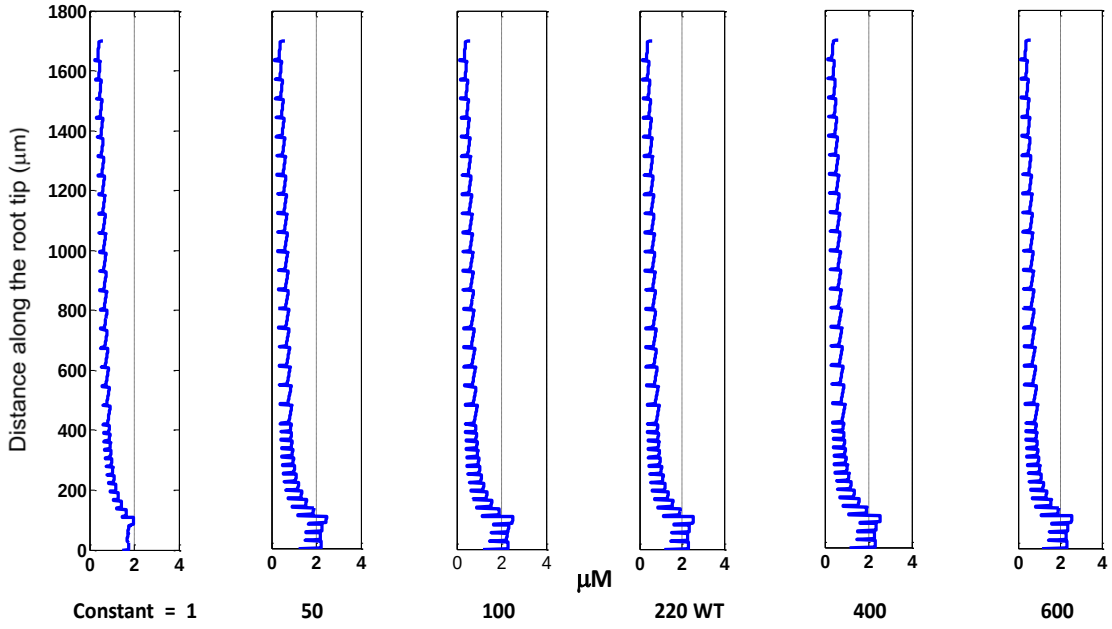

Figure 2.31: Auxin concentration profile for varied AUX1 diffusion
At very low diffusion rates the auxin maximum at the QC is very weak, but is quickly established at a diffusion rate of 50 μm^2 sec^{-1} and thereafter remains stable (diffusion constant from 1 to 600 μm^2 sec^{-1}; WT = 220 μm^2 sec^{-1})

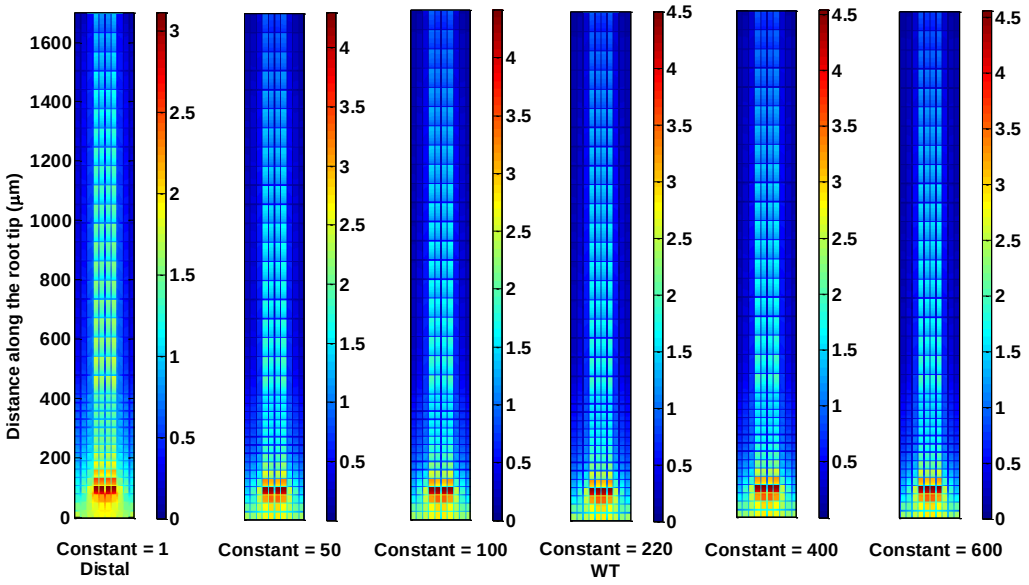

Figure 2.32: Auxin concentration maps for varied AUX1 diffusion
The auxin maximum exists at the QC over the full range of diffusion constants (diffusion constant from 1 to 600 $\mu m^2 sec^{-1}$; WT = 220 $\mu m^2 sec^{-1}$, colour bar units µM)

2.6.6 Auxin decay rates

The rate of auxin decay was varied from the WT value of k3 = 0.002 sec^{-1}. As expected, at higher rates the average root auxin concentration declined and at lower rates it increased; however, at all values tested the classic auxin pattern still occurred with a maximum in the QC region (Figure 2.33).

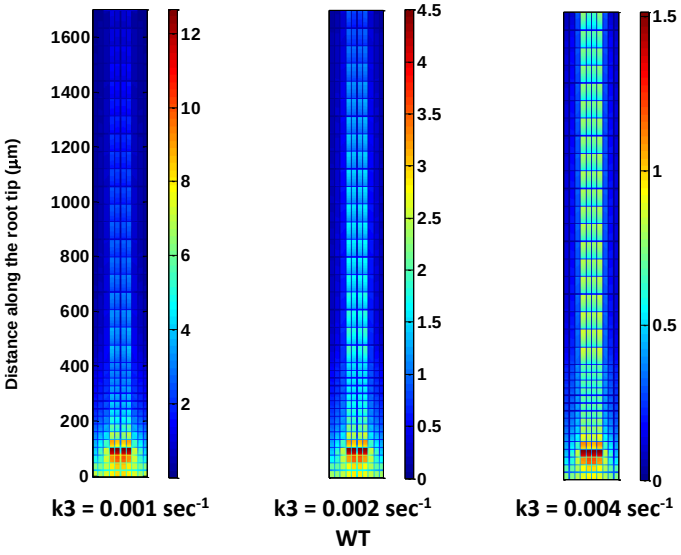

Figure 2.33: Auxin concentration maps for varied auxin decay
The auxin concentration increased at lower decay rates and decreased at higher rates; however, the auxin maximum at the QC is evident at all decay rates (decay rates from 0.001 to 0.004 sec^{-1}; colour bar units µM).

2.6.7 Tissue specific CK biosynthesis

As discussed earlier, in the model CK is assumed to be synthesised only in the central cell files to represent predominant tissue specific biosynthesis and to give a lateral concentration gradient similar to experimental results.

To test the sensitivity of auxin patterning and concentrations to assumptions on tissue specific CK biosynthesis, a version of the model was run where CK was synthesised in all root cells, which resulted in increased CK concentration and a different CK concentration pattern in the root. When CK was synthesised in all root cells, CK concentration increased nearly 3-fold and the lateral CK distribution was very different with higher concentration in the epidermal cell files and lower in the vascular cells (Figure 2.34b, Figure 2.35b). In the tissue specific biosynthesis model the CK concentration maximum occurred in the pericycle cell files, similar to experimental results.

Even with these significant changes in CK concentration and distribution in the root, the auxin patterns and profiles for both model versions were very similar (Figure 2.34a, Figure 2.35a). There was a slight decrease in the average root concentration of auxin when CK biosynthesis was restricted to the pericycle and vascular cells.

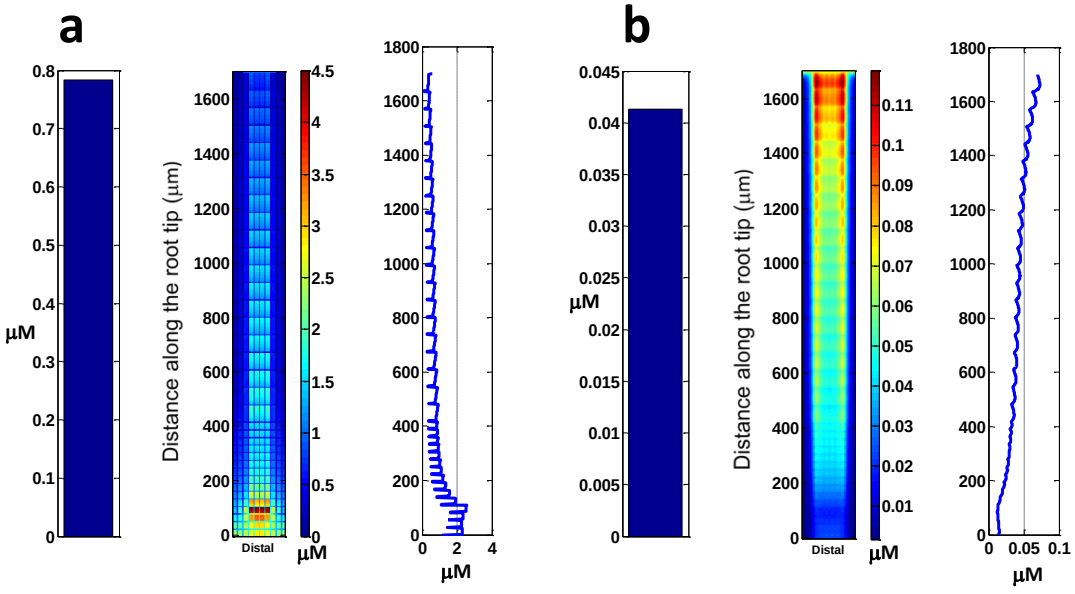

Figure 2.34: CK synthesis in central cell files (a) auxin (b) cytokinin results
Auxin and CK average concentrations, concentration colour maps and profiles. Lateral CK model patterning is similar to experimental results with a maximum near the pericycle cell files. Auxin patterning and average concentration is similar to the model version where CK is synthesised in all cells, see Figure 2.35 (WT; colour bar units μM).

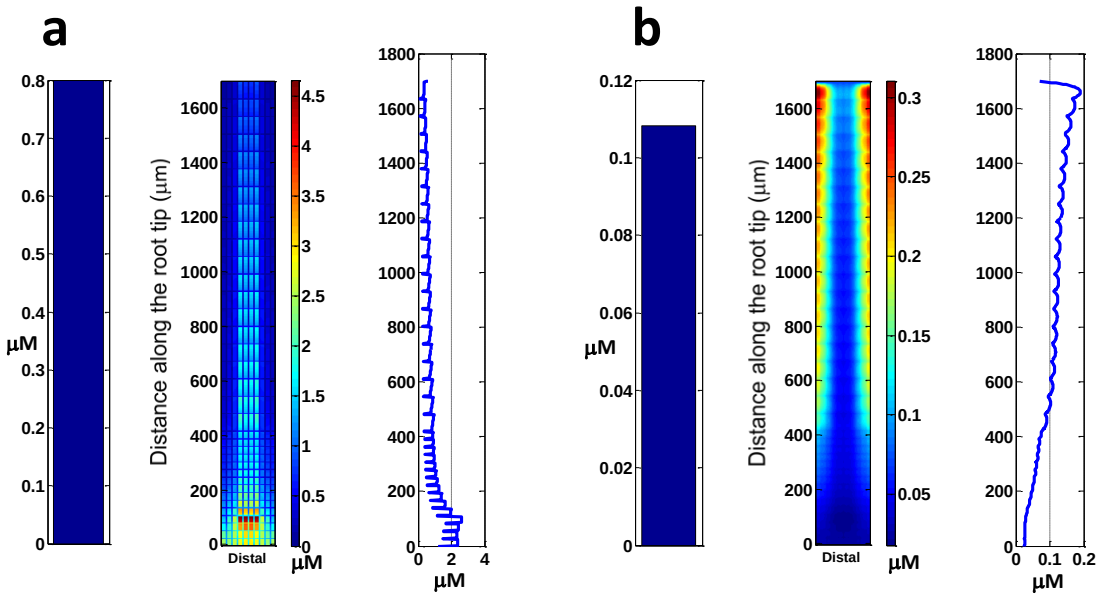

Figure 2.35: CK synthesis in all cells (a) auxin (b) cytokinin results
Auxin and CK average concentrations, concentration colour maps and profiles. Lateral CK patterning differs from experimental results with a maximum in the epidermal cells. Auxin patterning and average concentration is similar to the model version where CK is synthesised in the central cell files, see Figure 2.34 (WT; colour bar units µM).

2.6.8 *AUX1* gene expression rates

The rate constant for *AUX1* expression was varied from k1a = 0.01 to 2.5 µM sec^{-1} (WT setting = 0.8 µM sec^{-1}). The level of expression of *AUX1* determines the rate of auxin influx into the cells and therefore (together with PINp) the distribution of auxin between the cell walls and cytosol, and also the rate of transport of auxin through the root and auxin accumulation in the QC region. Average auxin root concentration shows a slight bell shaped response to increasing rates of *AUX1* expression (Figure 2.36).

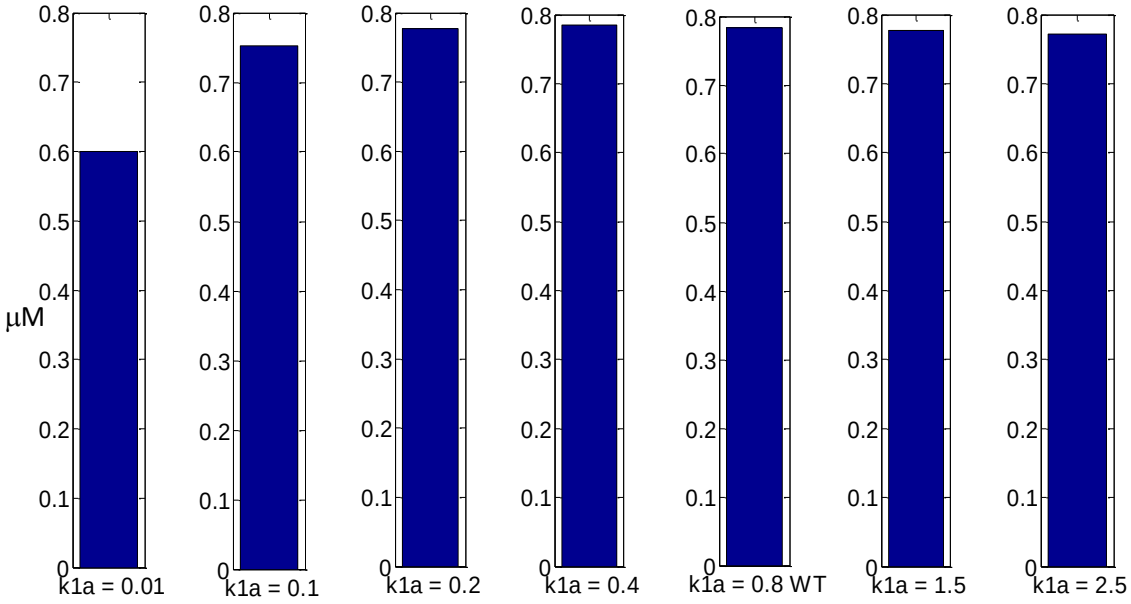

Figure 2.36: Average auxin concentrations for varied *AUX1* expression
Shows a slight bell shaped response to variation in expression rates (expression rate constant k1a = 0.01 to 2.5 μM sec^{-1}; WT = 0.8 μM sec^{-1})

The auxin concentration profile at low rates of *AUX1* expression shows that auxin is concentrated in the cell walls, with slightly higher cell wall auxin concentrations at the proximal end of the root and no auxin maximum (Figure 2.37). As the expression rate increased an auxin maximum was established as auxin was released from the cell walls and accumulated in the QC region. The size of the auxin maximum progressively increases as auxin is removed from the cell walls by the action of higher concentrations of the AUX1 influx carrier. The gradual establishment of the auxin maximum is also illustrated by the auxin concentration colour maps (Figure 2.38). Both the reallocation of auxin from the cell wall to the cytosol and the emergence of the auxin maximum are better illustrated in an enlarged auxin concentration colour map of the QC region (Figure 2.39).

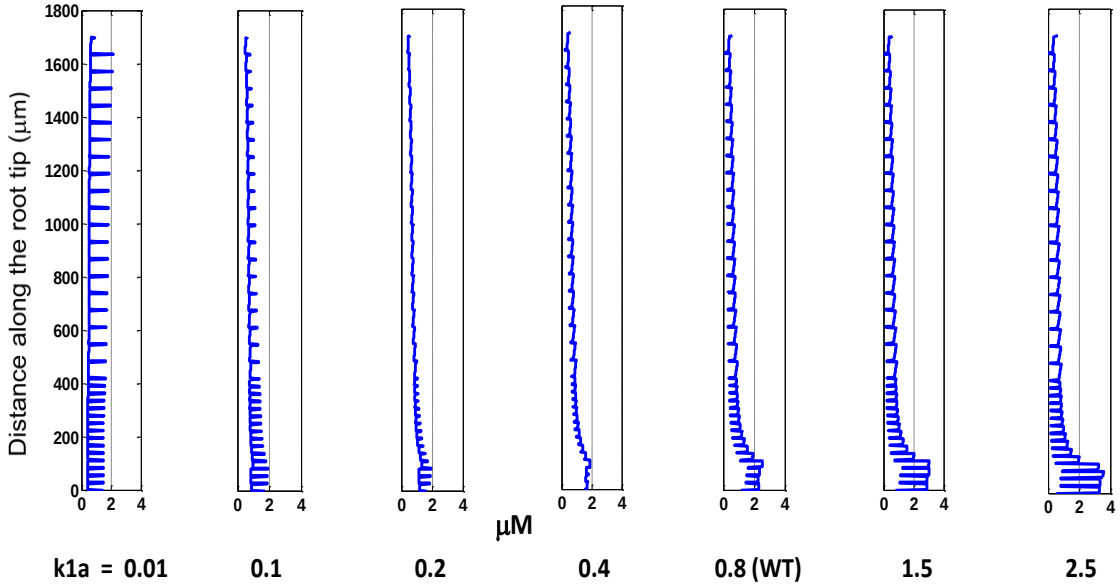

Figure 2.37: Auxin concentration profiles for varied *AUX1* expression
At very low expression rates, auxin is concentrated in the cell walls, with no auxin maximum at the QC; as expression rates increase auxin is reallocated to the cytosol, and the auxin maximum and the longitudinal auxin trend progressively emerge (expression rate constant k1a = 0.01 to 2.5 μM sec^{-1}; WT = 0.8 μM sec^{-1})

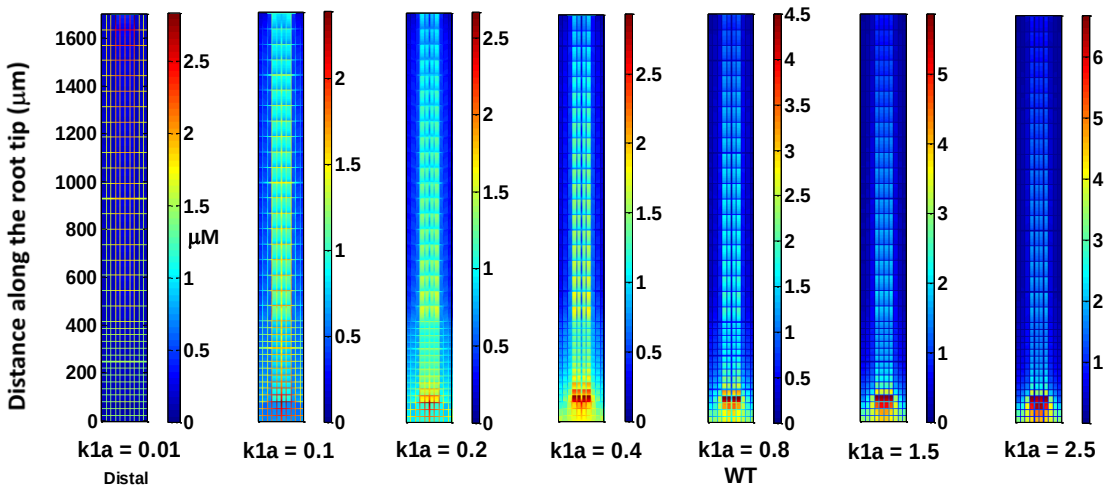

Figure 2.38: Auxin concentration maps for varied *AUX1* expression
At very low expression rates, there is no auxin concentration maximum at the QC; as expression rates increase the auxin maximum emerges and progressively increases (rate constant k1a = 0.01 to 2.5 μM sec^{-1}; WT = 0.8 μM sec^{-1}; colour bar units μM)

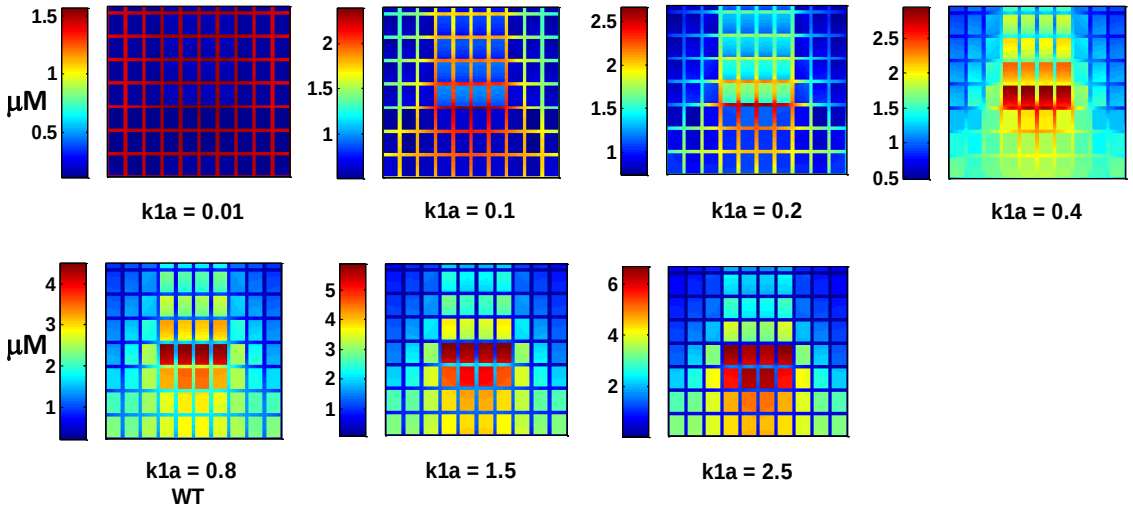

Figure 2.39: Auxin QC concentration maps for varied *AUX1* expression
This enlarged image of the distal 4 cell tiers shows that at very low expression rates, auxin is concentrated in the cell walls with no auxin maximum at the QC; as expression rates increase auxin is reallocated from the cell wall to the cytosol and the auxin maximum emerges (rate constant k1a = 0.01 to 2.5 μM sec^{-1}; WT = 0.8 μM sec^{-1}).

2.6.9 *PIN* gene expression rates

The PIN proteins act as auxin efflux transporters to remove auxin from the cell. Depending on the location in the root they have asymmetrical localisation on the cell face to direct auxin flow in certain directions to create Polar Auxin Transport (PAT). The placement of the PIN proteins is critical for the accumulation of auxin in the QC and the establishment of the auxin maximum (Grieneisen *et al*., 2007).

The model was run with different levels of *PIN* expression to see how this affected the auxin maximum and to test model sensitivity to the value of the parameter determining *PIN* expression (k20a). The average auxin concentrations in the root gradually decline with increasing *PIN* expression rates (Figure 2.40), likely due to increased auxin efflux from the root which is determined by PIN concentration at the root/shoot border of epidermal cells.

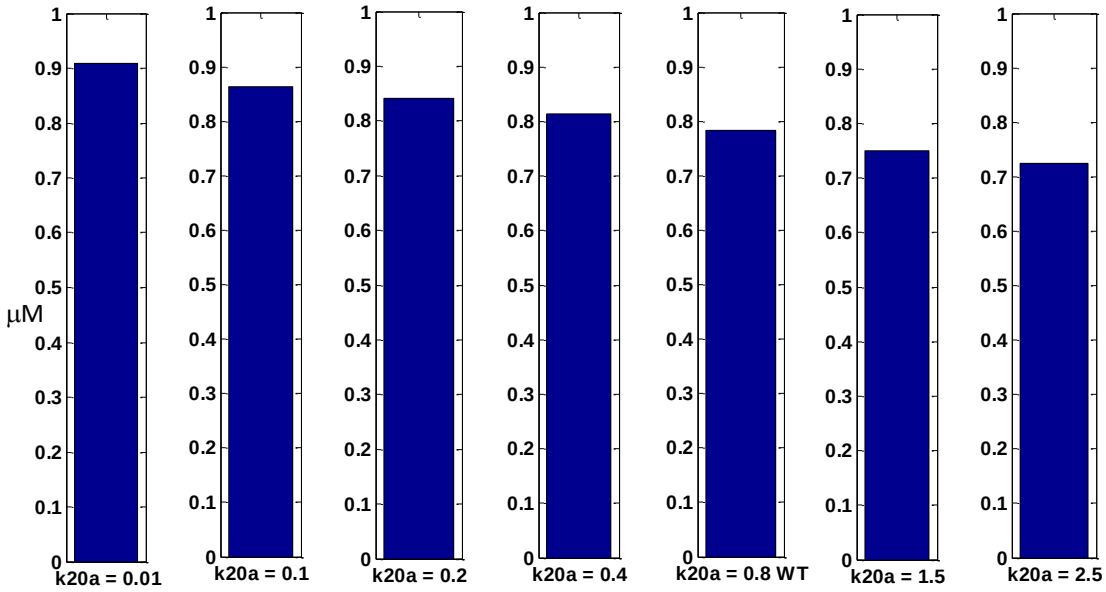

Figure 2.40: Average auxin concentrations for varied *PIN* expression
Average root auxin concentration progressively decreases with increasing *PIN* expression rates due to increased auxin efflux from the root in the epidermal cell files (rate constant k20a = 0.01 to 2.5 μM sec^{-1}; WT = 0.8 μM sec^{-1}).

At low levels of *PIN* expression there is a high concentration of auxin at the proximal cell tiers, as seen in the auxin profiles and colour maps (Figure 2.41, Figure 2.42), since the reduction in PIN proteins is preventing auxin transport down the root. The lack of PIN proteins also reduces the lateral transport of auxin, preventing accumulation in the QC region and the establishment of the auxin maximum. As the *PIN* expression rates increase the auxin concentration at the border progressively decreases, auxin is accumulated in the QC region and the maximum established. As the expression rate increases above the WT value, the auxin concentration in the cell walls increases and exceeds that in the cytosol. This is particularly apparent at very high levels of expression (k20a = 2.5 μM sec^{-1}) in Figure 2.41, where the action of the PIN efflux proteins exceeds that of the AUX1 influx proteins, resulting in increased cell wall auxin content. The auxin concentration colour map (Figure 2.42) shows the establishment of the auxin maximum as the *PIN* expression rates increase and then the formation of an abnormal maximum at high levels of *PIN* expression with very high auxin concentration in the cell walls in the QC region. The enlarged colour map of the QC region (Figure 2.43) illustrates more clearly how auxin is driven into the cell walls as the *PIN* expression rate is increased above

WT. This can be rescued by coincidently overexpressing the *AUX1* gene (k1a & k20a = 2.5 μM sec^{-1}, Figure 2.43) such that increased cell influx offsets increased efflux, so reducing the the auxin content of the cell walls. These results show that auxin patterning is fairly robust for *PIN* expression rates in the region of the WT value but that patterning deteriorates as the expression rates deviate further from WT.

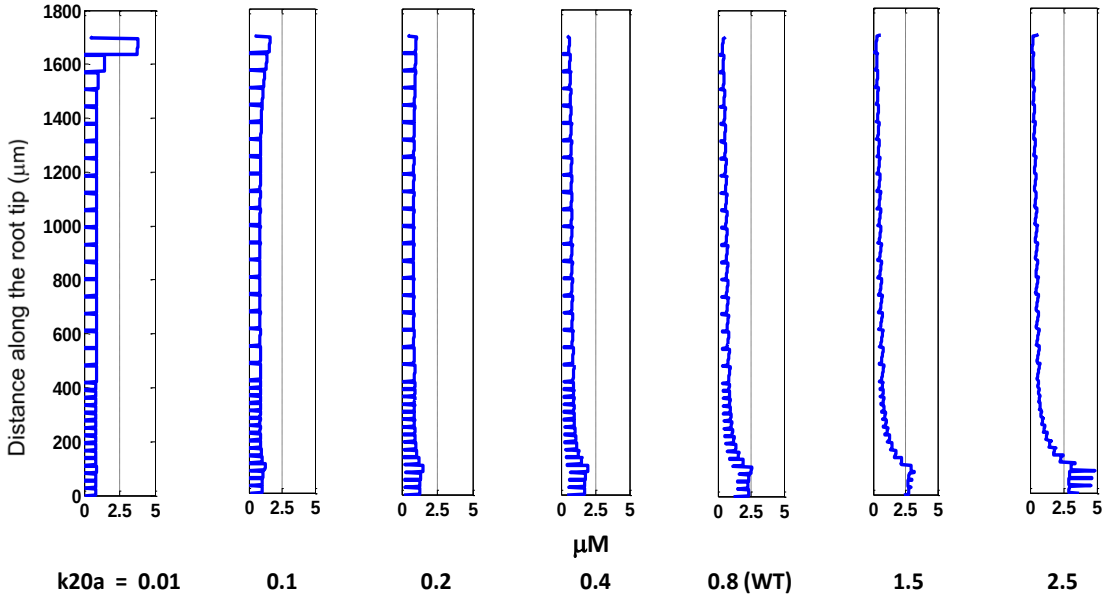

Figure 2.41: Auxin concentration profiles for varied *PIN* expression
At low expression rates auxin is concentrated in the cytosol, and there is high auxin concentration in the proximal cell tiers, since low PIN concentration is preventing auxin transport down the root, and no auxin maximum occurs at the QC; as expression rates increase, this situation is reversed and at very high expression rates the excess allocation of auxin to the cell walls can be clearly seen in the region of the QC (rate constant k20a = 0.01 to 2.5 μM sec^{-1}; WT = 0.8 μM sec^{-1}).

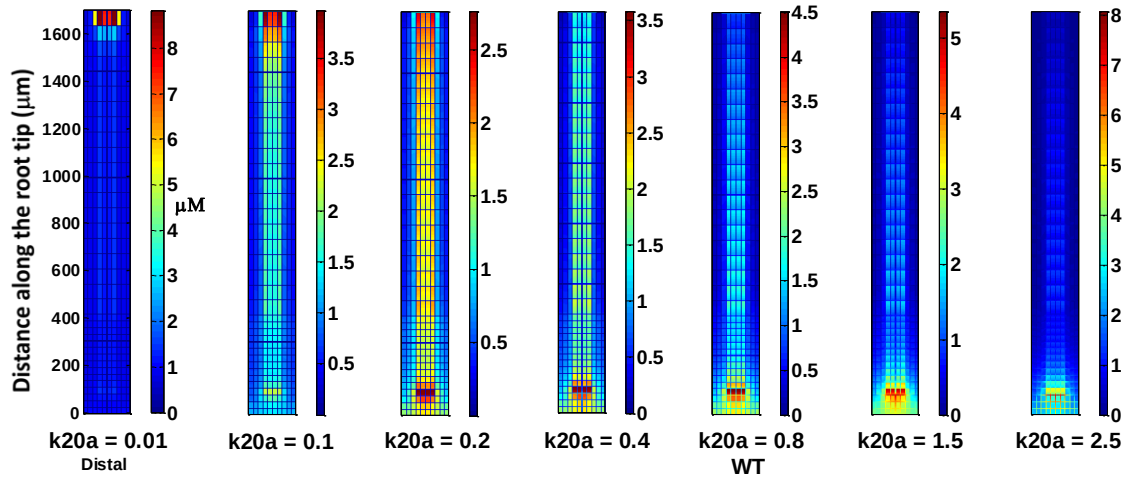

Figure 2.42: Auxin concentration maps for varied *PIN* expression

At low expression rates there is a high auxin concentration in the proximal cell tiers, since low PIN concentration is preventing auxin transport down the root, with no apparent auxin maximum at the QC; as expression rates increase, this situation is reversed and at very high expression rates excess allocation of auxin to the cell walls can be seen in the region of the QC (rate constant k20a = 0.01 to 2.5 μMsec^{-1}; WT = 0.8 μMsec^{-1}; colour bar units in μM).

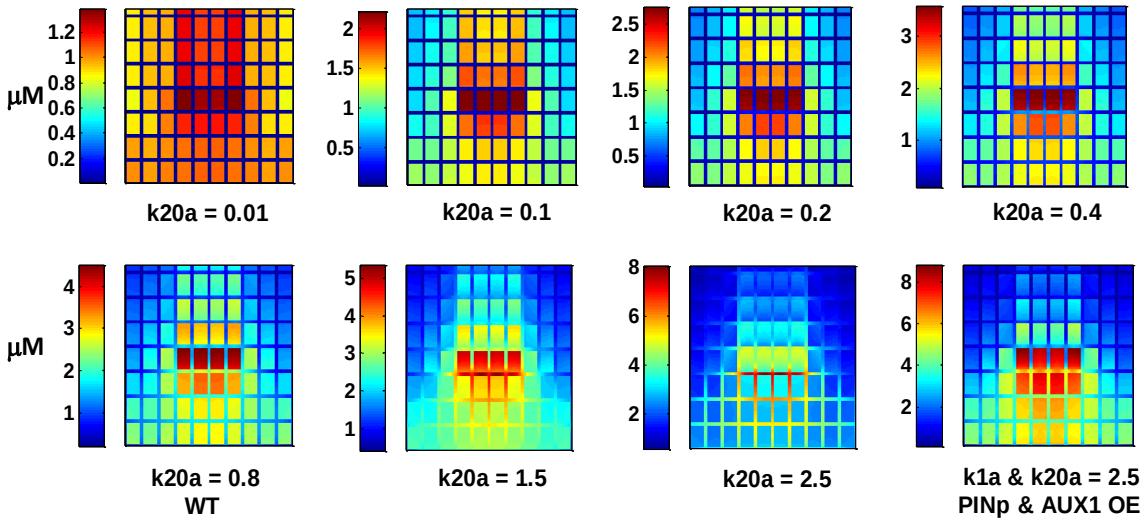

Figure 2.43: Auxin concentration maps at QC for varied *PIN* expression

The exploded colour map of the QC shows the emergence of the auxin maximum at the QC as *PIN* expression rates increase, and also the reallocation of auxin from the cytosol to the cell walls at very high expression rates; very high *PIN* expression rates are rescued by increased *AUX1* expression as seen in the *PINp & AUX1* OE image (*PIN* expression rate constant k20a = 0.01 to 2.5 μM sec^{-1}; *PIN* OE k20a =2.5 μM sec^{-1}; *AUX1* OE k1a = 2.5 μM sec^{-1}; WT k20a = 0.8 μM sec^{-1}; WT k1a = 0.8 μM sec^{-1}).

2.7 Comparison between experimental results and model predictions

In previous work (section 2.5) comparisons between experimental and model results were used to fit the model and calibrate parameters values, and then the model was tested for sensitivity to parameter value variation from WT settings. In this section model predictions are compared with additional experimental results to assess how well the model explains hormonal crosstalk and gene expression interactions and patterning.

2.7.1 Shoot to root auxin flux

Experimental measurements of the shoot to root transport of auxin in inflorescent stem segments are shown for WT, the *pls* null mutant and the double mutant *pls etr1-1* (Figure 2.44), where *etr1-1* is a gain of function (high activation, ethylene insensitive, low downstram ethylene signalling) mutant. *pls* showed a significant decline in shoot to root transport while the double mutant recovered to approximately WT levels of transport.

Relative shoot to root transport at the proximal border of the pericycle and vascular cell files was measured in the model (Figure 2.45) and exhibited similar trends although the double mutant recovered to levels slightly higher than WT.

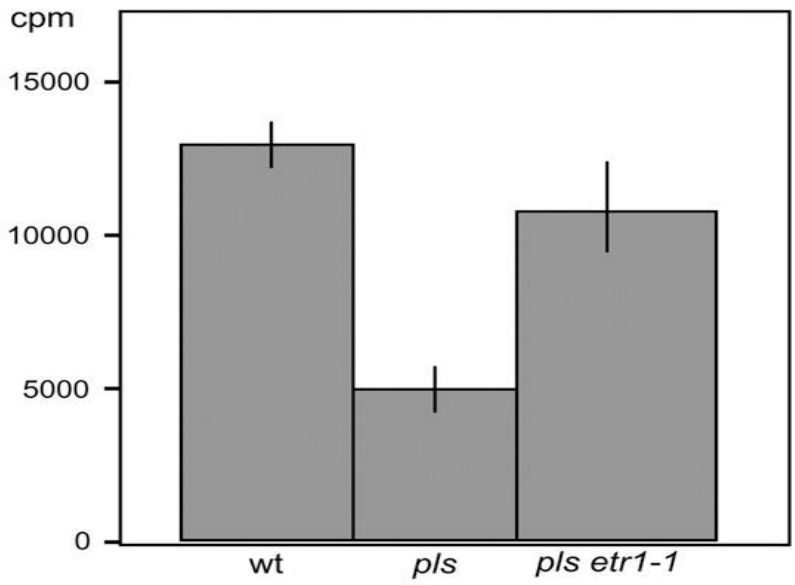

Figure 2.44: Relative experimental shoot to root auxin transport
(Chilley *et al*., 2006)

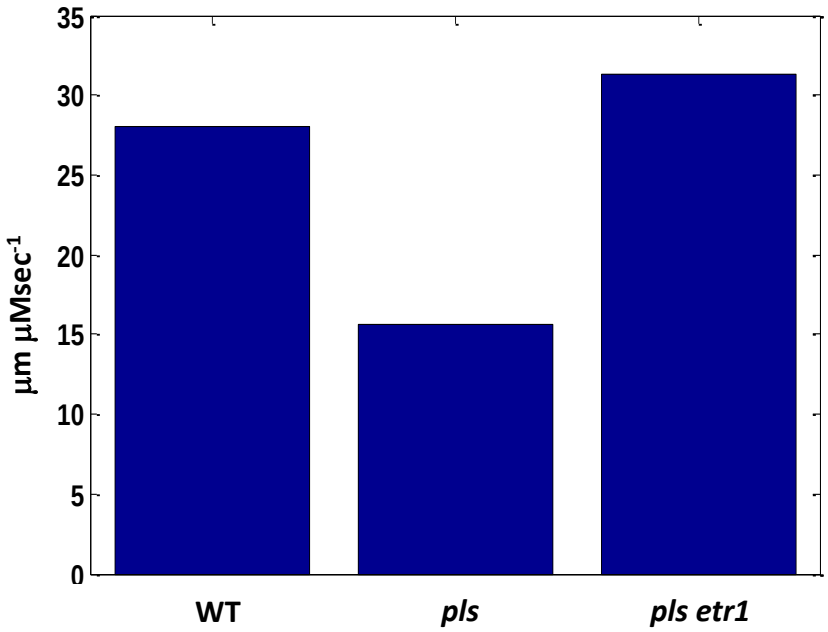

Figure 2.45: Relative model shoot to root auxin transport
With similar trends to experimental results in Figure 2.44

2.7.2 ET concentration profile

A relative ET response profile was derived from an experimental image (Martin-Rejano *et al*., 2011) using ImageJ and compared to the ET concentration profile from the WT model (Figure 2.46). Both profiles showed increasing ET response/concentration towards the proximal end of the root.

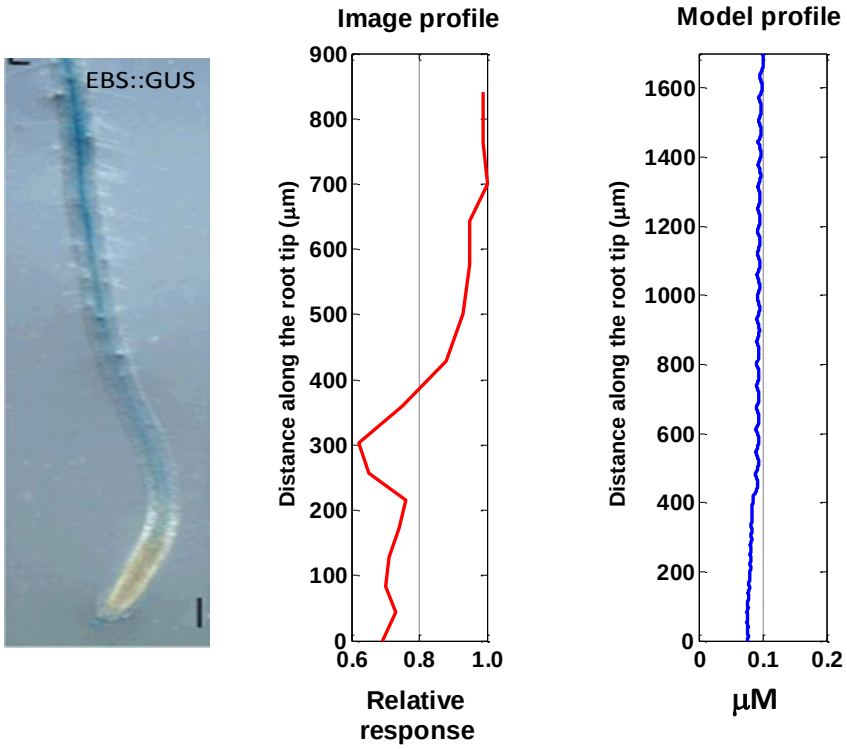

Figure 2.46: ET response and model concentration profiles
Both experimental and model profiles show proximally increasing average ET concentration (image from Martin-Rejano *et al*., 2011)

2.7.3 *POLARIS* (*PLS*) expression pattern

Gene expression patterning was also examined using an experimental image of *PLS* expression patterning and comparing this to model concentrations. The profiles generated from the image and from the model gave similar results with a PLS concentration maximum near the distal end and the concentration declining proximally along the root (Figure 2.47 b,c).

As shown in the hormonal crosstalk network (Figure 2.9), the *PLS* gene of *Arabidopsis*, which transcribes a short mRNA encoding a 36-amino-acid peptide (Casson *et al*., 2002; Chilley *et al*., 2006), is important for establishing crosstalk between auxin, ethylene, and cytokinin. Here, both experimental analysis and modelling are used to further investigate control of *PLS* gene expression patterning. Experimental imaging of PLS protein accumulation in the wild-type root (Figure 2.47a) shows a concentration maximum near the distal region, with the concentration declining proximally through the MZ. This is similar to the expression of the *PLS* gene as monitored by *PLS* promoter-GUS analysis

(Casson *et al*., 2002; Chilley *et al*., 2006). The PLS concentration profile generated from the experimental fluorescence image (Figure 2.47b) illustrates this patterning graphically. The spatiotemporal modelling of hormonal crosstalk predicts the same trend (Figure 2.47c), indicating that the hormonal crosstalk network controls the patterning of *PLS* gene expression and protein accumulation. Modelling calculations reveal that the rate of *PLS* transcription reaches a maximum in the distal part of the root (Figure 2.48), resulting in the patterning of *PLS* expression (Figure 2.47). As indicated in Figure 2.47d, if *PLS* transcription is not regulated by auxin, the modelled patterning of *PLS* expression is not in agreement with experimental observation. This reflects the predominant role of auxin in the regulation of *PLS* expression.

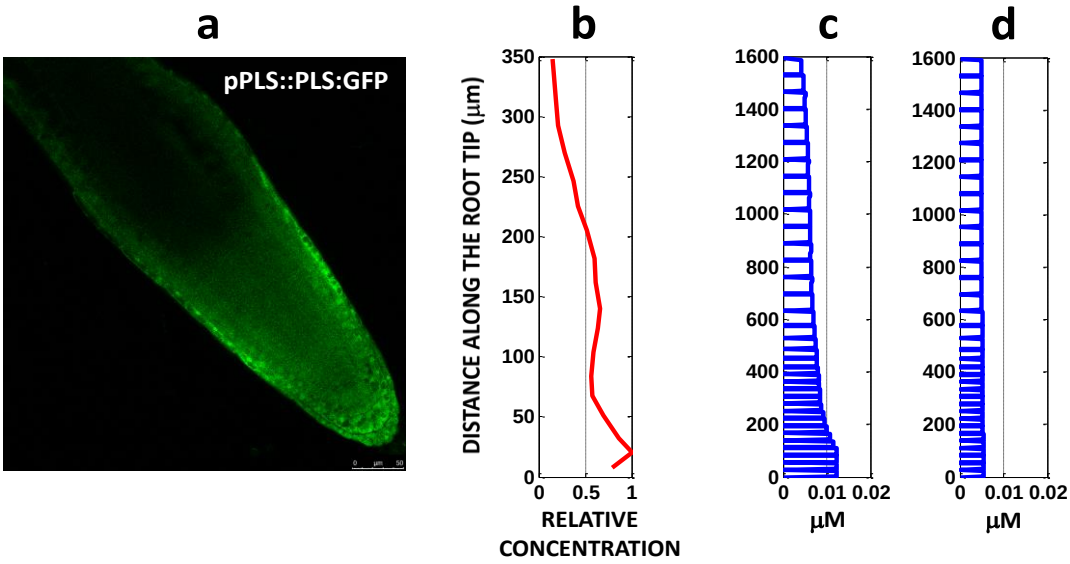

Figure 2.47: Experimental and model *PLS* gene expression patterning
(a) Image of *PLS* gene expression and PLS protein accumulation, (b) PLS protein concentration profile derived from image, (c) Model prediction of the PLS protein concentration profile is similar to experimental results. (d) Model prediction of the PLS protein concentration profile differs from experimental results if auxin regulation of *PLS* transcription is removed from the hormonal crosstalk network, indicating the importance of auxin in *PLS* regulation

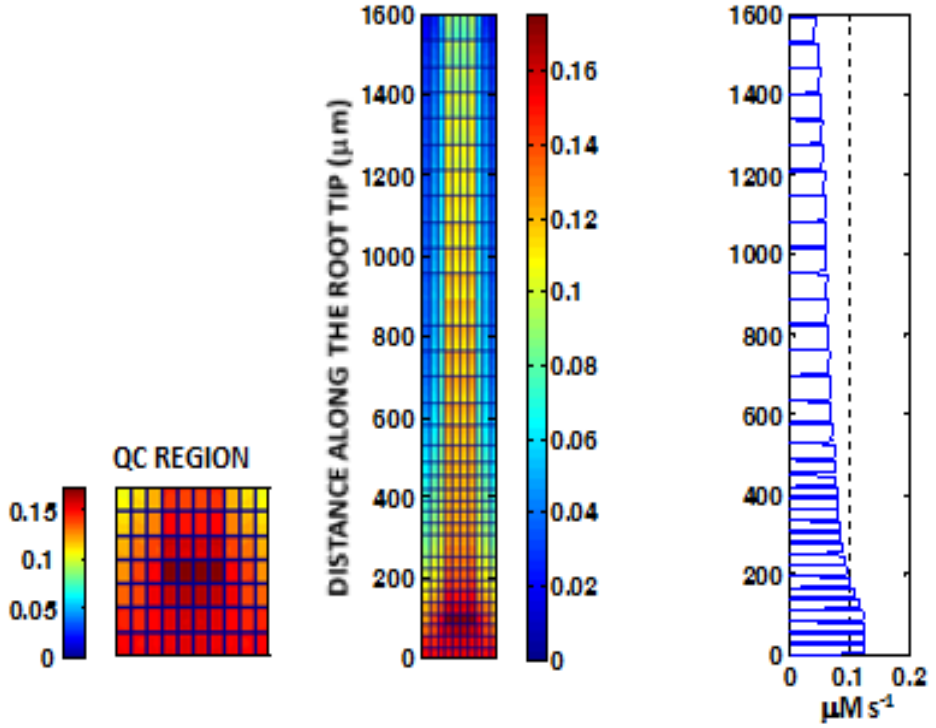

Figure 2.48: *PLS*m transcription patterning in WT

PLSm transcription is at a maximum at the distal end of the root similar to experimental results, see Figure 2.47a (colour bar units μM s^{-1})

2.7.4 PIN concentration trends in WT and mutants

The relative experimental PIN1 protein concentrations in WT, PLSox transgenic, and *pls, etr1* (the *etr1-1* mutant with gain of function, high activation, low downstream ethylene signalling) and *pls etr1* mutants (Figure 2.49) were measured (Liu *et al*., 2013) using ImageJ to extract data from fluorescent PIN1 protein images. The relative PIN concentrations predicted by the model (Figure 2.50) show similar concentration trends to those observed experimentally, (especially when standard errors are considered), apart from *etr1* which appeared to be relatively low in the model. A comparison between the model and PIN2 experimental results showed similar trends, but again with low model results for *etr1.*

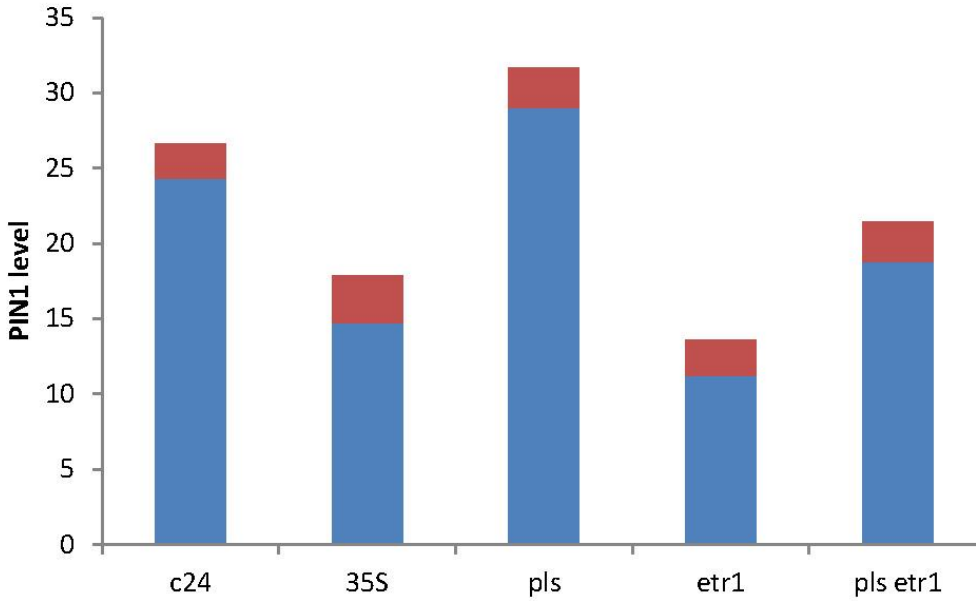

Figure 2.49: Relative experimental PIN in WT(c24), 35S(PLSox), *pls, etr1*, *pls etr1* (*etr1* is the *etr1-1* gain of function mutant; red bar = standard error; Liu *et al*., 2013)

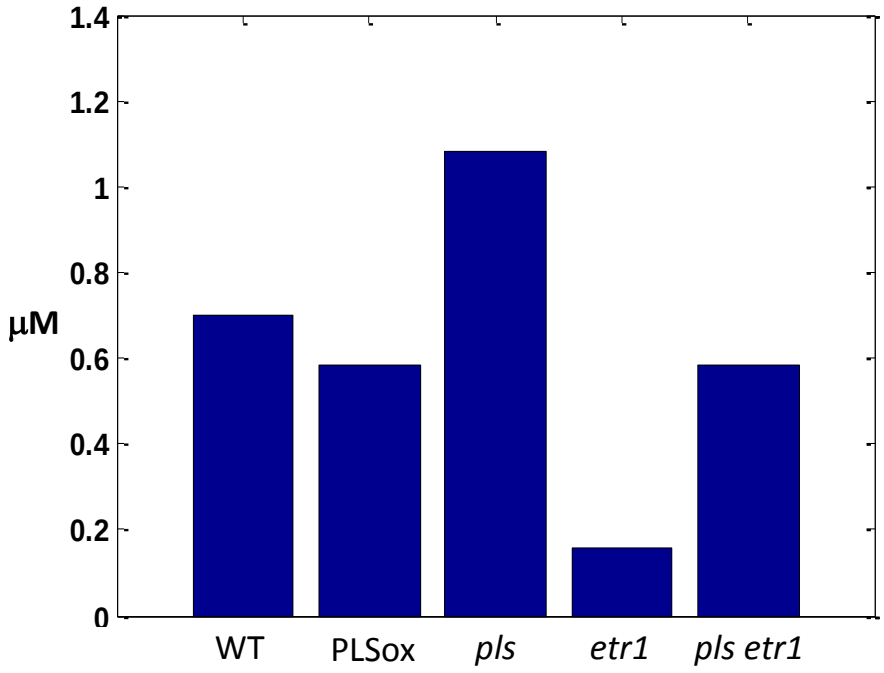

Figure 2.50: Relative model PIN concentration in WT, PLSox and mutants Model average root concentrations in wild-type, PLSox over-expressor, and *pls*, *etr1* and *pls etr1* mutants, show a similar qualitative trend to experimental results in Figure 2.49

2.7.5 PIN concentration profiles

ImageJ was used to extract relative concentration data from experimental images of PIN1 and PIN2 proteins in WT, and *pls, etr1* (ethylene insensitive, gain-of-function)*, pls etr1* mutants, and the PLSox overexpressor and the data used to plot PIN concentration profiles. These image profiles were compared to model profiles for the WT and mutants.

The PIN1 images (Figure 2.51) show that PIN1 proteins localise mainly to the vascular cell files, with a weak signal in the epidermal and cortical tissues consistent with other experimental results (Blilou *et al*., 2005), which appears to be up-regulated in the *pls* mutant image. Relative PIN1 concentrations in the vascular tissue were derived from the areas defined by the central column of rectangles in each image, using ImageJ, plotted and then compared to profiles from the vascular and pericycle cell files from the model (Figure 2.52). The model profile is a plot of the average PIN concentration in the vascular and pericycle cells for each cell tier cross-section of the root rather than each grid point cross-section since the large difference between PIN concentrations in the plasma membrane and cytosol make grid point plots more difficult to read. The images represent a region in the model root from approximately 5 to 25 cell tiers from the tip (denoted by the arrow), however some images vary. PIN model trends are in general similar to PIN1 trends generated from the images, except for the *pls etr1* double mutant.

In addition, each of the model profiles shows an increase in concentration at the 16^{th} cell tier which is believed to be due to the sudden increase in cell length from 28 to 64 μm at that point in the model root structure. This change in cell length effects the averaging since while the cell lengthens the thickness of the cell wall remains the same, so proportionately increasing the cytosolic area where PIN biosynthesis can occur. This is tested later when the model is run with a root structure with a gradual increase is cell length at the transition zone between the MZ and EZ.

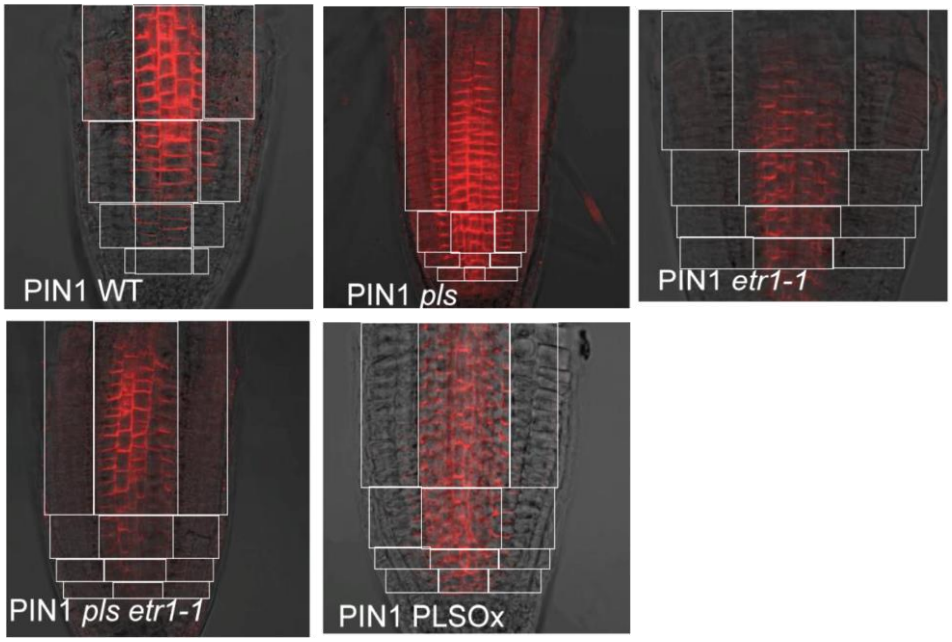

Figure 2.51: PIN1 images for WT, mutants and PLSox
(Liu *et al*., 2013)

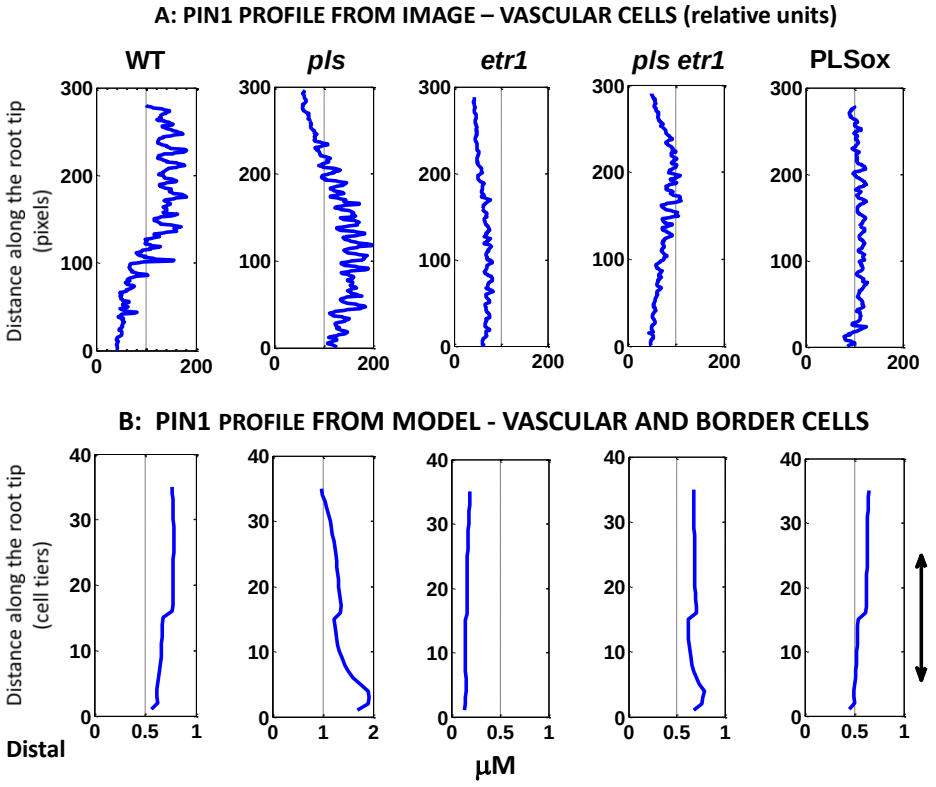

Figure 2.52: PIN1 concentration profiles (A) experimental and (B) model
Experimental profile generated from the vascular cell files in Figure 2.51 using ImageJ; the arrow denotes the region of the model plot that corresponds to the images; model and experimental results are similar except for the double mutant.

The same process was followed for the PIN2 images (Figure 2.53). The data were captured from the 2 external columns of rectangles shown in the images and then combined; however given the location of the PIN2 proteins in the lateral root cap, epidermis and cortical cells, and the tapering root shape, it was more difficult to capture data for PIN2 than data for the PIN1 proteins in the central vascular region. Image and model concentration profiles were plotted and compared (Figure 2.54). There was a reasonable match in concentration trends in the WT and PLSox but not for the mutants. Possibly this is due to the overly simplistic structure of the root model where the region of PIN2 expression/localization is a simple rectangle of cells consisting of the 2 exterior cell files of equal width extending for the full length of the root. In comparison, the region of PIN2 expression/localization in a real root is not a simple rectangle of cells but consists of the lateral root cap (which only extends to the EZ zone) and the epidermal and cortical cell files starting about 5 cell tiers above the QC region (Muller *et al*., 1998).

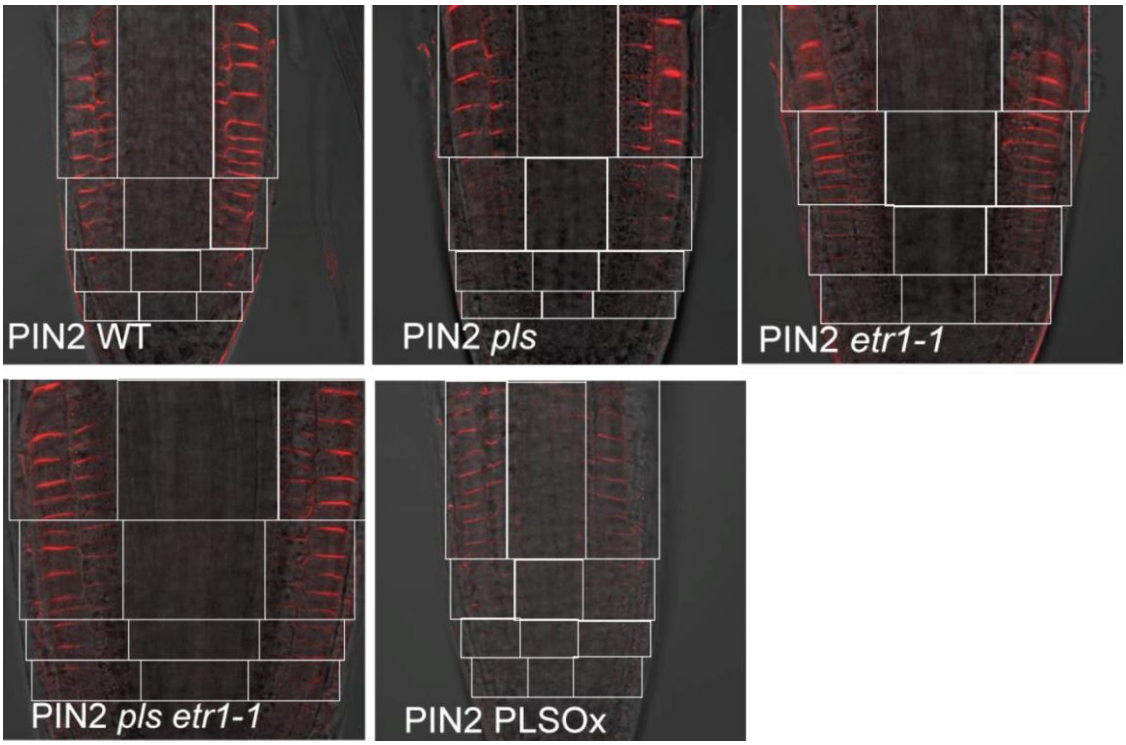

Figure 2.53: PIN2 images for WT, mutants and PLSox
(Liu *et al*., 2013)

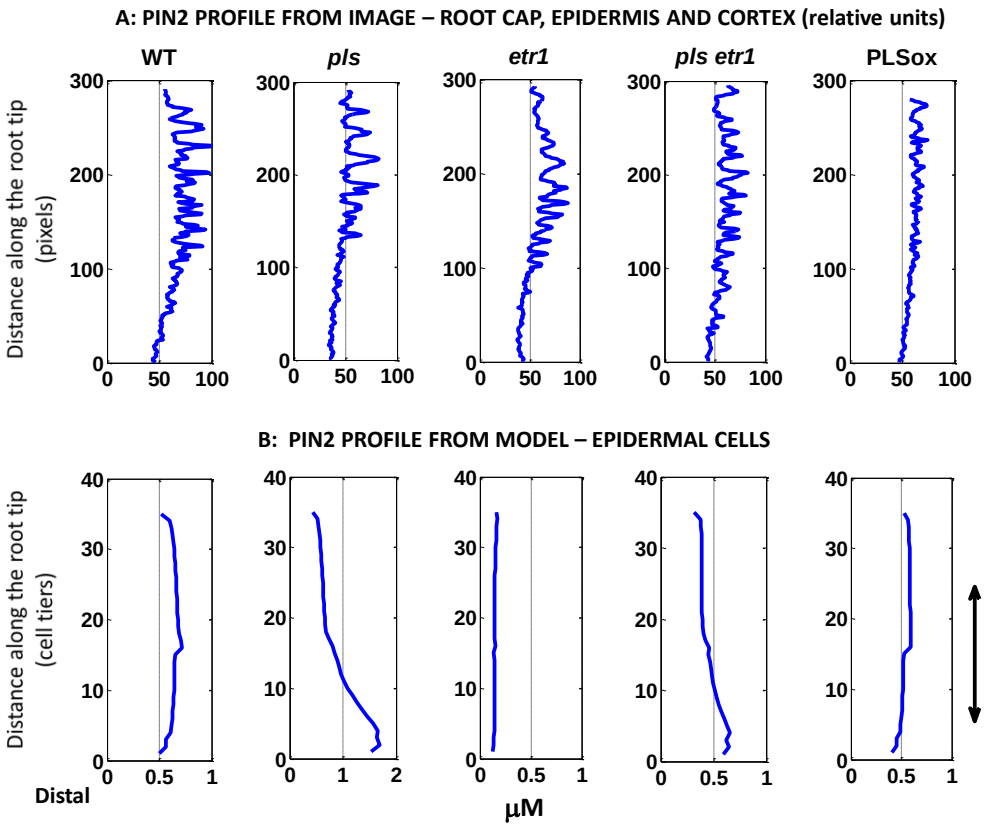

Figure 2.54: PIN2 concentration profiles (A) experimental and (B) model
Experimental profile generated from the epidermal, cortical and root cap cells in Figure 2.53 using ImageJ; the arrow denotes the region of the model plot that corresponds to the images; model and experimental results are similar for WT and PLSox but not for the mutants.

2.7.6 Auxin patterning in the *aux1* mutant

Images of auxin patterning in the WT and *aux1* null mutant show a decrease in auxin response in the mutant (Figure 2.55) compared to the WT. The images were scanned using ImageJ and the resulting auxin response profiles compared to profiles from the model (Figure 2.56). Since additional auxin influx carriers exist such as LAX2 (Figure 2.15), LAX3 and ABCB, the *aux1* null mutant was modelled with a 50% knockdown of *AUX1* since LAX2, LAX3 and ABCB influx proteins are not represented in the model. Model auxin profiles were similar to experimental profile trends derived from the images, with the auxin concentration of the *aux1* mutant being slightly lower than the WT, especially in the QC and columella, and both profiles then decreasing proximally along the root tip to reach approximately the same concentration levels.

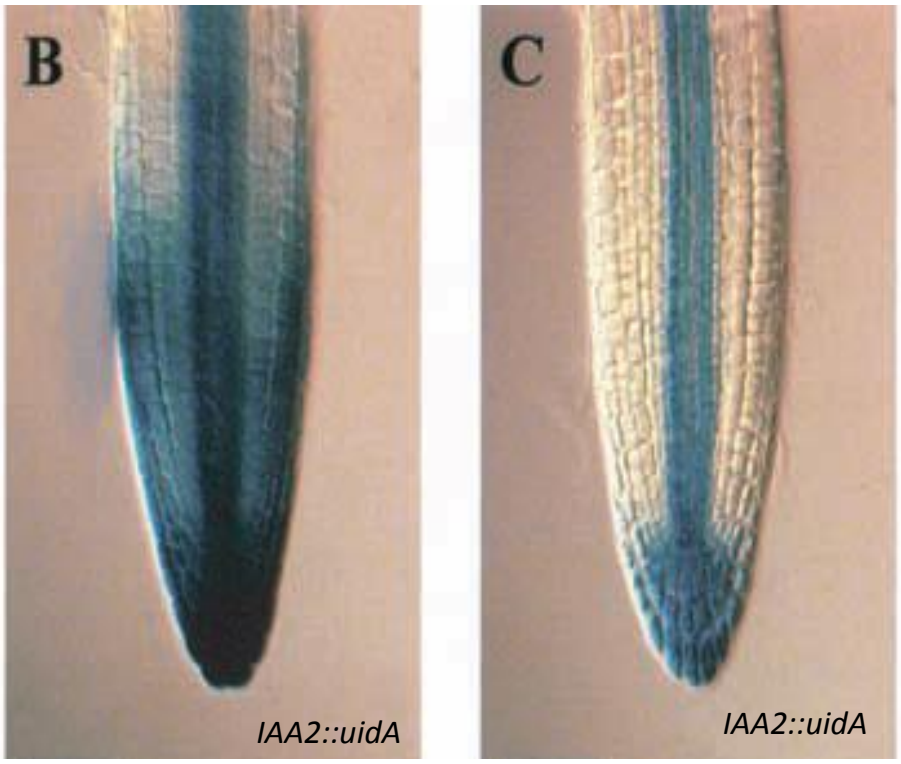

Figure 2.55: Auxin patterning in (B) WT (C) *aux1* mutant
(Swarup *et al*., 2001)

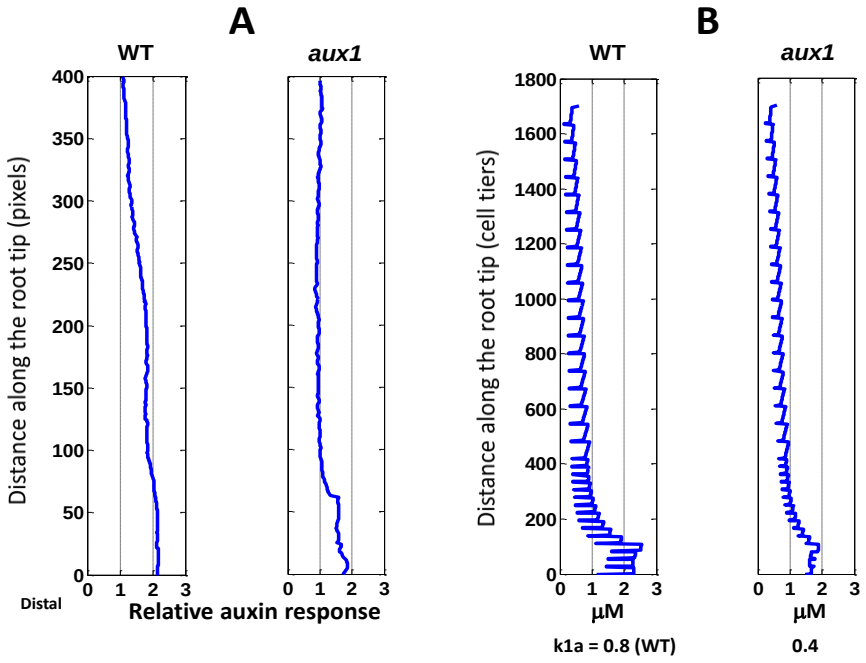

Figure 2.56: Auxin profiles in WT and *aux1,* (A) experimental (B) model
Experimental response profiles generated from Figure 2.55 using ImageJ; model and experimental profile trends are similar, with *aux1* concentrations slightly lower than in WT, especially in the QC and columella.

2.8 Gradual cell growth in the Transition Zone

In the model root structure, the cells increase in length from 28 to 64 μm when they move from the MZ into the EZ, at cell tier 16 from the distal end of the root, consistent with Grieneisen *et al*. (2007).

An alternative version of the model was developed, incorporating a more realistic gradual increase in cell length as cells moved through the TZ from the MZ to the EZ, to investigate whether this had any effect on model patterning. Cortical cell lengths were shown to increase at a relatively constant rate from 28 to 64 μm over a root distance of approximately 280 μm in 10 DAG plants (Beemster and Baskin, 1998). The lengths of the cells in the model root structure were increased at the same rate from 28 μm at the proximal end of the MZ by 15% per cell tier to a length of 64 μm over 7 cell tiers into the EZ. The length of these 7 cell tiers was 28 μm, 32 μm, 36 μm, 42 μm, 48 μm, 56 μm and 64 μm. The root map was changed accordingly but the total number of cell tiers remained at 35, which meant that the overall model root length was marginally reduced by 106 μm. Results for the gradual growth (GG) model were very similar to those from the original model. The GG root model, having more realistic cell elongation in the TZ, was therefore used to generate additional data for comparison with experimental results.

2.8.1 Auxin patterning in the gradual growth (GG) root model.

WT auxin concentration patterning and profiles appeared unchanged by the gradual increase in cell length in the TZ (Figure 2.57) compared to results from the original model where there was a sudden change in cell length at the MZ to EZ boundary (Figure 2.18). Auxin concentration profiles were also analysed for three different regions of the model root (epidermal, pericycle, and vascular cell files, extended to include the QC and columella). Figure 2.58 shows that the concentration profiles for the three regions follow similar trends to the original model, with the auxin maximum predominantly established in the central vascular tissues at or close to the QC.

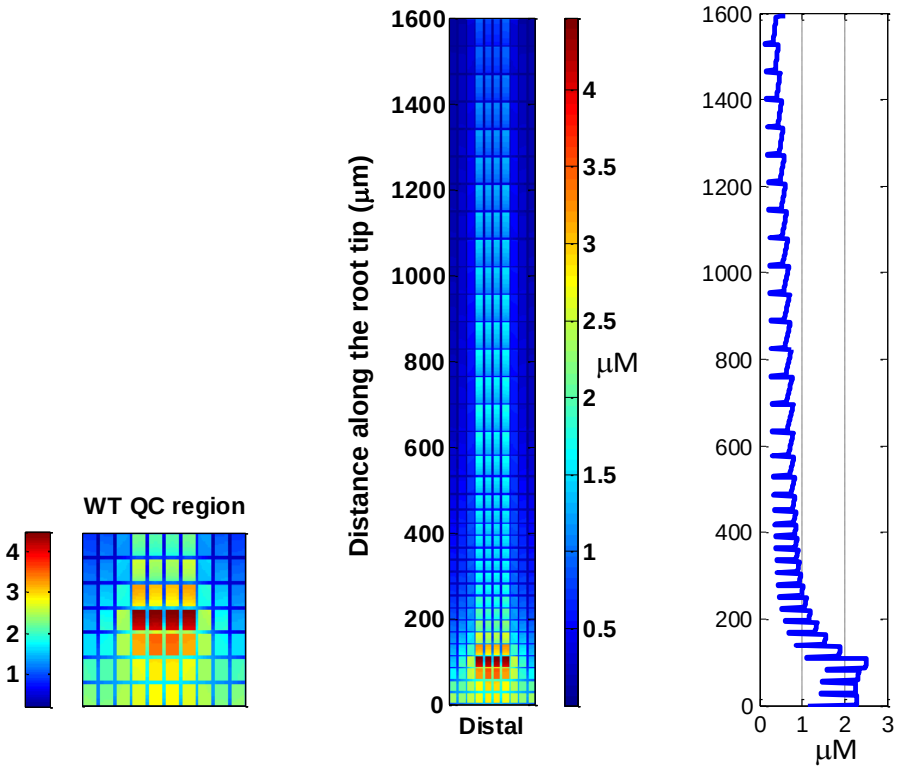

Figure 2.57: Auxin WT colour map and profile (GG model)
With an auxin maximum at the QC and proximally decreasing concentration profile.

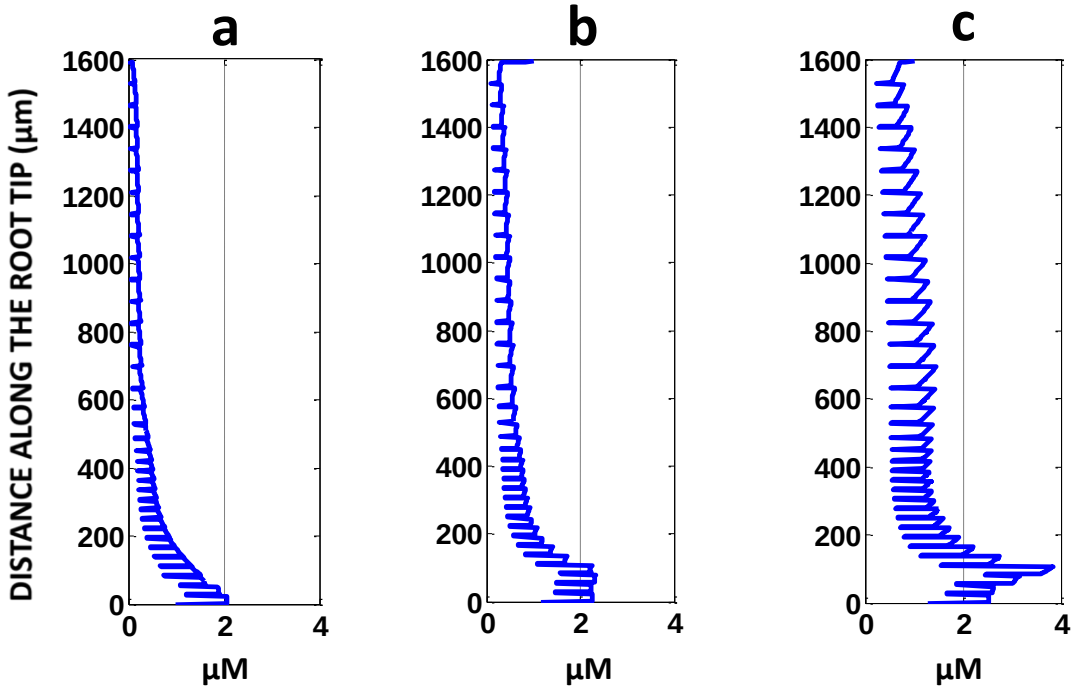

Figure 2.58: GG Model WT auxin profiles for three different regions
The auxin maximum is predominantly established in the central tissues at or close to the QC. (a) epidermal (b) pericycle (c) vascular.

It has been shown that auxin response can be regulated by different effectors. Response is therefore not necessarily equivalent to auxin concentration (Vernoux *et al*., 2011; Cho *et al*., 2014) and results can depend on the reporter mechanisms used. Experimental results, using the synthetic auxin reporter DII-VENUS, allow improved quantitative comparison between experimental images and modelling results (Brunoud *et al*., 2012). DII-VENUS is a fluorescent reporter expressed under the *35S* promoter; it is localised to the nucleus, quickly degrades in the presence of auxin, and is thought to more accurately represent relative auxin levels than other reporters which rely on promoters that are activated further downstream in the auxin signalling pathway and are therefore subject to additional regulation (Brunoud *et al*., 2012; Band *et al*., 2014). When combined with propidium iodide staining for cell membranes, it is also possible to measure the relative intensity of DII-VENUS fluorescence and so the relative auxin response (the inverse of DII-VENUS levels) at a cellular scale (Band et al., 2014).

While modelling results are similar to auxin IAA2::GUS response (Figure 2.13), it was decided to also use DII-VENUS imaging to compare relative experimental auxin response levels to auxin concentration patterning using the GG model. Figure 2.59 compares auxin response (using DII-VENUS) with modelling results. In the meristematic zone and QC, the modelled concentration profile is similar to the experimental auxin response profile derived from DII-VENUS data; however, in the elongation zone, the modelled concentration profile is not in agreement with experimental DII-VENUS imaging which indicates increasing auxin response compared to decreasing concentrations in the model, due to an apparent increase in auxin response in the epidermal cells of the EZ.

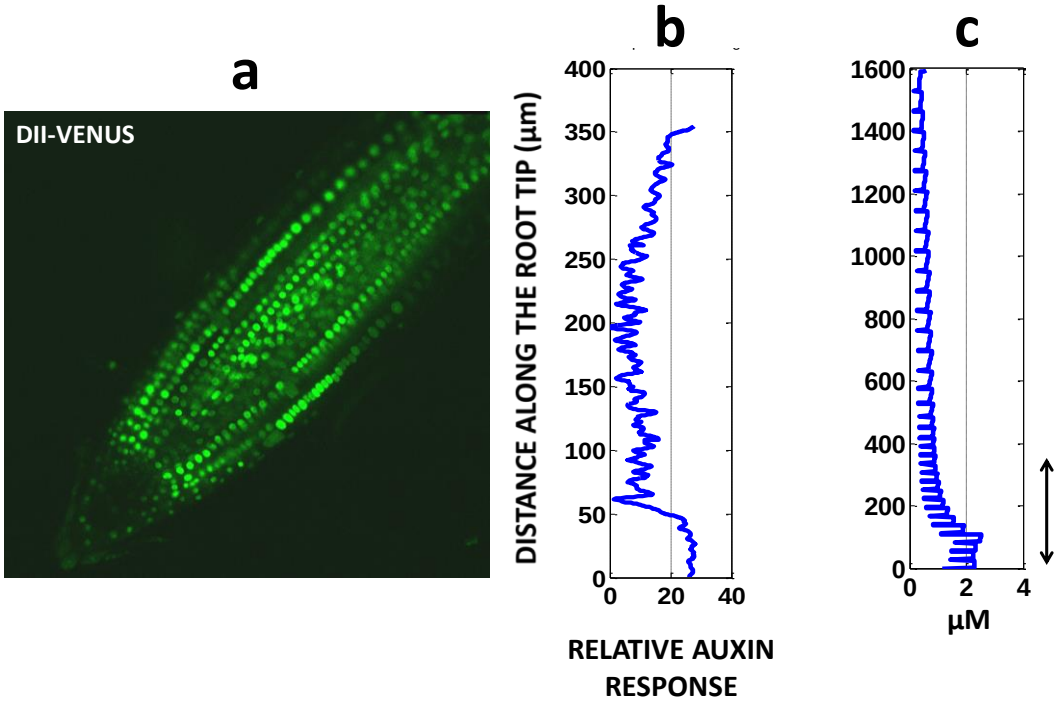

Figure 2.59: WT DII-VENUS response and model auxin profiles
(a) Experimental image of WT DII-VENUS response, (b) relative auxin response profile (inverse of DII-VENUS response) derived from the experimental image, (c) GG model WT auxin concentration profile. The experimental image profile approximately corresponds to the region in the model denoted by the arrow. Both profiles exhibit increased auxin in the QC region, but the experimental profile starts to increase at the 250 position along the root tip while the model does not.

It was also possible to compare experimental data (Figure 1K, Band *et al*., 2014) and model results on a 'cell-type' basis. The relative fluorescence of different cell types using the DII-VENUS reporter is shown in Figure 2.60.

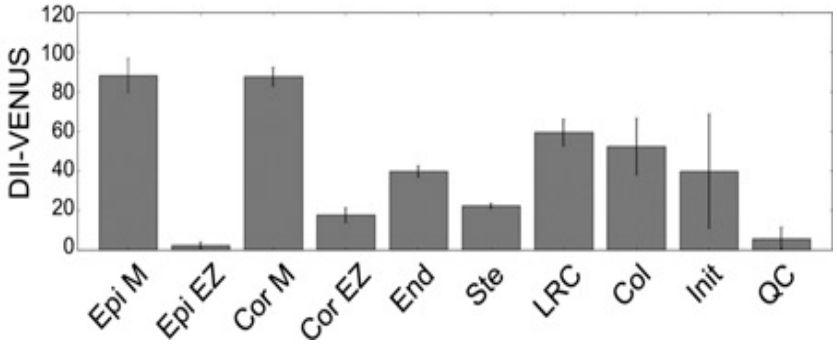

Figure 2.60: Measures of DII-VENUS levels in different cell types
Epi, epidermis; Cor, cortex; End, endodermis; Ste, stele; Col, columella; Init, columella initials; QC, quiescent centre; M, meristem; EZ, elongation zone (Figure 1K, Band *et al*., 2014)

Regions of the GG model root can be approximately mapped to the cell definitions used in Band *et al*. (2014), as follows. The model root map is 35 cells long with 10 cell files (Figure 2.61). The cell files are first classified into 3 'types' which are full root-length files and so can include columella and quiescent centre (QC) cells. There are 4 'epidermal' cell files (Type 1), 2 'pericycle/border' files (Type 2) and 4 'vascular files' (Type 3). The model root can also be divided into 4 'areas' (Figure 2.61), the QC, the elongation and meristematic (excluding the QC) zones, and the columella.

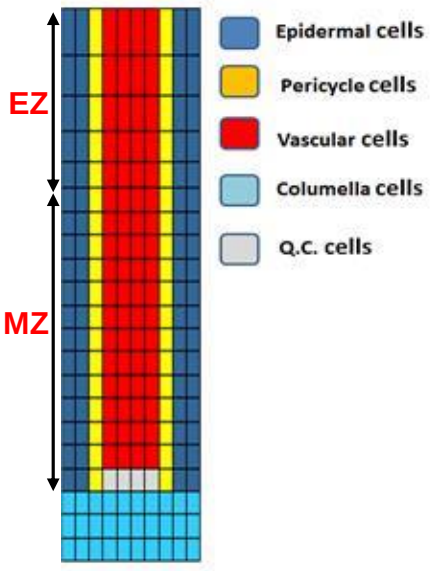

Figure 2.61: The GG model root map.
With gradual cell elongation from the MZ to the EZ
(MZ, meristematic zone. EZ, elongation zone. QC, quiescent centre)

Using combinations of 'Area' and 'Type' it was possible to define regions in the model root map which approximate to the cell types specified by Band *et al*. (2014). Since the root architecture in this paper was significantly more complex than the relatively simple structure used in the model, several approximations were necessary. The epidermis and cortex cells in the Band *et al*. (2014) paper were both mapped to the epidermis (Type 1) in the model, the endodermis in the paper was mapped to the pericycle (Type 2), the columella cells in the paper were mapped to the group of columella cells (included in Types 1, 2 and 3), and there was no match in the model for the columella initials or the lateral root cap. Table 2.6 shows the specific mapping of the model to the Band *et al*. (2014) cells using area/cell type combinations.

Table 2.6: Cell type mapping between experimental and model results

Cell type from Band *et al*. (2014)	Map to model cells, defined by type and area		
	Model cell code	**Root Area**	**Type 1, 2 or 3**
Epi M – epidermis, meristem	MZ T1	Meristematic zone	Type 1
Epi EZ – epidermis, elongation zone	EZ T1	Elongation zone	Type 1
Cor M – cortex, meristem	MZ T1	Meristematic zone	Type 1
Cor EZ – cortex, elongation zone	EZ T1	Elongation zone	Type 1
End – endodermis	MZ T2	Meristematic zone	Type 2
Ste – stele	MZ T3	Meristematic zone	Type 3
LRC – lateral root cap	LRC	No match	No match
Col – columella	COL T1-3	Columella	Type 1, 2 and 3
Init – columella initials	INIT	No match	No match
QC – quiescent centre	QC T3	QC	Type 3

The experimental DII-VENUS levels for different cell types (Figure 2.60) were converted into auxin response levels relative to the QC (set at 100) assuming an inverse relationship between auxin and DII-VENUS (Table 2.7). Average model auxin concentrations were calculated for corresponding regions within the model root map and the data scaled, with the QC again set to 100 (Table 2.7).

Table 2.7: Auxin DII-VENUS response and model data

(relative DII-VENUS fluorescence read from Figure 2.60; relative auxin response is the inverse of DII-VENUS fluorescence relative to the QC which is set at 100; average model auxin concentration is relative to the QC which is set at 100)

DATA DERIVED FROM Band *et al.* (2014)			MODEL DATA		
CELL TYPE	**RELATIVE DII-VENUS FLUORESCENCE**	**RELATIVE AUXIN RESPONSE (QC=100)**	**CELL CODE**	**AVERAGE MODEL CONCENTRATION (μM)**	**AVERAGE AUXIN CONCENTRATION (QC = 100)**
Epi M	85	6	MZ T1	0.73	21
Epi EZ	3	166	EZ T1	0.19	6
Cor M	85	6	MZ T1	0.73	21
Cor EZ	10	50	EZ T1	0.19	6
End	40	13	MZ T2	1.03	30
Ste	20	25	MZ T3	1.47	42
LRC	55	9	LRC	No match	No match
Col	45	11	CO T1-3	2.15	62
Init	35	14	INIT	No match	No match
QC	5	100	QC T3	3.48	100

The relative auxin response from Band *et al*. (2014) (Figure 2.62a) and the relative auxin concentrations from the model (Figure 2.62b) were then plotted in descending order of the Band *et al*. (2014) results, so that experimental and model trends could be easily compared.

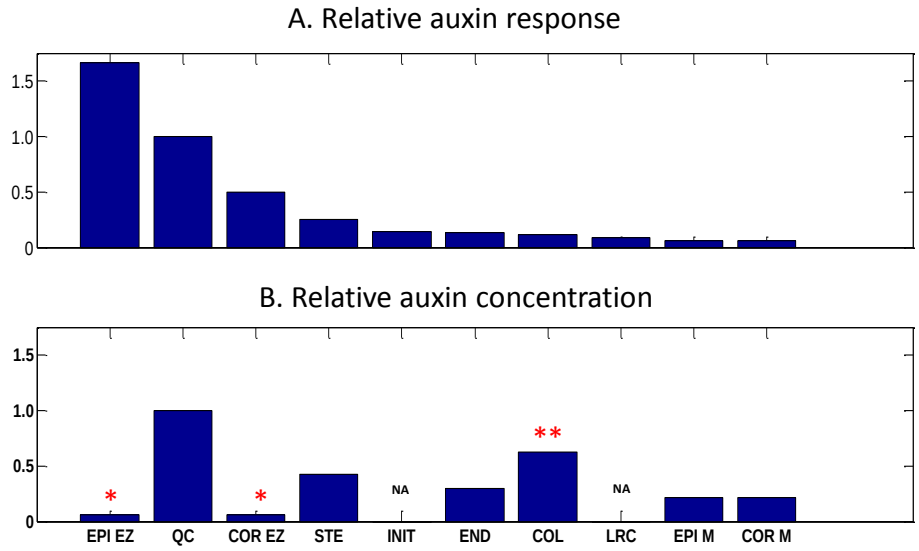

Figure 2.62: Auxin levels relative to QC (A) experimental (B) model.
* and ** indicate cell types where the model auxin level is below or above the experimental trend (Band *et al*., 2014). EPI, epidermis; COR, cortex; END, endodermis; STE, stele; COL, columella; INIT, columella initials; QC, quiescent centre; M, meristem; EZ, elongation zone; NA, data not available in modelling results.

The trend of the modelled auxin levels for 5 cell types (QC, stele, endodermis, epidermis meristem, and cortex meristem) is similar to the experimentally observed trend (Band *et al*., 2014); however, the model levels in the epidermis and cortex in the elongation zone (labelled ***** in Figure 2.62b) and the columella (labelled ****** in Figure 2.62b) are markedly different. These discrepancies between modelling results and experimental observations could be explained as follows.

DII-VENUS experimental levels rely on the rates of expression and decay of DII-VENUS. DII-VENUS expression is under the control of the *35S* promoter, while the rate of decay depends both on the levels of auxin and the auxin co-receptors TIR1 and AFB1-5 (Brunoud *et al*., 2012). Homogenous expression of *35S* and the auxin co-receptors is therefore necessary to allow representative comparison of relative auxin levels using the DII-VENUS reporter. It was reported that DII-VENUS fluorescence was ubiquitous in *tir1 afb1 afb2 afb3* quadruple mutant roots (where DII-VENUS is not subject to auxin regulated decay due to the mutation of *TIR1* and *AFB1)*, and that the quadruple mutant was also significantly less sensitive to auxin (Brunoud *et al*., 2012); however, the co-receptors *TIR1, AFB1* and *AFB3* were shown to have very low relative

expression in the columella and lateral root cap cells (Figure S5, Brunoud *et al*., 2012). This could result in a reduced rate of decay of DII-VENUS, a relatively high DII-VENUS response and therefore the underestimation of relative experimental auxin levels in these cell types, so accounting for the difference between the Band *et al*. (2014) and model results for the columella. Using a non-degradable reporter, mDII-VENUS, the *35S* promoter was shown to have significantly increased expression in the transition and elongation zones of the epidermis and cortex (Fig S6 A,B in Brunoud *et al*., 2012), which again could result in underestimation of relative experimental auxin levels in these areas. The DII-VENUS data in the literature (Band *et al*., 2014) suggest that auxin responses in the epidermis and cortex elongation zone are higher than all other regions of the root except the QC. Therefore, by taking into account the possibility of increased *35S* expression in these tissues, auxin responses in the epidermis and cortex elongation zone could possibly exceed those in the QC. This result is not apparent in experimental imaging using the auxin reporter IAA2::GUS (Figure 1.3). This discrepancy leads to a number of possibilities: (a) the non-degradable reporter, mDII-VENUS, does not fully reflect *35S* expression levels in the elongation and transition zones, (b) other unknown factors may suppress DII-VENUS in these zones or (c) there is additional suppression of the IAA2::GUS reporter in the transition and elongation zones resulting in variable reporter sensitivity to auxin in different regions of the root. As noted in Band *et al*. (2014) the higher auxin response derived using DII-VENUS data in the elongation zone brings into question the hypothesis that a gradual decrease in auxin levels from the QC maximum determines root developmental zones (Blilou *et al*., 2005; Grieneisen *et al*., 2007). After taking the above factors into account, the modelling results are in reasonably good agreement with experimental results derived using DII-VENUS data from Band *et al*. (2014).

DII-VENUS expression was also used to estimate and plot relative auxin trends for different cell layers in the meristematic zone (Figure 2.63; from Figure 2B, Brunoud *et al*., 2012). No attempt was made to plot auxin levels in the columella and root cap, possibly because of the low expression levels of the auxin co-receptors observed in these cell types, as previously discussed.

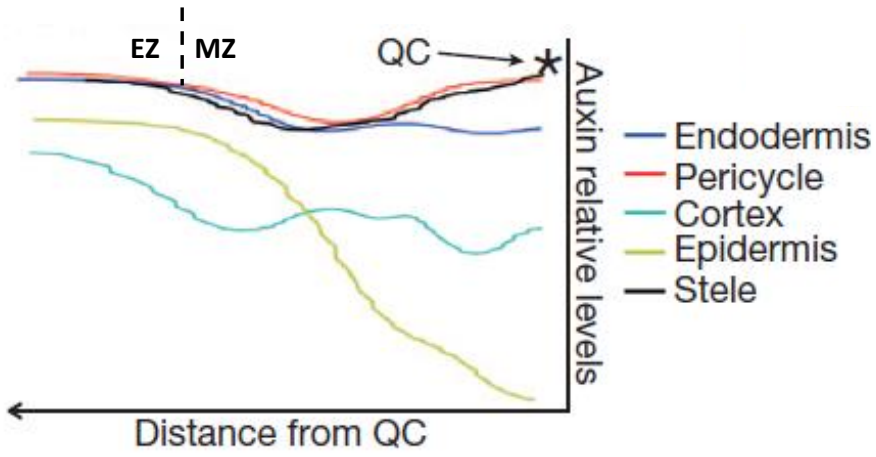

Figure 2.63: Relative auxin trends in different cell types.
QC, quiescent centre. MZ, meristematic zone. EZ, elongation zone
(Figure 2B, Brunoud *et al*., 2012)

Experimental and model auxin trends were compared for different cell types in the meristem proximal to the QC, using experimental data (Figure 2.63) and model data from Figure 2.58. Since the root architecture in the literature (Brunoud *et al*., 2012) is more complex than in the model, cell types are approximately matched using the following table.

Table 2.8: Matching experimental cell file data to the model

Cell type in the literature (Brunoud *et al*., 2012)	Corresponding model cell type
stele	vascular, meristem
endodermis and pericycle	pericycle, meristem
cortex and epidermis	epidermis, meristem

The models results (Figure 2.58) show that vascular, pericycle and epidermal cells have a high, medium and low auxin level, respectively. This trend is in agreement with experimental observations (Figure 2.63). Therefore, auxin

concentration patterning generated by the model, with an auxin maximum established at or close to the QC, is similar to both experimental IAA2::GUS and DII-VENUS response patterns.

2.8.2 Ethylene and cytokinin concentrations in the *pls* mutant

The accumulated concentration of cytokinin is described in the hormonal crosstalk network as the balance between its biosynthesis and its removal (Figure 2.9), with auxin negatively regulating cytokinin biosynthesis (Nordstrom *et al*., 2004). The model predicts that, in the *pls* mutant, the average endogenous cytokinin concentration for the root is increased to c. 1.9-fold of that in wild-type (Figure 2.64). Experimental measurements show that different cytokinins have significantly different fold changes, however, the general trend is that endogenous cytokinin concentrations in the *pls* mutant are significantly increased, with a median fold change of 1.42 (Table 1 in Liu *et al*., 2010). Experimentally it has been shown that *PLS* transcription does not affect ethylene concentration (Chilley *et al*., 2006). The GG model results (Figure 2.64) are therefore consistent with experimental observations.

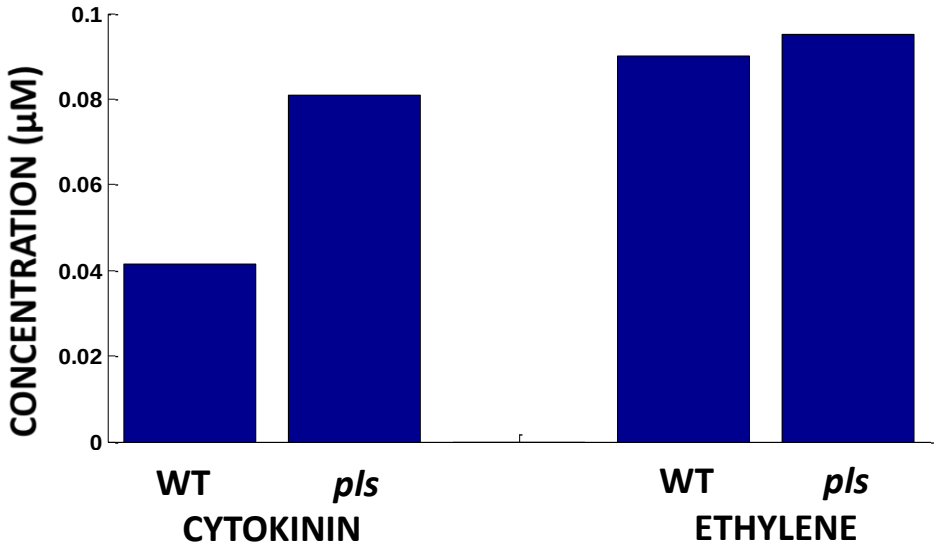

Figure 2.64: Model cytokinin and ethylene concentrations in WT and *pls*. Model results for average CK and ET concentrations in WT and pls are consistent with experimental results.

2.8.3 AUX1 patterning

The increased epidermal and cortical auxin response in the elongation zone compared to the meristematic zone indicated by DII-VENUS patterning (Figure 2.60; Figure 2.63) was suggested to be the result of tissue specific patterning of AUX1, supported by AUX1-YFP imaging (Figure 2.65) which shows high AUX1 levels in the lateral root cap, in the proximal meristematic and elongating epidermal cells and the elongating cortical cells. The Band *et al*. (2014) model originally assumed AUX1 patterning from the literature with AUX1 predominantly located in the epidermal elongation zone, the lateral root cap and the columella (Swarup *et al*., 2001; Swarup *et al*., 2005). Using a new AUX1::YFP reporter they showed that *AUX1* was also expressed in the elongating cortical cells. It was suggested that this expression pattern restricted flux between the outer layers and the stele, promoting increased auxin response in the elongating epidermal and cortical cells and shoot-ward auxin flux through the epidermis and cortex in the elongation zone. From their model results, they concluded that periclinal PIN placement had little effect on auxin reflux, that overall auxin distribution was not significantly affected by polar placement of PIN proteins and, while PIN protein polarity determined the direction of auxin flux, it was AUX1 levels that determined cellular auxin concentrations.

The experimental image (Figure 2.65) exhibits variable AUX1 concentrations and trends in different parts of the root, with high AUX1 levels in the lateral root cap, medium levels in the columella and surrounding the QC, proximally increasing levels in the epidermis and cortex, and proximally decreasing levels in what appears to be the pericycle or specific vascular cell files. In contrast, our model follows the Grieneisen *et al*. (2007) paper which does not include a root cap structure and assumes ubiquitous non-polar AUX1 placement, to which is added promotion of *AUX1* expression by ethylene signalling. Model results for AUX1 patterning (Figure 2.66) are in part similar to experimental imaging (Figure 2.65), with AUX1 levels increasing proximally in the epidermis, and higher AUX1 levels in the outer cell layers compared to the central cell cylinder. However the model does not exhibit the elevated experimental AUX1 levels in the columella and near the QC or the proximally declining AUX1 levels in the

central cylinder. In this work, AUX1 activity is positively regulated by downstream ethylene signalling based on experimental observation (Fig. 7B in Ruzicka *et al*., 2007). The differences between modelling and experimental results might indicate that, in addition to ethylene, other effectors also regulate AUX1 activity. Model results could possibly be enhanced by including a root cap structure and more realistic root geometry, allowing the investigation of tissue specific regulation of key components such as *AUX1* on hormonal cross-talk and patterning.

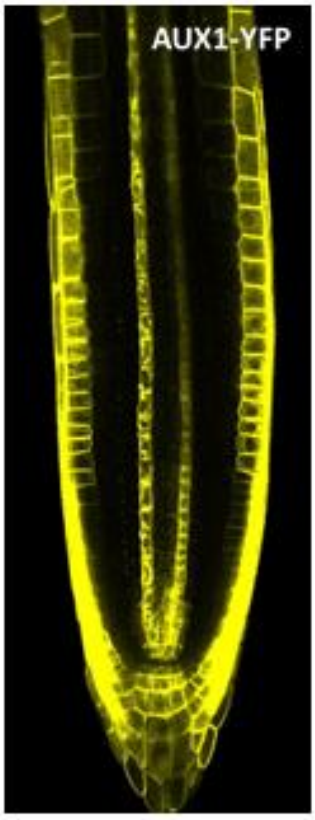

Figure 2.65: AUX1 experimental patterning
Localisation of AUX1 using AUX1::YFP reporter shows elevated AUX1 levels in the columella, lateral root cap, epidermal and cortical cells, with a proximally declining concentration in the central cylinder (Band *et al*., 2014)

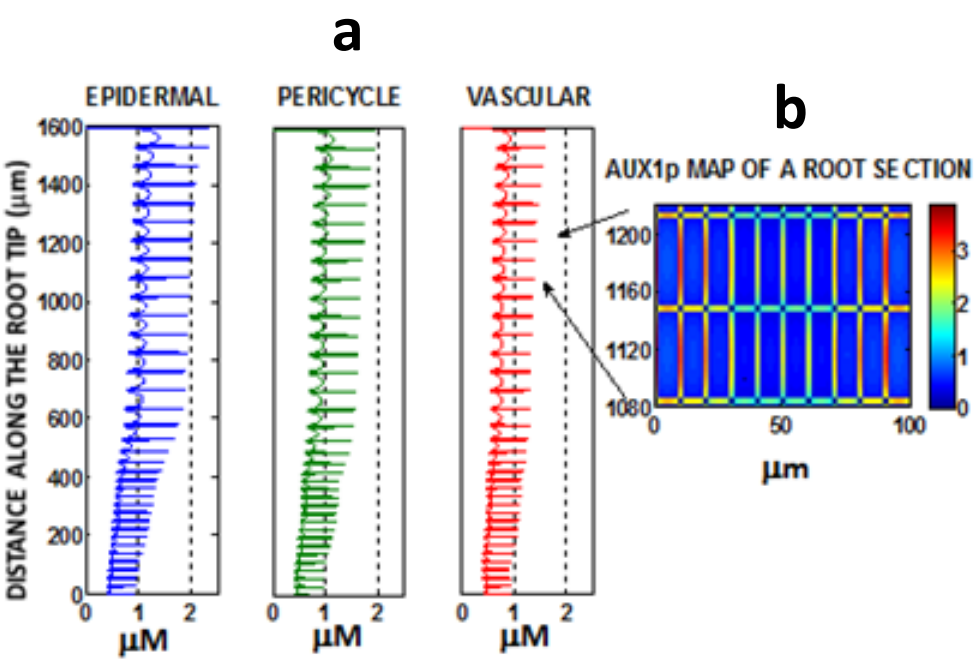

Figure 2.66: AUX1 model concentration profiles and image
(a) AUX1 concentration profiles for 3 regions; epidermal region includes the epidermal cell files extended to include the columella, similarly the pericycle region includes columella cells, and the vascular region includes QC and columella cells (b) colour map image of a root section (colour map units μM)

2.8.4 PIN profiles in the GG root model

The effect of the sudden change in cell length at the MZ/EZ boundary in the original root model can be seen in the PIN profiles (Figure 2.52B, Figure 2.54B), which show a sudden slight increase in PIN average cell concentrations at the point where cell lengths increase at the MZ/EZ boundary. Trends in PIN profiles for the vascular/pericycle cell files in the GG model (Figure 2.67) were unchanged from the previous model (except for a smoothing of the increase in PIN concentration observed at the MZ/EZ boundary in the original root model) and are in general similar to PIN1 trends generated from the images (apart from the *pls ert1* double mutant).

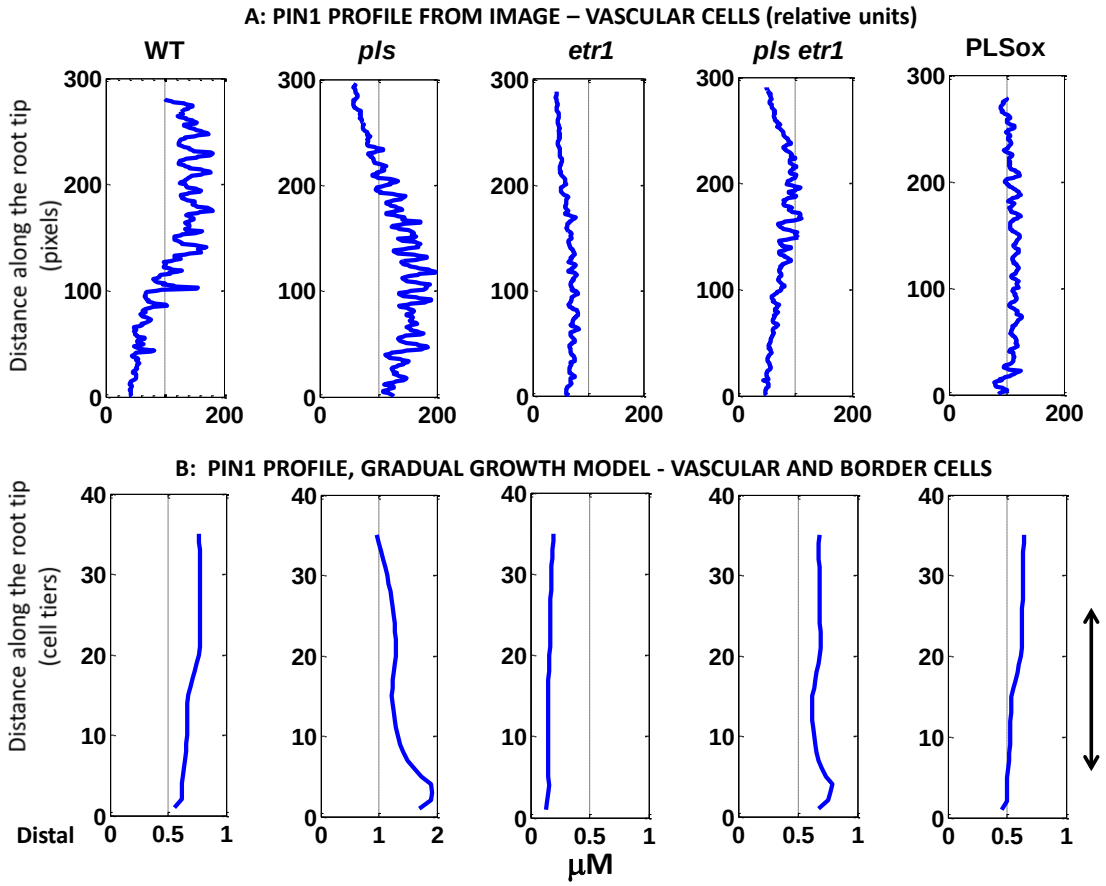

Figure 2.67: PIN1 concentration profiles (A) experimental (B) model
Experimental profile generated using Figure 2.51 and ImageJ; model and experimental results are similar except for the double mutant; the arrow denotes the region of the model plot that corresponds to the images. The model profiles are similar to the previous model except for a smoother increase at the MZ/EZ boundary.

Modelling analysis further revealed that PIN1 patterning in wild-type, mutant and PLSox transgenic roots reflect changes in the *PIN1* transcription rate resulting from different contributions of auxin, ethylene and cytokinin. For example, modelled PIN1 patterning in the wild-type shows that the level of PIN1 generally decreases from the proximal region to the distal region of the root; however, in the *pls* mutant, an opposite trend emerges (Figure 2.67B). Model calculations show that, in the *pls* mutant, the *PIN1* transcription rate significantly increases at the region near the root tip (Figure 2.68). Further analysis reveals that, in the wild-type, the downstream component of ethylene signalling, designated X, is suppressed as a result of the action of PLS at the region near the tip (Figure 2.69), due to an increasing PLS concentration from the proximal to the distal end of the root, predominantly as a result of the positive regulation

of *PLS* expression by auxin (Figure 2.69; also see section 2.7.3 '*POLARIS (PLS)* expression pattern'). In the *pls* mutant, the suppression of X is relaxed owing to the loss of PLS function. This enhances the rate of PIN1 biosynthesis at the region near the tip and therefore PIN1 patterning shows an increasing concentration trend from the proximal to the distal region. In addition, in the *pls* mutant, auxin concentration decreases (Figure 2.12) and cytokinin concentration increases (Figure 2.64). As auxin positively regulates, and cytokinin negatively regulates *PIN1* transcription, the increase in *PIN1* transcription rate at the region near the tip also reflects the relative effects of both auxin and cytokinin signalling. Therefore, the combined contribution of auxin, ethylene and cytokinin result in opposite trends in PIN1 patterning in wild-type and *pls* mutant roots. This example demonstrates that spatiotemporal hormonal crosstalk, which describes simultaneous actions of multiple hormones and the associated genes, is necessary for specifying the patterning of PIN1 in the root. Figure 2.67 further shows that the modelled patterning trend of PIN1 for wild-type, *pls, etr1* and PLSox is similar to the corresponding experimental trend. However, a noticeable difference for the *pls etr1* double mutant can be identified. This indicates the current limitation of the model for analysing this double mutant.

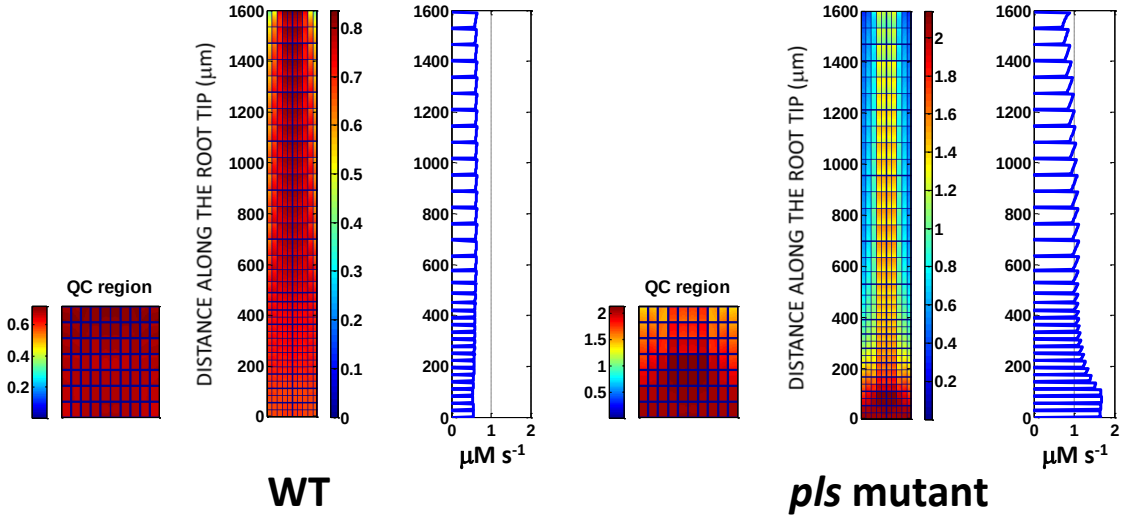

Figure 2.68: Model results for *PIN* transcription rate in WT and *pls*
The *pls* mutant shows significantly increased *PIN* transcription in the distal root compared to WT.

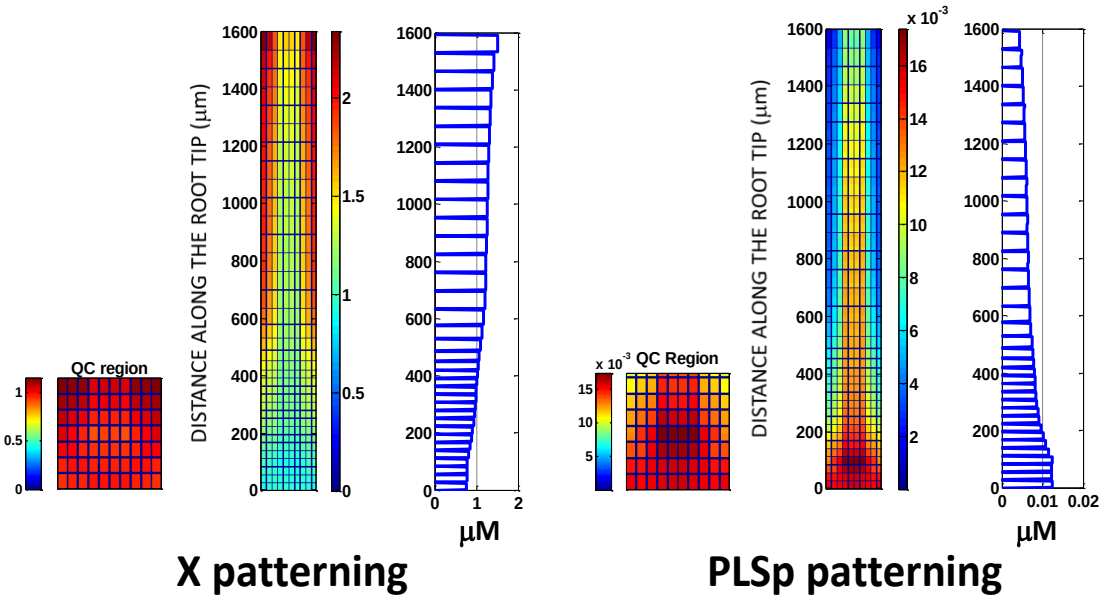

Figure 2.69: Model WT pattern of X (downstream ET signalling) and PLSp Exhibits the inhibition of X (downstream ET signalling) by high PLS protein concentration in the distal root.

2.8.5 PIN and AUX1 permeability and auxin patterning

Additional work was done using the GG model to investigate relationships between PIN and AUX1 permeability and WT auxin patterning. Manually adjusting (unknown) PIN and AUX1 permeability parameters reveals that both PIN and AUX1 permeability must be restricted to certain ranges in order to generate a model auxin concentration patterning that is similar to experimental IAA2::GUS response patterning. For example, if both PIN and AUX1 permeability are low, the auxin gradient towards the distal region of the root is gradually smoothed out due to reduced auxin transport through the root, and if PIN permeability increases, an increase in AUX1 permeability is required to maintain similar auxin patterning to experimental data (Figure 2.70).

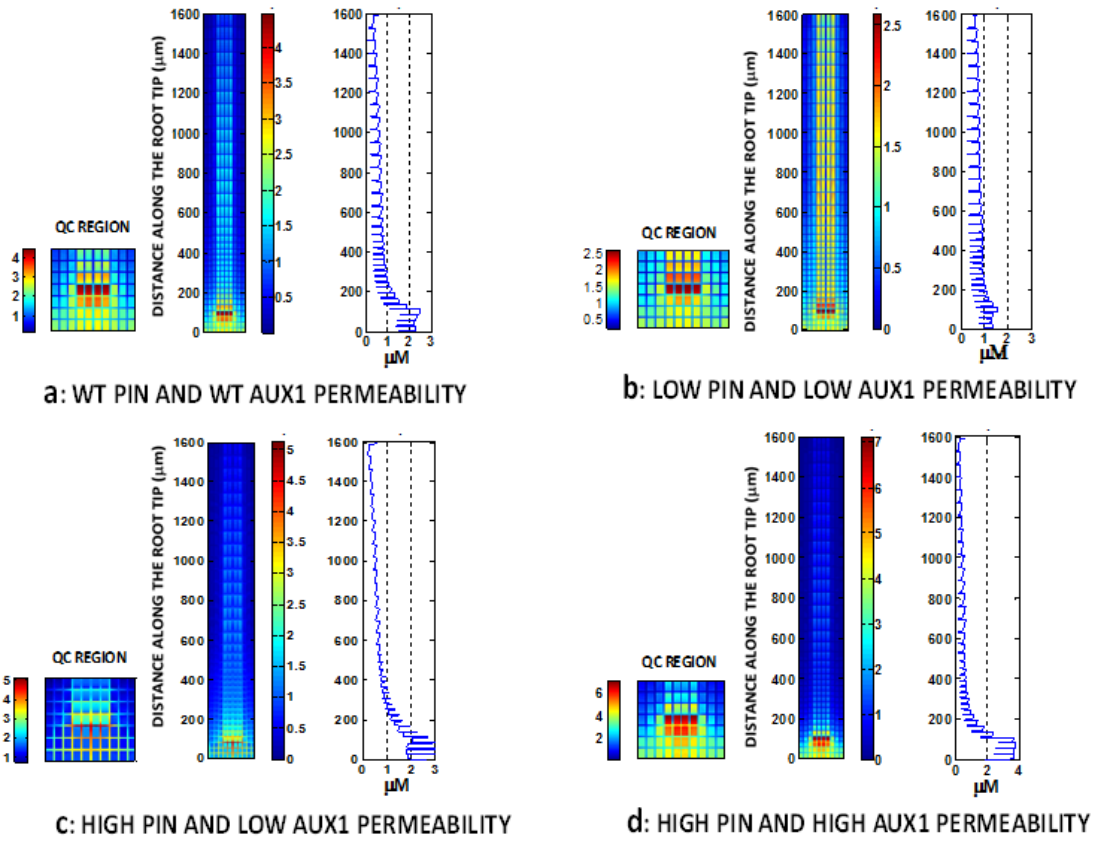

Figure 2.70: Auxin patterning for different PIN and AUX1 permeabilities
(a) Auxin patterning for WT PIN, AUX1 permeability (b) low PIN and AUX1 permeability reduces the auxin maximum (c) high PIN and low AUX1 permeability drives auxin into the cell wall and reduces the cytosolic maximum in the QC (d) high PIN combined with high AUX1 permeability rescues auxin maximum (colour bar units, μM).

Although the auxin gradient has been hypothesized to be sink-driven (Friml *et al*., 2002) and computational modelling has suggested that auxin efflux carrier permeability may be sufficient to generate the gradient (Grieneisen *et al*., 2007; Wabnik *et al*., 2010), recent work shows that AUX1 is also essential to create the auxin gradient at the root tip (Band *et al*., 2014). The above modelling results support the view that both PIN and AUX1 permeability work together to generate auxin patterning. If AUX1 permeability is not varied in the model such that it becomes a limiting factor for auxin transport, the importance of AUX1 permeability for generating an auxin gradient cannot be revealed, as demonstrated in a previous study where the effects of varying AUX1 permeability were not reported (Grieneisen *et al*., 2007). The combined roles of the auxin efflux and influx carriers in establishing auxin patterning are further investigated in Chapter 4.

2.9 Summary

2.9.1 WT Parameter calibration matched most fit criteria

The single cell model was embedded into a multicellular root structure to produce a 2-D spatial root model of hormonal crosstalk and gene expression. Parameters were initially set at values established in the multicellular root and single cell models and then calibrated either by reference to the literature (for certain diffusion and permeability constants) or by matching experimental results to fit criteria (in particular auxin concentration trends in mutants and auxin patterning) to produce a WT parameter set.

For the selected WT parameter set, the model matched most fit criteria. The average auxin WT root concentration was similar to experimental data. Experimental auxin concentration trends for WT and *pls, pls etr1* mutants and the PLSox transgenic compared favourably to model results (Figure 2.11, Figure 2.12) and, although the *pls etr1* double mutant in the model did not exhibit recovery to near WT values as observed experimentally, model results did show that auxin concentration in the *pls etr1* double mutant was higher than in *pls*, therefore the trends are qualitatively correct. These quantitative differences between model and experimental auxin concentration may possibly be due to the fact that the experimental results were for whole seedlings and not for separated roots and shoots (Chilley *et al*., 2006), especially since additional data in this paper for separated WT root and shoots showed significant variations in root and shoot concentrations depending on the age of the plant, with WT root concentrations being more or less than shoot concentrations depending on age. Also there are 5 ethylene receptors which are not functionally equivalent and can act in dimers and clusters with CTR1, with possible crosstalk between clusters (Yoo *et al*., 2009; Mayerhofer *et al*., 2012), making it difficult to model the overall effect of the *etr1-1* (gain-of-function, ethylene insensitive) mutant by just one variable in the model.

Experimental auxin response images compared favourably with modelled concentration colour maps and the concentration profiles derived from the experimental images matched model results (Figure 2.13).

In the model, auxin carrier proteins PIN and AUX1 were predominantly located to the plasma membrane which was consistent with experimental results (Figure 2.16). However, AUX1 patterning only partially matched experimental results (Figure 2.65, Figure 2.66) possibly indicating that additional factors regulate *AUX1* expression, as indicated by a recent paper proposing that cytokinin inhibits *AUX1* (Street *et al*., 2016).

The trend in average CK root concentration in the WT and *pls* mutant (Figure 2.64) was similar to experimental results. The lateral CK concentration trends across the root showed interesting similarities, with CK maxima observed in the region of the border/pericycle cell files in both the model and the image (Figure 2.17). These results could possibly be due to a combination of minimal CK biosynthesis in the epidermal/cortical cell files with suppression of CK biosynthesis by higher auxin concentrations towards the centre of the vascular cylinder.

The CK concentration profile produced by the model did not match the longitudinal concentration trends in profiles derived from experimental images (Figure 2.17). The modelled longitudinal CK concentration profile increased with distance towards the proximal end of the root tip, presumably due in part to reduced suppression of CK biosynthesis by auxin, whereas in experimental images there is a decrease in the concentration with distance up the root tip.

In this version of the model CK inhibits auxin biosynthesis and auxin inhibits CK biosynthesis (Nordstrom *et al*., 2004). However additional results (Jones *et al*., 2010) seem to indicate a different relationship where CK promotes auxin biosynthesis in young developing tissues and CK inhibits its own biosynthesis through the induction of CK oxidases.

In previous work (Liu *et al*., 2013), hormonal crosstalk network analysis revealed that both sets of experimental results (Nordstrom *et al*., 2004; Jones *et al*., 2010) can be incorporated into the network, leading to the same conclusions about other regulatory relationships of hormonal crosstalk. Later on in this work, CK patterning is examined in greater detail and both cases are analysed with similar modelling results. Therefore, the conclusions drawn from this work are applicable to both cases and questions surrounding CK and auxin interactions

do not necessarily detract from other model results. The above results do however suggest that there are additional regulatory factors controlling CK patterning (see Chapter 5) and, although auxin patterning appears to be relatively insensitive to the CK and auxin relationship assumptions, given the developmental importance of both CK and auxin, it will be essential to develop an experimentally based model with improved CK patterning to enhance the predictive capabilities of the model.

2.9.2 The model proved robust to variations in the WT parameter values

Model parameters were initially set to values taken from the Grieneisen *et al*. (2007) and Liu *et al*. (2013) models. While certain parameters for diffusion and permeability were adjusted to match data from the literature, most of the WT parameter values used in the model were unknown and difficult or impossible to verify experimentally. It is therefore important to test whether the model results are heavily dependent on specific (and unknown) parameter values. Testing was performed on a number of parameters to see if the model was overly sensitive to variation in values around the WT. The model was tested for changes in diffusion rates, auxin decay, and tissue specific CK biosynthesis which resulted in changes in CK concentration. The diffusion constants and the rate of expression for *AUX1* and *PIN* were also varied to test the sensitivity of auxin patterning to modifications in parameter values for these auxin transport proteins.

Changes to the auxin diffusion constant around the WT had minimal effect on average auxin concentrations and auxin patterning, except at very low diffusion rates when auxin transport was minimal and patterning did not occur. Changes to the CK and ET diffusion rates had even less impact on auxin concentrations and patterning than the auxin diffusion rate.

The PIN protein diffusion rate affected the proportion of PIN proteins at the plasma membrane compared to the cytosol. At very low diffusion rates PIN proteins were predominantly localised to the cytosol, limiting auxin transport and preventing the formation of the auxin maximum. As the diffusion rate increased, PIN at the plasma membrane increased which in turn increased the rate of auxin efflux and the strength of the auxin maximum. The auxin maximum was

formed over a wide range of PIN diffusion values around the WT value. Similarly the localisation of AUX1 to the plasma membrane was reduced at low AUX1 diffusion rates; however, the formation of the auxin maximum was very robust to changes in the AUX1 diffusion rate indicating that the concentration of PIN at the plasma membrane is the limiting factor for auxin pattern formation in the model. This is believed to be in part a result of our assumptions on AUX1 and PIN permeability rates, based on the literature, where AUX1 permeability is greater than PIN permeability.

The coordinated rates of expression of *PIN* and *AUX1* control auxin transport through the root. The relative expression of these transport proteins determines the proportion of auxin in the cytosol compared to the cell walls, with high relative *PIN* expression driving auxin into the cell walls and high relative *AUX1* expression retaining auxin in the cytosol. The importance of the coordinated activity of these transport proteins is demonstrated in the model by the rescue of *PIN* overexpression by the overexpression of *AUX1*. Again the model showed relatively robust behaviour to variation in expression rate parameter values around the WT.

Given the previous discussion on CK patterning and the interactions between CK and auxin, it was critical to test the sensitivity of the model to changes in CK parameter values. Auxin patterning proved very robust to changes in parameters controlling CK diffusion, tissue specific biosynthesis and the resulting CK concentration changes.

Auxin decay rates were also tested and auxin patterning was still maintained at decay rates of 50% and 200% of WT.

In summary the results showed that the model does not rely on a specific set of WT parameter values and it is possible to define multiple WT parameter sets that meet the fit criteria and produce correct predictions. Therefore the model is robust since it does not depend on a unique set of parameter values that could not be experimentally verified.

2.9.3 Model sensitivity to changes in cell length

The root structure defined by Grieneisen *et al*. (2007) contained a sudden change in cell length from 28 to 64 μm as cells moved from the MZ to the EZ. This produced a sharp change in average cell concentrations in the PIN concentration profiles. A more realistic version of the model root map was developed to simulate a gradual increase in cell length in this transition zone, with no effect on overall patterning apart from smoothing the profiles for average PIN cell concentration through the transition zone. This result could indicate that the model is relatively insensitive to cell size; however, more extensive simulations would be required to provide confirmation and this is effectively addressed in Chapter 3 with the introduction of a realistic root structure.

2.9.4 The model explains most concentration trends and patterning

After completion of parameter calibration, simulations were performed to test if the model could explain/predict additional concentration trends and patterning. While the model matched observed auxin patterning and profiles, and to a large degree the concentration trends for mutants, and also importantly the high concentrations of the auxin carrier proteins PIN and AUX1 at the plasma membrane compared to the cytosol in the WT model (matching the localisation of PIN and AUX1 observed in experimental images), these results could not be used to measure the predictive capability of the model since they were used as part of the initial calibration process.

The observed trend of auxin flux from shoot to root for different mutants was matched by the model except that results for the double mutant *pls etr1* were slightly high compared to WT; however, double mutants tend to be very difficult to model, particularly with multiple ET receptors and complex ET signalling.

ET and PLS experimental images were scanned and model concentration profiles compared very favourably with profiles derived from the images. Images of auxin response patterning in the WT and *aux1* mutant were also scanned and the experimental auxin response profiles matched model concentration profiles.

Model results for PIN root concentrations for different mutants largely matched the concentration trends observed experimentally, especially when error bars are taken into account.

PIN1 and 2 images for the WT, *pls, etr1, pls etr1* mutants and the PLSox transgenic were scanned to test how PIN1 and 2 concentration profiles compared to model PIN profiles for the vascular cylinder (for PIN1) and the epidermal layers (for PIN2). The model profiles for PIN in the vascular cylinder were a reasonable match to the PIN1 profiles generated from the images; however, the PIN2 profiles only matched for WT and the PLSox transgenic. This could in part be due to the relative ease of scanning images in the vascular column compared to scanning external cell layers and then combining the data, or be due to the fact that the model only contained a single generalised PIN protein rather than representing different types of PIN proteins located in different cell types in the root. Possibly a more complex model of the PIN proteins and their positioning and individual regulation would give a better match between the model and experimental results.

CHAPTER 3 : DEVELOPMENT OF AN ANATOMICALLY REALISTIC MODEL ROOT

DEVELOPMENT OF AN ANATOMICALLY REALISTIC MODEL ROOT

3.1 Introduction

A major challenge in plant developmental biology is understanding how development is coordinated by interacting hormones and genes. The regulated formation of auxin gradients provides a key mechanism controlling plant growth, tropisms and development through the provision of positional and vectorial information (Vanneste and Friml, 2009). *Arabidopsis* root development is coordinated via an auxin concentration maximum in the root tip (Sabatini *et al*., 1999). The auxin maximum specifies the hypophysis and quiescent centre (QC), regulates root meristem formation, and positions the stem cell niche (SCN) (Sabatini *et al*., 1999). An auxin minimum also defines a developmental window for lateral root initiation (Dubrovsky *et al*., 2011), while transport of auxin produced in a new lateral root primordia regulates lateral root emergence (Peret *et al*., 2013). Low rates of polar auxin transport balance cell differentiation and division to prevent meristem growth, while high polar auxin transport promotes cell division over differentiation (Moubayidin *et al*., 2010). These and many other studies show that understanding the quantitative properties of auxin patterning is essential for understanding the regulation of root development.

The work so far has been based on a relatively simple rectangular root map, with AUX1, PIN1 and PIN2 placement consistent with Grieneisen *et al*. (2007). The next logical step was to replace the original rectangular root map with a more anatomically realistic digital root map based on experimental imaging. The realistic root includes additional cell files and cell types, with varying cell lengths and widths, which more accurately represents the cell geometry of the root tip and, in particular, includes a lateral root cap which experiments have shown to be important for transporting auxin from the distal region to the elongation zone (Swarup *et al*., 2005; Band *et al*., 2014). Development of a realistic root map achieves several goals by:

- testing if the initial model patterning results were dependent on the rectangular root architecture,

- allowing experimental data to be used to more accurately place the auxin influx and efflux carriers and to introduce additional carriers such as PIN3, PIN4, PIN7 and LAX2 and LAX3 into the auxin transport system,
- supporting the definition of an improved wild-type root model to match wild-type experimental results and,
- in particular, enabling more accurate comparison between modelled patterning results and experimental imaging of hormonal response, gene expression and protein concentrations, by cell groups, cell layers or tissue type.

3.2 Realistic root cell geometry

The digitised root structure was based on an image (Figure 3.1a) downloaded from www.simuplant.org (Band *et al*., 2014) which was originally generated from confocal image stacks of roots stained with propidium iodide to define root geometry and cell organization. Software (SurfaceProject) was developed (Band *et al*., 2014) to process the confocal image stack data to produce the image of a 2-D root structure, showing individual cells, cell layers and cell types (Figure 3.1b).

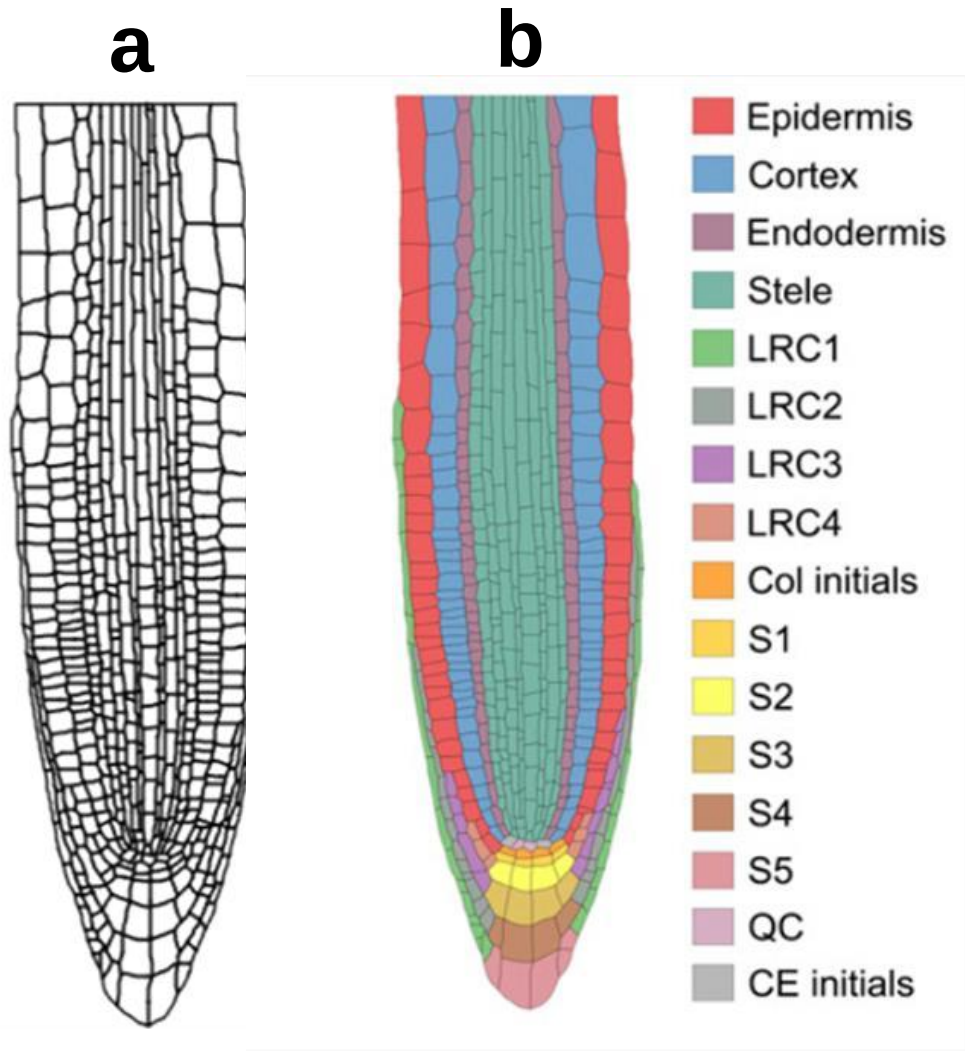

Figure 3.1: (a) SimuPlant Image (b) Root structure

2-D root structure based on confocal image data; LRC lateral root cap; S1 to S5 columella; Col columella; CE cortical endodermis; QC quiescent centre (Band *et al*., 2014)

The SimuPlant image (Figure 3.1a) was initially downloaded and then digitised by scanning with ImageJ and the grid point data saved as a Microsoft® Excel file. The scanned image produced an initial digital root map which contained multiple imperfections and discontinuities in the cell wall structures. To correct these, a series of error-checking MATLAB® programs was developed. The digital map was first searched for discontinuities in the cell walls which were corrected by interpolation from the break in a wall along points of weak ImageJ signal until another wall point was encountered. The revised digital map was searched again, using the MATLAB® program tool-kit, for abnormal groups of cell wall grid points (GPs) and discontinuities, which were identified and

removed. These processes were repeated several times since it was possible for the correction of one type of error to create another. The resulting file was formatted to highlight the cell walls to allow a visual check of the digitised root for remaining abnormalities or discontinuities. Finally all cytosolic GPs were coded to 0 and cell wall GPs to 1, with GPs outside the root set to 9 and then the digital map was visually checked against the 2-D root structure from Band *et al*. (2014) (Figure 3.1b). The next step was to create an individual cell wall for each cell. This was achieved by duplicating all cell wall GPs and then replacing the double wall at the exterior of the root with a single wall. The resulting root map was again searched for larger blocks of cell wall GPs which were each individually checked and corrected as necessary. The final map was visually checked for any wall discontinuities or abnormalities and a few manual adjustments made. In the resulting root map, some cell wall GPs were adjacent to cytosolic points, having a nearest neighbour (NN) cytosolic point to the N, S, E or W. Other wall GPs did not have a NN cytosolic point, especially at multiple cell junctions, and could therefore be considered as forming an extra-cellular space. Figure 3.2 compares the digital realistic root generated using the above procedures with the root structure from Band *et al*. (2014) which was generated from confocal image stacks. As can be seen, the final digital realistic root map is a good representation of the root structure generated from confocal imaging. The above procedures could be used to convert any scanned cell structure image, such as Figure 3.1a, into a digital map.

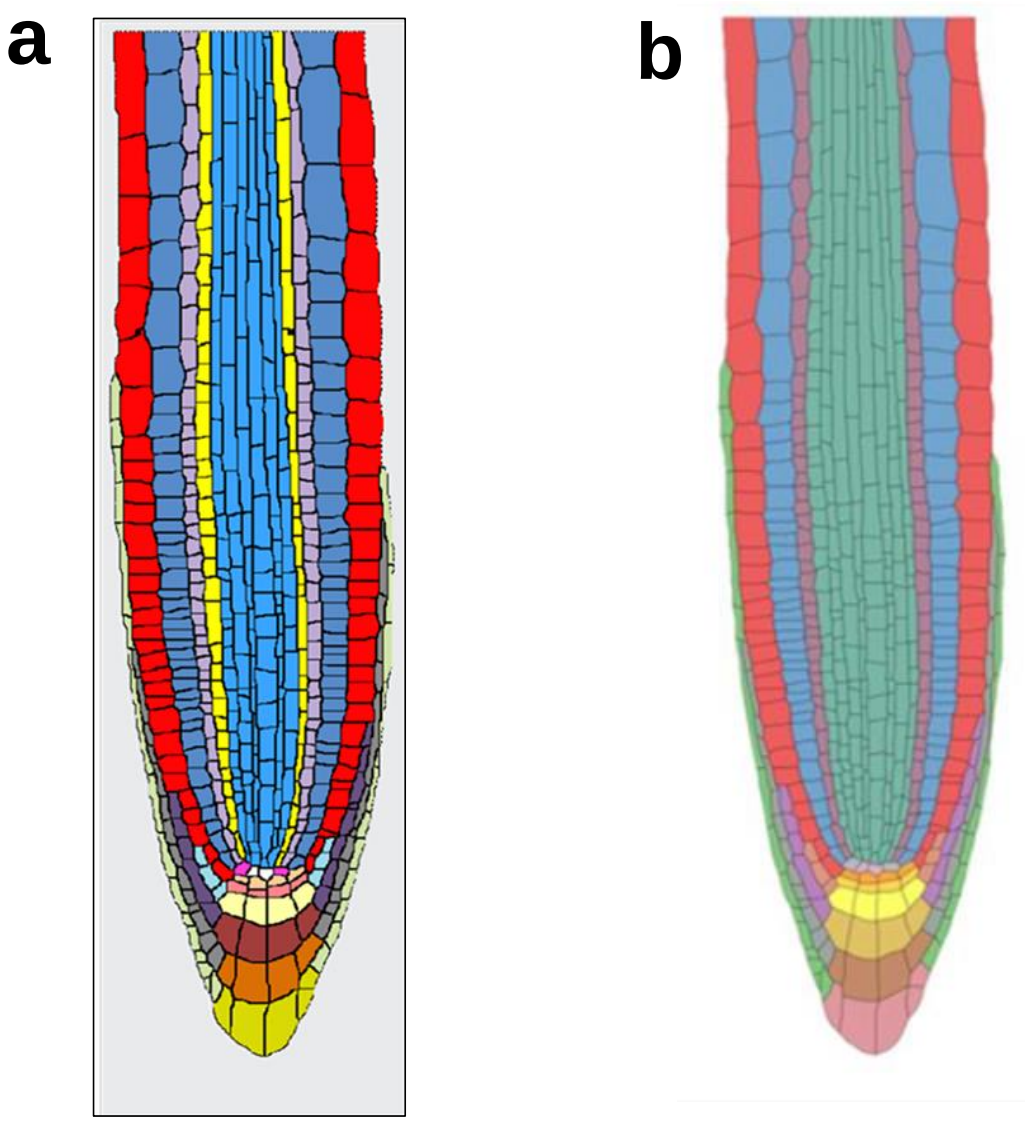

Figure 3.2: (a) Digital realistic root (b) Root structure (Band *et al*., 2014)
The digital realistic root is very similar to a root structure derived from confocal imaging. (colouring is to assist in comparison of cell layers and tissues)

The above process resulted in a final digital root map matrix containing 374,900 grid points defining 501 cells. Having set up the basic root map, it was then necessary to assign properties to the individual GPs within the map; for example defining auxin carrier properties to each GP at the plasma membranes of each cell, for each influx or efflux carrier. To facilitate this process mirror root maps were generated to define the properties of each auxin carrier. Given the need to be able to easily set up and then revise these mirror root maps, and given the number of GPs in the root matrix, it was necessary to develop a tool-kit of MATLAB® programs to allow efficient (and accurate) definition and map revision. In addition it was important set up the GP data such that it was

possible to analyse subsequent model results not only for the whole root but also by individual cell, cell layer or group of cells. To achieve this, an additional 'cell-number' map was established where each cell was allocated an individual number, which was assigned to each cytosolic GP within the cell. The cell numbers used (and available) for each cell type are summarised in Table 3.1.

Table 3.1: Numbers assigned to each cell in the root map
(NA – not applicable)

	Description of cell type (Figure 3.1**b)**	**Total number of individual cells (right, left sides)**	**Available number range for cells at right side of root**	**Available number range for cells at left side of root**
1	QC	2, NA	100-104	NA
2	Cortical endodermal (CE) initials	2, NA	105-109	NA
3	Columella initials	4, NA	100-119	NA
4	Columella S1	4, NA	120-129	NA
5	Columella S2	4, NA	130-139	NA
6	Columella S3	4, NA	140-149	NA
7	Columella S4	4, NA	150-159	NA
8	Columella S5	5, NA	160-169	NA
9	Lateral Root Cap (LRC1)	12, 16	200-219	220-239
10	LRC2	12,14	250-269	270-289
11	LRC3	8,5	300-319	320-339
12	LRC4	3,3	350-369	370-389
13	Epidermis	28,31	500-549	550-599
14	Cortex	38,41	600-649	650-699
15	Endodermis	39,42	700-749	750-799
16	Pericycle	23,33	800-849	850-899
17	6 Vascular cell files			
	(a) Outer pair	21,26	900-949	950-999
	(b) Middle pair	23,22	1000-1049	1050-1099
	(c) Inner pair	19,16	1100-1149	1150-1199
	TOTAL NUMBER OF CELLS	**501**		

In the cell-number map, the plasma membrane for each cell was divided into 4 regions defining the apical, basal, and left and right lateral cell faces. The combination of cell-number and cell-face data allows MATLAB® programs to be used to assign auxin carrier properties by cell type, cell number and cell face and also enables reports to be generated on a cell level or even cell face basis, as shown in later results. The cytosolic GPs within each cell are assigned a unique number (Table 3.1) and each cell-face plasma membrane GP is assigned a number indicating whether it is part of the right lateral (5), basal (6), left lateral (7) or apical face (8). A sample of the 'cell-number' map showing data for one of the QC cells (number 100) is shown in Figure 3.3.

1071	5	7	1118	1118	1118	1118	1118	1118	1118	5	7	920	920	920	920
6	5	7	1118	1118	1118	1118	1118	1118	1118	5	7	920	920	920	920
1	1	7	1118	1118	1118	1118	1118	1118	1118	5	7	920	920	920	5
1	1	7	6	6	6	6	6	6	6	5	7	6	6	6	5
7	8	8	8	8	8	8	8	8	8	8	8	8	8	8	5
7	100	100	100	100	100	100	100	100	100	100	100	100	100	100	5
7	100	100	100	100	100	100	100	100	100	100	100	100	100	100	5
7	100	100	100	100	100	100	100	100	100	100	100	100	100	100	5
7	100	100	100	100	100	100	100	100	100	100	100	100	100	100	5
7	100	100	100	100	100	100	100	100	100	100	100	100	100	100	5
7	100	100	100	100	100	100	100	100	100	100	100	100	100	100	5
7	100	100	100	100	100	100	100	100	100	100	100	100	100	6	5
7	100	100	100	100	100	100	100	100	100	100	100	100	6	6	8
7	6	6	100	100	100	100	100	100	100	100	100	100	6	8	8
8	8	6	6	100	100	100	100	100	100	100	100	6	6	8	111
112	8	8	6	6	6	100	100	100	100	100	6	6	8	8	111
112	112	8	8	8	6	6	6	100	100	6	6	8	8	111	111
112	112	112	112	8	8	8	6	6	6	6	8	8	111	111	111
112	112	112	112	112	112	8	8	5	7	8	8	111	111	111	111
112	112	112	112	112	112	112	112	5	7	111	111	111	111	111	111

Figure 3.3: Example cell-number data for QC cell 100
(100) - cytosol GP values for cell number 100; plasma membrane GP values defining cell faces, (5) - right lateral cell face, (6) - basal face, (7) - left lateral face and (8) - apical face

3.3 Placement of the auxin carriers in the realistic root

Localisation of PIN efflux (PIN1,2,3,4,7) and AUX1/LAX influx carriers (AUX1, LAX2,3) at the plasma membrane (PM) is derived from experimental imaging and implicitly includes ABCB transporter activity. Since the ABCB family can reversibly redirect auxin flux (Yang and Murphy, 2009), it is assumed that ABCB activity can be incorporated into the basal activity of all PIN proteins and AUX1/LAX influx carriers. The base level (lowest) activities for both efflux and

influx carriers are non-polar and it is assumed that the lowest levels of PIN proteins implicitly include the efflux activities of both PIN and ABCB and similarly the lowest level of AUX1/LAX includes the influx activites of AUX1/LAX and ABCB.

PIN (PIN1,2,3,4,7) carrier polarity definitions are based on experimental data. In the cytosolic spaces, the crosstalk network controls metabolism of two efflux carriers (PIN1 and PIN2) and the hormones auxin, ethylene and cytokinin. The network allows quantitative description of PIN1 and PIN2 regulation by the three hormones and enables study of the relationship between auxin, PIN1 and PIN2 patterning. The crosstalk networks for other auxin carriers (PIN3,4,7 and AUX1, LAX2,3) cannot be constructed due to insufficient experimental data, as discussed later in sections 3.3.2 and 3.3.3, therefore the localisation and levels of these carriers are prescribed based on experimental imaging.

3.3.1 PIN1 and PIN2 auxin efflux carriers

Once the digital root map had been defined, with an individual cell wall structure for each cell and unique cell numbers, it was necessary to assign the levels and localisation of the polar PIN efflux carriers and the non-polar AUX1/LAX influx carriers to the PM (included in the cell wall properties). PIN1 and PIN2 carrier levels are regulated by the crosstalk network, in the same way as earlier work (Chapter 2). The network also regulates the rate that the cytosolic PIN proteins are cycled to and from the PM. The model does not differentiate between PIN1 and PIN2 (apart from polarity localisation) and since they are regulated in the same way by the network and are essentially the same entity, for clarification and to distinguish them from the prescribed carriers (PIN3, PIN4 and PIN7), PIN1 and PIN2 are jointly referred to as PIN12 (or PINm or PINp in the equations). Depending on the location in the root, the plasma membrane GPs are assigned different properties to define the rate of transfer of the PIN12 proteins from the cytosolic GPs to the NN plasma membrane. The PIN12 transfer rates (low, medium or high) were based on experimental images from various publications. It was assumed that PIN12 are differentially expressed everywhere in the root tip, therefore as a default, all PIN12 transfer rates to the plasma membrane were initialised at a low non-polar level and then transfer rates at selected cell faces were reset to medium or high based on experimental

images. The map in Figure 3.4 summarises the transfer rate settings that define PIN12 polarity (Red = high, Green = medium, Blue = low).

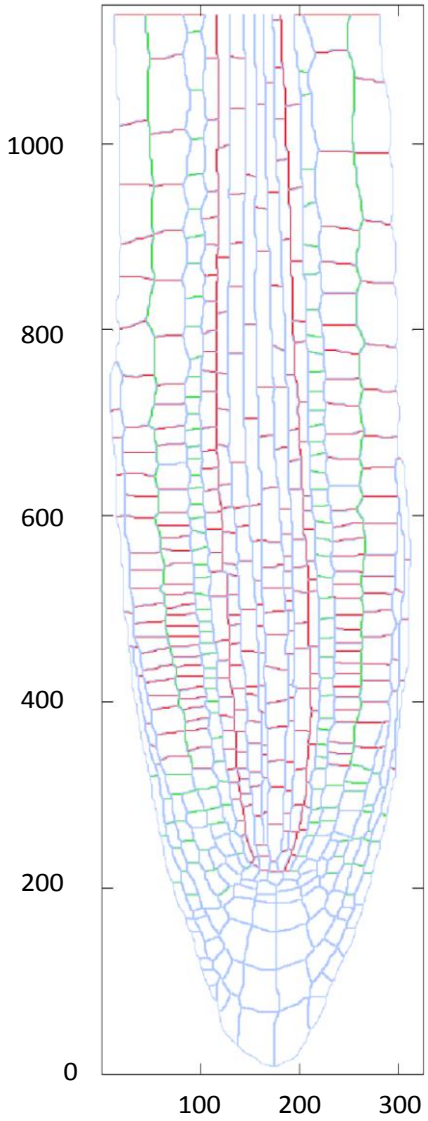

Figure 3.4: PIN12 transfer rates to the plasma membrane
(Red = High, Green = Medium, Blue = Low; relative axis units).

PIN12 transfer rates in the lateral root cap cells were set at medium (Green) on the apical cell faces from approximately the 200 level from the distal end of the root (Figure 3.4) up to approximately the 325 level after which they were set to high (Red) on the apical cell faces (Laskowski *et al*., 2008). In the epidermal cells, the transfer rates were left at low (Blue) on all cell faces for the first 3 cells proximal to the QC. For the next 3 cells they were set at medium on the apical faces and low on the lateral and basal faces, and thereafter set at high on the apical face and low on the lateral and basal faces (Laskowski *et al*., 2008; Muller *et al*., 1998). For the cortical cell files for the first 3 cells proximal to the

QC the transfer rates were set to low at all faces. For the next 3 cells the rates were set to medium on the basal face and low on the inner and outer lateral and apical faces. The rates were then set to high on the basal face, medium on the outer lateral and low on the inner lateral and apical faces through the meristematic zone (MZ) to approximately the 650 level. As the cells move out of the MZ there is a basal to apical polarity shift and the transfer rates were then set at high on the apical cell face, medium on the outer lateral face and low on the basal and inner lateral faces (Kleine-Vehn *et al*., 2008; Muller *et al*., 1998). The outer lateral settings in the cortical cells were based on Figure 1D from Kleine-Vehn *et al*. (2008). In the vascular cylinder and pericycle, the transfer rates were set to high at the basal face of all cells and high on the inner lateral of the pericycle cells (Friml *et al*., 2002), while the rates at the remaining vascular and pericycle cell faces were set at low. For the endodermis cells, the transfer rates were set at medium on the basal face and at low on the inner and outer lateral and apical faces (Friml *et al*., 2002). At the root-shoot border, the transfer rates are set at high for the epidermis, cortex and endodermis cells and zero for the pericycle and vascular cells.

3.3.2 PIN3, PIN4 and PIN7 auxin efflux carriers

As previously noted, PIN3, PIN4 and PIN7 efflux carrier concentration levels and polar localisation (Figure 3.5) are not regulated by the network but have prescribed concentrations at selected cell faces based on experimental imaging from the literature (Blilou *et al*., 2005), with concentration levels adjusted to produce WT auxin patterning. The model has 4 possible concentration levels (only 3 are used) for each PIN3,4,7 efflux carrier, for which concentrations are assigned by the user at model run time so that concentrations can be easily adjusted when searching for WT auxin patterning. PIN3 has non-polar localisation at a high level in the columella S1 and S2. It is localised at a high level at the basal face and a medium level at the inner and outer lateral and apical faces of the vascular cells in the elongation zone (EZ). In the pericycle cells in the EZ, it has a high level of localisation at the inner lateral and basal faces, and a medium level at the outer lateral and apical faces (Figure 3.5). PIN3 has non-polar localisation at a low level in all other cells. PIN4 has non-polar localisation at a medium level in the QC and initials and their immediate

neighbours. In the other cells in the distal meristematic zone (MZ) it is localised at a high level at the basal face and a medium level at the apical and inner and outer lateral faces. In all other cells, PIN4 has non-polar localisation at a low level at all cell faces (Figure 3.5). PIN7 is localised at a medium or high level at all cell faces in the pericycle and vascular cells in the MZ and EZ and in columella S1 and S2 cells. In the pericycle cells it is localised at a high level on the inner lateral and basal faces and a medium level at the apical and outer lateral faces. In the vascular cells it is localised at a high level at the inner and outer lateral and basal faces and a medium level on the apical face. It is localised in a non-polar distribution at a high level at all faces of the columella S1 and S2 cells. At all other cells PIN7 has non-polar low level localisation (Figure 3.5). At the root-shoot border, PIN3, PIN4 and PIN7 are set to zero.

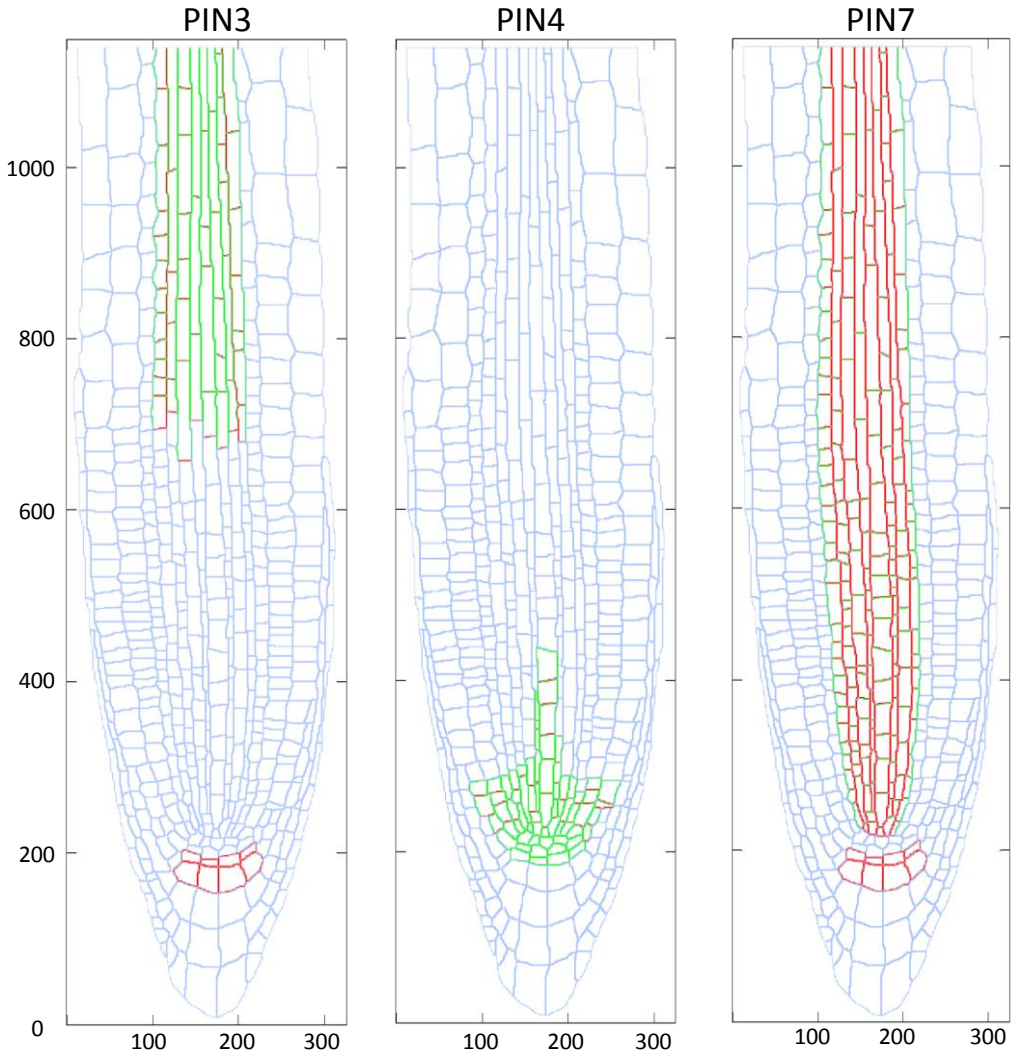

Figure 3.5: PIN3, PIN4 and PIN7 level and localisation
Relative level and localisation of prescribed auxin efflux carriers
(Red = high, Green = medium, Blue = low; relative axis units)

3.3.3 AUX1, LAX2 and LAX3 auxin influx carriers

The non-polar localisation of the auxin influx carriers AUX1, LAX2 and LAX3 (Figure 3.6) is again based on experimental imaging (Band *et al*., 2014) with concentrations adjusted to achieve WT auxin patterning. The model allows 15 concentration levels for AUX1, 8 levels for LAX2 and 4 levels for LAX3 (but only 3 were used for each carrier to define WT). Specific concentrations are assigned to each level by the user at model run time. AUX1 is localised at a medium level in the lateral root cap, a medium level in the EZ and proximal MZ of the epidermis, and a medium level in the cortical cells in the EZ. It is localised at a medium level in the cortical and epidermal cells just proximal to the QC, a high level in the columella S1-S4, and a medium level in the columella S5. In all other cells AUX1 is localised at a low level. LAX2 is localised at a high level in the vascular and pericycle cells in the mid to distal region of the MZ, and in the QC and columella initials, and at zero concentration in all other cells. LAX3 is localised at a high level in the columella S2 and at a zero concentration in all other cells. At the root-shoot border, AUX1, LAX2 and LAX3 are set to zero.

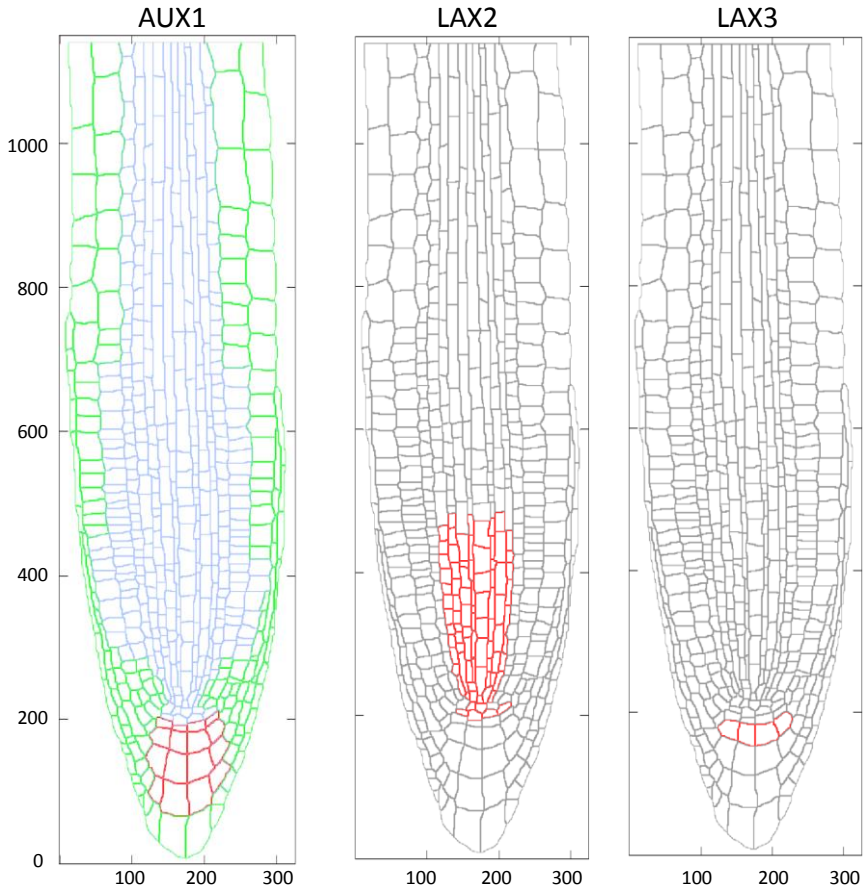

Figure 3.6: AUX1, LAX2 and LAX3 levels and localisation
(Red = high, Green = medium, Blue = low, Grey is zero concentration; relative axis units)

3.4 Definition of a new model for the realistic root

The crosstalk network remains the same as in the previous work except for the regulation of the AUX1 auxin influx carrier and the introduction of additional influx carriers (LAX2, LAX3) and efflux carriers (PIN3, PIN4, PIN7).

The regulatory relationships between auxin, ethylene, cytokinin and polar PIN1 and PIN2 proteins were previously established by iteratively combining experimental measurements with modelling analysis (Liu *et al*., 2010; Liu *et al*., 2013; in this work and as published in Moore *et al*., 2015a; Rowe *et al*., 2016).

In the earlier work, AUX1 activity was positively regulated by downstream ethylene signalling based on experimental observation (Figure 7B in Ruzicka *et al*., 2007). Model results for AUX1 patterning (Figure 2.66) were in part similar to experimental imaging (Figure S8 in Band *et al*., 2014) with AUX1 levels increasing proximally in the epidermis, and higher AUX1 levels in the outer cell layers compared to the central cell cylinder. However, the model did not exhibit the elevated experimental AUX1 levels in the columella and near the QC, or the proximally declining AUX1 levels in the central cylinder. The differences between model and experimental results could indicate that, in addition to ethylene, other effectors may also regulate AUX1 activity, such as cytokinin inhibition of *AUX1* as proposed in a recent paper (Street *et al*., 2016). It was therefore concluded that the existing crosstalk network between AUX1 and the three hormones (auxin, ethylene and cytokinin) cannot be fully established and that AUX1 patterning cannot be sufficiently predicted using the model network.

Extensive examination of published experimental data also reveals that it is currently impossible to construct a network between the three hormones and the other auxin carriers (PIN3, PIN4, PIN7, LAX2, LAX3) due to insufficient data and the complexity of crosstalk between hormones and auxin carriers. For example, experimental and modelling analysis has suggested that spatial expression patterning of the influx carrier *LAX3*, observed in cell reshaping and separation necessary for lateral root emergence, is affected by expression of the efflux carrier *PIN3* (Peret *et al*., 2013). However, other modelling and experimental analysis suggests that the induction of *PIN3* is not required to explain the ”all-or-nothing” expression of *LAX3* in this process (Mellor *et al.,*

2015). The feedback of GH3, which is an important component in the auxin-degradation pathway, may also have a role in *LAX3* expression (Mellor *et al.,* 2016). Furthermore, a recent study has shown that the regulation of *PIN3* and *PIN7* expression by auxin and cytokinin in root development follows different mechanisms (Lavenus *et al.,* 2016; Wang *et al.,* 2015). These examples show the complexity of crosstalk between auxin, its carriers and other hormones.

Given the above, it was concluded that PIN3, PIN4, PIN7, AUX1, LAX2 and LAX3 level and localisation should be prescribed based on experimental data.

In the model developed for the realistic root, the revised crosstalk network (Figure 3.7) controls metabolism in the cytosolic spaces of the PIN1 and PIN2 efflux carriers but not the influx carrier AUX1, and of the hormones auxin, ethylene and cytokinin. The network therefore allows quantitative description of PIN1 and PIN2 regulation by the three hormones and enables study of the relationship between auxin, PIN1 and PIN2 patterning.

The kinetic equations and parameters used in this model version are the same as in the rectangular root model (see Table 2.3, Table 2.4 and Table 2.5) except for a few minor changes. Since AUX1 is prescribed, AUX1 biosynthesis is set to zero (k1a = 0 in reaction v26 in Table 2.3) so that the values for AUX1m and AUX1p remain at zero. *AUX1* is therefore not regulated by the network, and AUX1p is not cycled to and from the plasma membrane. Three new variables are introduced (AUX1, LAX2 and LAX3) to represent the prescribed concentrations of these auxin influx carriers, and the auxin influx equations use the total AUX1, LAX2 and LAX3 concentrations to calculate auxin influx into the cell (Table 2.5). The regulation of PINm and PINp (Table 2.3) and PINp cycling to and from the plasma membrane (Table 2.4) remain unchanged. Three new variables (PIN3, PIN4 and PIN7) were introduced to represent the prescribed concentrations of the new auxin efflux carriers and these concentrations are added to the concentration of PINp in the equations for calculating auxin efflux (Table 2.5). An example of the placement of the auxin carriers PIN3 and AUX1 in the root structure is shown in Figure 3.8. The border concentrations for auxin, ethylene and cytokinin are handled in the same way as in the rectangular root. Similar to the rectangular root model, cytokinin biosynthesis is set to zero in the epidermis, cortex and endodermis cell files and occurs in all other cells.

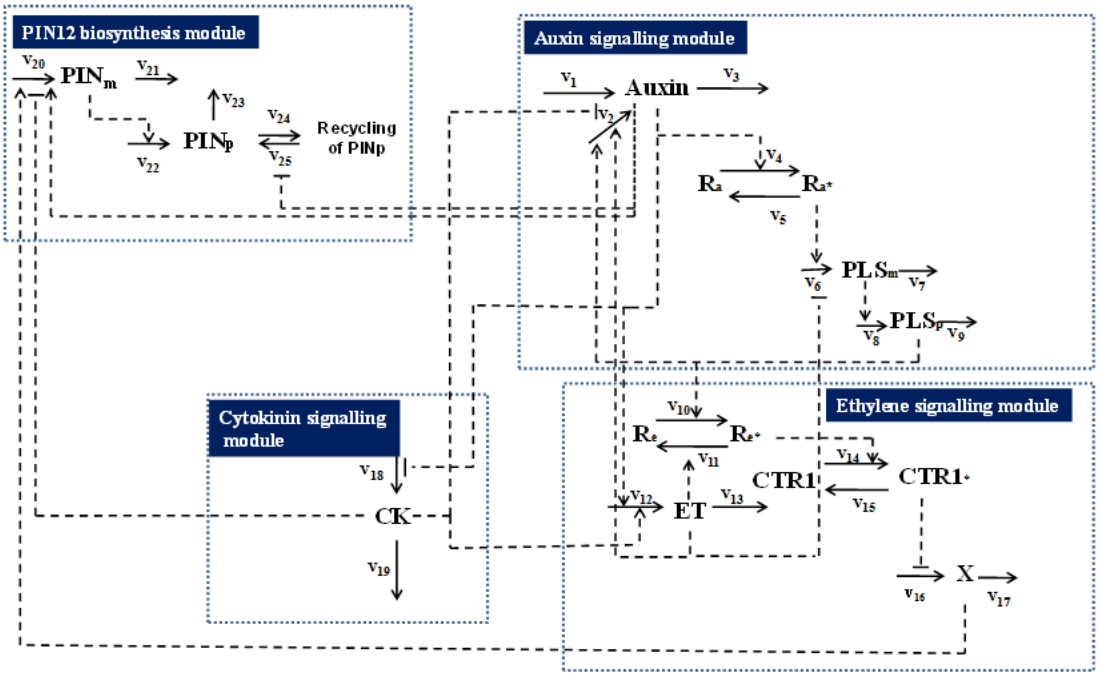

Figure 3.7: Hormonal crosstalk network for the realistic root

→ mass conversion links; - - · positive and negative regulatory links; ----- auxin transport links

Symbols: Auxin, auxin hormone; ET, ethylene; CK, cytokinin; PINm, PIN mRNA; PINp, PIN protein; PLSm, POLARIS mRNA; PLSp, POLARIS protein; X, downstream ethylene signalling; Ra*, active form of auxin receptor; Ra, inactive form of auxin receptor; Re*, active form of ethylene receptor ETR1; Re, inactive form of ethylene receptor ETR1; CTR1*, active form of CTR1; CTR1, inactive form of CTR1

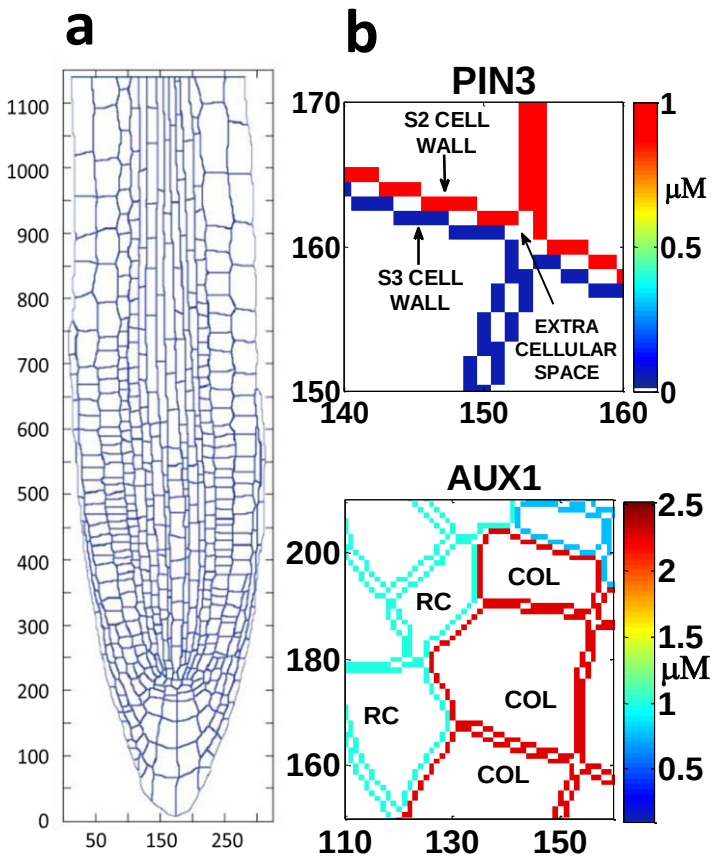

Figure 3.8: Model root with (a) cell geometry (b) sample carrier placement (S2 and S3, columella tier 2 and 3 cells; COL, columella; RC, root cap).

3.5 Results for the wildtype realistic root

The above model and root maps were used with varying concentration levels for the prescribed auxin influx and efflux carriers AUX1, LAX2 and LAX3, and PIN3, PIN4 and PIN7 to generate a reference wildtype realistic root model for the next stage of the work. Details of the root map file names and the prescribed auxin carrier concentration settings for generating the final wildtype realistic root can be found in the model running instructions (Appendix 1).

The realistic root model integrates actual cell geometries and the level and polar or non-polar localisation of auxin efflux and influx carriers, with a variety of experimental data on hormonal crosstalk. This compares to earlier work (Chapter 2) based on a simple rectangular root structure lacking realistic cell geometry, which did not have a lateral root cap or extra-cellular space and did not include the LAX2,3 and PIN3,4,7 auxin carriers.

3.5.1 Auxin patterning

Figure 3.9 shows auxin patterning for the wildtype model root, including an auxin concentration map, enlarged colour map images of the elongation zone and quiescent centre, and the auxin concentration profile. The model reproduces the auxin maximum located at the quiescent centre and shows increased auxin concentration in the epidermis in the elongation zone compared to the vascular tissues, with a corresponding increase in the auxin concentration profile trend in this region. This matches the DII-VENUS experimental profile results (Figure 2.59), unlike the previous WT model for the rectangular root. This is in part due to the outward lateral polarity settings for PIN12 in the cortex, which tend to drive auxin into the epidermis in the elongation zone, together with the prescribed concentration settings for AUX1 in the epidermis and cortex which act to retain auxin in these cells compared to the vascular cylinder, combined with the rate of auxin biosynthesis (see 3.5.6).

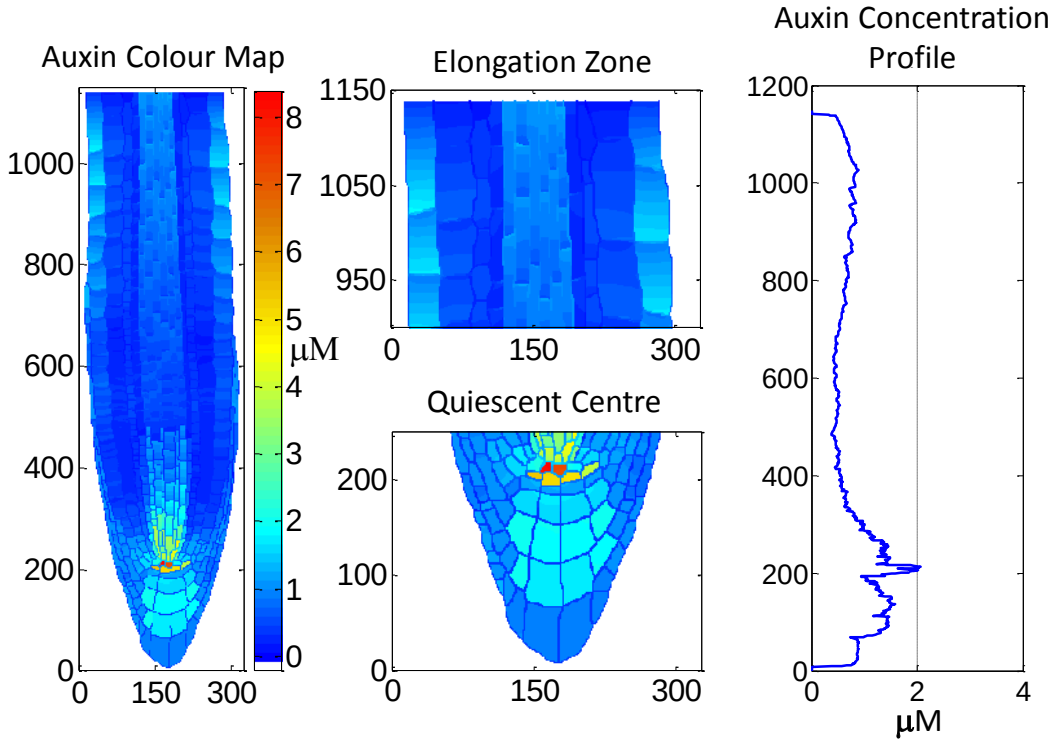

Figure 3.9: Auxin patterning in the WT realistic root model
Showing the auxin concentration map, enlarged colour map images of the EZ and QC, and the auxin concentration profile. The realistic root model results are a better match than the rectangular root model to the DII-VENUS experimental results (Figure 2.59), exhibiting increased auxin in the EZ epidermal cells and a proximally increasing auxin concentration profile in the EZ.

The average auxin concentrations were also plotted by cell type (Figure 3.10) and showed similar results to those generated previously for the rectangular root, where the trend for five cell types (QC, stele, endodermis, epidermis meristem and cortex meristem) is similar to the trend observed experimentally (Figure 2.62). These recent realistic root results showed similar discrepancies from the DII-VENUS experimental results, as discussed in section 2.8.1.

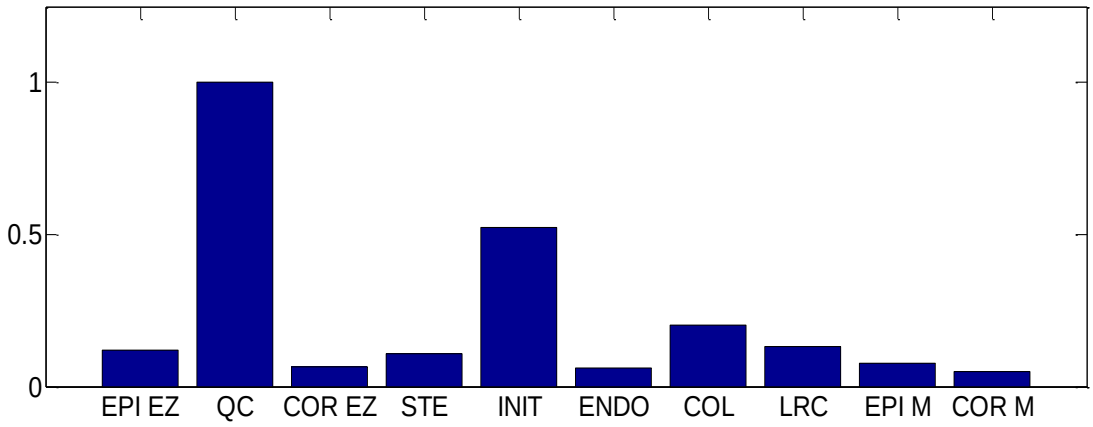

Figure 3.10: Auxin levels relative to QC for the WT realistic root
(EPI, epidermis; COR, cortex; END, endodermis; STE, stele; COL, columella; INIT, columella initials; QC, quiescent centre; M, meristem; EZ, elongation zone)

The introduction of the realistic root allowed detailed comparison between model results and experimental auxin response trends in selected cell files. In a fairly recent study using a novel R2D2 auxin reporter, the auxin response was imaged in selected cell files above the initials and the relative responses plotted (Liao *et al*., 2015). The auxin model concentration was plotted for the same cell files and exhibited similar trends (Figure 3.11).

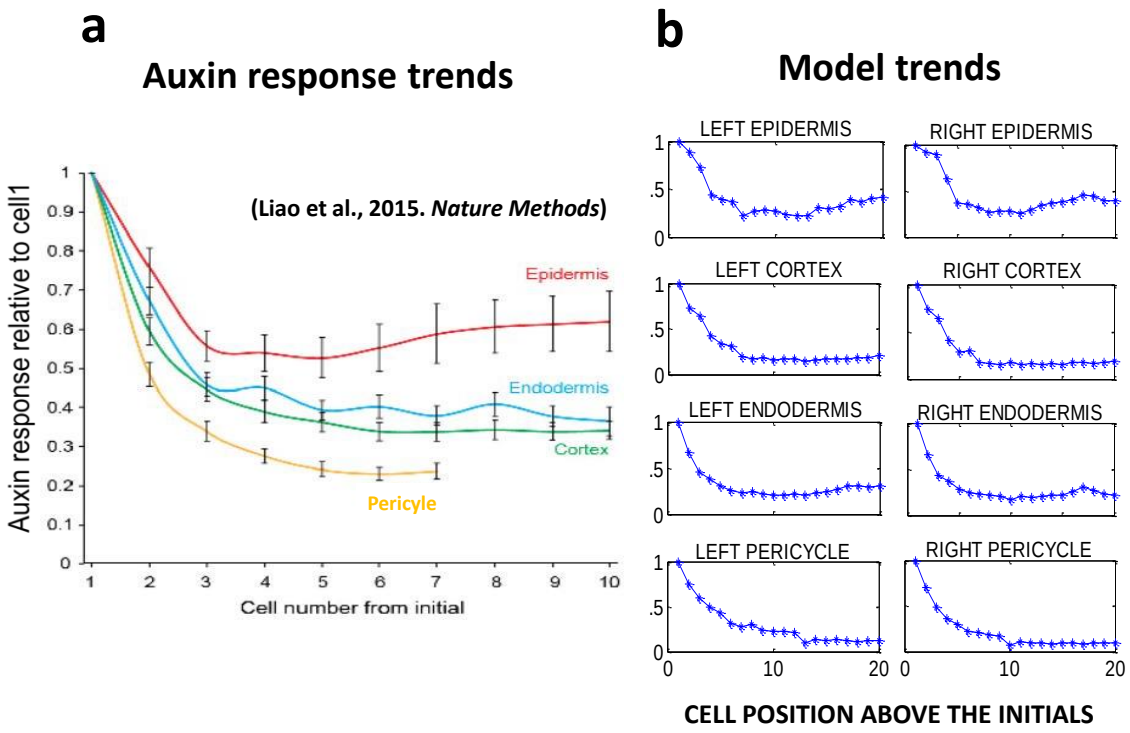

Figure 3.11: Relative auxin response and concentration trends
(a) Relative auxin response trends in cell files above the initials (Liao *et al*., 2015)
(b) Relative auxin concentration trends from the model for the same cell files. Model and experimental results show similar trend results.

3.5.2 PIN1 and PIN2 patterning

Similar to the rectangular root model (Figure 2.52, Figure 2.54), the WT realistic root model also predicts that total PIN1 and PIN2 levels generally decrease from the proximal to distal region of the root (Figure 3.12), consistent with experimental observations (Figure 1 in Liu *et al*., 2013; Figure 3B in Bishopp *et al*., 2011a; Figure 5 in Rowe *et al*., 2016).

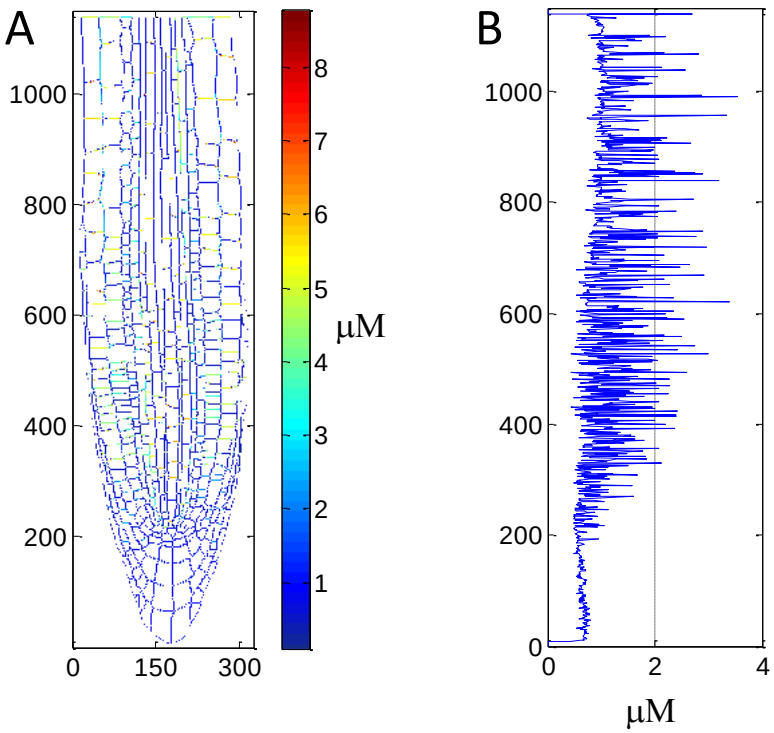

Figure 3.12: WT model PIN(1&2) concentration patterning.
(A) Concentration colour map of PIN12 at the plasma membrane
(B) Concentration profile for PIN12 at the plasma membrane, showing the trend of the average cross-sectional concentration along the root tip, and consistent with experimental results.

3.5.3 Ethylene patterning

Ethylene concentration patterning in the realistic root (Figure 3.13) is similar to the rectangular root and experimental observations (Figure 2.46) with modelled ethylene concentration gradually increasing proximally along the root tip.

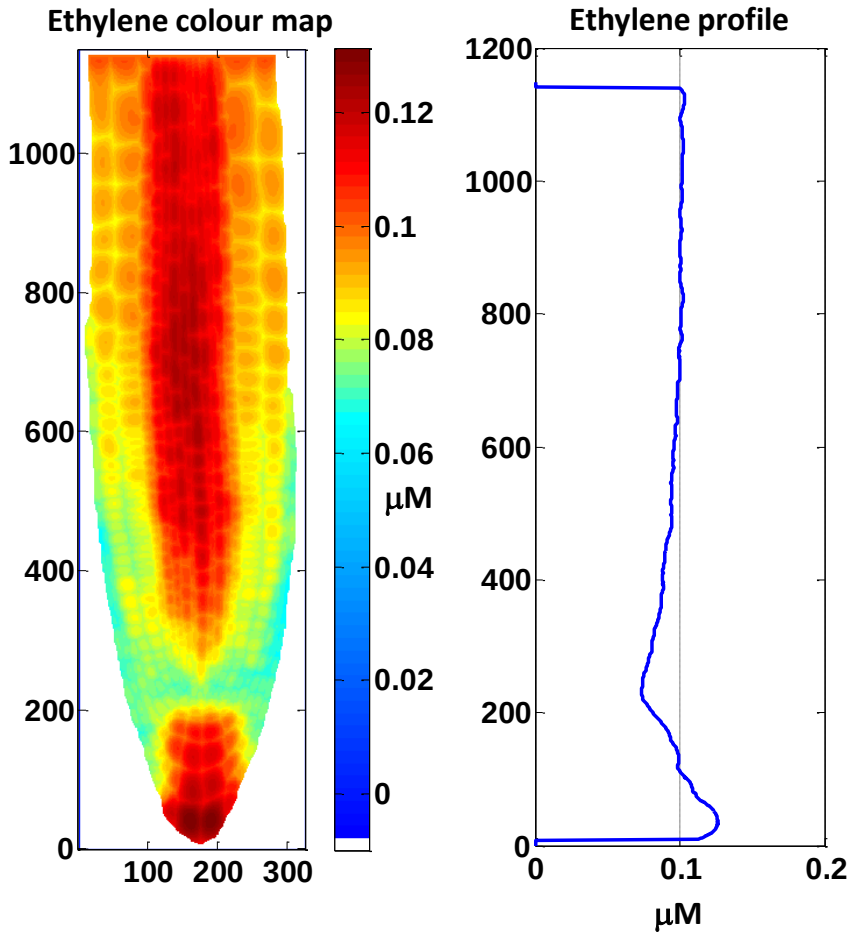

Figure 3.13: Ethylene concentration patterning in the realistic root
Similar to the rectangular root and experimental observations with the ET concentration profile increasing proximally.

3.5.4 Cytokinin patterning

Cytokinin patterning in the realistic root (Figure 3.14) appears somewhat improved compared to the rectangular root (Figure 2.17) since there is a marked decrease in profile concentration in the cross-section containing the QC and a proximally decreasing concentration profile, both of which can be observed from experimental response results (Figure 2.17). These improvements are driven by auxin patterning since auxin inhibits cytokinin, with high auxin concentrations in the root cross-section containing the QC and an increasing auxin profile concentration in the elongation zone due to the relative increase in auxin in the vascular cells in the EZ (Figure 3.9).

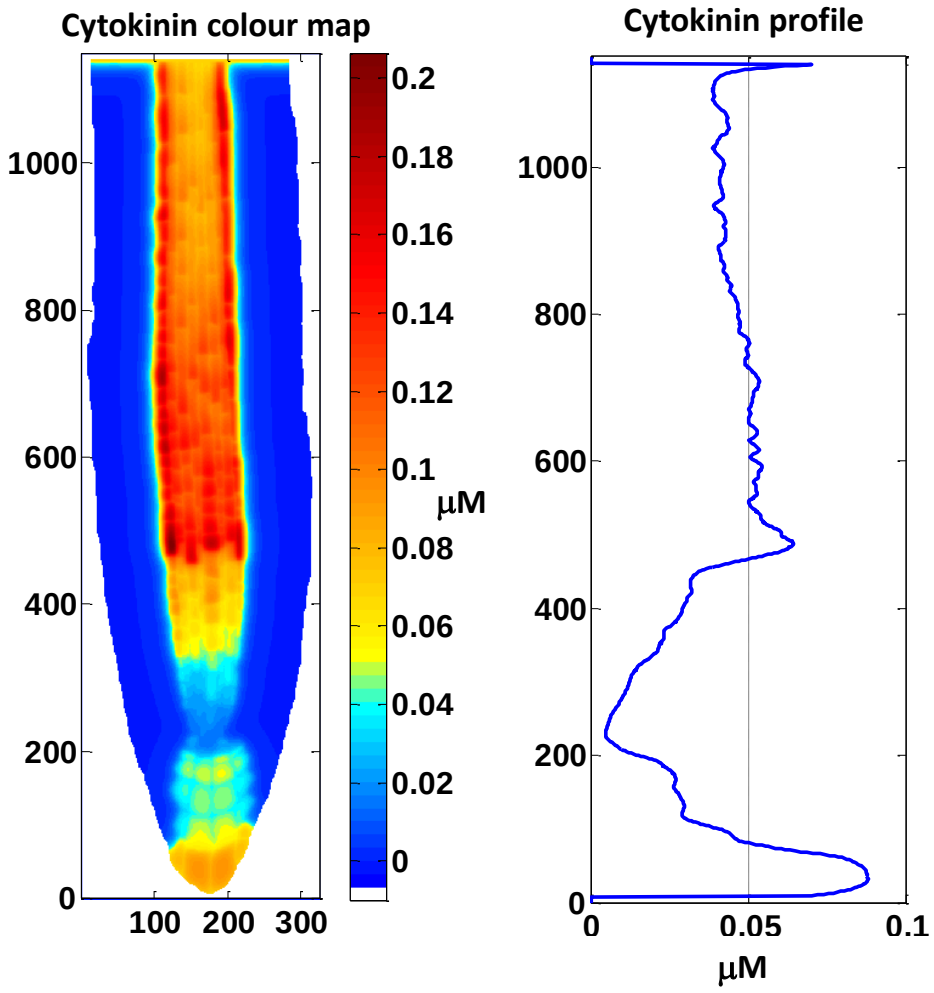

Figure 3.14: Cytokinin patterning in the realistic root
Showing somewhat improved patterning compared to the rectangular root with a marked decrease in profile concentration in the cross-section containing the QC and a proximally decreasing concentration profile, both of which can be observed in experimental response results (Figure 2.17).

3.5.5 POLARIS (PLS) patterning

Results for PLS protein concentrations in the realistic root (Figure 3.15) were similar to experimental *PLS* expression patterning and to the rectangular root concentration patterning (Figure 2.47), with a higher level at the distal root tip which decreases proximally through the MZ.

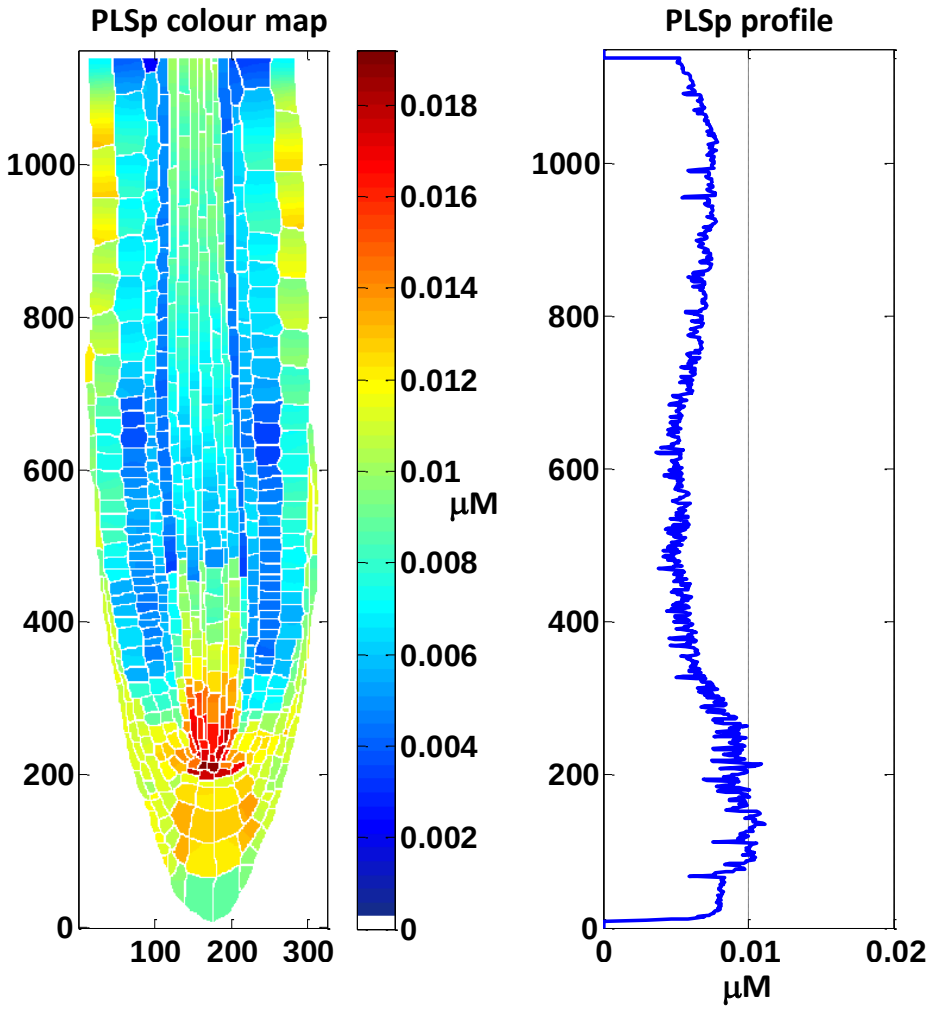

Figure 3.15: PLS protein patterning in the realistic root
Similar to experimental *PLS* expression patterning and to the rectangular root concentration patterning, with a higher level at the distal root tip which decreases proximally through the MZ.

3.5.6 Auxin biosynthesis rate patterning

Figure 3.16 shows model predictions for auxin biosynthesis rate patterning, where auxin biosynthesis rates are higher towards the distal *Arabidopsis* root tip, specifically in the QC and columella. In the epidermal cells of the elongation zone, rates are also relatively high. These predictions for auxin biosynthesis rate patterning are similar to those found by experimental observations (Figure 5 in Petersson *et al*., 2009). Note that the realistic root model does not include the region of lateral root development seen in the proximal part of the Petersson *et al*., 2009) figure and therefore modelling predictions can only be compared after excluding this region.

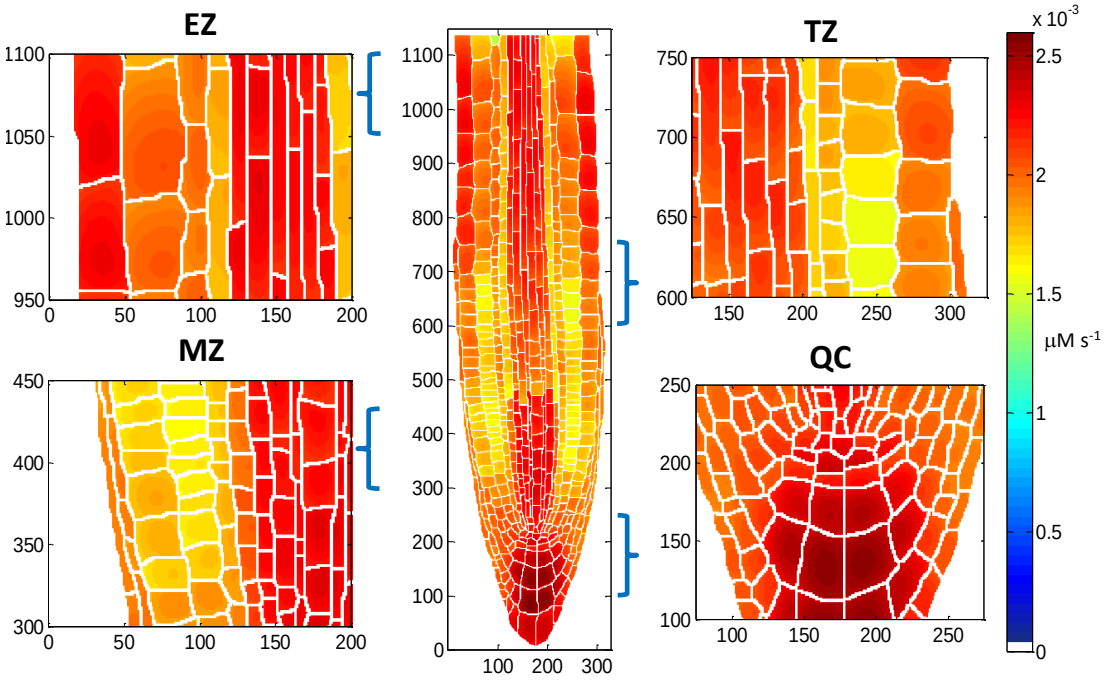

Figure 3.16: Auxin biosynthesis rate pattern in the realistic root
Predictions for auxin biosynthesis rate patterning are similar to experimental observations (Figure 5 in Petersson *et al*., 2009); EZ, elongation zone; TZ, transition zone; MZ, meristematic zone; QC, quiescent centre region.

3.5.7 PIN1 and PIN2 patterning after loss of PINs 3, 4 and 7

Figure 3.17 shows modelling predictions for combined PIN1 and PIN2 concentration patterns after 100% loss of PIN3 or PIN4 or PIN7 and for the combined 100% loss of PIN3, PIN4 and PIN7. When PIN3, PIN4 or PIN7 level is reduced to zero, modelling results predict that the PIN1 expression domain extends further into the elongation zone. These predictions are similar to experimental observations (Figure 6 in Omelyanchuk *et al*., 2016). In addition, after reducing total PIN3,4 and 7 concentration to zero, modelling results predict that PIN12 concentration increases in the plasma membrane of vascular cells. This is similar to experimental observations for the *pin3pin4pin7* triple mutant (Blilou *et al*., 2005). Modelling analysis reveals that the model is also able to predict changes in PIN1 profile trends for other mutants (Figure 2.52).

These model predictions assume that, for a *pin* mutant, the dynamics of PIN1 and PIN2 are regulated by hormonal crosstalk while other (non-mutated) auxin influx and efflux transporters remain unchanged. Also, since both PIN1 and

PIN2 are regulated by the same hormonal crosstalk network (Moore *et al*., 2015a), and are effectively the same entity in the model, the change in PIN1 patterning for *pin2* mutant has not been studied.

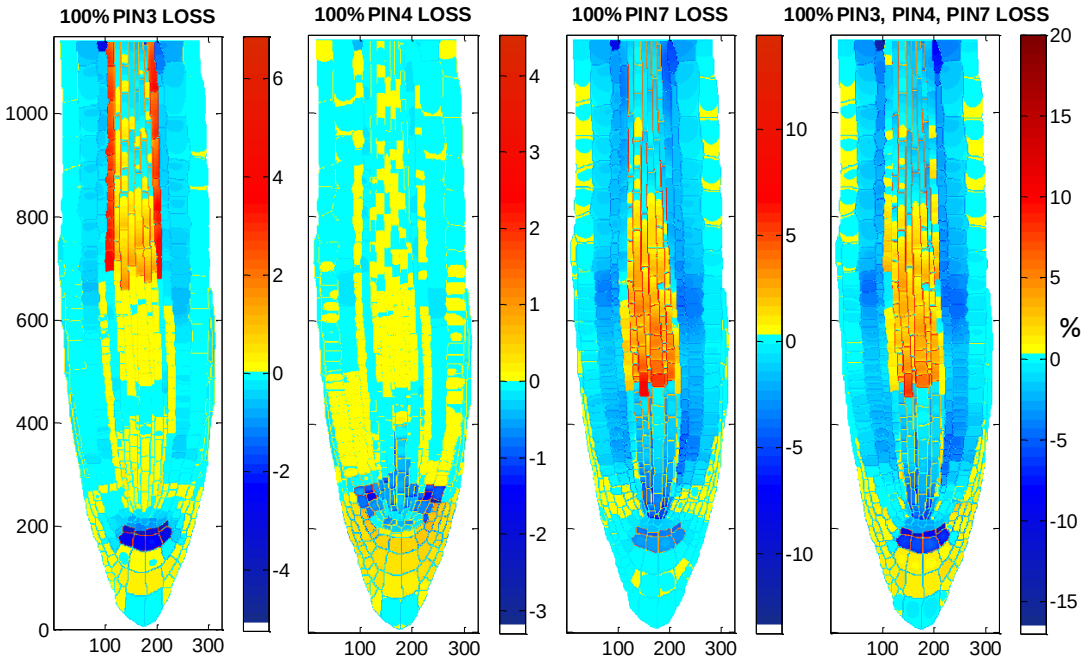

Figure 3.17: PIN1 and 2 patterning after PIN3, 4 and 7 loss
This figure shows percentage difference of PIN1/2 concentration from WT. From left to right, PIN3, PIN4, PIN7 or total PIN3,4,7 concentration is set to zero. Model predictions on combined PIN1 and PIN2 concentration patterns after 100% loss of PIN3 or PIN4 or PIN7 or after the combined 100% loss of PIN3, PIN4 and PIN7 are similar to experimental observation since *PIN1* expression domain extends further into the EZ when PIN3, PIN4 or PIN7 level is reduced to zero (Omelyanchuk *et al*., 2016), and PIN1 concentration increases in the plasma membrane of vascular cells in the *pin3pin4pin7* triple mutant (Blilou *et al*., 2005).

3.5.8 Auxin patterning with reduced apoplastic auxin diffusion

Experimental measurement has shown that the auxin apoplastic diffusion constant is lower than that in water (Kramer *et al*., 2007). Figure 3.18 shows the effects on auxin patterning of reducing the auxin diffusion constant in the cell wall from the WT setting of 220 $\mu m^2 s^{-1}$. Interestingly, modelling results predict that decreasing the auxin diffusion constant in the cell wall favours auxin accumulation in QC.

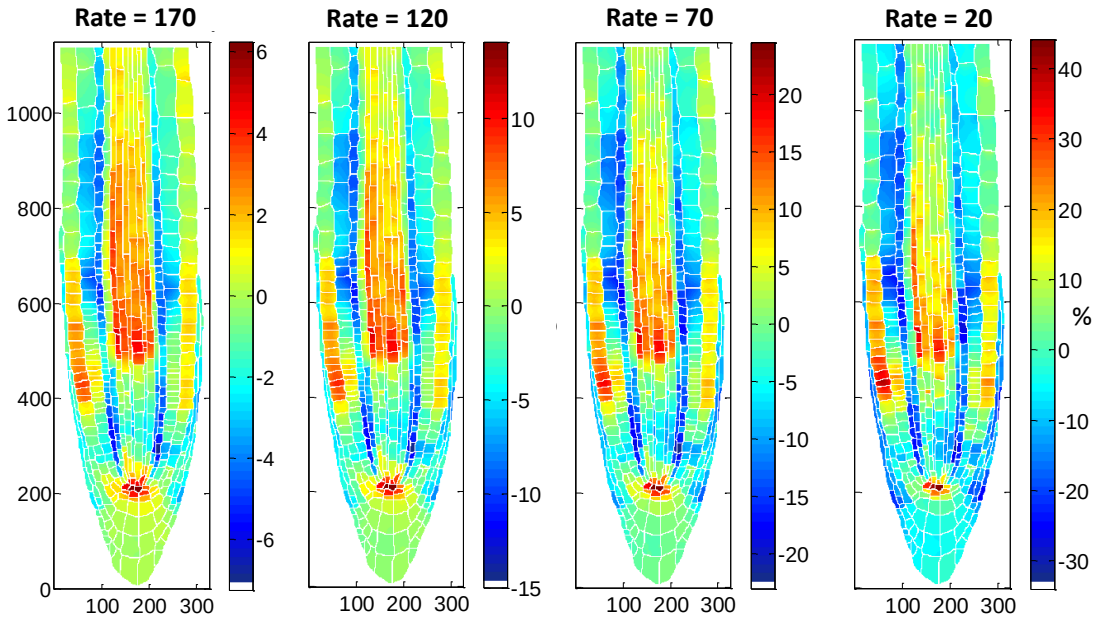

Figure 3.18: Auxin patterning with reduced auxin apoplastic diffusion rates
Showing the percentage difference from WT cytosolic auxin concentrations for reduced auxin diffusion constants in the cell wall of 170, 120, 70 and 20 $\mu m^2\ s^{-1}$, exhibiting an increasing auxin maximum at the QC (WT diffusion rate = 220 $\mu m^2\ s^{-1}$).

3.5.9 Effects on auxin patterning of changing auxin influx levels

The effects of varying the levels of auxin influx carriers on auxin patterning were also analysed (Figure 3.19). The results support the suggestion that non-polar AUX1/LAX carriers act to retain cellular auxin (Band *et al*., 2014). Specifically, increasing or decreasing the level of AUX1/LAX carriers affects the auxin concentration accordingly. These results reveal how non-polar AUX1/LAX quantitatively contributes to auxin patterning, in particular to the emergence of the auxin maximum, where reduced AUX1/LAX levels weaken the auxin maximum at the QC while increased levels reinforce the maximum.

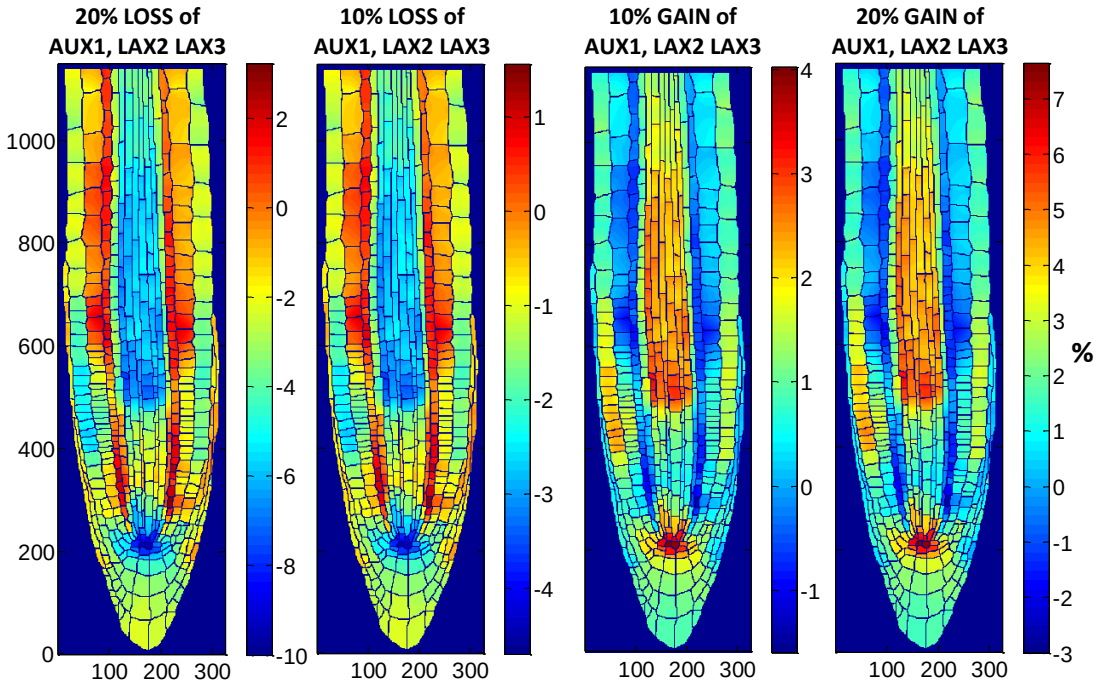

Figure 3.19: Auxin patterning with changed auxin influx levels.
This figure shows percentage difference from WT cytosolic auxin concentrations for changes in the concentrations of the AUX1, LAX2 and LAX3 auxin influx carriers. From left to right, the AUX1, LAX2 and LAX3 carrier concentrations are all adjusted by -20%, -10%, +10% or +20%, respectively. Reduced AUX1/LAX levels weaken the auxin maximum at the QC while increased levels reinforce the maximum.

3.6 Summary

The realistic root model developed in this chapter integrates a root structure incorporating actual cell geometries, the level and polar or non-polar localisation of all auxin influx (AUX1, LAX2,3) and efflux carriers (PIN1,2,3,4,7), with a variety of experimental data on hormonal crosstalk. Since the ABCB family of auxin carriers can reversibly redirect auxin flux, the role of ABCB transporters has been incorporated into PIN and AUX1/LAX non-polar basal activity to simplify modelling analysis. Therefore, the current research has integrated all known important auxin transporters for cell to cell communication with a wide range of experimental data on the crosstalk between PIN1,2 and three hormones, auxin, ethylene and cytokinin (Liu *et al*., 2010; Liu *et al*., 2013; Moore *et al*., 2015a).

The results for the realistic root with actual cell geometry demonstrate that earlier results were not dependent on using a simple rectangular root structure,

and that initial results were confirmed (and to an extent improved) by the use of a realistic root map with additional auxin carriers. Furthermore, as demonstrated in section 3.5.1 on auxin patterning, the implementation of a realistic root allowed increased in-depth comparison between experimental and model results for selected cells or regions in the root.

Since the model integrates the properties of auxin influx and efflux transporters with those of auxin biosynthesis and degradation, the model is also able to make several predictions that are similar to experimental observations, as follows:

- the model predicts (Figure 3.12) that PIN1 and PIN2 levels generally decrease from the proximal to distal region of the WT root. This reveals that PIN1 and PIN2 patterning is the result of the integrative actions of a hormonal crosstalk network in *Arabidopsis* root,
- predictions for combined PIN1 and PIN2 concentration patterns after 100% loss of PIN3 or PIN4 or PIN7 or for the combined 100% loss of PIN3, PIN4 and PIN7 (Figure 3.17) showed a proximal shift in the PIN1 expression domain,
- after reducing total PIN3, 4 and 7 concentration to zero, PIN1 and PIN2 concentration increased in the plasma membrane of vascular cells (Figure 3.17),
- earlier modelling analysis revealed that the model is able to predict changes in PIN1 concentration profiles for other mutants (Figure 2.52),
- since auxin biosynthesis and degradation are also processes included in the hormonal crosstalk network, the model is able to make predictions on auxin biosynthesis rate patterning (Figure 3.16) demonstrating high auxin biosynthesis rates towards the distal *Arabidopsis* root and a relative increase in biosynthesis in the epidermal cells of the elongation zone. Moreover, the model also predicts that, in the transition zone, patterning of auxin biosynthesis is complex. These modelling predictions reveal that understanding the patterning of auxin biosynthesis requires the study the biosynthesis, degradation and transport of auxin as an integrated crosstalk system, similar to that described in this work.

Since the model developed in this study has integrated auxin biosynthesis, degradation and transport, effects of any parameters relating to these processes can also be analysed using the model. For example, the model indicated that reducing the apoplastic auxin diffusion rate results in increased accumulation of auxin at the QC (Figure 3.18). In addition, the effects of varying levels of auxin influx (or efflux) carriers on auxin patterning can also be analysed (Figure 3.19) supporting the idea that AUX1/LAX carriers act to retain cellular auxin and contribute to the creation of the auxin maximum at the QC.

The results described in Chapters 2 and 3 therefore reinforce the concept that experimental data can be integrated into a systems model that is able to reproduce and analyse key patterning characteristics and behaviour.

CHAPTER 4 : RECOVERY PRINCIPLE GIVES INSIGHTS INTO AUXIN PATTERNING

RECOVERY PRINCIPLE GIVES INSIGHTS INTO AUXIN PATTERNING

4.1 Introduction

As described in detail above, auxin gradient formation in the *Arabidopsis* root is predominantly regulated by auxin transport proteins (Zazimalova *et* al., 2010), including PIN-FORMED (PIN) proteins (Adamowski and Friml, 2015), the AUX1/LIKE-AUX1 (AUX1/LAX) family of influx carriers (Swarup and Peret, 2012), and ABCB transporters (Geisler and Murphy, 2006; Cho and Cho, 2012). Auxin gradients are hypothesized to be sink-driven (Friml *et al*., 2002), and modelling has suggested that PIN efflux carriers can generate the gradient (Grieneisen *et al*., 2007), while other studies indicate that AUX1/LAX influx carriers are required for creating auxin distribution patterning at the root tip (Band *et al*., 2014; Swarup *et al*., 2005). Importantly, it has been suggested that non-polar AUX1/LAX influx carriers create tissues containing high auxin concentrations by auxin retention, while polar PIN carriers control directional auxin transport within these tissues (Band *et al*., 2014). Therefore both auxin efflux (Grieneisen *et al*., 2007; De Rybel *et al*., 2014; Xuan *et al*., 2016) and influx carriers (Band *et al*., 2014; Xuan *et al*., 2016) are considered important for generating auxin patterning, although their relative contributions are not clear. It has also been proposed that the dynamic recycling of both the influx and efflux carrier proteins to and from the plasma membrane enables the cell to respond quickly to environmental changes by adjusting auxin flow and patterning (Kleine-Vehn *et al*., 2006).

While it is known that polar PIN carriers direct auxin movement differentially and non-polar AUX1/LAX carriers act to retain cellular auxin, one key question is how the combined transport activity of the polar PIN and non-polar AUX1/LAX carriers can potentially control auxin pattern formation. Important auxin carrier properties include their concentration and localisation. Concentration is controlled by gene expression and protein turnover, and localisation by polar or non-polar recycling and distribution to the plasma membranes (Adamowski and Friml, 2015; Swarup and Peret, 2012). A critical component of understanding auxin pattern formation requires investigation of how concentration and localisation of influx and efflux carriers could potentially work together to

generate pattern. The following questions need to be addressed. First, while maintaining non-polar AUX1/LAX localisation but at different concentration levels, can auxin patterning be maintained without changing PIN polarity; and, while maintaining polar PIN localisation but at different levels, does auxin pattern maintenance require changes in AUX1/LAX localisation? Answers to this question will determine how influx and efflux carrier levels and localisation combine to control auxin pattern formation and clarify the individual roles of polar PIN and non-polar AUX1/LAX carriers in maintaining auxin patterning. Second, can auxin pattern recovery lead to auxin carrier pattern recovery? Answers will address the role of auxin in regulating the patterning of its own transporters. Third, for the same auxin pattern generated by different influx and efflux carrier combinations, are the influx and efflux carrier levels spatially correlated? Answers to the above questions will reveal how auxin patterning is controlled by combined influx and efflux carrier patterning.

The realistic root model, described in Chapter 3 (with no changes to the network or parameters), which incorporates the activities of polar PIN and non-polar AUX1/LAX carriers (implicitly including the activity of the reversible ABCB carriers), is used to investigate the roles of the auxin influx and efflux carriers in auxin patterning and how they potentially can coordinate their activities for auxin pattern formation. The model integrates (1) a root structure with cell geometries derived from confocal microscopy imaging where each cell has a cytosolic space, plasma membrane and cell wall, and where adjacent plasma membrane and cell wall entities are represented by a single model identity containing both cell wall and plasma membrane properties and referred to as either a cell wall or plasma membrane depending on the context and properties under discussion; (2) PIN and AUX1/LAX carrier localisation based on experimental imaging; (3) PIN polarity; and (4) experimental data describing hormonal crosstalk between efflux carriers (PIN1 and PIN2) and hormones (auxin, ethylene, cytokinin). The hormonal crosstalk network is a mixed-type network that integrates gene expression, signal transduction and metabolic conversions. In particular, it includes auxin biosynthesis and degradation, auxin transport facilitated by both influx and efflux carriers, and hormonal crosstalk regulatory relationships. Therefore, the network incorporates both auxin metabolism and

transport into an integrated system and, as demonstrated in Chapter 3, reproduces auxin patterning similar to experimental observations.

To facilitate this work, a general principle was formulated for quantitative auxin pattern recovery after perturbation of one or other carrier types to demonstrate how relationships between influx and efflux carrier level and localisation possibly combine to quantitatively control auxin patterning and the emergence of specific auxin patterns. The use of this principle demonstrated that the relationship between influx and efflux carriers, not their individual activity, regulates auxin patterning. This principle also allows relationships between level and localisation of influx and efflux carriers for a target auxin pattern to become searchable and enables auxin concentration and its influx and efflux carriers to be studied as an integrated system. In addition, the model makes various predictions that can be validated experimentally.

4.2 Quantitative recovery of an auxin pattern: 'The Recovery Principle'

Since the model integrates a wide range of experimental data and reproduces key features of auxin response patterning, it is possible to investigate how the combined activities of PIN and AUX1/LAX carriers can potentially control auxin pattern formation, provided that a general principle for quantitative auxin pattern recovery following perturbation of transporter activity can be developed. Such a principle can reveal how specific auxin patterning can be generated by the relationship between influx and efflux carriers, rather than the independent activities of individual carrier types.

The recovery principle is an iterative process designed to study steady-state patterning; it therefore requires each iteration to be computed for a sufficiently long simulation time for all components to reach steady state values.

Since AUX1/LAX influx carriers at the plasma membrane direct auxin from the cell wall to the cytosol, an iterative recovery principle for resetting AUX1/LAX concentrations, to recover auxin patterning after PIN carrier perturbation, can be formulated as follows. At each iteration step ‘i’ (from 1 to n):

a) $A_{p,i}$ is the AUX1/LAX concentration at a plasma membrane GP ‘p’. At iteration 1, $A_{p,1}$ is equal to the AUX1/LAX initial concentration (e.g. WT), before any adjustments have occurred.

b) $[Auxin]_{p,i}$ is the auxin concentration at a plasma membrane GP ‘p’.

c) $[Auxin]_{c,i}$ is the auxin concentration at a NN cytosolic GP ‘c’ connecting to the adjacent plasma membrane GP ‘p’ referenced in (b).

d) $[Auxin]_{p,0}$ and $[Auxin]_{c,0}$ are the respective target recovery auxin concentrations (e.g. WT) at the plasma membrane GP ‘p’ and the NN cytosolic GP ‘c’, before any PIN perturbation.

e) At iteration 1, $[Auxin]_{p,1}$ and $[Auxin]_{c,1}$ are the auxin concentrations after the initial PIN perturbation and before any AUX1/LAX adjustments.

f) $$R_{p,i} = \frac{\left|[Auxin]_{p,i} - [Auxin]_{p,0}\right|}{[Auxin]_{p,0}},$$ (equation 1a)

is the absolute relative difference of auxin concentration at the plasma membrane GP ‘p’ from the target recovery concentration before PIN perturbation.

g) $$R_{c,i} = \frac{\left|[Auxin]_{c,i} - [Auxin]_{c,0}\right|}{[Auxin]_{c,0}},$$ (equation1b)

is the absolute relative difference of auxin concentration at the NN cytosolic GP ‘c’ from the target recovery concentration before PIN perturbation.

h) At iteration ‘i’ the AUX1/LAX concentration is adjusted at each plasma membrane GP ‘p’ using either the plasma membrane auxin concentration relative to the target concentration (equation 2) or the NN cytosolic auxin concentration relative to target (equation 3), whichever is greater.

$$A_{p,i+1} = \frac{[Auxin]_{p,i}}{[Auxin]_{p,0}} A_{p,i} \quad \text{if} \quad R_{p,i} > R_{c,i}, \quad \text{(equation 2)}$$

$$A_{p,i+1} = \frac{[Auxin]_{c,0}}{[Auxin]_{c,i}} A_{p,i} \quad \text{if} \quad R_{p,i} \leq R_{c,i}, \quad \text{(equation 3)}$$

Where $A_{p,i+1}$ is the 'new' AUX1/LAX concentration, calculated by adjusting the 'old' AUX1/LAX concentration ($A_{p,i}$) using the above equations.

The recovery principle, equations 1-3, has the following biological significance. To recover the original target auxin pattern after initial PIN perturbation, the current auxin pattern at iteration 'i' is compared to the target pattern and then AUX1/LAX patterning is reset at all plasma membrane GPs in the root matrix, using equations 1-3. Since changing the auxin concentration at any single GP results in changes at all neighbouring GPs, a change at any location will change concentrations across the whole root. Therefore, for each iteration, AUX1/LAX is reset simultaneously at all root locations. The AUX1/LAX adjustments at each plasma membrane GP are calculated using the auxin concentration at the plasma membrane or NN cytosolic GP, whichever differs most from the target value, following equations 1-3.

Specifically, at iteration 'i', if $R_{p,i} > R_{c,i}$, the AUX1/LAX activity should be adjusted based on the plasma membrane auxin concentration relative to target, using the factor $\frac{[Auxin]_{p,i}}{[Auxin]_{p,0}}$, following equation 2. Therefore, if say $\frac{[Auxin]_{p,i}}{[Auxin]_{p,0}} > 1$, total AUX1/LAX concentration is increased, resulting in a decrease in auxin concentration at the cell wall GP which in turn results in increased auxin concentration at the NN cytosolic GP. Similarly, if $R_{p,i} \leq R_{c,i}$, AUX1/LAX activity should be adjusted so that auxin concentration at the

cytosolic GP changes towards its target value by using the factor $\frac{[Auxin]_{c,r}}{[Auxin]_{c,i}}$, following equation 3.

Thus, after all plasma membrane GPs in the root are compared simultaneously to target and new AUX1/LAX concentrations calculated for each plasma membrane GP, a new AUX1/LAX concentration pattern is generated which in turn generates a new auxin pattern. The recovery process then moves to the next iteration when this new auxin pattern is compared to target and the AUX1/LAX concentration pattern again reset following the recovery principle. As this process is repeated, the auxin pattern gradually approaches the target concentration pattern until, after multiple iterations, the original target auxin pattern is recovered.

Therefore, the recovery principle is a generic, biologically based, iterative relationship that establishes how auxin efflux and influx carriers can coordinate their activities to control the emergence of a specific auxin pattern.

The recovery principle can also be used to search for the level and localisation of PIN efflux carriers necessary to recover AUX1/LAX perturbations, as summarised in section 4.8 “Quantitative recovery after AUX1/LAX changes can require modified PIN polarity”.

4.3 Auxin pattern recovery after PIN3,4,7 perturbations

Figure 4.1 presents an example of auxin pattern recovery after total PIN3, 4 and 7 concentration is decreased by 75% of its wildtype value. After reducing total PIN3, 4 and 7 by 75%, the maximum deviation in auxin concentration from WT is ca. 80% across the whole root (Figure 4.1). Using the recovery principle to reset AUX1/LAX, this difference reduces to ca. 10% after 5 iterations, and after 85 iterations it reduces to ca. 0.3%, indicating that wildtype root auxin patterning is fully recovered (Figure 4.1). Therefore after a 75% PIN3, 4, 7 reduction, wildtype auxin patterning can be rescued by resetting AUX1/LAX following the recovery principle. This indicates that the relationship between influx and efflux carriers, rather than their individual activities, is potentially one method of maintaining or controlling auxin homeostasis.

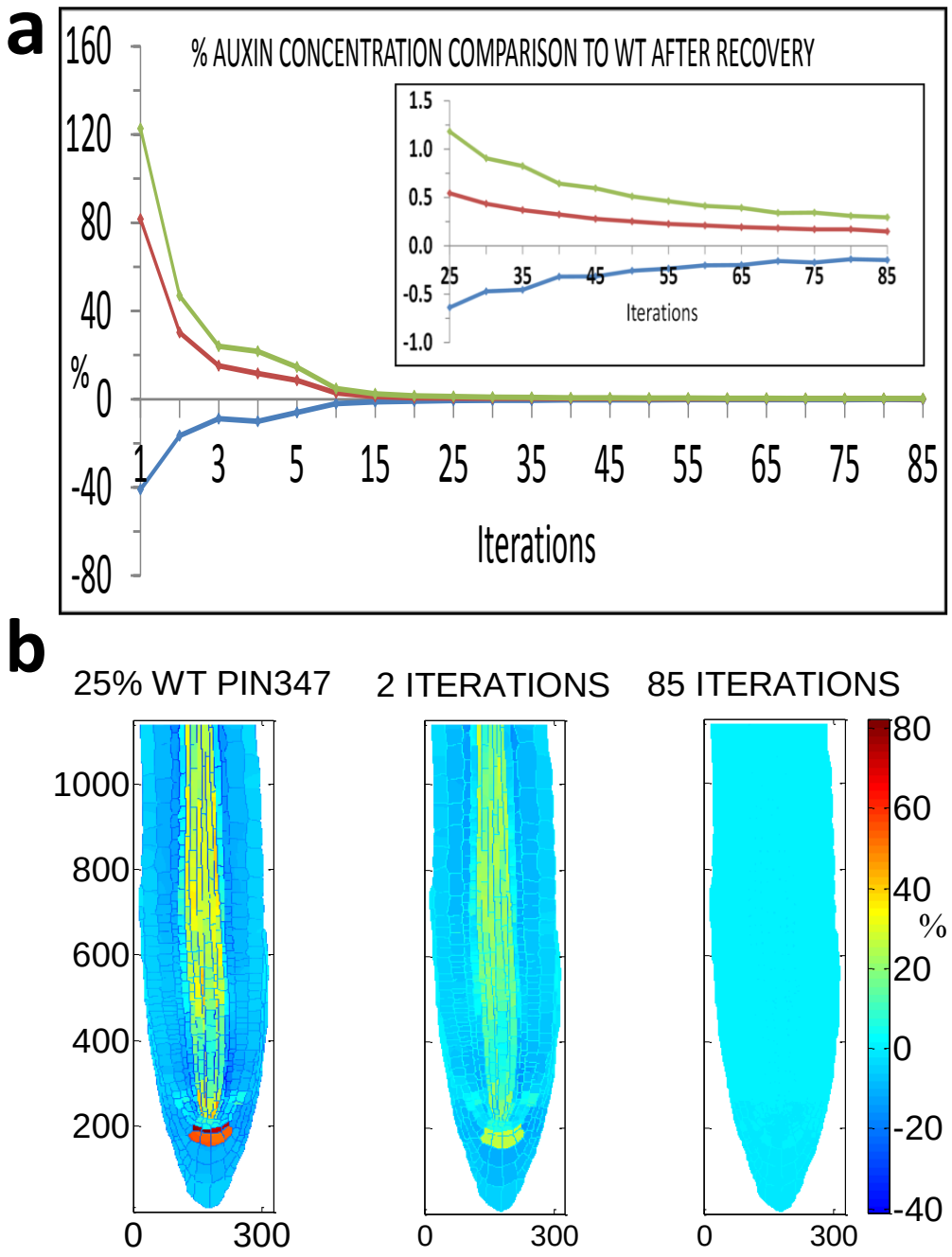

Figure 4.1: Auxin pattern recovery after 75% PIN3,4,7 loss

Pattern recovery after 75% decrease in total wildtype PIN3,4,7 concentrations, using the recovery principle over 85 iterations. **(a)** Progressive auxin percentage difference from wildtype in the whole root. Blue curve shows the maximum auxin percentage difference below wildtype in the root at each iteration. Red curve shows the maximum auxin percentage difference above wildtype in the root at each iteration. Green curve shows the maximum range of the percentage difference from wildtype within the root, calculated by adding the absolute values of the blue and red curves at each iteration. **(b)** Colour map images of the percentage difference from wildtype auxin concentrations after the initial perturbation of 75% loss of PIN3,4,7, then after 2 recovery iterations, and at full recovery after 85 iterations. Symbol % is the percentage difference relative to corresponding wildtype value.

Five additional cases were examined for total PIN3, 4 and 7 concentrations set at 0%, 50%, 150%, 175% and 200% of wildtype and for all cases the recovery principle fully recovered a reference wildtype auxin pattern **(**Figure 4.2**,** Figure 4.3, Figure 4.4, Figure 4.5 and Figure 4.6). Therefore, it is clear that wildtype auxin patterning can emerge from multiple combinations of interlinked levels and localisation of influx and efflux carriers. Thus, PIN and AUX1/LAX influx carrier combinations possibly act to control auxin pattern formation to achieve a target pattern.

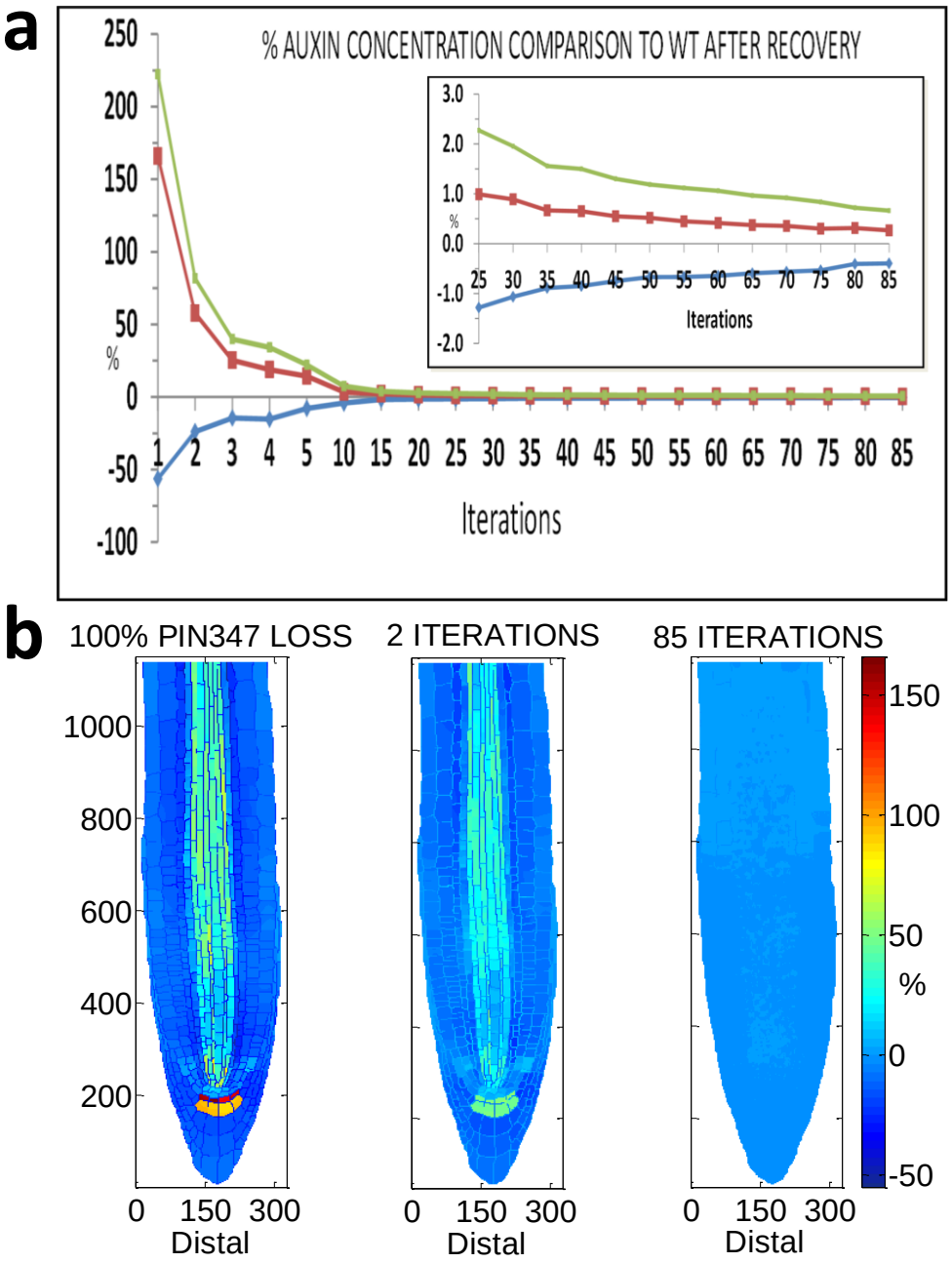

Figure 4.2: Auxin pattern recovery after 100% PIN3,4,7 loss

Pattern recovery after 100% decrease in total wildtype PIN3,4,7 concentrations, using the recovery principle over 85 iterations. **(a)** Progressive auxin percentage difference from wildtype in the whole root. Blue curve shows the maximum auxin percentage difference below wildtype in the root at each iteration. Red curve shows the maximum auxin percentage difference above wildtype in the root at each iteration. Green curve shows the maximum range of the percentage difference from wildtype within the root, calculated by adding the absolute values of the blue and red curves at each iteration. **(b)** Colour map images of the percentage difference from wildtype auxin concentrations after the initial perturbation of 100% loss of PIN3,4,7, then after 2 recovery iterations, and at full recovery after 85 iterations. Symbol % is the percentage difference relative to corresponding wildtype value.

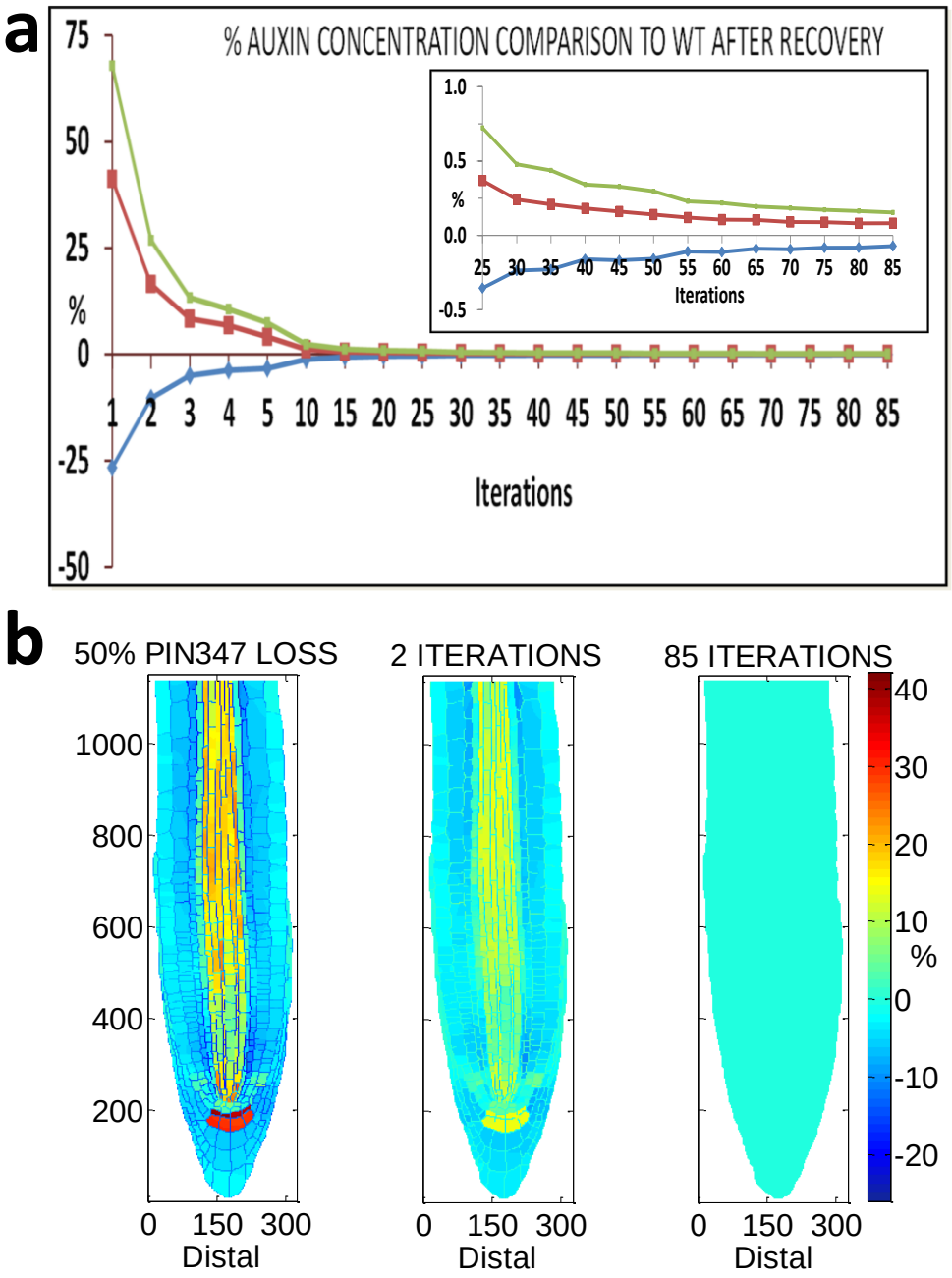

Figure 4.3: Auxin pattern recovery after 50% PIN3,4,7 loss

Pattern recovery after 50% decrease in total wildtype PIN3,4,7 concentrations, using the recovery principle over 85 iterations. **(a)** Progressive auxin percentage difference from wildtype in the whole root. Blue curve shows the maximum auxin percentage difference below wildtype in the root at each iteration. Red curve shows the maximum auxin percentage difference above wildtype in the root at each iteration. Green curve shows the maximum range of the percentage difference from wildtype within the root, calculated by adding the absolute values of the blue and red curves at each iteration. **(b)** Colour map images of the percentage difference from wildtype auxin concentrations after the initial perturbation of 50% loss of PIN3,4,7, then after 2 recovery iterations, and at full recovery after 85 iterations. Symbol % is the percentage difference relative to corresponding wildtype value.

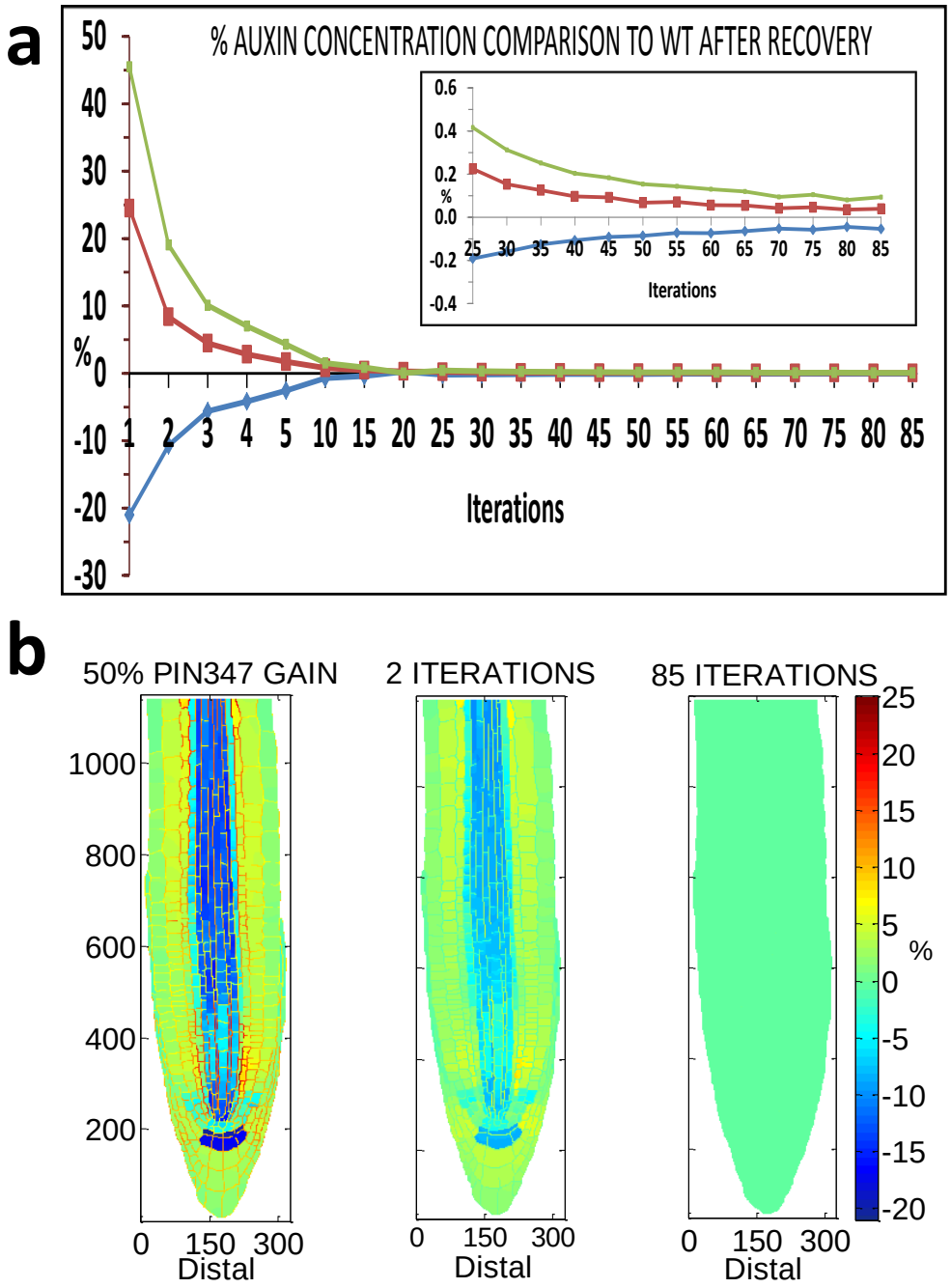

Figure 4.4: Auxin pattern recovery after 50% PIN3,4,7 gain

Pattern recovery after 50% gain in total wildtype PIN3,4,7 concentrations, using the recovery principle over 85 iterations. **(a)** Progressive auxin percentage difference from wildtype in the whole root. Blue curve shows the maximum auxin percentage difference below wildtype in the root at each iteration. Red curve shows the maximum auxin percentage difference above wildtype in the root at each iteration. Green curve shows the maximum range of the percentage difference from wildtype within the root, calculated by adding the absolute values of the blue and red curves at each iteration. **(b)** Colour map images of the percentage difference from wildtype auxin concentrations after the initial perturbation of 50% gain of PIN3,4,7, then after 2 recovery iterations, and at full recovery after 85 iterations. Symbol % is the percentage difference relative to corresponding wildtype value.

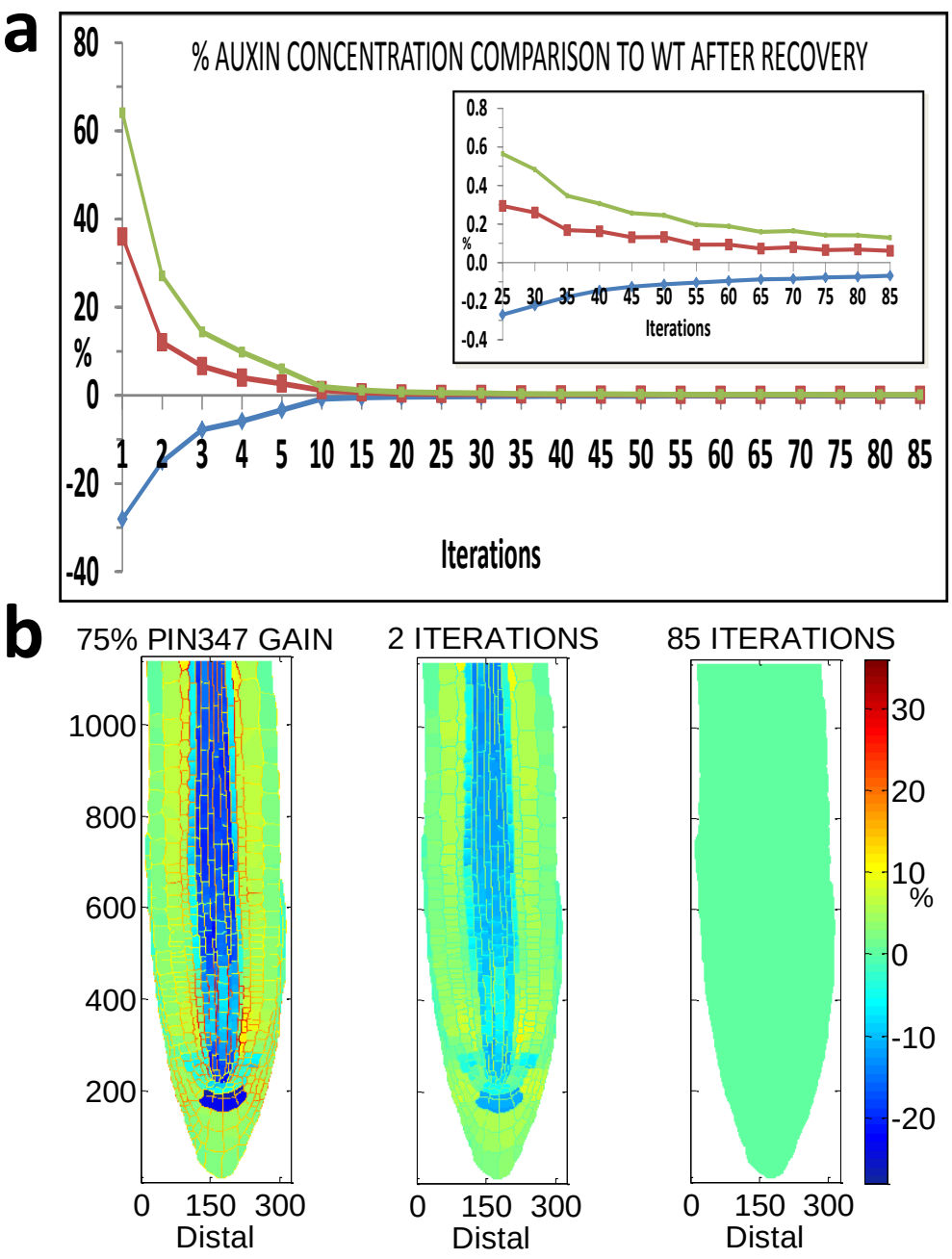

Figure 4.5: Auxin pattern recovery after 75% PIN3,4,7 gain

Pattern recovery after 75% gain in total wildtype PIN3,4,7 concentrations, using the recovery principle over 85 iterations. **(a)** Progressive auxin percentage difference from wildtype in the whole root. Blue curve shows the maximum auxin percentage difference below wildtype in the root at each iteration. Red curve shows the maximum auxin percentage difference above wildtype in the root at each iteration. Green curve shows the maximum range of the percentage difference from wildtype within the root, calculated by adding the absolute values of the blue and red curves at each iteration. **(b)** Colour map images of the percentage difference from wildtype auxin concentrations after the initial perturbation of 75% gain of PIN3,4,7, then after 2 recovery iterations, and at full recovery after 85 iterations. Symbol % is the percentage difference relative to corresponding wildtype value.

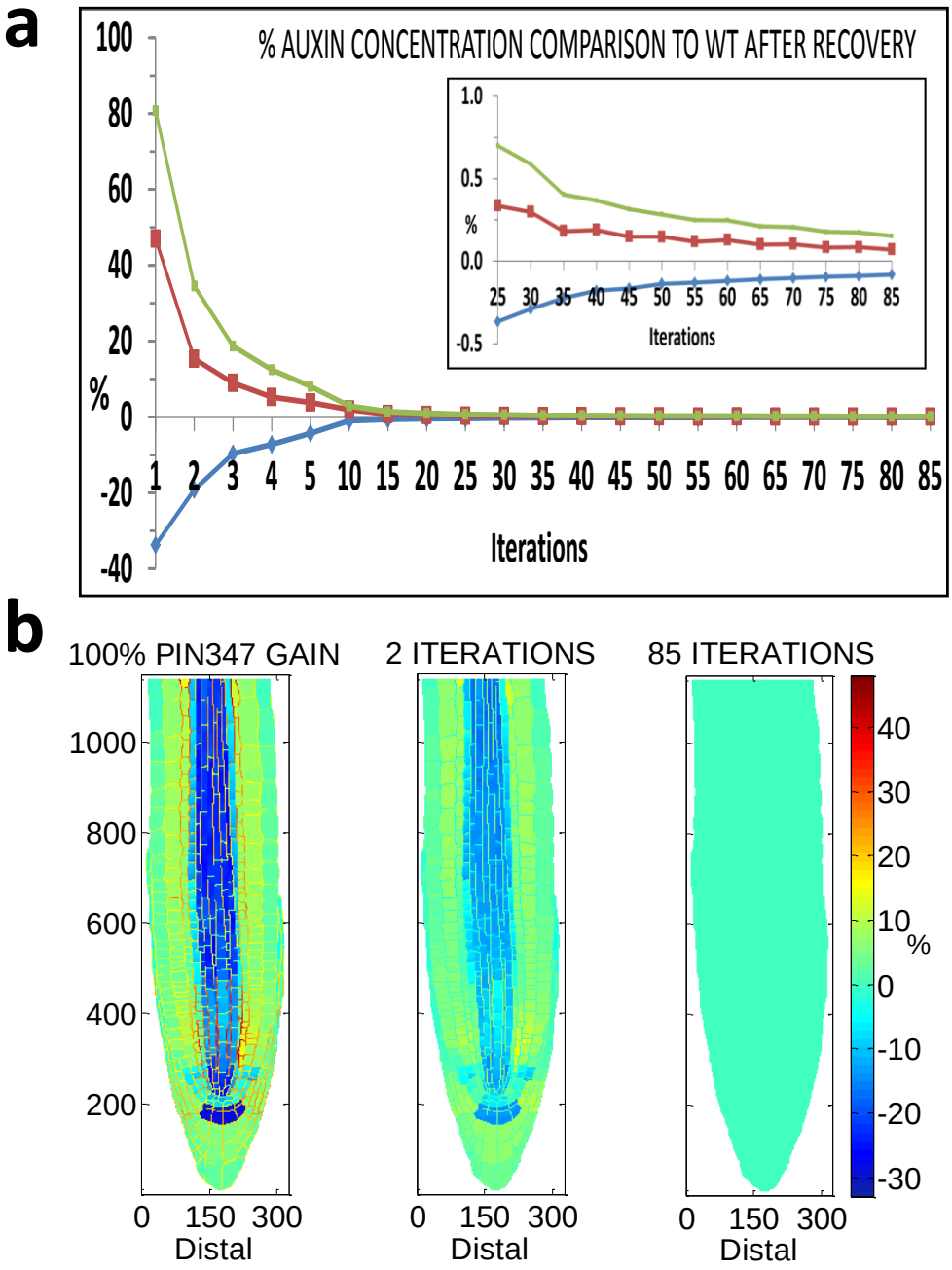

Figure 4.6: Auxin pattern recovery after 100% PIN3,4,7 gain

Pattern recovery after 100% gain in total wildtype PIN3,4,7 concentrations, using the recovery principle over 85 iterations. **(a)** Progressive auxin percentage difference from wildtype in the whole root. Blue curve shows the maximum auxin percentage difference below wildtype in the root at each iteration. Red curve shows the maximum auxin percentage difference above wildtype in the root at each iteration. Green curve shows the maximum range of the percentage difference from wildtype within the root, calculated by adding the absolute values of the blue and red curves at each iteration. **(b)** Colour map images of the percentage difference from wildtype auxin concentrations after the initial perturbation of 100% gain of PIN3,4,7, then after 2 recovery iterations, and at full recovery after 85 iterations. Symbol % is the percentage difference relative to corresponding wildtype value.

4.4 Non-uniform, polar AUX1/LAX required for recovery

The computed AUX1/LAX carrier patterns for wildtype auxin pattern recovery reveal that, when PIN carriers maintain their polarity but change levels, pattern recovery requires non-uniform and polar distribution of AUX1/LAX**.** AUX1/LAX concentrations can vary at the same cell face and AUX1/LAX influx carrier polarity can also be identified. In recovery from 75% loss of total PIN3, 4 and 7, regions of vascular and pericycle cells exhibit higher average AUX1/LAX levels at apical cell faces (Figure 4.7). This polarity can be similar or opposite to total PIN (total of PIN1,2,3,4,7) polarity depending on root location and the original perturbation (Figure 4.8).

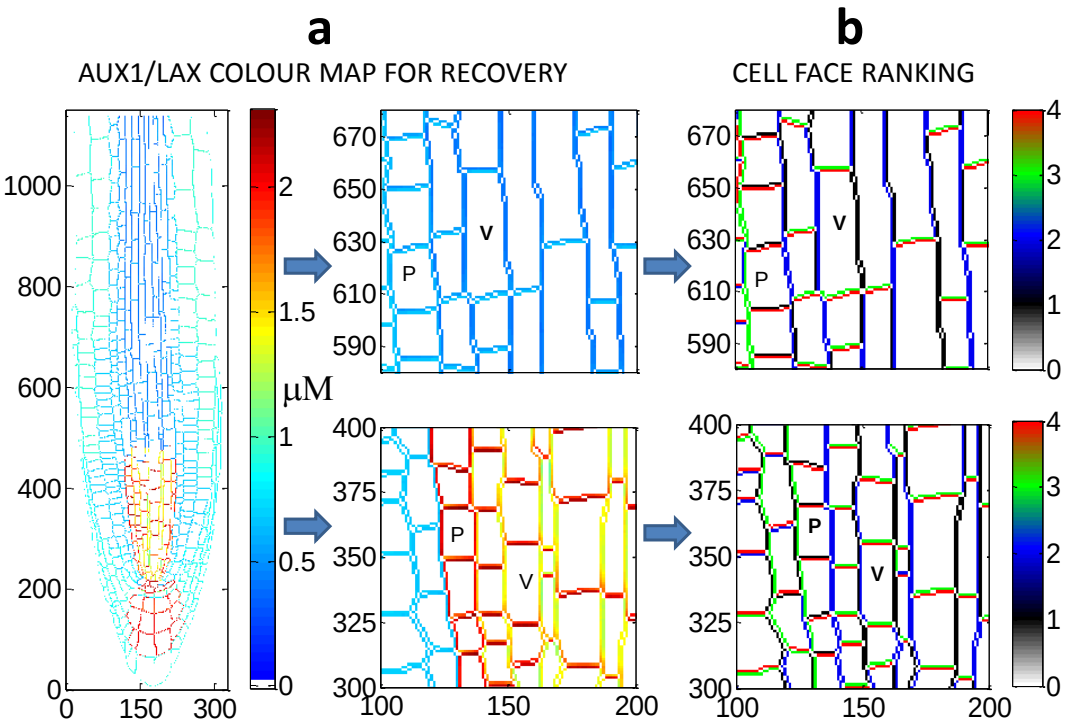

Figure 4.7: AUX1/LAX recovery pattern after 75% PIN3,4,7 loss.
(a) AUX1/LAX concentration colour map for auxin pattern recovery from 75% loss in WT total PIN347, requires non-uniform and polar distribution of AUX1/LAX. (b) AUX1/LAX average cell face concentrations are ranked 1 to 4 (1 low to 4 high) for each cell, showing polar distribution of AUX1/LAX influx carriers. This is calculated by averaging the data in each cell face in (a) and by ranking them in terms of the average values. P: pericycle cell, V: vascular cell.

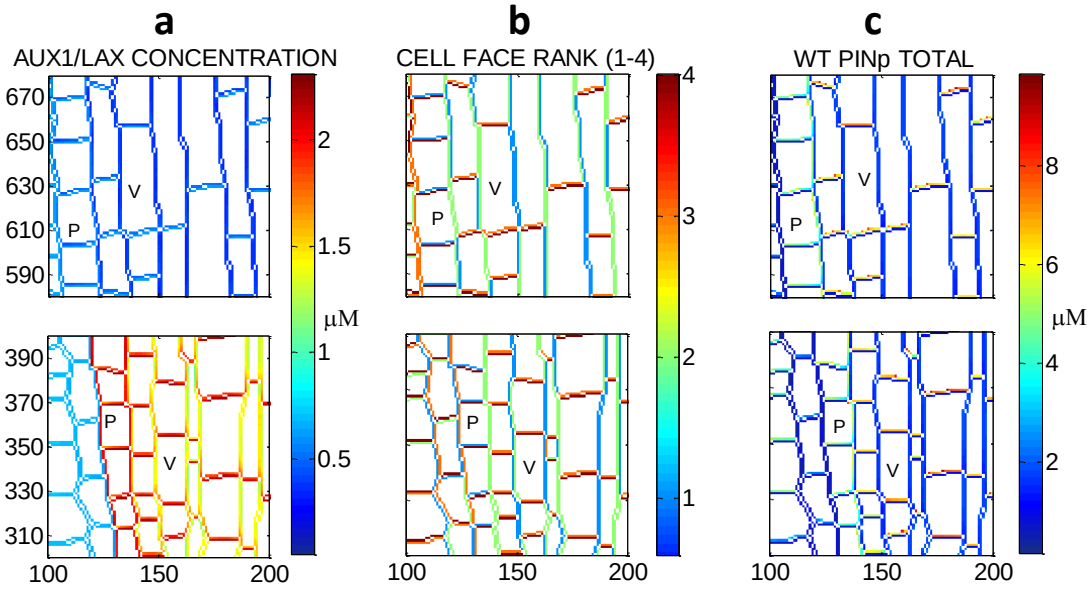

Figure 4.8: Enlarged AUX1/LAX recovery pattern after 75% PIN3,4,7 loss. For two enlarged regions of the root, AUX1/LAX concentration patterning required for auxin pattern recovery from 75% loss in WT total PIN347, AUX1/LAX cell face concentration ranking for recovery, and wildtype total PINp patterning. (a) AUX1/LAX colour map for recovery requires non-uniform and polar distribution of AUX1/LAX. (b) AUX1/LAX average cell face concentrations are ranked 1 to 4 (1 low to 4 high) for each cell and model imaging of the concentration rankings demonstrates polar AUX1/LAX distribution. (c) Polar distribution of total PINp (total PIN1,2,3,4,7) in WT (P – pericycle cell, V – vascular cell).

Experimentally, in many cells AUX1/LAX appears to have non-polar distribution (Band *et al*., 2014; Peret *et al*., 2012); however, AUX1 polarity does exist and is observed in protophloem cells (Kleine-Vehn *et al*., 2006). In the wildtype, polar PIN and non-polar AUX1/LAX carriers combine to generate wildtype auxin patterning. When total wildtype PIN3,4,7 is perturbed, wildtype auxin pattern recovery requires non-uniform and polar distribution of AUX1/LAX influx carriers. This highlights the importance of polarity in combined PIN and AUX1/LAX carrier activity to generate a specific quantitative auxin pattern.

4.5 Auxin pattern recovery leads to PIN1 and PIN2 pattern recovery

Auxin pattern recovery also leads to quantitative recovery of PIN1 and 2 patterning (Figure 4.9). After reducing total PIN3,4,7 concentration, modelling results predict that PIN1 and 2 concentration increases in the plasma membrane of vascular cells (Figure 4.9). This is similar to experimental

observations for the *pin3pin4pin7* triple mutant (Blilou *et al*., 2005). After auxin recovery, the level and patterning of both total PIN3,4,7 and AUX1/LAX differ from their original WT patterning; however, PIN1 and 2 levels and patterning return to their original values (Figure 4.9). This reflects the regulation of PIN1 and PIN2 level and patterning by hormonal crosstalk and demonstrates the mutual regulation of auxin and its transporters via hormonal crosstalk. Therefore, the recovery principle reveals that the patterning of auxin concentration and of the influx and efflux carriers are interlinked.

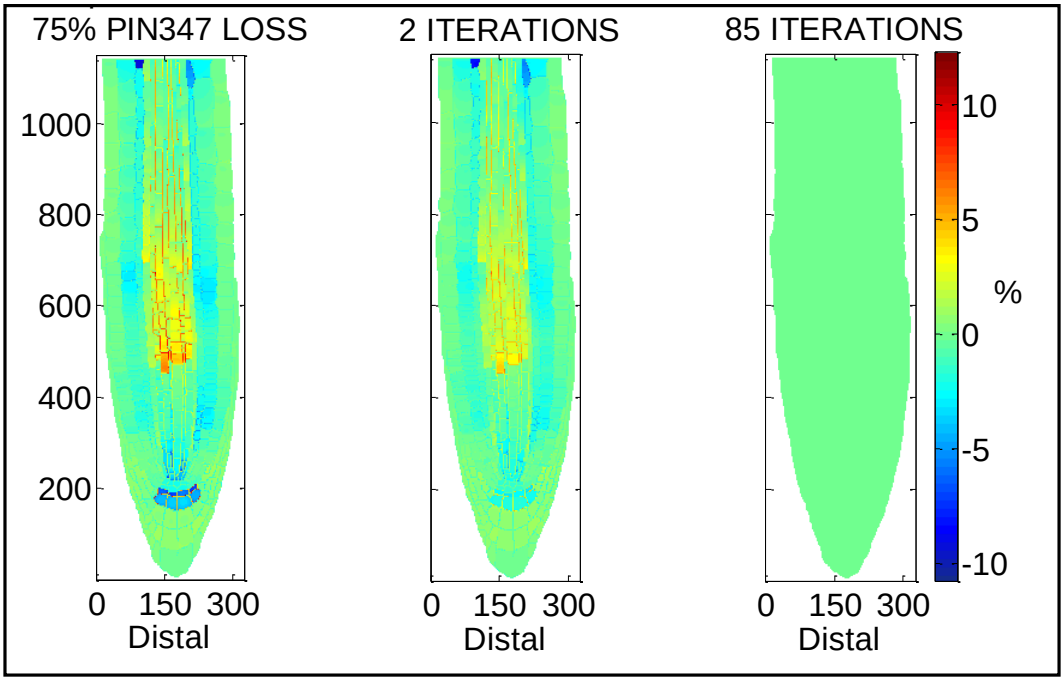

Figure 4.9: PIN12 pattern recovery

PINp12 pattern recovery after 75% decrease in total wildtype PIN3,4,7 concentrations, using the recovery principle over 85 iterations. Colour map images of the % deviation of PINp12 from WT concentrations in the root after the initial perturbation of 75% loss of PIN3,4,7, then after 2 recovery iterations, and full recovery after 85 iterations.

4.6 Uniform AUX1/LAX distribution changes the recovered auxin pattern

To further explore the roles of PIN and AUX1/LAX carriers in generating auxin patterning, after recovery from perturbations in PIN3,4,7 the AUX1/LAX concentrations at the plasma membrane are averaged for each individual cell in the root for the six recovery cases investigated. Although averaging does not change the total AUX1/LAX level at the plasma membrane of any given cell, it guarantees a uniform AUX1/LAX distribution at the plasma membrane of each

cell. After averaging, AUX1/LAX carriers have uniform non-polar cellular distribution, however the average varies between cells. Figure 4.10 shows that uniform AUX1/LAX distribution leads to changes in auxin patterning compared to the equivalent non-uniform AUX1/LAX distribution. This demonstrates that, while non-uniform polar AUX1/LAX distribution can recover wildtype auxin patterning, the corresponding uniform distribution cannot. Therefore, while the same level of AUX1/LAX influx carriers is maintained, uniform distribution generates a specific auxin pattern that differs from the pattern generated by non-uniform distribution, indicating the importance of uniform and non-uniform (or non-polar and polar) distribution of AUX1/LAX influx carriers in controlling auxin patterning.

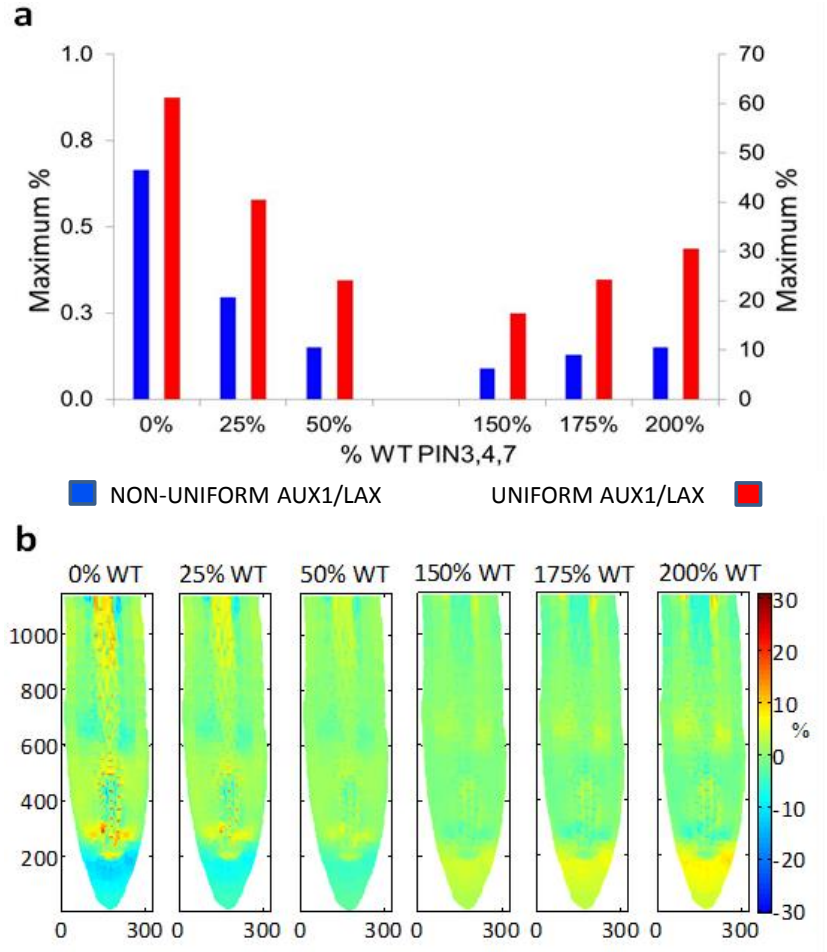

Figure 4.10: Auxin pattern recovery by uniform and non-uniform AUX1/LAX Comparison of recovery from 6 different total PIN3, 4 and 7 concentrations set at 0%, 25%, 50%, 150%, 175% and 200% of wildtype. (a) Maximum percentage difference of auxin concentration from WT after recovery by non-uniform (blue bar, left y-axis) and uniform (red bar, right y-axis) AUX1/LAX distribution, for the 6 cases. (b) Colour maps of percentage difference of auxin concentration from WT after recovery by uniform AUX1/LAX distribution, for each case, none of which exhibit full recovery. Symbol % is the percentage difference relative to corresponding wildtype value.

4.7 PIN and AUX1/LAX for a specific auxin pattern are not spatially correlated

Six cases of wildtype auxin patterning recovery were investigated, revealing that multiple combinations of interlinked PIN and AUX1/LAX patterns can lead to the same target auxin pattern. Biologically, polar PIN carriers differentially direct and deplete cellular auxin, while AUX1/LAX carriers act to retain cellular auxin. Further insights into how PIN and AUX1/LAX carriers can combine to generate specific auxin patterning were gained by exploring whether multiple combinations of interlinked PIN and AUX1/LAX patterns for generating the same auxin pattern exhibit spatially proportional correlation. Any correlation would imply that the effect on auxin patterning of changing polar PIN activity can be compensated by proportionately changing AUX1/LAX activity.

Figure 4.11 reveals the spatial complexity of relationships between influx and efflux carriers. Different PIN and AUX1/LAX pattern combinations, that maintain the same auxin pattern, do not exhibit spatially proportional correlation. Although auxin patterning is recovered, the ratio of total PIN in '75% PIN3,4,7 loss' to wildtype recovery is generally not equal to the corresponding ratio for AUX1/LAX. This reveals that the effects on auxin patterning of changing polar PIN activity are not compensated by a proportional change in AUX1/LAX activity. Another level of complexity is that relationships between PIN and AUX1/LAX for maintaining an auxin pattern depend on the absolute levels of these carriers. Comparing Figure 4.11(a) and Figure 4.11(b), shows that 75% reduction of PIN3,4,7 and 75% increase of PIN3,4,7 require different relationships between PIN and AUX1/LAX to maintain the same auxin patterning. This complexity exists for all six cases investigated (where total PIN3, 4 and 7 concentrations are set at 0%, 25%, 50%, 150%, 175% and 200% of wildtype) (Figure 4.11, Figure 4.12, Figure 4.13). Therefore, PIN and AUX1/LAX patterning for maintaining an auxin pattern do not have a spatially proportional correlation.

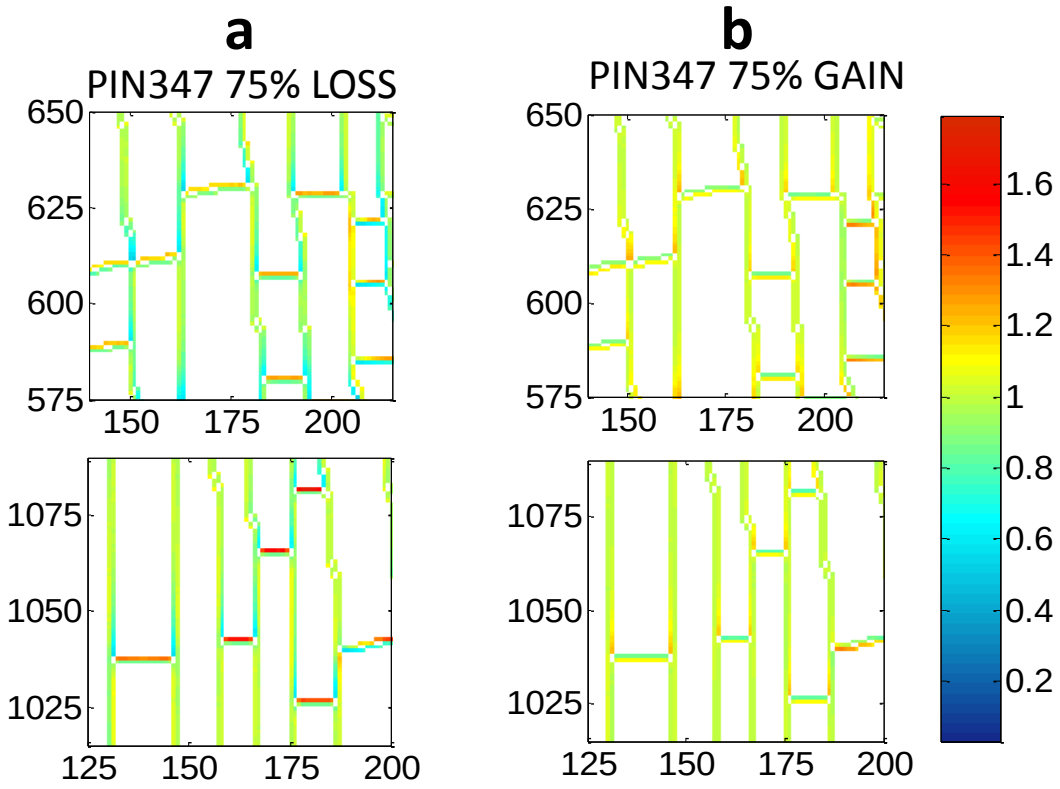

Figure 4.11: PIN and AUX1/LAX pattern combinations giving the same target auxin pattern are not correlated (example 1)

This figure shows the **RATIO OF TWO RATIOS = RATIO1/RATIO2** where **RATIO1 = (TOTAL PIN AFTER RECOVERY) / (TOTAL PIN IN WILDTYPE**) **RATIO2 =** (**TOTAL AUX1,LAX AFTER RECOVERY) / (TOTAL AUX1,LAX IN WT**). (a) Recovery from 75% PIN347 loss. (b) Recovery from 75% PIN347 gain. Both (a) and (b) show the same two regions of the root, and they demonstrate that, although auxin patterning is recovered for both cases, the ratio of ratios is generally not unity and is also not constant, implying that PIN and AUX1/LAX patterns that maintain the same auxin pattern do not exhibit spatially proportional correlation. Comparing figures (a) and (b) shows that this ratio of ratios is different for 75% loss of PIN3,4,7 and for 75% gain of PIN3,4,7, implying that 75% loss of PIN3,4,7 and 75% gain of PIN3,4,7 require different relationships between PIN and AUX1/LAX to maintain the same auxin patterning.

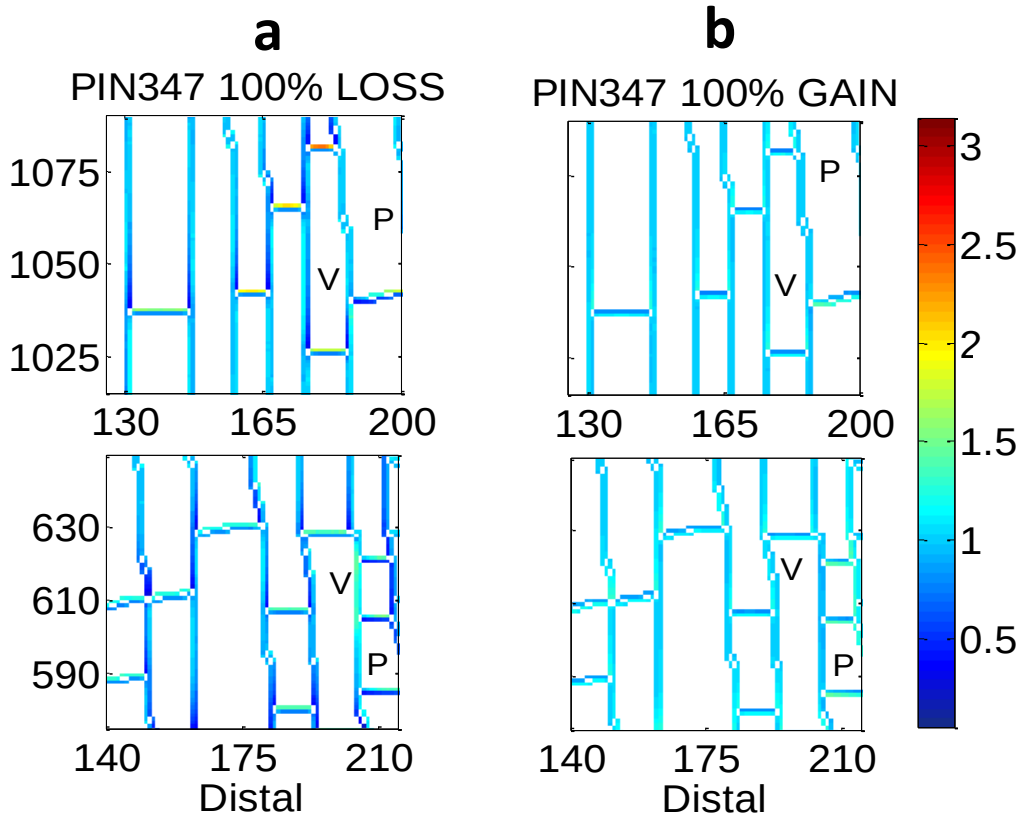

Figure 4.12: PIN and AUX1/LAX pattern combinations giving the same target auxin pattern are not correlated (example 2)

This figure shows the **RATIO OF TWO RATIOS = RATIO1/RATIO2** where **RATIO1 = (TOTAL PIN AFTER RECOVERY) / (TOTAL PIN IN WILDTYPE**) **RATIO2 =** (**TOTAL AUX1,LAX AFTER RECOVERY) / (TOTAL AUX1,LAX IN WT**). (a) Recovery from 100% PIN347 loss. (b) Recovery from 100% PIN347 gain. Both (a) and (b) show the same two regions of the root, and they demonstrate that, although auxin patterning is recovered for both cases, the ratio of ratios is generally not unity and is also not constant, implying that PIN and AUX1/LAX patterns that maintain the same auxin pattern do not exhibit spatially proportional correlation. Comparing figures (a) and (b) shows that this ratio of ratios is different for 100% loss of PIN3,4,7 and for 100% gain of PIN3,4,7, implying that 100% loss of PIN3,4,7 and 100% gain of PIN3,4,7 require different relationships between PIN and AUX1/LAX to maintain the same auxin patterning. P: pericycle; V: vascular.

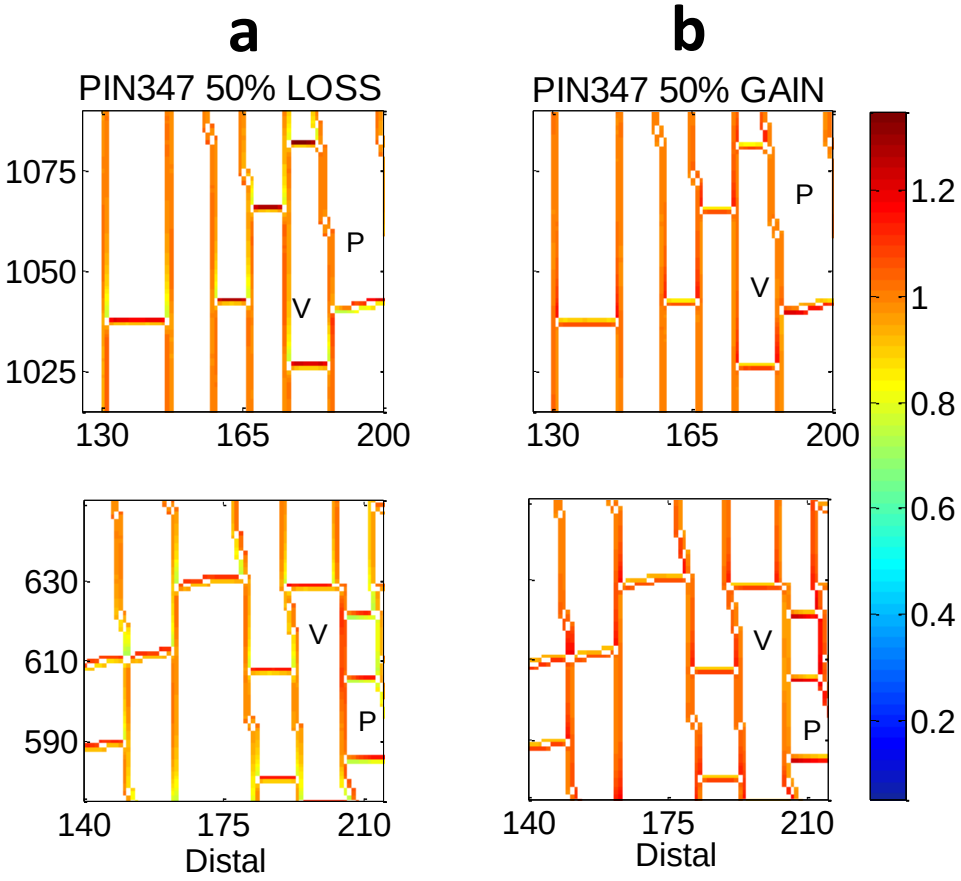

Figure 4.13: PIN and AUX1/LAX pattern combinations giving the same target auxin pattern are not correlated (example 3)

This figure shows the **RATIO OF TWO RATIOS = RATIO1/RATIO2** where **RATIO1 = (TOTAL PIN AFTER RECOVERY) / (TOTAL PIN IN WILDTYPE**) **RATIO2 =** (**TOTAL AUX1,LAX AFTER RECOVERY) / (TOTAL AUX1,LAX IN WT**). (a) Recovery from 50% PIN347 loss. (b) Recovery from 50% PIN347 gain. Both (a) and (b) show the same two regions of the root, and they demonstrate that, although auxin patterning is recovered for both cases, the ratio of ratios is generally not unity and is also not constant, implying that PIN and AUX1/LAX patterns that maintain the same auxin pattern do not exhibit spatially proportional correlation. Comparing figures (a) and (b) shows that this ratio of ratios is different for 50% loss of PIN3,4,7 and for 50% gain of PIN3,4,7, implying that 50% loss of PIN3,4,7 and 50% gain of PIN3,4,7 require different relationships between PIN and AUX1/LAX to maintain the same auxin patterning. P: pericycle; V: vascular.

4.8 Quantitative recovery from AUX1/LAX changes requires modifed PIN polarity

At different PIN levels, maintaining an auxin pattern can require non-uniform and polar AUX1/LAX distribution (Figure 4.7). A uniform AUX1/LAX distribution leads to deviations from target auxin patterning (Figure 4.10), demonstrating the significance of polarity in PIN and AUX1/LAX carrier combinations for generating a specific auxin pattern.

The recovery principle can also be used to search for the level and localisation of PIN required for recovery after AUX1/LAX carriers are perturbed, by considering the role of PIN carriers in auxin transport from the cytosol to cell wall. To recover auxin patterning by adjusting PIN after AUX1/LAX perturbation, the recovery principle requires that equations 2 and 3 are replaced by equations 4 and 5.

$$PIN_{p,i+1} = \frac{[Auxin]_{p,0}}{[Auxin]_{p,i}} PIN_{p,i} \quad \text{if} \quad R_{p,i} > R_{c,i} \qquad \text{(equation 4)}$$

$$PIN_{p,i+1} = \frac{[Auxin]_{c,i}}{[Auxin]_{c,0}} PIN_{p,i} \quad \text{if} \quad R_{p,i} \leq R_{c,i} \qquad \text{(equation 5)}$$

$PIN_{p,i+1}$ is the searched 'new' PIN concentration, calculated by adjusting the 'old' PIN concentration ($PIN_{p,i}$) using the above equations. At the first iteration (i=1), $PIN_{p,i}$ is equal to the initial PIN concentration (e.g. WT), before any adjustments have occurred.

The recovery principle shows that, at different levels of uniformly localised AUX1/LAX, maintenance of auxin pattern requires changes in PIN polarity (Figure 4.14).

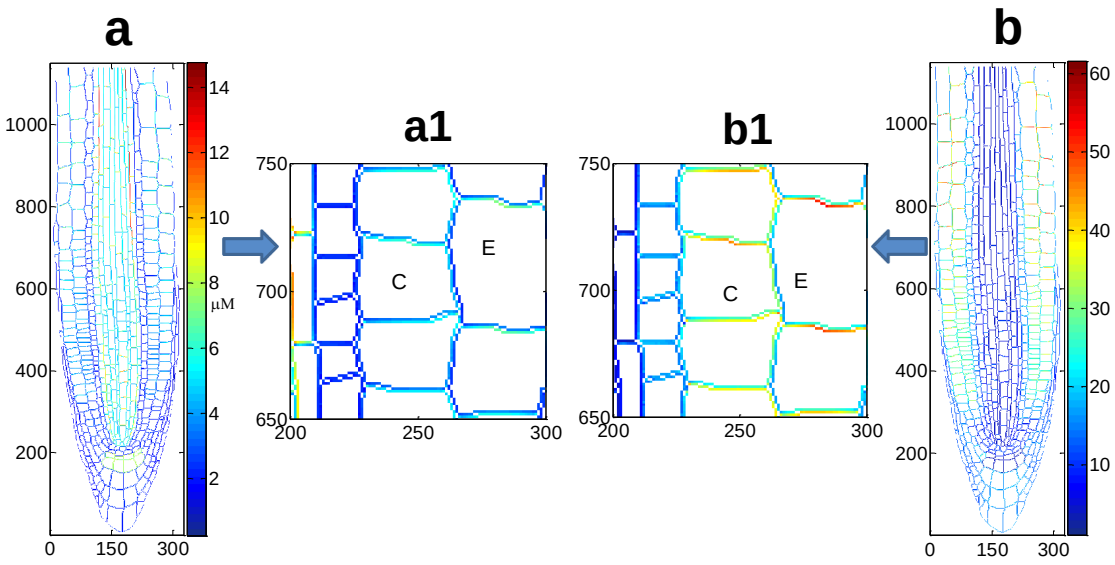

Figure 4.14: PIN3,4,7 polarity after recovery from 50% AUX1/LAX gain compared to WT PIN3,4,7 polarity

The polarity of PIN3,4,7 after wildtype auxin pattern recovery from a 50% gain in AUX1/LAX level, is different from PIN3,4,7 polarity in wildtype. **(a)** Colour map of total PIN3,4,7 after recovery to wildtype auxin patterning. (**a1)** Shows an enlarged view of this map in selected epidermal and cortical cells. (**b**) Colour map of the ratio of PIN3,4,7 after auxin pattern recovery to wildtype PIN3,4,7, therefore there are no units. (**b1)** shows an enlarged view of this map in the epidermal and cortical cells, corresponding to the region shown in (a1). Total PIN3,4,7 has no polarity in the wildtype epidermal and cortical cell files (Figure 3.5), however total PIN3,4,7 polarity can be observed in these cells after recovery in (a1), where there is greater PIN3,4,7 concentrations at the apical cell faces. This is confirmed in (b1) where the red/brown/yellow colours indicate a consistently larger proportional increase in PIN3,4,7 after recovery compared to wildtype at the apical faces of these cells. This result shows that, in these epidermal and cortical cells, the polarity of PIN3,4,7 after wildtype auxin pattern recovery from a 50% gain in AUX1/LAX level, is different from PIN3,4,7 polarity in wildtype. C: cortical cells. E: epidermal cells.

When AUX1/LAX levels are increased to 50% above wildtype, wildtype auxin patterning can be recovered, but the searched PIN3,4,7 polarity differs from wildtype. The searched total PIN3,4,7 localisation in epidermal cells displays polarity that does not exist in wildtype (Figure 4.14), indicating that the corresponding relationship between influx level and efflux polarity, rather than the individual activity of either the influx or efflux carriers, controls auxin pattern formation.

4.9 Recovery principle allows searchable relationships for influx and efflux carriers

The recovery principle reveals that the same wildtype reference auxin pattern can emerge from multiple combinations of interlinked, but not spatially proportionally correlated, levels and localisation of influx and efflux carriers. This principle reveals novel aspects of auxin patterning control and enables the search for unknown PIN and AUX1/LAX carrier combinations that generate a known (and not necessarily wildtype) target auxin pattern (Figure 4.15).

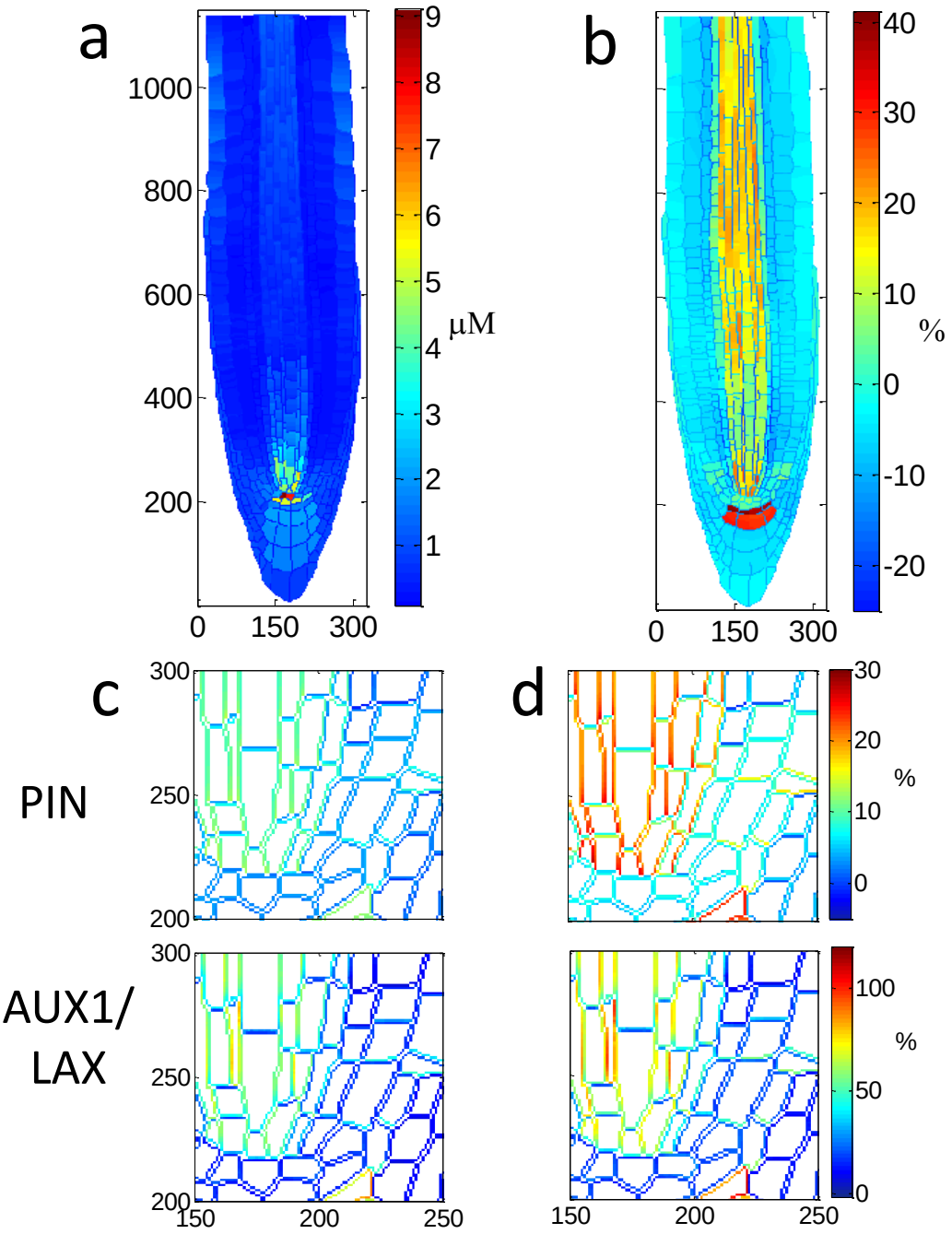

Figure 4.15: Different PIN and AUX1/LAX combinations can generate the same target pattern

Recovery from a 15% gain in PIN3,4,7 and from a 30% gain in PIN3,4,7, to the same target auxin pattern shows that two very different combinations of interlinked PIN and AUX1/LAX can lead to the same auxin pattern. **(a**) Auxin concentration colour map for the target auxin pattern created by a 50% loss in PIN3,4,7. **(b)** The percentage difference of target auxin pattern from the WT. **(c)** Total PIN and AUX1/LAX percentage comparison to WT for recovery to target from a 15% gain in PIN3,4,7 for a selected area of the root. **(d)** Total PIN and AUX1/LAX percentage comparison to WT for recovery to target from a 30% gain in PIN3,4,7 for the same selected area of the root. In (c) and (d), symbol % is the percentage difference relative to corresponding wildtype value.

The recovery principle discovers two interlinked PIN and AUX1/LAX pattern combinations (Figure 4.15c,d) that both recover a known target auxin pattern (Figure 4.15a,b). Although PIN patterning in Figure 4.15c and Figure 4.15d differ significantly, when combined with their corresponding AUX1/LAX patterns they generate the same target auxin pattern. Thus, for a known target auxin pattern, the recovery principle can search for multiple PIN and AUX1/LAX pattern combinations that achieve target patterning. Therefore by using the recovery principle, relationships between level and localisation of influx and efflux carriers become searchable.

4.10 Summary

The model developed to this point integrates a variety of experimental data and makes various predictions that can be experimentally validated. Formulation of the recovery principle also enables the model to be used to provide further insights into the control of auxin patterning and gradients in *Arabidopsis* root.

For reasons given above, the PIN3,4 and 7 auxin efflux carriers and the AUX1/LAX auxin influx carrier concentrations are prescribed and not established by the crosstalk network; therefore, the model cannot 'predict' or 'explain' how specific perturbations in one carrier set would affect the level and polarity of PIN3,4,and 7 or AUX1/LAX; however, since the hormonal crosstalk network for PIN1,2 can be established (Moore *et al*., 2015a), effects of the prescribed auxin carriers on PIN1,2 patterning can be predicted (Figure 3.17) and compared with experimental observations. Although it is not possible to 'predict' all relationships between the influx and efflux carriers, the recovery principle allows us to theoretically explore how the two carrier types could potentially coordinate their activity to establish and maintain auxin patterning and the possible implications for carrier concentration levels and polarity. In doing so, it is possible to effectively integrate the analysis of both carrier sets with auxin patterning rather than investigate the activity of one or other carrier type in isolation.

This work is done within the existing crosstalk network, which includes auxin biosynthesis and degradation mechanisms. By formulating a recovery principle, it reveals how the level and localisation of both influx and efflux carriers are

possibly interlinked with the other network processes to quantitatively control auxin pattern formation and how multiple combinations of levels and localisation of efflux and influx carriers could generate the same auxin pattern. Therefore, a specific auxin pattern is not necessarily uniquely determined by just a single efflux and influx carrier combination.

The relationship between levels and localisation of the carriers plays a key role in determining a specific auxin pattern. When efflux carriers retain their original polarity but their levels are increased or decreased, both influx carrier level and polarity require simultaneous adjustment to maintain the original auxin pattern (Figure 4.16a). Similarly, at different levels of influx carriers with the same non-polar localisation, both the level and polarity of efflux carriers must also be simultaneously changed to maintain auxin patterning. Therefore, the relationship between influx and efflux level and polarity rather than the separate activity of either influx or efflux carriers, potentially controls auxin pattern formation.

Since the recovery principle shows that the same auxin pattern can possibly emerge from multiple combinations of interlinked, but not spatially proportionally correlated, levels and localisation of both influx and efflux carriers, this enables searchable relationships between influx and efflux activity to achieve a specific auxin pattern (Figure 4.16b) where, given a target auxin pattern and the patterning of one carrier set, then the required patterning of the other carrier set can be generated. In addition, a recovered auxin pattern leads to quantitative PIN1 and 2 pattern recovery. Therefore, auxin concentration, and influx and efflux carrier patterning are all potentially interlinked into an integrated system.

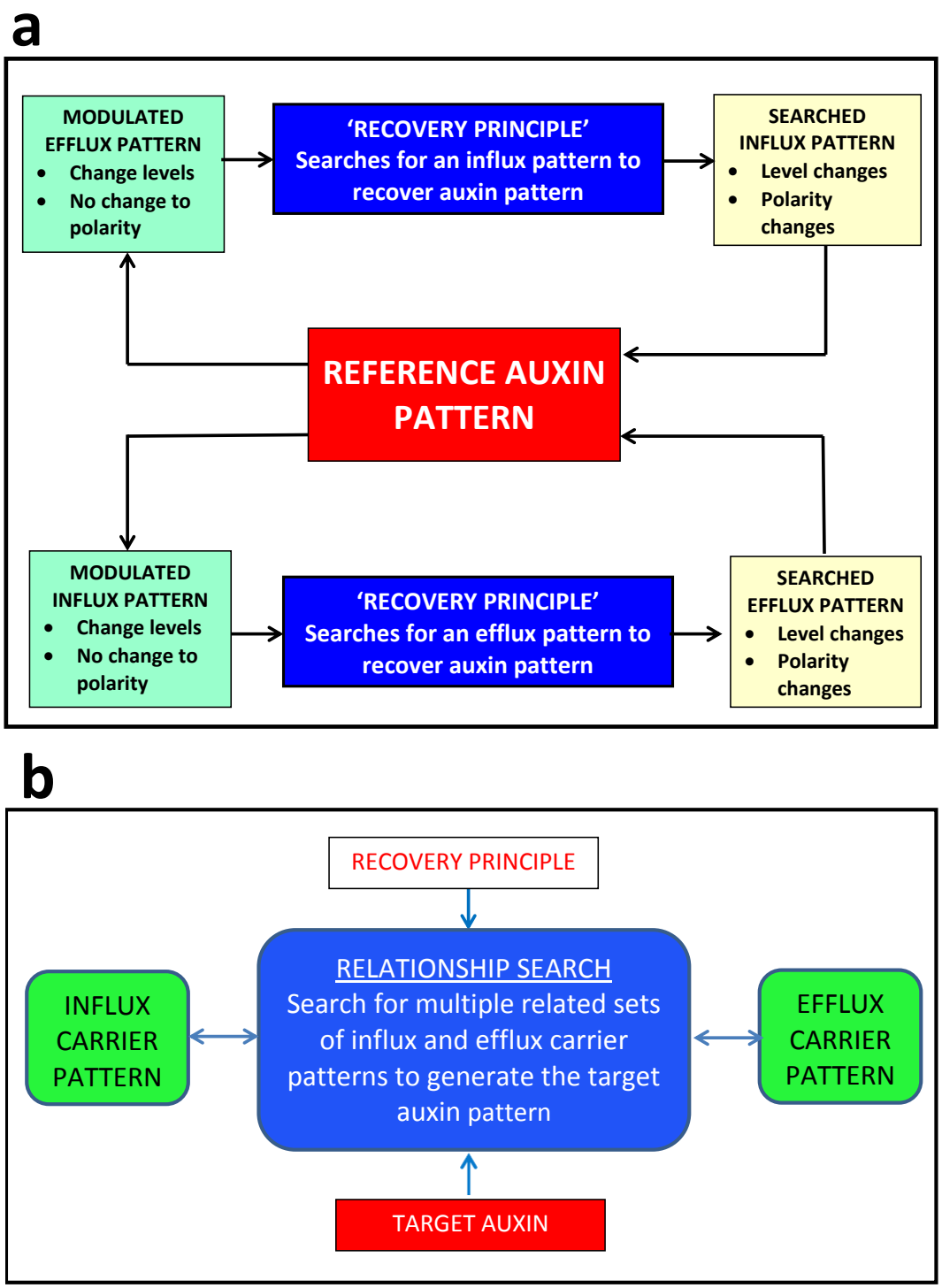

Figure 4.16: The recovery principle and auxin carriers and patterning
(**a**) For recovery, changes in level in either the influx or efflux carriers require changes in both the polarity and level of the opposing carrier. (**b**) The recovery principle makes it possible to search for influx and efflux carrier combinations that achieve a target auxin pattern.

CHAPTER 5 : ALTERNATIVE NETWORK FOR CYTOKININ PATTERNING

ALTERNATIVE NETWORK FOR CYTOKININ PATTERNING

5.1 Introduction

Cytokinin is developmentally significant as demonstrated by the role it plays in conjunction with auxin in defining the developmental pathway of callus cells (Skoog and Miller, 1957), in delay of senescence (reviewed by Zhang and Zhou, 2013), in the regulation of PIN auxin efflux carriers (Ruzicka *et al*., 2009; Bishopp *et al*., 2011a), and in determining the size of the root meristem and the length of the root (Dello Ioio *et al*., 2007; Werner *et al*., 2003). It has been demonstrated that cytokinin predominantly has tissue-specific biosynthesis (Miyawaki *et al*., 2004) and that it is transported in the phloem (Bishopp *et al*., 2011b). It has also recently been shown that cytokinin transporter proteins (PUP14) actively import cytokinin from the apoplast into the cytoplasm for degradation (Zurcher *et al*., 2016), potentially reducing cytokinin signalling at the plasma membrane.

In both rectangular and realistic root models (Chapters 2 - 4), cytokinin biosynthesis does not occur in the epidermis, cortex and endodermal cell files, and cytokinin flux occurs by diffusion. The relationships between auxin, cytokinin and ethylene are based on results from Nordstrom *et al*. (2004) which show that auxin inhibits cytokinin biosynthesis in the whole seedling, on Nordstrom *et al*. (2004) and Eklof *et al*. (1997) which demonstrate that cytokinin inhibits auxin, and on Stepanova *et al*. (2007) and Swarup *et al*. (2007) which show that auxin biosynthesis is stimulated by ethylene. However, it was also found that cytokinin promotes auxin biosynthesis in young developing tissue (Jones *et al*., 2010), auxin upregulates cytokinin biosynthesis through *SHY2* and *IPT5* genes (Dello Ioio *et al*., 2008), and auxin promotes cytokinin biosynthesis through TM05 and LOG4 (De Rybel *et al*., 2014).

In the Nordstrom *et al*. (2004) paper, auxin and CK biosynthesis rates were measured by deuterium labelling and mass spectrometry in 3 week old plants. Results indicated that different types of CK (iP and Z type) were predominantly synthesised in either the shoot (Z) or the root (iP) and that while biosynthesis of the Z type CK was inhibited by auxin, the biosynthesis of iP type CK was not inhibited and even potentially promoted by the application of auxin. Therefore

an alternative conclusion from this paper is that while auxin inhibits CK biosynthesis in the whole plant, it might not inhibit CK biosynthesis in the root and could even promote it. This paper also examined the effects of CK on auxin biosynthesis, where the application of CK inhibited auxin biosynthesis; however this was a delayed reaction and it was suggested that it was possibly mediated by plant developmental changes rather than metabolic interaction.

Results from Jones *et al*. (2010), again using deuterium labelling, suggested that CK promotes auxin biosynthesis in young developing tissues and that CK promotes its own degradation through the induction of CK oxidases. They proposed that the apparent contradiction with Nordstrom *et al*. (2004) could have been because the Nordstrom *et al*. (2004) results were based on 3 week old whole plants while Jones *et al*. (2010) separated young growing tissues from 10 day old seedlings.

The model results for cytokinin patterning in the rectangular and the realistic root both show discrepancies compared to experimental imaging results (Figure 2.17 and Figure 3.14). Given these discrepancies, the developmental importance of cytokinin, and the different proposed relationships where cytokinin either inhibits (Nordstrom *et al*., 2004) or promotes (Jones *et al*., 2010) auxin biosynthesis, and where auxin either inhibits (Nordstrom *et al*., 2004) or promotes cytokinin synthesis (Dello Ioio *et al*., 2008), it was decided to use the GG model to test different relationships for mutual auxin and cytokinin regulation to see if these resulted in any significant changes to the patterning results from previous chapters, and in particular to see if modelled cytokinin results, for both patterning and comparative average concentration in WT and *pls,* could simultaneously match experimental results. The cytokinin patterning results for the existing crosstalk network (where auxin inhibits CK and CK inhibits auxin biosynthesis) were compared to results from a new version of the GG model in which cytokinin promotes auxin biosynthesis (Jones *et al*., 2010) and auxin inhibits cytokinin biosynthesis (Nordstrom *et al*., 2004). A second model revision was considered (but discarded) where cytokinin promotes auxin biosynthesis (based on Jones *et al*., 2010) and auxin promotes cytokinin biosynthesis (based on Dello Ioio *et al*., 2008) since, while possibly improving cytokinin patterning it would have resulted in a reduction in cytokinin

concentration in the *pls* mutant given that PLS promotes auxin and auxin promotes cytokinin.

Comparative results between the existing and a revised GG model (where cytokinin promotes auxin and auxin inhibits cytokinin) are shown for auxin (Figure 5.1) and cytokinin (Figure 5.2). The two models display very similar patterning results, with no improvement in cytokinin patterning. In addition, there was no significant difference between the two models in patterning and concentration results for all other species and mutants.

To explore further modifications in the relationships between auxin and cytokinin, where say they each promote the biosynthesis of the other, while achieving both improved cytokinin patterning and the correct relative average cytokinin concentration for the *pls* mutant and wildtype, would however require additional regulatory links for cytokinin that do not exist in the current models.

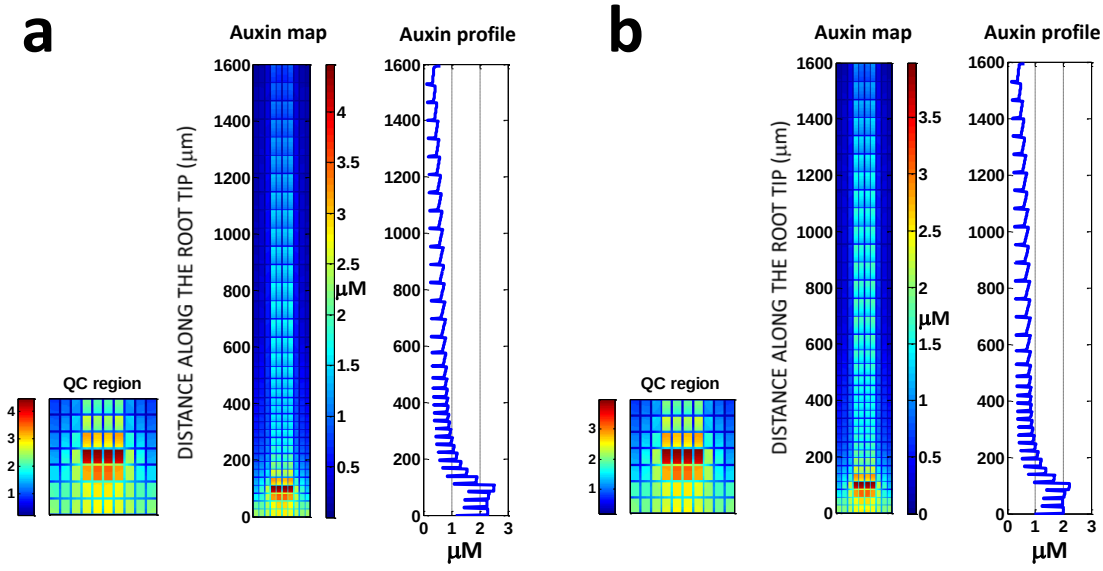

Figure 5.1: Auxin patterning if (a) CK inhibits or (b) CK promotes auxin and auxin inhibits CK (using the GG model). Auxin patterning is very similar for both model versions, with a maximum occurring at the QC, similar average profile concentration levels, and a proximally decreasing concentration trend.

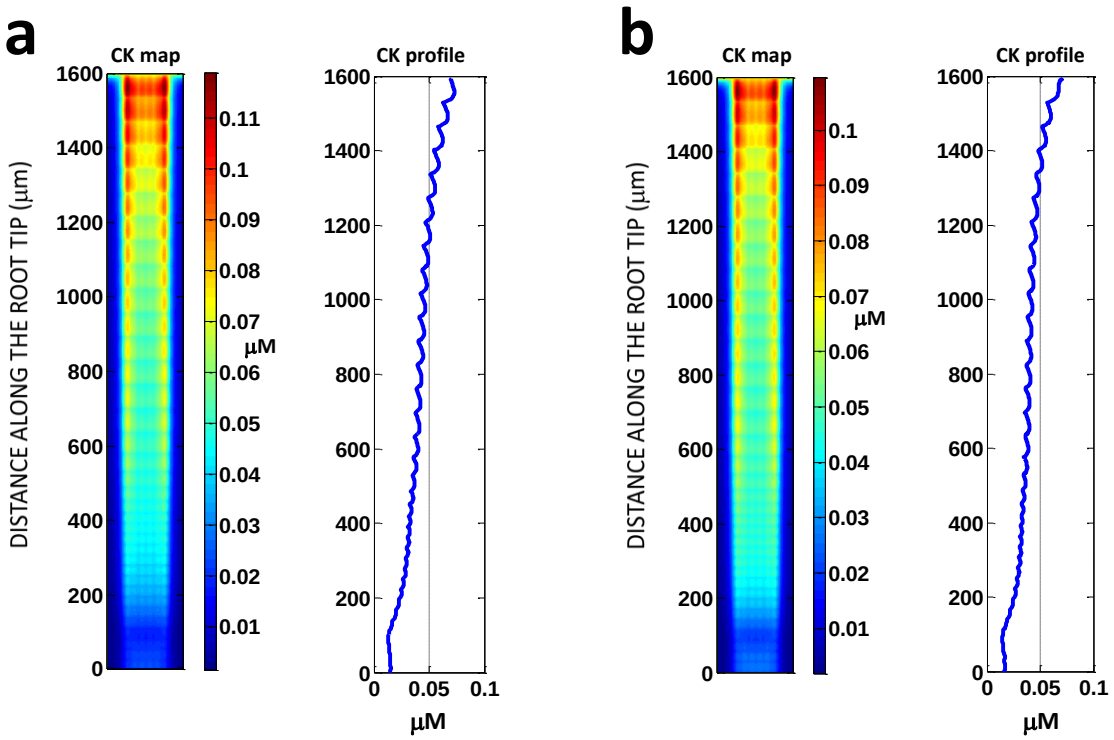

Figure 5.2: CK patterning if (a) CK inhibits or (b) CK promotes auxin and auxin inhibits CK (using the GG model). CK patterning is similar in both model versions, with higher concentrations in the central vascular tissues, similar average profile concentration levels, and a proximally increasing concentration trend.

Given the above results, it was decided to search the literature for additional mechanisms for the regulation of cytokinin and to use these relationships to build an alternative experimentally based crosstalk model in an attempt to reproduce previous model results, while improving the match between experimental and modelled cytokinin patterning.

5.2 Crosstalk network revisions

Cytokinin concentrations are determined by the balance between biosynthesis and degradation. Biosynthesis is regulated by rate limiting steps involving the IPT group of enzymes, while irreversible cytokinin degradation occurs through the action of a set of cytokinin oxidases (Werner *et al*., 2003; Werner *et al*., 2006). Cytokinin signalling acts through receptors at the plasma membrane and the ER and then through a phospho-relay cascade to activate a set of Type-B ARR transcription factors that include as targets the Type-A ARRs which, while not transcription factors, act as inhibitors of Type-B ARRs (To *et al*., 2007).

Therefore, within this initial pathway cytokinin limits its own responses. Cytokinin is also self-regulated by the activity of cytokinin oxidase (CKX) where increased CK treatment initially increases CKX activity and then reduces it (Figure 4 in Chatfield and Armstrong, 1986).

A type-B ARR of particular interest is ARR2 which appears to have unique properties whereby phosphorylated ARR2 is rapidly degraded by the proteasome while other type-Bs are not (Kim *et al*., 2012). Non-degradable ARR2 was found to increase cytokinin sensitivity in a number of developmental processes and to upregulate Type-A ARRs. It appears that ARR2 proteolysis is involved in regulating cytokinin responses in developmental processes mediated by cytokinin (Kim *et al*., 2012). Multiple ARR2 binding motifs found in the promoter regions of cytokinin-induced genes have led to the suggestion that ARR2 could act as a master regulator of cytokinin signalling responses (Hwang and Sheen, 2001).

ARR2 also links the cytokinin pathway into the ethylene pathway (Hass *et al*., 2004). It is found to bind the *ERF1* promoter and upregulate *ERF1*. A stabilized phosphorylated (active) ARR2 showed an ethylene response in the absence of ethylene even in the presence of AVG, an inhibitor of ethylene biosynthesis. The *arr2* null mutant has reduced ethylene response, which is rescued by expressing *ARR2* under the control of the *35S* promoter. There are also links in the other direction from the ethylene pathway into the cytokinin pathway (Hass *et al*., 2004) via ARR2. The ethylene receptor ETR1 appears to phosphorylate ARR2 since the ethylene sensitive *etr1-7* (Cancel and Larsen, 2002) loss-of-function mutant (low receptor activity and high downstream ethylene signalling) has reduced levels of phosphorylated ARR2 (Hass *et al*., 2004). It was concluded (Hass *et al*., 2004) that an ETR1 dependent phosphorelay regulated ARR2 phosphorylation and activity. An additional link between the ET and CK pathways is that EIN3 inhibits the commonly used cytokinin reporter *ARR5* (El-Showk *et al*., 2013; Shi *et al*., 2012).

There are also multiple links between the cytokinin and auxin pathways. Auxin upregulates *IPT* genes through SHY2 (Dello Ioio *et* al., 2008; Kushwah *et al*., 2011), and type-B ARRs ARR1 and ARR12 in turn promote *SHY2* (Dello Ioio *et* al., 2008; El-Showk *et al*., 2013) which inhibits *ARF* in the auxin signalling

pathway. Auxin also promotes the transcription of *AHP6*, an inhibitor of the cytokinin signalling pathway (Bishopp *et al*., 2011a).

From the above it is evident that the signalling pathways of these three hormones are heavily interlinked, even without considering regulation of say auxin transporters and the resulting effect on auxin patterning and therefore on the patterning of all other hormones and proteins. A schematic of these links is shown in Appendix 2 (Figure Ap 2.1), which while inevitably incomplete and likely requiring update from recent research, provides a useful reference map and shows the complexity of relationships between the pathways. Each link in the map is annotated, referring to notes with supporting references.

As noted above, ARR2 is suggested to be a central type-B ARR within the cytokinin signalling pathway, with links to and from the ethylene pathway. Microarray analysis suggests that ARR2 promotes cytokinin oxidase expression and activity since cytokinin oxidase mRNA is reduced -2.9 fold in the *arr2* null mutant and increased by +14.1 fold with stabilized activated ARR2, which mimics phosphorylation but cannot be degraded (supplementary tables, Hass *et al*., 2004). Therefore ETR1 ethylene receptor activity, by phosphorylating ARR2 and increasing ARR2 activity (Hass *et al*., 2004), appears to be able to regulate cytokinin concentrations and response through ARR2 and cytokinin oxidase. As such, it is proposed that active ETR1 receptors (in the absence of ET) result in ARR2 phosphorylation and increased ARR2 activity, which in turn results in increased CKX activity and reduced cytokinin. In the presence of ethylene (and for the *pls* mutant), ETR1 activity is reduced which decreases ARR2 phosphorylation and activity and so reduces CKX and increases cytokinin concentrations, which is consistent with the effects of the *pls* mutant on cytokinin concentrations compared to wildtype.

This provides a potential additional link in the crosstalk network for the regulation of cytokinin. Based on the above experimental results, it was therefore decided to develop an alternative model and calibrate a new wildtype realistic root, where downstream ethylene signalling (X) inhibits cytokinin degradation (Hass *et al*., 2004), cytokinin promotes auxin biosynthesis (Jones *et al*., 2010) and auxin promotes cytokinin synthesis (Dello *Ioio et* al., 2008).

5.3 The revised model

The revised model is a modified version of the model from Chapter 3 and 4, which used the realistic rootmap with prescribed levels and localisation of the auxin influx and efflux carriers PIN3, PIN4, PIN7, AUX1, LAX2 and LAX3. A comparison of the realistic root network and the modified network is shown in the following simplified schematic (Figure 5.3).

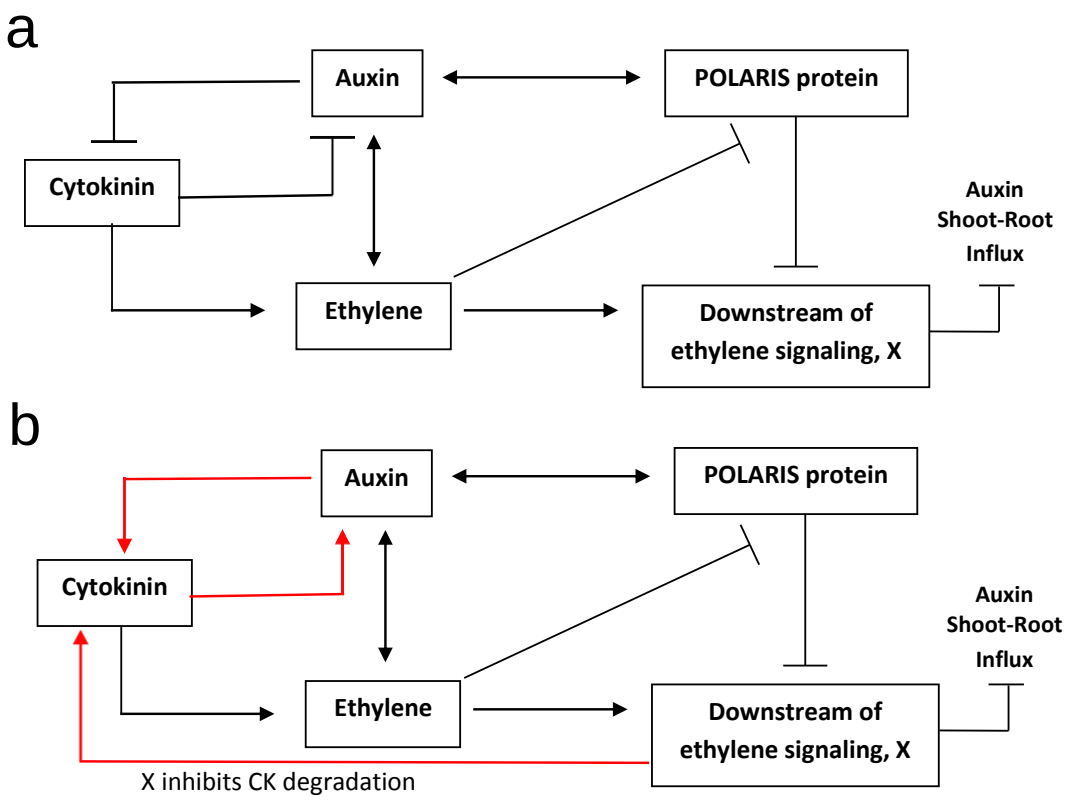

Figure 5.3: Schematic of (a) the original network (b) the revised network
The red lines show modified or additional network links compared to the original network

The equations were modified and the model recalibrated by adjusting certain parameters so that the model matched experimental patterning and concentration results. Changes to the realistic root model equations and data files are listed below. These include modifications to the auxin carrier concentrations, to the equations for biosynthesis and decay (Table 5.1), carrier cycling to and from the plasma membrane (Table 5.2), and auxin influx and efflux (Table 5.3), and show the reference V-numbers for the rate equations:

- AUX1m transcription is set to zero therefore AUX1p = 0 and no cycling occurs to and from the plasma membrane. This change is already included in the realistic root model (V26 and V27).
- New variables are introduced for the PIN3,4, and 7 and AUX1, LAX2 and LAX3 auxin carriers, with prescribed concentrations at the plasma membrane (already included in realistic root model).
- The cell numbers at the distal end of the two epidermal cell files are 527 and 580. For the cell numbers 524 to 526 and 578 to 579 (proximal to the distal epidermal cells), the apical face settings in the PIN12 map were changed from 1 (low) to 2 (medium) to increase auxin efflux.
- The AUX1 prescribed concentration settings at all cell faces in columella S5 cells were increased from setting 2 to 3 to increase auxin influx.
- cytokinin promotes auxin biosynthesis (V2, Table 5.1)
- auxin promotes cytokinin biosynthesis (V18, Table 5.1)
- cytokinin is synthesized in all cells (V18, Table 5.1)
- X inhibits cytokinin degradation (V19, Table 5.1)
- Auxin efflux is based on the total concentration of PIN12, PIN3, PIN4 and PIN7 (Table 5.3). This change is already included in realistic root model.
- Auxin influx is based on the total concentration of AUX1, LAX2 and LAX3 (Table 5.3). This change is already included in realistic root model.
- The prescribed concentration settings for PIN3, PIN4, PIN7 and AUX1, LAX2, LAX3 were the same as for the previous realistic root model in Chapters 3 and 4 except for LAX2 level 3 setting which was reduced from 1.75 to 0.75, effectively reducing auxin influx by LAX3
- The detailed run instructions, including the rootmap file names and prescribed concentration settings, can be seen in Appendix 3. Note that to achieve steady state the model run time was increased from 20,000 to 30,000 secs.

Table 5.1: Hormonal crosstalk rate equations for the cytokinin model
(for species biosynthesis, decay, activation and inactivation at each grid point; the parameters highlighted in red have had their values changed or are new compared to the realistic root model)

Species	Rate equations and parameter values	Notes
AUXIN		
V1 Background biosynthesis	k_2	Only in the cytosol
V2 Variable biosynthesis	$\frac{k_{2a}[ET][CK]}{(k_{2d}+k_{2e}[ET])(1+[CK]/k_{2b})} \quad \frac{[PLSp]}{(k_{2c}+[PLSp])}$	Only in the cytosol
V3 Decay	$k_3[Auxin]$	In the cytosol and cell walls
Parameters	k2 = 0.001 μM s^{-1}; k2a = 1.25 s^{-1}; k2b=0.01 μM; k2c = 0.02 μM; k2d = 1.0; k2e = 0.0 μM^{-1}; k3 = 0.001 s^{-1}	
References	Jones *et al*., 2010; Liu *et al*., 2010; Ljung, 2013; Stepanova *et al*., 2007; Swarup *et al*., 2007; Tivendale *et al*., 2014; Zhao, 2010	
Ra*		
V4 Rate of activation	$k_4[Auxin](RaT - Ra^*)$	Only in the cytosol. The receptor switches between active and inactive, with total RaT remaining constant.
V5 Rate of inactivation	$k_5 Ra^*$	Only in the cytosol
Parameters	k4 = 20.0 μM^{-1} s^{-1}; k5 = 1.0 s^{-1}	
References	Liu *et al*., 2010; Ljung, 2013; Mockaitis and Estelle, 2008; Vanneste and Friml, 2009	
PLSm		
V6 Rate of transcription	$\frac{k_6[Ra^*]}{1+\frac{[ET]}{k_{6a}}}$	Only in the cytosol
V7 Rate of decay	$k_7[PLSm]$	Only in the cytosol
Parameters	k6 = 0.0197 s^{-1}; k6a = 3.0 μM; k7 = 1.0 s^{-1}; for *pls* null mutant k6 = 0.0 s^{-1}; for PLSox k6 = 0.045 s^{-1}	
References	Casson *et al*., 2002; Chilley *et al*., 2006; Liu *et al*., 2010; Ljung, 2013; Mockaitis and Estelle, 2008; Vanneste and Friml, 2009	

PLSp		
V8 Rate of translation	$k_8[PLSm]$	Only in the cytosol
V9 Rate of decay	$k_9[PLSp]$	Only in the cytosol
Parameters	k8 = 1.0 s^{-1}; k9 = 1.0 s^{-1}	
References	Casson *et al*., 2002; Chilley *et al*., 2006; Liu *et al*., 2010; Ljung, 2013; Mockaitis and Estelle, 2008; Vanneste and Friml, 2009	
Re*		
V10 Rate of activation	$(k_{10} + k_{10a}[PLSp])([\mathrm{Re}T] - [\mathrm{Re}^*])$	Only in the cytosol. The receptor switches between active and inactive with the total ReT remaining constant.
V11 Rate of inactivation	$k_{11}[\mathrm{Re}^*][ET]$	Only in the cytosol
Parameters	k10=0.0003 s^{-1}; k10a=5.0 $\mu M^{-1} s^{-1}$; k11=4.0 $\mu M^{-1} s^{-1}$; for the *etr1* mutant k11 = 0.025 $\mu M^{-1} s^{-1}$	
References	Diaz and Alvarez-Buylla, 2006; Liu *et al*., 2010; Wang *et al*., 2002	
ET		
V12 Rate of biosynthesis	$k_{12} + k_{12a}\left(\frac{[Auxin]}{(k_{12b} + k_{12d1}[Auxin])} \frac{[CK]}{(k_{12c} + k_{12d2}[CK])}\right)$	Only in the cytosol. Michaelis Menten kinetics for the rate of biosynthesis regulated by Auxin and CK.
V13 Rate of decay	$k_{13}[ET]$	In the cytosol and cell walls
Parameters	k12 = 0.1 $\mu M\ s^{-1}$; k12a = 0.02 $\mu M^{-1} s^{-1}$; k12b = 0.1; k12c = 0.1; k12d1 = 0.1 μM^{-1}; k12d2 = 1.0; k13 = 1.0 s^{-1}	
References	Liu *et al*., 2010; Stepanova *et al*., 2007; Tanimoto *et al*., 1995; Vogel *et al*., 1998;	
CTR1*		
V14 Rate of activation	$k_{14}[\mathrm{Re}^*]([CTR1T] - [CTR1^*])$	Only in the cytosol. The receptor switches between active and inactive, with the total CTR1T remaining constant.
V15 Rate of inactivation	$k_{15}[CTR1^*]$	Only in the cytosol
Parameters	k14 = 3.0 $\mu M^{-1} s^{-1}$; k15 = 0.085 s^{-1}	
References	Diaz and Alvarez-Buylla, 2006; Liu *et al*., 2010; Wang *et al*., 2002	

X		
V16 Rate of pathway activation	$k_{16} - k_{16a}[CTR1^*]$	Only in the cytosol. Pathway inhibition is regulated by active CTR1.
V17 Rate of pathway inactivation	$k_{17}[X]$	Only in the cytosol
Parameters	k16 = 0.3 μM s^{-1}; k16a = 1.0 s^{-1}; k17 = 0.1 s^{-1}	
References	Diaz and Alvarez-Buylla, 2006; Liu *et al*., 2010	
CK		
V18 Rate of biosynthesis	$\frac{k_{18a}[Auxin]}{1+\frac{[Auxin]}{k_{18}}}$	In the cytosol of all cells
V19 Rate of decay	$\frac{k_{19}k_{18e}[CK]}{k_{18c}+k_{18d}[X]}$ $k_{19}[CK]$	In the cytosol of all cells In all cell walls
Parameters	k18 = 10.0 μM; k18a = 0.5 μM s^{-1}; k18c = 1.0 μM ; k18d = 10.0; k18e = 100.0 μM; k19 = 1.0 s^{-1}	
References	Dello Ioio *et al*., 2008; Hass *et al*., 2004; Liu *et al*., 2010;	
PINm		
V20 Rate of transcription	$\frac{k_{20a}[X][Auxin]}{(k_{20b}+[CK])(k_{20c}+[Auxin])}$	Only in the cytosol
V21 Rate of decay	$k_{21a}[PINm]$	Only in the cytosol
Parameters	k20a = 0.8 μM s^{-1}; k20b = 1.0 μM; k20c = 0.3 μM; k21a = 1.0 s^{-1}	
References	Chandler, 2009; Liu *et al*., 2010; Liu *et al*., 2013; Nordstrom *et al*., 2004; Paciorek *et al*., 2005; Ruzicka *et al*., 2007; Ruzicka *et al*., 2009; Swarup *et al*., 2007; Vanneste and Friml, 2009	
PINp		
V22 Rate of translation	$k_{22a}[PINm]$	Only in the cytosol
V23 Rate of decay	$k_{23a}[PINp]$	In the cytosol and plasma membrane
Parameters	k22a = 1.0 s^{-1}; k23a = 0.75 s^{-1}	
References	Chandler, 2009; Liu *et al*., 2010; Liu *et al*., 2013; Nordstrom *et al*., 2004; Paciorek *et al*., 2005; Ruzicka *et al*., 2007; Ruzicka *et al*., 2009; Swarup *et al*., 2007;	

	Vanneste and Friml, 2009	
AUX1m		
V26 Rate of transcription	$k_{1a}[X]$	Only in the cytosol.
V27 Rate of decay	$k_{26}[Aux1m]$	Only in the cytosol
Parameters	k1a = 0.0 μM s^{-1}; k26=1.0s^{-1}	AUX1m = 0 since it is not transcribed. All influx carrier localization and levels are prescribed by the user
References	Ruzicka *et al.*, 2007; this work.	
AUX1p		
V28 Rate of translation	$k_{27}[Aux1m]$	Only in the cytosol but AUX1p = 0 since there is no AUX1m transcription.
V29 Rate of decay	$k_{28}[Aux1p]$	In the cytosol and plasma membrane
Parameters	k27 = 1.0 s^{-1}; k28 = 1.0 s^{-1}	
References	This work	

Table 5.2: PIN12 cycling rate equations for the cytokinin model
(PIN3, PIN4, PIN7, AUX1, LAX2 and LAX3 localization and levels are prescribed)

Species	Rate equations and parameter values	Notes
PINp		
V24 Rate of localisation of PINp to the plasma membrane	$k_{24a}(i)[PINpi]$	[PINpi] is the PIN12 protein concentration at the cytosolic GP. k24a(i) depends on the property of the NN plasma membrane GP (i) as shown in the parameter values.
V25 Rate of removal of PINp from the plasma membrane	$\frac{k_{25a}[PINpm]}{(1+[Auxin]_0 / k_{25b})}$	[PINpm] is the PIN12 protein concentration at the plasma membrane GP. $[Auxin]_0$ is the auxin concentration at the NN cytosolic GP.
Parameters	k24a(1)=1.0 s^{-1}; k24a(2) = 5.0 s^{-1}; k24a(3)=20.0 s^{-1}; k24a(4) = 0.0 s^{-1}; k24a(5) = 20.0 s^{-1} K25a = 1.0 s^{-1}; k25b = 1.0 μM	
References	Grieneisen *et al*., 2007; Liu *et al*., 2013; Paciorek *et al*., 2005. This work.	
AUX1p		
V30 Rate of localisation of AUX1p to the plasma membrane	$k_{29}[Aux1pi]$	[AUX1pi] is the AUX1 concentration at the cytosolic GP; however no cycling occurs since AUX1p = 0
V31 Rate of removal of AUX1p from the plasma membrane	$k_{30}[Aux1pm]$	[AUX1pm] is the AUX1 concentration at the plasma membrane GP; however no cycling occurs since AUX1p = 0
Parameters	k29 = 10.0 s^{-1}; k30 = 1.0 s^{-1}	
References	This work	

Table 5.3: Species flux for the cytokinin model
(between nearest neighbour, NN, grid points A to B)

Species	A → B		Flux equation	Notes
Auxin diffusion	0	0	$Auxindiff\ (cell)\ ([Auxin]_A - [Auxin]_B)/\Delta x$	Diffusion in the cytosol
	1 or 2 or 3	1 or 2 or 3	$Auxindiff\ (wall)\ ([Auxin]_A - [Auxin]_B)/\Delta x$	Diffusion in the cell wall
	4 or 5	any	No diffusion from GP 4 and 5	Border to cytosol
	any	4 or 5	No diffusion to GP 4 and 5	Cytosol to border
Parameters			Auxindiff(cell) = 220 $\mu m^2\ s^{-1}$ Auxindiff(wall) = 220 $\mu m^2\ s^{-1}$; Δx = 2.0μm	
References			Kramer *et al*., 2011; Rutschow *et al*., 2011; This work.	
Auxin efflux permeability	0	1,2 or 3	$\frac{1}{\Delta x}\,p(A,B)\,\frac{k_{3b}[TOTALPIN]_B[Auxin]_A}{k_{3a}+[Auxin]_A beta}$	Efflux from the cell. p(A,B) = 1 TOTALPIN is the total of PIN12, PIN3, PIN4, PIN7 concentrations
	0	4	Above equation but zero flux	p(A,B) = 0
	0	5	Above equation and flux occurs	Efflux from the root to the shoot. p(A,B) = 1
Parameters			p(A,B) is a switch determining if permeability can occur from A to B and is = 0 or 1 Δx = 2.0μm (scaling constant); k3a = 1.0μM; k3b = 0.8 $\mu m^2\ s^{-1}$; beta = 0	Optional Michaelis Menten kinetics depending on the value of beta
References			Kramer *et al*., 2011; This work	
Auxin influx permeability	1, 2 or 3	0	$\frac{1}{\Delta x}\,p(A,B)\,\frac{k_{31}[AUXLAX]_A[Auxin]_A}{k_{31a}+[Auxin]_A k_{31b}}$	Influx into the cell. AUXLAX is the total of AUX1, LAX2, LAX3 concentration. p(A,B) = 1
	4	0	$\frac{1}{\Delta x}\,p(A,B)\,\frac{k_{32a}[Auxin]_A}{1+[X]_B/k_{32b}}$	Influx, shoot to root p(A,B) = 1
	5	0	Same equation as 4 to 0 but zero flux since p(A,B) = 0	Influx, shoot to root. p(A,B) = 0
Parameters			p(A,B) is a switch determining if permeability can occur from A to B and is = 0 or 1; Δx = 2.0μm (scaling constant); k31 = 2.0 $\mu m^2\ s^{-1}$; k31a = 1.0μM; k31b = 0; k32a = 10 $\mu m^2\ s^{-1}$; k32b = 1.0 μM	Optional Michaelis Menten kinetics depending on the value of k31b
References			Chilley *et al*., 2006; Kramer, 2004; Rutschow *et al*., 2014; Suttle, 1988.	

			This work.	
ET diffusion	0, 1, 2, 3, 4 or 5	0, 1, 2, 3, 4 or 5	$ETdiff\ ([ET]_A - [ET]_B)/\Delta x$	ET diffuses between all GP of the same or different types whether in the cytosol or cell wall with the same diffusion coefficient
Parameters			ETdiff = 600 $\mu m^2\ s^{-1}$; Δ x = 2.0μm	
References			This work	
CK diffusion	0, 1, 2, 3, 4 or 5	0, 1, 2, 3, 4 or 5	$CKdiff\ ([CK]_A - [CK]_B)/\Delta x$	CK diffuses between all GP of the same or different types whether in the cytosol or cell wall with the same diffusion coefficient
Parameters			CKdiff = 220 $\mu m^2\ s^{-1}$; Δx = 2.0μm	
References			Mellor and Bishopp, 2014. This work	
All other species diffusion	0	0	$Otherdiff\ ([Other]_A - [Other]_B)/\Delta x$	Diffuse within the cytosol only and do not cross the PM and enter the cell wall (for PIN12p recycling see Table 5.2)
Parameters			Otherdiff = 220 $\mu m^2\ s^{-1}$; Δx = 2.0μm	
References			This work	

5.4 Results for the new wildtype root

The alternative crosstalk network model, containing experimentally based revised relationships between auxin, cytokinin and downstream ethylene signalling, was executed with the simulation time increased from 20,000 to 30,000 secs to achieve steady state.

Auxin patterning (Figure 5.4) is very similar to both the previous model and experimental imaging, with a maximum occurring in the QC region, a proximally diminishing concentration in the vascular cylinder, and an increase in concentration in the epidermal cell file in the elongation zone. Relative auxin concentrations in the cells files above the initials using the R2D2 reporter

(Figure 5.5) and relative auxin concentration in WT, *pls* mutant and the PLSox transgenic (Figure 5.6) show similar trends to experimental observations.

Ethylene patterning (Figure 5.4) was similar to experimental observations (Figure 2.46), with higher levels in the columella, then declining in the meristematic region followed by increasing levels in the elongation zone.

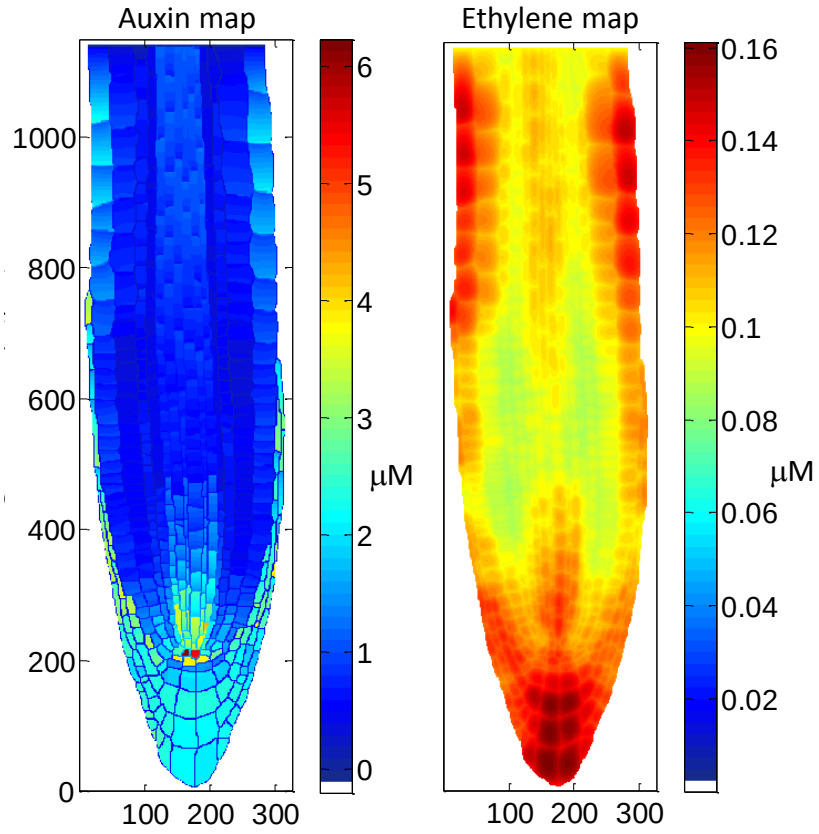

Figure 5.4: Auxin and ethylene concentration colour maps
showing model outcomes similar to experimental results

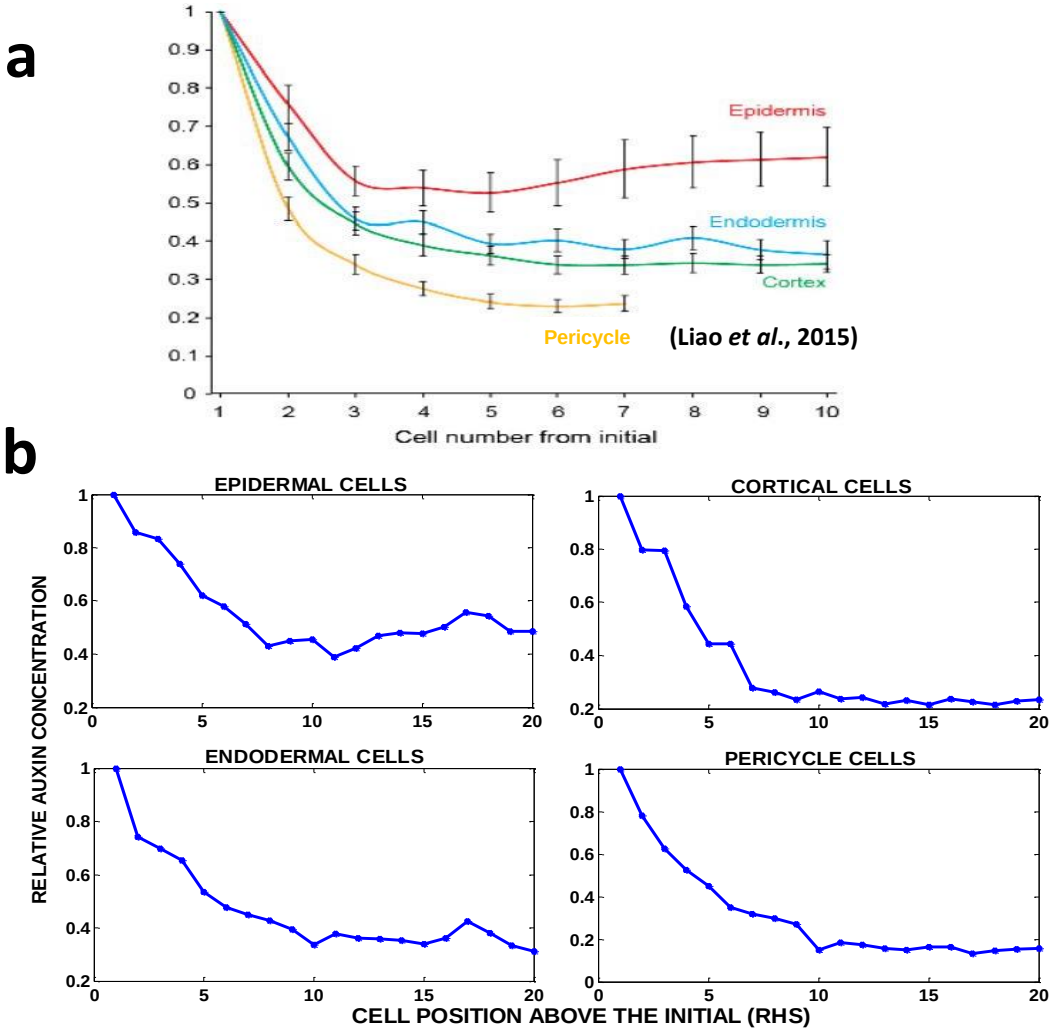

Figure 5.5: Relative auxin response and concentration trends
(a) Relative auxin response trends in cell files above the initials (Liao *et al*., 2015)
(b) Relative auxin concentration trends from the model (RHS, right hand side)

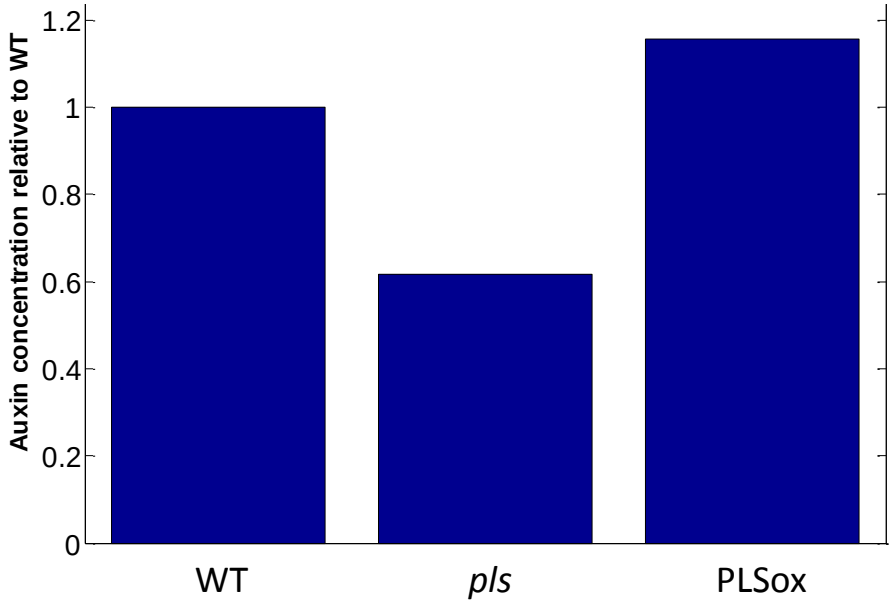

Figure 5.6: Average auxin concentration trend
demonstrating similar trend to experimental results

Experimental data for cytokinin patterning is shown in Figure 5.7 where (a) shows relative cytokinin concentrations using cell sorting and mass spectrometry techniques (Antoniadi *et al*., 2015), (b) relative cytokinin response patterning using the ARR5::GUS reporter (Werner *et al*., 2003), and (c) relative cytokinin response using a synthetic reporter TCSn::GFP based on type-B ARR promoters (Zurcher *et al*., 2013) which is reported to be more sensitive to cytokinin than the ARR5 reporter. All three images show slightly different results; (a) represents cell concentration measurements, while (b) and (c) are based on reporters with different cytokinin sensitivity (and possibly varied sensitivity to different cytokinins) which can also potentially be differentially influenced by other signalling pathways which link into the cytokinin pathway. Nevertheless, all 3 images show high concentrations or response in the columella, with a proximally diminishing signal in the vascular cylinder. (a) and (c) suggest higher concentrations in the lateral root cap, and both the reporter images (b) and (c) have a low signal in the QC region, not observed in (a).

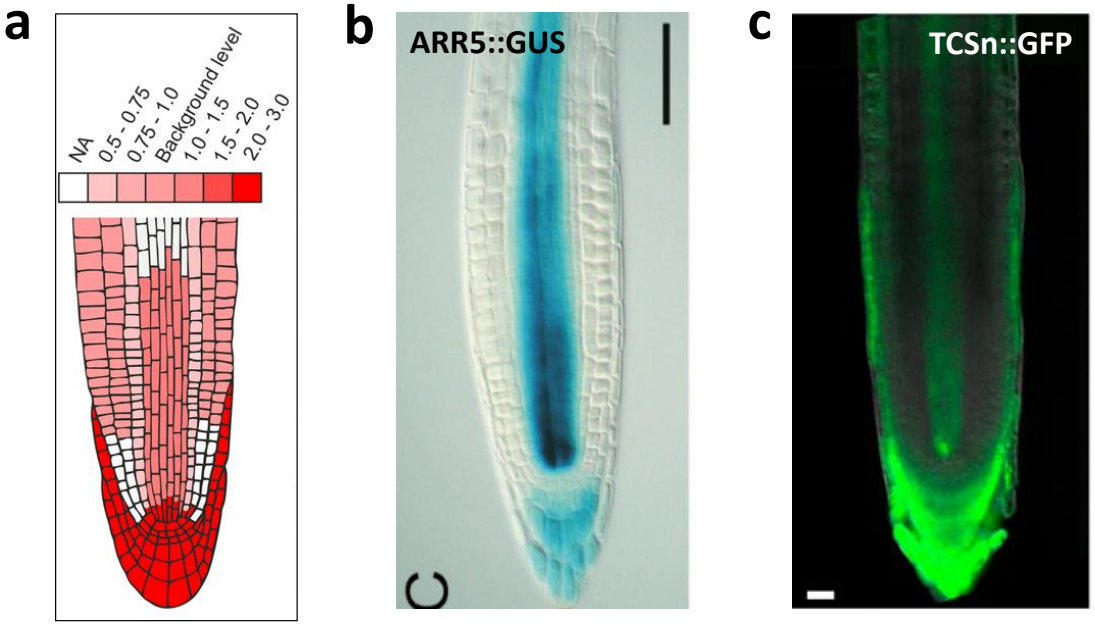

Figure 5.7: Experimental cytokinin concentration and response data
(a) Cytokinin relative concentration using cell sorting and mass spectrometry (Antoniadi *et al*., 2015). (b) Cytokinin response using the ARR5::GFP reporter (Werner *et al*., 2003). (c) Cytokinin response using the TCSn::GFP reporter (Zurcher *et al*., 2013).

Model results for cytokinin concentration patterning were compared to experimental measurements using the cell sorting method, and to cytokinin response patterning using the more sensitive TCSn::GFP cytokinin reporter (Figure 5.8). Model results were very similar to experimental results with high cytokinin signalling in the columella and lateral root cap, a proximally decreasing signal in the central vascular cylinder and a lower signal between the vascular cylinder and the outer lateral cell files. One area of difference appears in the QC region where the TCSn::GFP response image (Figure 5.8c) gives a lower signal than both the model (Figure 5.8b) and the measured cytokinin concentration (Figure 5.8a).

The model results for average cytokinin and ethylene concentrations in the wildtype and *pls* mutant (Figure 5.9) were similar to prior model results and experimental observation (Figure 2.64) with increased cytokinin concentrations but an insignificant change in ethylene concentration in the *pls* mutant.

Model results for PLS protein (Figure 5.10) and auxin biosynthesis patterning (Figure 5.11) were similar to previous model and experimental results.

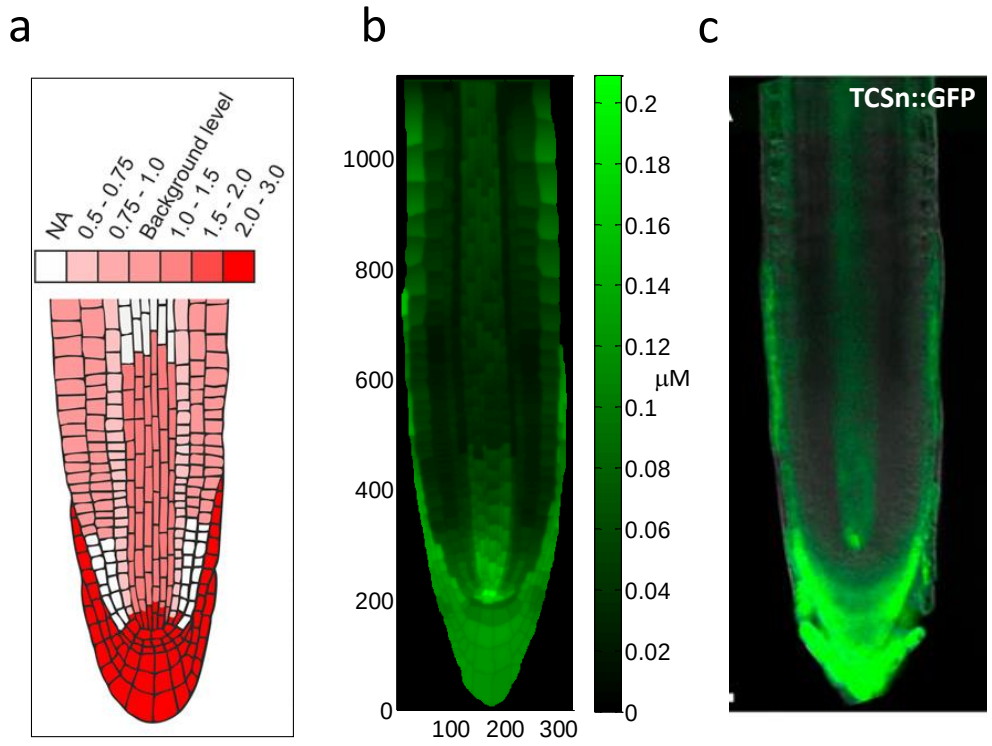

Figure 5.8: Comparison of experimental and model cytokinin patterning
(a) Cytokinin concentration map from cell sorting and mass spectrometry (Antoniadi *et al*., 2015). (b) Model cytokinin concentration colour map. (c) Cytokinin response using TCSn::GFP reporter (Zurcher *et al*., 2013).

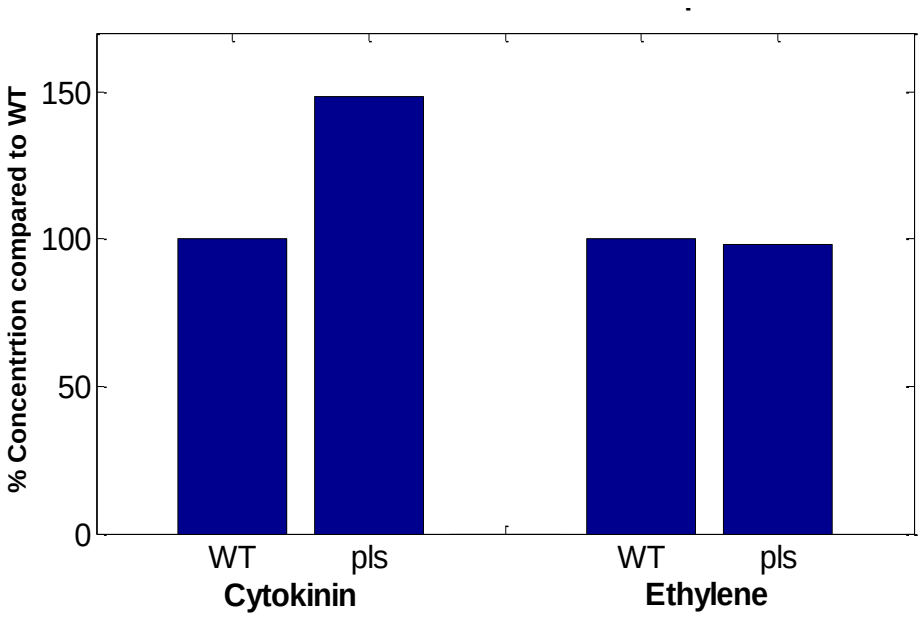

Figure 5.9: Relative model CK and ET concentrations in WT and *pls*
Similar to experimental and previous model results.

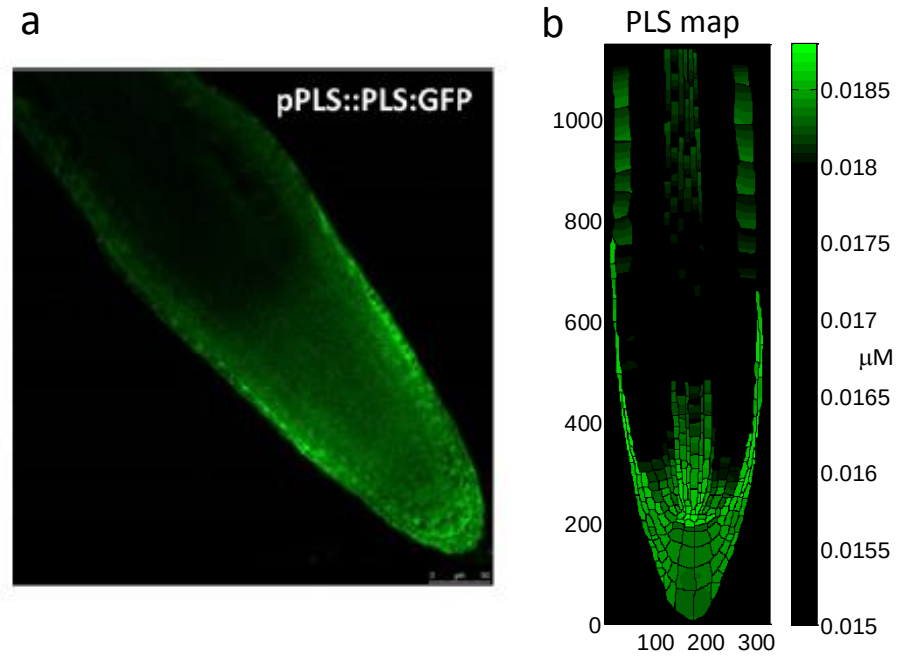

Figure 5.10: PLS protein patterning (a) experimental (b) model
Model results similar to experimental results and to previous model results.

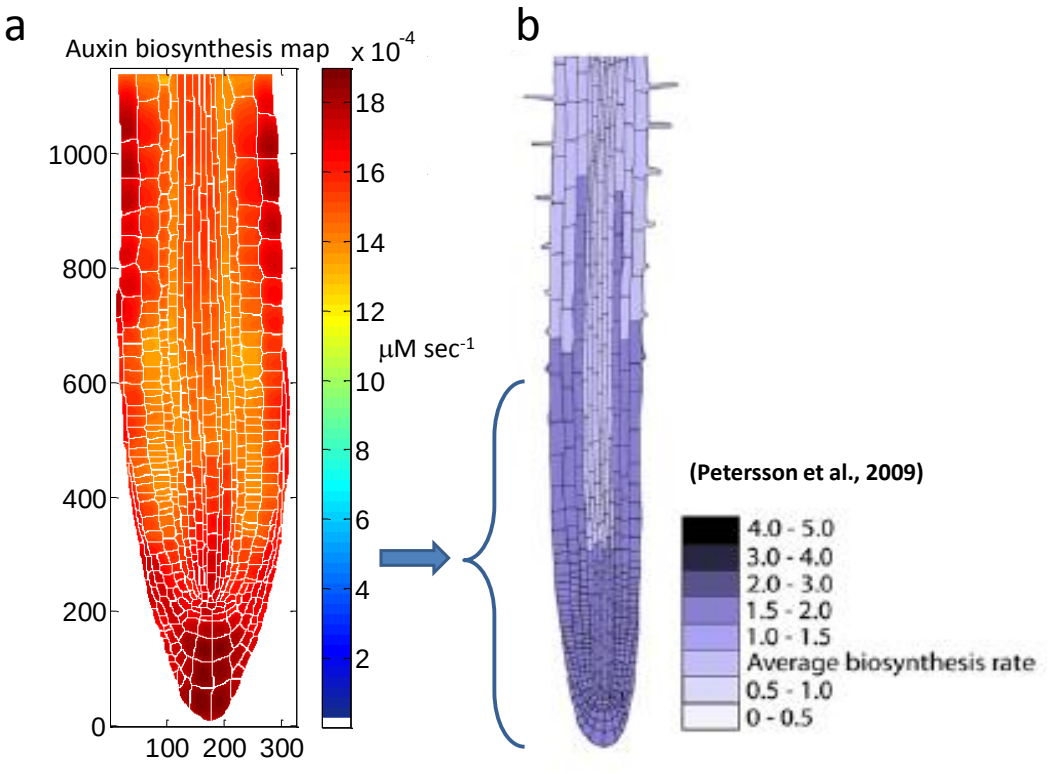

Figure 5.11: Auxin biosynthesis patterning (a) model (b) experimental
The model root in (a) corresponds to the bracketed region of the experimental root (b). Model results are similar to experimental results and to previous model results

5.5 Summary

To make it possible to use this model to investigate detailed expression patterning of developmental genes regulated by hormonal crosstalk between auxin, ethylene and cytokinin, it is particularly important that the model can achieve representative cytokinin patterning while maintaining correct patterning of other hormones and proteins. As described above, the model was revised using a set of alternative relationships between auxin, cytokinin and ethylene signalling based on additional experimental evidence from the literature. The goal was to maintain the similarities between previous model and experimental results while improving the match between experimental and model cytokinin patterning. As seen from the above results (Figure 5.8), cytokinin concentration patterning now compares favourably with both experimental response imaging and concentration measurements. While generating improved patterning, the model results for comparative average cytokinin concentrations in WT and *pls* mutant (Figure 5.9) remain similar to experimental observations and there is

minimal change in model results for all other species. With the improvement in cytokinin patterning, the revised model now demonstrates more complete pattern matching to experimental results than models developed earlier in this work. The patterning improvement is created by building in a relationship between ethylene signalling and cytokinin degradation. Experimental evidence points to links between ethylene signalling and components in the cytokinin signalling pathway such as type-B ARR2 (Hass *et al*., 2004) and type-A ARR5, 7, 15 (Shi *et al*., 2012) response regulators, where ARR2 potentially regulates cytokinin oxidase (and in turn cytokinin levels), and type-A ARRs regulate the activity of the type-B ARRs and other cytokinin target genes. Type-A ARR regulation of cytokinin oxidase and cytokinin levels has also been demonstrated in rice (Hirose *et al*., 2007).

Figure 5.8 compares the model to experimental CK patterning results. It also compares two different patterning results from cytokinin concentration measurements and from cytokinin response imaging using the synthetic TCSn::GFP reporter (based on type-B ARR promoters), with the two experimental results showing pattern differences in the QC region. Figure 5.7b also shows experimental CK response patterning using the reporter ARR5::GUS (a type-A ARR promoter), again showing variation from the other two experimental patterns. One reason for the differences could be that response imaging using reporter constructs measures hormone signalling which is not necessarily equivalent to hormone concentrations. Hormone signalling response will depend on the promoter used in the reporter construct and where it is positioned in the signalling pathway. The further along the pathway the promoter is located, the more likely it is to be influenced by signalling inputs from other pathways, so creating potential differences between actual hormone concentration and downstream response patterning. As such, imaging using reporter constructs is a reflection of multiple signalling inputs. In addition, different reporters could possibly have varied sensitivity to the different cytokinins which in turn do not necessarily have the same concentration patterning, potentially creating additional variability between response images generated by different reporters.

The difference between the two experimental results for cytokinin patterning (Figure 5.8) could be due to the influence of auxin and ethylene concentrations on cytokinin response (see Figure Ap 2.1 in Appendix 2 for the more complex network). Auxin inhibits the phospho-relay cascade and cytokinin response through AHP6 (Bishopp *et al*., 2011a) and, given the relatively high auxin concentrations in the QC, it is possible that cytokinin signalling response (both type-B and type-A activation) could be suppressed in this region, as seen in the type-B promoter based TCSn::GFP (Figure 5.8c) and the type-A promoter based ARR5::GUS response images (Figure 5.7b). This could explain the difference between ARR5::GUS and TCSn::GFP response imaging and the experimental CK concentration measurements and model results in the QC region, where both the model and experimental concentration measurements indicate higher relative cytokinin concentrations. Ethylene concentrations could also affect cytokinin response imaging in the QC region. Increased ethylene inactivates ETR1 and reduces ARR2 activity (a type-B ARR) and also increases EIN3, resulting in reduced ARR5 (a type-A ARR) which is an inhibitor of type-B ARRs used in the promoter construct of the TCSn::GFP reporter. So ethylene potentially both positively and negatively regulates type-B promoters and so cytokinin response through at least two pathways.

Furthermore, it has been shown that the *pls* mutant is hyper-responsive to exogenous cytokinin application (Casson *et al*., 2002) which is possibly a further indicator of the complexity of the linkages between hormone signalling pathways and hormone response. Referring to the more complex network (Figure Ap 2.1 in Appendix 2), the *pls* mutant could result in increased response to exogenous cytokinin by at least 2 pathways. First, in the *pls* mutant ETR1 is inactivated removing downstream ET signalling inhibition and so downregulating *ARR5*, therebye reducing inhibition of the type-B ARRs which upregulate CK responsive genes. Second, auxin is reduced in the *pls* mutant, resulting in downregulation of *AHP6* which further reduces inhibition of CK response.

pls null mutants also show reduced responsiveness to auxin (Casson *et al*., 2002). Again referring to the more complex network in Appendix 2, this could be explained by increased CK concentrations in the *pls* mutant resulting in the

upregulation of type-B ARRs and so the upregulation of *SHY2*, which inhibits the auxin signalling pathway.

Therefore, the revised network suggests an even more complex role for the small PLS protein in hormone crosstalk, including auxin biosynthesis and signalling, ethylene response and downstream signalling, and also in the activation of the ETR1 receptor and the consequent effect on CK degradation and response. This is even further complicated by the effects of CK on *PIN* expression and PIN localisation at the plasma membrane which in turn affects auxin transport, concentration and patterning (Ruzicka *et al*., 2009; Bishopp *et al*., 2011a).

In addition, it has been demonstrated that cytokinin is transported from the shoot to root in the phloem (Bishopp *et al*., 2011b) and more recently that PUP14 cytokinin influx transporters remove cytokinin from the apoplast and import it into the cell for degradation (Zurcher *et al.*, 2016) which, in combination with local biosynthesis, degradation and diffusion could influence cytokinin concentration and signal patterning in the root tip. Interestingly, in a different context for root development analysis, it has also been shown that an additional component is required to position cytokinin signal patterning (Muraro *et al*., 2014).

Therefore, the combination of the analysis in this work with the information in the literature indicates that the patterning of cytokinin concentration, response and signalling requires further experimental study and a more complex model network to further improve model comparison with experimental results.

CHAPTER 6 : DISCUSSION

DISCUSSION

6.1 Introduction

Experimental information accumulated over many years indicates that, in root development, hormones and the associated regulatory and target genes form a network in which relevant genes regulate hormone activities and hormones regulate gene expression. Functionally important patterns of hormone distribution, hormone responses and gene expression are presumed to emerge from these interactions and, although many individual links in the crosstalk network have been established including complex feedback relationships, for example ethylene activates the biosynthesis of auxin locally in the root tip (Stepanova *et al*., 2007; Swarup *et al*., 2007) and both auxin and cytokinin can synergistically activate the biosynthesis of ethylene (Chilley *et al*., 2006; Stepanova *et al*., 2007), little is known about how patterning is generated. The importance of understanding pattern development is reinforced by numerous experimental analyses showing that auxin patterning, with a localized concentration maximum in the root tip, is pivotal for correct root development (Sabatini *et al*., 1999).

The goal of this project was to build a 2-D spatiotemporal model of hormonal crosstalk to reproduce experimental patterning of auxin, cytokinin and ethylene hormones, gene expression, and associated regulatory and transport proteins, and to simultaneously reproduce observed average hormone concentration trends in wildtype and mutants. The work involved several phases in which the model was progressively developed to improve the replication of experimentally observed hormone and gene expression patterning and to investigate in more detail the roles of auxin transporters in pattern formation.

The development of this series of integrative models, each of which combine experimental data with the construction of a hormonal crosstalk network, a 2-D spatial root structure for cell–cell interactions, and spatiotemporal modelling, demonstrates that the spatiotemporal dynamics of hormonal crosstalk establishes a causal relationship for the amount of auxin, ethylene, cytokinin, PIN protein and PLS protein, as well as the mechanisms for generating patterning in these hormones and proteins.

6.2 The rectangular root model

The original rectangular root model was based on a multicellular auxin transport model (Grieneisen *et al*., 2007) and single cell crosstalk models (Liu *et al*., 2010; Liu *et al*., 2013), where the crosstalk network from the single cell models was essentially embedded into each cell of the multicellular auxin transport model. The parameters of the model were calibrated from the literature, or by matching experimental results, to generate an initial wildtype parameter set. This initial model matched most fit criteria: the average auxin concentration was similar to experimental measurements, trends in auxin concentration in wildtype, mutants and the transgenic PLSox over-expressor were qualitatively correct, colour map images and profiles of auxin concentration matched experimental observations, and the PIN and AUX1 carriers predominantly located to the plasma membrane. AUX1 patterning was only a partial match to experimental imaging suggesting that additional factors could regulate *AUX1* expression, and, while the average cytokinin concentration in wildtype and *pls* mutant showed similar trends to experimental results, cytokinin results did not match experimental patterning images in this initial model; nevertheless, alternative network relationships between auxin and cytokinin were analysed and found not to significantly affect other model results. Further research was conducted (Chapter 5) in an attempt to improve cytokinin patterning while maintaining the similarity between model and experimental results for other species.

The model was tested to see if it was overly sensitivity to parameter variation around wildtype values. Testing was performed on a number of parameters including diffusion, biosynthesis and decay rates, and the model proved robust to variation in these parameter values. The model was also tested for variation in the rates of diffusion and expression of the auxin carriers PIN and AUX1 which influence auxin transport through the root. Again the model proved robust, with the auxin maximum forming over a wide range of values.

The model was revised to include a more realistic graduated change in cell length in the transition zone (the Gradual Growth model) compared to the

sudden length change used in the original Grieneisen *et al*. (2007) model, with the only impact being to smooth out some of the sudden (but minor) transitions in the concentration profiles.

The model matched observed auxin patterning and profiles and to a large degree the average concentration trends for mutants. Similarly, experimental results for auxin flux from shoot to root for different mutants were matched by the model, except that results for the double mutant *pls etr1* were slightly high compared to WT. However, double mutant interactions are complex and tend to be very difficult to model especially when there are multiple non-equivalent ethylene receptors which can act in clusters, each of which could independently or as a group affect ethylene signalling, and there is also evidence of multiple ethylene signalling pathways (see Appendix 2). ET and PLS experimental imaging data compared favourably with model results as did the auxin concentration profiles for wildtype and the *aux1* mutant.

Experimental analysis has shown that PIN content in *Arabidopsis* varies in response to a range of hormones and that hormonal interactions determine PIN localization patterns (Liu *et al*., 2013). Auxin positively regulates levels of several PIN proteins in different developmental contexts (Blilou *et al*., 2005; Laskowski *et al*., 2006; Chapman and Estelle, 2009; Vanneste and Friml, 2009) by a signalling pathway regulating transcription (Woodward and Bartel, 2005), and by promoting accumulation at the plasma membrane (Paciorek *et al*., 2005). Ethylene also up-regulates PINs (e.g. PIN2, Ruzicka *et al*., 2007) while cytokinin negatively regulates PIN1, PIN2 and PIN3, but positively regulates PIN7 (Ruzicka *et al*., 2009; Bishopp *et al*., 2011a). In this work, to be consistent with Grieneisen *et al*. (2007), the investigation initially concentrates on PIN1 and PIN2. In addition, since PIN3 (which is negatively regulated by cytokinin) and PIN7 (positively regulated by cytokinin) are in part localized at similar positions in the root (Ruzicka *et al*., 2009; Bishopp *et al*., 2011a), it may be reasonable to assume that the overall effects of cytokinin on both PIN3 and PIN7 have a reduced net effect on auxin transport. PIN concentrations are also influenced by other genes; for example, in the *pls* mutant, both PIN1 and PIN2 increase (Liu *et al*., 2013).

During *Arabidopsis* root development, both the amount and patterning of hormones, proteins and auxin carriers are interlinked. For example, in the wild-type root, PIN1 concentrations generally decrease from the proximal to the distal region (Figure 2.67) and PLS generally increases from the proximal end to the distal end (Figure 2.47). However, in the *pls* mutant, PIN1 concentrations generally increase from the proximal to the distal end. In addition, in the *pls* mutant, the average auxin, ethylene and cytokinin concentration or response in the root is reduced, remains approximately constant, and is increased, respectively (Chilley *et al*., 2006; Liu *et al*., 2010), while the average PIN1 concentration increases (Liu *et al*., 2013).

Model results for PIN root concentrations for different mutants largely matched experimentally observed concentration trends. The predominant localization of the PIN and AUX1 carrier proteins to the plasma membrane was consistent with experimental imaging. Model PIN concentration profiles were also compared to PIN1 and PIN2 profiles derived from experimental images for different mutants and the PLSox transgenic. Model PIN profiles in the vascular cylinder compared favourably with the experimental PIN1 data; however, PIN2 profiles only matched for wildtype and PLSox possibly due to the difficulty of scanning and combining the data from the epidermal regions of the root images. Also the model only represented a single PIN protein so did not model possible differences in regulation of level and localization between PIN1 and PIN2.

The work on testing model sensitivity to variation in PIN and AUX1 rates of expression and diffusion demonstrated the importance of coordination between the influx and efflux carriers in establishing patterning, as investigated in greater depth in Chapter 4. In order for the model root to generate auxin patterning similar to experimental results, the permeability of both the PIN and AUX1 auxin carrier proteins is important and must be limited to certain ranges. It can be concluded that both PIN and AUX1 proteins work together to generate auxin patterning similar to experimental results. It has also been suggested that AUX1 influx must be at least equal to PIN efflux to avoid auxin depletion in the cells (Kramer, 2004).

Previous modelling results have suggested that either the auxin efflux carrier PIN activity (Grieneisen *et al*., 2007; Wabnik *et al*., 2010) or the AUX1 activity

(Band *et al*., 2014) are essential to create the auxin gradient at the root tip. The importance of the coordination of the properties and regulation of the PIN and AUX1 auxin carrier proteins is emphasised by the model results. These suggest that the coordination of AUX1 and PIN processes should also include transcription, translation and decay, diffusion rates, concentration at the plasma membrane and protein recycling, to maintain the AUX1 to PIN balance and prevent auxin from being trapped in the cytosol or cell walls, so facilitating correct auxin transport and formation of the auxin maximum.

6.3 The realistic root model

The initial work in Chapter 2 involved combining previous studies by embedding a single cell crosstalk model into a simple rectangular multicellular root structure to try to reproduce 2-D hormone and gene expression patterning in the root tip. Further work would obviously be limited by continuing to compare experimental imaging from a 'real' root with model results from a simple rectangular root; therefore, it was necessary to produce a much more realistic digital root map and wildtype root structure for use with the existing model. As demonstrated, the final realistic digital root map was a good reproduction of published images. The digital realistic root map was of increased resolution containing approximately 375,000 pixels compared to the rectangular root with 85,000 pixels, and also importantly contained more identifiable and defined root structures and regions within the root tip, in particular the lateral root cap, to allow cell-scale comparison with experimental images.

Much of the work in this phase of the project involved creating a realistic digital root map from published images originally derived from confocal image stacks. This required the development of a series of programs to take the original flawed data from a scanned image and then iteratively refine and correct the data to produce a final rootmap to match the original imaging, with each cell having a cytosol and cell wall, and including some extra-cellular space.

Since the crosstalk network did not accurately reproduce AUX1 patterning, it was decided to prescribe the level and location of wildtype AUX1 auxin influx carriers based on experimental imaging. At the same time additional auxin carriers LAX2, LAX3, PIN3, PIN4 and PIN7, for which insufficient regulatory

knowledge was available to include in the network, were similarly prescribed based on experimental data. The reversible ABCB carriers were implicitly included in the non-polar base activity of other influx and efflux carriers. As such, all important known auxin influx and efflux carriers were included in the realistic root model.

Using the same parameter value set and crosstalk relationships, the realistic root model reproduced all the results from the rectangular root and similarities to experimental observations, including additional predictions regarding the effects of the loss of PIN3, PIN4 and PIN7 on PIN1 and PIN2 patterning and predictions on auxin biosynthesis patterning that were similar to experimental results. This demonstrated that the original results were not dependent on the artificial rectangular root structure. The realistic root model also enabled more detailed comparison of auxin concentration trends in selected cells as demonstrated by the similarity between model and experimental R2D2 reporter results on relative auxin response trends in cell files proximal to the initials. Auxin patterning in the realistic root was also a better match to experimental patterning, showing increased auxin concentrations in the epidermal cells in the elongation zone, not evident in the rectangular root model, and likely due to the action of AUX1 to retain auxin in these cells. While there were some improvements in cytokinin patterning, the model still exhibited limitations in matching experimental results and also still relied on somewhat artificially limiting cytokinin biosynthesis to the central cell files instead of being fully controlled by the crosstalk network.

The results further reinforce the concept that individual elements of experimental data can be integrated into a larger model of a biological system to be able to reproduce and better understand such complex characteristics as hormone and gene expression patterning.

6.4 The roles of auxin influx and efflux carriers in auxin patterning

At this stage of the project, the model integrated experimental crosstalk data into a realistic root map to produce patterning results that were similar in most cases to those observed experimentally. The next step was to use the existing

model to further investigate the roles of the influx and efflux carriers in establishing auxin patterning.

Experimental evidence shows that the quantitative properties of auxin gradients are important factors in regulating *Arabidopsis* root development. Auxin gradient formation is predominantly regulated by influx and efflux carriers that play distinct roles in controlling cellular auxin concentrations by moving auxin into and out of each cell. Directional auxin movement is coordinated by the combined activities of polar PIN efflux proteins, and AUX1/LAX influx proteins, that can have both non-polar (Peret *et al*., 2012) and polar (Kleine-Vehn *et al*., 2006) localisation depending on cell type.

The roles of influx and efflux carriers in plant development have been the subject of extensive investigation. Existing research predominantly explains experimental observations by the activity of either the auxin influx carriers (Swarup *et al*., 2001; Swarup *et al*., 2005; Dharmasiri *et al*., 2006; Ugartechea-Chirino *et al*., 2010; Peret *et al*., 2012; Fàbregas *et al*., 2015; Robert *et al*., 2015), or the activity of efflux carriers (Adamowski and Friml, 2015; references therein), or the ABCB transporters (Geisler *et al*., 2005; Geisler and Murphy, 2006; Cho *et al*., 2007; Cho and Cho, 2012), rather than analysing the integrated action of all carrier types. Although accumulated experimental evidence demonstrates that both auxin influx and efflux carriers have roles in plant development, a major obstacle for elucidating auxin patterning is the lack of a methodology to integrate the functions of these carriers. Previous modelling analysis has made efforts to study the actions of both influx and efflux carriers, but tends to emphasize the independent activities of either the efflux (Grieneisen *et al*., 2007) or the influx carriers (Band *et al*., 2014). The model developed in this work effectively integrates the function of all of these important known auxin transporters, rather than treating them as separate independent entities, to assist understanding of the coordinated action of the auxin carriers in auxin pattern formation.

To quantitatively investigate the integrated roles of the two carrier families in driving auxin patterning, it was necessary to develop a process which, after perturbing auxin patterning by changing the distribution of one carrier type, could generate the adjustments required to the other carrier type to rescue the

original patterning. In doing so, it would then be possible to better understand the integrated roles of the influx and afflux carriers.

An iterative process was developed, the ‘Recovery Principle’, where after adjustments to either carrier type, and consequent perturbation of auxin patterning, the distribution of the other carrier type was progressively adjusted to eventually recover the original auxin patterning before perturbation. Use of the recovery principle allowed the theoretical investigation of how the level and localisation of the influx and efflux carriers are potentially interlinked to generate auxin patterning. It was shown that multiple combinations of influx and efflux carriers could potentially generate the same auxin patterning, and that after pattern perturbation by changes to one carrier set, then pattern recovery relied on changes to both the level and localisation of the other carrier set. The theoretical existence of multiple combinations of influx and efflux carrier sets that achieve the same target auxin patterning, raises the possibility that perturbations in one carrier type, due to say environmental conditions or stress, could potentially be compensated by adjustments to the other carrier type to maintain auxin homeostasis. Interestingly, it has been suggested that dynamic recycling of auxin carrier proteins could enable the cell to adjust concentrations of auxin carriers at the plasma membrane to respond quickly to environmental changes, by adjusting auxin flow and patterning (Kleine-Vehn *et al*., 2006).

The recovery principle describes a methodology which allows the quantitative integrated analysis of the linkage between auxin and influx and efflux carrier patterning (Figure 4.16a), and as such, sheds light on the integrated actions of influx and efflux carriers and suggests that further understanding of the roles of auxin carriers in auxin patterning requires the study of the relationships between the carriers, as well as the study of each individual carrier.

This work also demonstrates that once auxin patterning is recovered using the recovery principle, PIN1 and PIN2 patterning also recovers due to the action of hormonal crosstalk, which suggests that auxin controls the patterning of its own transporters via hormonal crosstalk. Control of patterning of the other prescribed transporters can be elucidated in the future by conducting further experimental research and combining experimental data with modelling analysis. The design of specific experimental measurements will be critical to

provide the necessary data for constructing hormonal crosstalk networks for these transporters.

Mechanisms for self-organizing polar auxin transport and auxin pattern formation (where auxin flux and/or concentration patterning determine and in turn are determined by auxin carrier distribution) have been the subject of extensive study using mathematical models. A review discussed various models and mechanisms (van Berkel *et al*., 2013) which can be divided into flux-based or concentration-based models. However, they only consider the relationships between auxin and PIN efflux carriers. This work reveals that the relationships between influx and efflux level and polarity (rather than separate influx or efflux carrier activity) could control polar auxin transport and auxin pattern formation. In addition, a recent modelling study has suggested that auxin influx carriers can play an important role in polarising PIN carriers by affecting extracellular auxin concentrations (Cieslak *et al*., 2015), therefore future research on possible mechanisms for polar auxin transport should study the combined roles of efflux and influx carriers, focussing on how the relationship between auxin and polar PIN depends on the levels and localisation of the influx carriers.

6.5 Improved cytokinin patterning

Previous models developed in this work generated relative average cytokinin root concentrations in wildtype and the *pls* mutant that were consistent with experimental results; however, model cytokinin concentration patterning exhibited significant discrepancies from experimental observations. Trials with alternative experimentally based relationships between auxin and cytokinin failed to improve patterning but did demonstrate that other model results were not dependent on these alternative auxin-to-cytokinin relationships.

Cytokinin is a developmentally significant hormone. The ratio of auxin to cytokinin is particularly important for balancing cell division and cell differentiation in the meristem, and therefore determines meristem size and regulates root length. For future development of this work, it was therefore essential that improvements were made to cytokinin patterning and that these were based on experimental data. As discussed in Chapter 5, additional literature searches revealed possible alternative experimentally based

relationships between auxin, cytokinin and ethylene signalling, where signalling from the ethylene pathway regulates cytokinin degradation and therefore concentration patterning.

Model results from this proposed alternative crosstalk network produced cytokinin patterning which closely matched two types of experimental data, one using cell sorting and mass spectrometry methods to directly measure cytokinin concentrations in various regions of the root, and the second from cytokinin reporter response imaging. The revised model yielded improved representation of cytokinin patterning, while other results still remained consistent with experimental data. Nevertheless, although the revised network is based on experimental data, it remains to be confirmed by additional experimental work.

Cytokinin patterning results from the revised model, while matching experimental concentration measurements, did not appear to fully reflect response imaging in the QC region. As discussed extensively in section 5.5 this could be due to differences between response and concentration, and possibly indicates that additional factors influence cytokinin patterning. To further improve CK patterning and comparisons between model and experimental results, model enhancements should include any such additional regulatory factors as well as the ability to generate CK response data to allow direct comparison between experimental response images and model response (rather than concentration) colour maps.

In the previous models, cytokinin patterning was partially improved by limiting cytokinin biosynthesis to the central cell files and removing it from the outer cell files. In the revised model, this artificial limitation on cytokinin biosynthesis was removed so that cytokinin biosynthesis occurred in all cells, but at different rates that were fully regulated by the network.

This latest model, while exhibiting significantly improved cytokinin patterning, does not represent two possibly important features of cytokinin transport and degradation noted earlier. Cytokinin has been shown to be transported in the phloem from the shoot to root in sufficient quantities to affect root development (Bishopp *et al*., 2011b); however, it was postulated that this long-distance cytokinin transport might only affect vascular development while cytokinin regulated development of other root tissues is driven by local biosynthesis,

decay and flux. Also, in a recent paper (Zurcher *et al*., 2016), cytokinin influx transporters PUP14 were identified which remove cytokinin from the apoplast into the cytosol where it is degraded. This implies that PUP14 transporters are potentially important in the regulation of cytokinin degradation. Should PUP14 transporters exhibit distribution patterning in the root, then another level of complexity is added to the patterning of cytokinin degradation and therefore to cytokinin patterning and signalling.

6.6 Conclusions

This project followed an iterative process to develop representative experimentally-based hormone and gene expression crosstalk models to explain pattern formation in the *Arabidopsis* root tip (Figure 6.1). Experimental data were initially reviewed to establish model relationships; the relationships were defined using standard kinetic equations; where available, published parameter values were utilized otherwise values were calibrated by fitting model outcomes to experimental results; and finally model predictions were tested against experimental imaging and data. The initial model was then progressively modified (based on additional experimental information) to produce increasingly representative comparisons with experimental results.

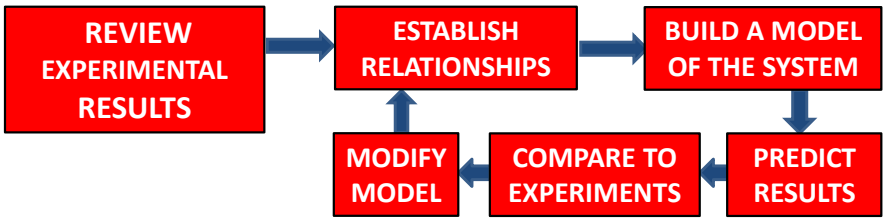

Figure 6.1: Iterative process to build the model

The model makes it possible to further investigate hormone and gene expression patterning in WT and mutants, in particular auxin pattern formation. Results suggest that auxin patterning is predominantly driven by directional auxin transport (consistent with Grieneisen *et al*., 2007) mediated by the concentration and localization of the influx and efflux carriers, since while auxin

patterning was fairly robust to all but extreme changes in rates of diffusion, biosynthesis and decay for many species, it proved more sensitive to changes in parameter values associated with auxin influx and efflux carriers (section 2.6). Even changing the regulatory relationships between auxin and cytokinin or implementing tissue-specific cytokinin biosynthesis had little impact on auxin pattern formation (section 2.6). It has been proposed that auxin patterning is the result of PIN efflux carriers directing auxin flux through the root, while the AUX1/LAX influx carriers act to retain cellular auxin and create the auxin maxima (Band *et al*., 2014); however, this work indicates that the regulation of auxin pattern formation could be more complex. The recovery principle in Chapter 4 demonstrates that auxin pattern homeostasis can theoretically be maintained by coordinating the concentration levels and polarity of the influx and efflux carriers at the plasma membrane. It has also been suggested that modification of carrier localization (to quickly adjust auxin patterning in response to environmental changes) could be achieved by modifying the rates of carrier recycling to the plasma membrane (Kleine-Vehn *et al*., 2006). Such a mechanism for adjusting auxin patterning assumes that it is possible that both the level and polarity of PIN and AUX1/LAX carriers can vary in response to environmental change; but, although AUX1 polarity is observed in protophloem cells (Kleine-Vehn *et al*., 2006), imaging data generally suggests a more uniform distribution of AUX1 at the cell faces. Nevertheless, since AUX1 permeability is thought to be greater than PIN permeability to prevent depletion of auxin in the cells (Kramer, 2004), minor AUX1 cellular polarity could be sufficient to achieve target auxin patterning, but at the same time be more difficult to observe experimentally. Similarly AUX1 polarity adjustments in response to changing environmental conditions could potentially modify auxin patterning through relatively small variation in AUX1 concentrations, again making it more difficult to experimentally observe polarity. Another interesting concept is that since root geometry constrains auxin directional flux it potentially also influences auxin accumulation and patterning, and in turn root development and root geometry. Therefore, influx and efflux carrier placement at the plasma membrane, auxin transport and accumulation, and root geometry could interact to determine auxin patterning and regulate root development.

While model results for PIN1 longitudinal concentration gradients matched experimental observations for WT and most mutants, PIN2 longitudinal patterning for the mutants did not, possibly indicating different or more complex regulatory pathways/factors for PIN1 and PIN2 localization and level. Similarly, AUX1 model patterning did not match experimental observations, suggesting additional regulatory factors influence AUX1 level and localisation, such as cytokinin (Street *et al*., 2016).

Comparison of multiple (and differing) experimental cytokinin patterning results, with each other and with modelling results (section 5.4), reveals possible limitations in the use of reporters as surrogate measures for concentration patterning. A good example is the regulation of *ARR5,* which is commonly used as a reporter mechanism for cytokinin (Zurcher *et al*., 2013). *ARR5* can be regulated by multiple pathways (see App 2.1). The Type-B ARRs are upregulated by cytokinin and in turn upregulate the Type-A ARRs, including *ARR5* (El-Showk *et al*., 2013; Kim *et al*., 2012; Zurcher *et al*., 2013). However, *ARR5* is downregulated by downstream ethylene signalling which is also regulated from the cytokinin pathway (El-Showk *et al*., 2013 and see section App 2.1). In the *pls* mutant, cytokinin levels increase (Table 1 in Liu *et al*., 2010), so potentially upregulating *ARR5*; however, downstream ethylene signalling also increases which downregulates *ARR5*. Ethylene, cytokinin and PLS upregulate auxin biosynthesis, which in turn upregulates *AHP6* which inhibits cytokinin signalling and *ARR5* (Bishopp *et al*., 2011a and section App 2.1). Reporter expression is further complicated by the fact that regulation pathways will very likely be non-linear, for example the bell-shaped regulation of cytokinin oxidase activity by cytokinin (Chatfield and Armstrong, 1986). This demonstrates the complexity of just some of the signalling pathways that control *ARR5* regulation and there are likely many additional hormone linkages which influence *ARR5* expression. The existence of cytokinin transport and influx carriers potentially further complicates the regulation of cytokinin concentration and the interpretation of experimental reporter imaging and patterning. This suggests the need for better understanding of the relationships between hormone concentrations and commonly used experimental reporters, to allow

improved interpretation of experimental imaging results for cytokinin and other hormones.

The difference between certain experimental and model results for ethylene receptor mutants (particularly the double mutant *pls etr1-1*), for example shoot to root auxin transport (Figure 2.44), average auxin concentration (Figure 2.12) and the PIN1 concentration profile (Figure 2.52) in the double mutant, and PIN1 concentrations in the single mutant (Figure 2.49), demonstrates the complexity of ethylene perception, which involves multiple receptors acting in different configurations and clusters (Yoo *et al*., 2009; Mayerhofer *et al*., 2012). The degree of receptor complexity makes it increasingly difficult to fully understand the regulation of downstream ethylene signalling, even before taking into account links to and from other signalling pathways, and is a further example of the intricacies of signalling pathways and multiple pathway interactions that have to be addressed to improve understanding of hormone pattern formation, gene expression and ultimately root development.

There are areas of the model which require revision to better reproduce experimental results; for example, the longitudinal trend in PIN2 concentration profiles, results for certain *etr1* mutants compared to wildtype as detailed above, and some features of cytokinin patterning. Model modifications could include long-distant cytokinin phloem transport, the influence of PUP14 patterning on cytokinin influx and degradation, separate networks for the regulation of PIN1 and PIN2 levels or localization, network additions for cytokinin regulation of PIN1, PIN3 and PIN7 auxin carrier placement in the vasculature (Bishopp *et al*., 2011a), enhanced regulation of *AUX1* expression including the recently demonstrated inhibition of *AUX1* by cytokinin (Street *et al*., 2016), network regulation of auxin carriers which currently have prescribed wildtype level and localization, the inclusion of additional hormones and genes, and more detailed downstream hormone signalling and linkages between the hormone signalling pathways (for example auxin inhibition of cytokinin signalling through AHP6).

Earlier discussions on comparisons between the model and experimental results for cytokinin patterning (above and section 5.4) raised the issue of potential differences between hormone concentrations and reporter imaging, often necessarily used as a surrogate measurement for concentration. A useful

model enhancement would therefore be the inclusion of commonly used reporter constructs into the hormone signalling pathways so that model predictions for both hormone concentration and specific reporter response patterning could be generated and compared to experimentally observed response imaging and concentration measurements. This would allow more accurate comparison and interpretation of model and experimental results. Potentially, such a model could also be used to assist in the design of novel hormone response reporters.

Despite the current limitations of this 2-D spatial model, the final version, including the latest modifications to improve cytokinin patterning, produces results which represent many key features of wildtype patterning for all species regulated by the network as well as concentration trends for WT and many mutants. It therefore provides an initial explanation of how hormonal crosstalk controls gene expression and patterning in the *Arabidopsis* WT and mutant roots.

This research has integrated a wide range of experimental data to establish a data-driven mechanistic model for both elucidating the control of hormone patterning and gene expression and for making various predictions, all within a realistic root map which enables detailed comparison to experimental results for individual regions, cell types or cell files within the root tip. Nevertheless, the current model is considered a starting point since it can only analyse the contribution to patterning (in particular auxin patterning) of those components that are included in the hormonal crosstalk network. Given that hormone signalling is the ultimate driver of gene expression and so root development, future research should include the integration of other hormones, signalling molecules and additional developmentally relevant gene expression processes into the model, followed by combined modelling and experimental studies to clarify the contribution of each process to patterning and root development.

Another area for model development could be the analysis of relationships between gene expression, hormone patterning and root growth which would require the inclusion of additional proteins and hormones. Recent studies have shown that growth and hormonal patterning can affect each other through gene expression, cell division, cell expansion and dilution (De Rybel *et al*., 2014;

Mahonen *et al*., 2014), therefore future research could investigate relationships between the spatiotemporal dynamics of hormonal crosstalk and growth. The effects of osmotic stress on root growth could also be researched by the addition of the hormone abscisic acid to the crosstalk network, based on experimental results from Rowe *et al*. (2016).

The model could potentially be used to further investigate how PIN polarity is established and maintained in a 2-D multicellular root. If it is the case that self-organizing PIN polarity is ultimately a function of hormone patterning and/or flux (as reviewed in van Berkel *et al*., 2013) then it could be possible to adapt the model such that PIN is initially set in a non-polar uniform distribution and is then iteratively adjusted, based on say auxin concentration or flux, to see if a final steady state is achieved and if the steady state PIN distribution exhibits polarity, levels and localisation similar to wildtype. In this proposed version of the model, auxin concentration gradients or flux would be factors in determining PIN distribution and polarity, which in turn would adjust auxin patterning until a steady state was established. If PIN polarity is in part established by auxin flux and/or patterning, then important parameters driving the model would be a combination of auxin influx at the shoot-root border and local auxin biosynthesis and decay in each cell.

In root development, the complexity of hormonal signalling includes many factors. The spatiotemporal dynamics of hormonal crosstalk, which integrates hormonal crosstalk at a cellular level with root structure, are able to explain two important factors – the level and patterning of hormones/hormone response and gene expression. Recent modelling and experimental work (Bargmann *et al*., 2013; Chickarmane *et al*., 2010; De Rybel *et al*., 2014; Hill *et al*., 2013) show that integration of regulatory networks into spatial root structures is a promising tool for elucidating mechanisms of development. By integrating more genes into the hormonal crosstalk network (Bargmann *et al*., 2013; De Rybel *et al*., 2014; Hill *et al*., 2013; Mintz-Oron *et al*., 2012) and enhancing the root structure to include further details of cell to cell communication (Chickarmane *et al*., 2010; De Rybel *et al*., 2014; Hill *et al*., 2013), it should be possible to expand the understanding of levels and pattern formation to include additional hormones and gene expression and, for example, the relationships between auxin

patterning and polarity, patterning of multiple efflux and influx carriers, and auxin metabolism (biosynthesis, degradation and conjugation).

The current crosstalk network is relatively simple when compared to the more detailed network in Appendix 2, which still only contains 3 hormones. Given that the network complexity will increase exponentially with additional hormone pathways, gene expression and pathway linkages, it is evident that the only way to analyse such complex biological networks as integrated systems is by a combined experimental and modelling approach. The last phase of this work, involving the development of an alternative crosstalk network for cytokinin regulation by ethylene signalling, is a good example of the advantages of this approach. The use of an experimentally based model allows accepted relationships in complex systems to be challenged by model outcomes and then alternative solutions, based on experimental data, proposed and investigated. This approach makes it possible to explore different relationships and gain a deeper understanding of the dynamics of complex biological systems.

Potentially this approach, with the tools already developed in this work, could also be used to investigate hormonal crosstalk and hormone and gene expression patterning for other regions of the *Arabidopsis* root and shoot.

APPENDICES AND BIBLIOGRAPHY

APPENDIX 1: RUNNING THE REALISTIC ROOT MODEL (WT200)

(USER INPUTS IN RED)

=====ROOT MODELLING PROGRAM vs29d WITH WT200 NETWORK=====

Input the RUN NUMBER: WT200
Input the time step and simulation time:
The time step (second)= 100
The simulation Time(s)= 20000

Input real root switch, 0 for rectangular root, 1 for real root: = 1

Input # data output sets/simulation time (recommend 1): = 1
SET MAX # OF DATA DUMPS ALLOWED (to restrict file size): = 5
This uses up to 300 MB of storage Is this OK? 0 = NO, 1 = YES: = 1

Input COMBINED PIN12347 START [ARRAY] ? NO = 0, YES = 1: 0

For RECOVERY ITERATIONS combined auxlax array must be input
Input COMBINED AUX1,LAX2,3 START [ARRAY] ? NO = 0, YES = 1: 0

AUTO RECOVERY BY AUXLAX OR PIN RE-SETS NO = 0, YES = 1: 0

SET START AUX1 concentrations (synthesis at 0) NO = 0, YES = 1: 1
SET START LAX2 concentrations NO = 0, YES = 1: 1
SET START LAX3 concentrations NO = 0, YES = 1: 1

SET START PIN3 concentration? NO = 0, YES = 1: 1
SET START PIN4 concentrations? NO = 0, YES = 1: 1
SET START PIN7 concentrations? NO = 0, YES = 1: 1

HORMONE FEEDING? Input 0 for NO or 1 for YES: 0

========== VALUE OF PARAMETERS ==========
Input START LEVEL 4 (MAX) PIN3 concentration (micro M) 0
Input START LEVEL 3 PIN3 concentration (micro M) 1
Input START LEVEL 2 PIN3 concentration (micro M) .25

Input START LEVEL 1 (MIN) PIN3 concentration (micro M) .06

Input START LEVEL 4 (MAX) PIN4 concentration (micro M) 0
Input START LEVEL 3 PIN4 concentration (micro M) .5
Input START LEVEL 2 PIN4 concentration (micro M) .1
Input START LEVEL 1 (MIN) PIN4 concentration (micro M) .02

Input START LEVEL 4 (MAX) PIN7 concentration (micro M) 0
Input START LEVEL 3 PIN7 concentration (micro M) 1
Input START LEVEL 2 PIN7 concentration (micro M) .25
Input START LEVEL 1 (MIN) PIN7 concentrations (micro M) .06

Input START LEVEL 15 (MAX) AUX1p concentration (micro M) 0
Input START LEVEL 14 AUX1p concentration (micro M) 0
Input START LEVEL 13 AUX1p concentration (micro M) 0
Input START LEVEL 12 AUX1p concentration (micro M) 0
Input START LEVEL 11 AUX1p concentration (micro M) 0
Input START LEVEL 10 AUX1p concentration (micro M) 0
Input START LEVEL 9 AUX1p concentration (micro M) 0
Input START LEVEL 8 AUX1p concentration (micro M) 0
Input START LEVEL 7 AUX1p concentration (micro M) 0
Input START LEVEL 6 AUX1p concentration (micro M) 0
Input START LEVEL 5 AUX1p concentration (micro M) 0
Input START LEVEL 4 AUX1p concentration (micro M) 0
Input START LEVEL 3 AUX1p concentration (micro M) 2.25
Input START LEVEL 2 AUX1p concentration (micro M) 1
Input START LEVEL 1 (MIN) AUX1p concentration (micro M) .75

Input START LEVEL 8 (MAX) LAX2 concentration (micro M) 0
Input START LEVEL 7 LAX2 concentration (micro M) 0
Input START LEVEL 6 LAX2 concentration (micro M) 0
Input START LEVEL 5 LAX2 concentration (micro M) 0
Input START LEVEL 4 LAX2 concentration (micro M) 0
Input START LEVEL 3 LAX2 concentration (micro M) 1.75
Input START LEVEL 2 LAX2 concentration (micro M) 0
Input START LEVEL 1 (MIN) LAX2 concentration (micro M) 0

Input START LEVEL 4 (MAX) LAX3 concentration (micro M) 0
Input START LEVEL 3 LAX3 concentration (micro M) 1.75
Input START LEVEL 2 LAX3 concentration (micro M) 0

Input START LEVEL 1 (MIN) LAX3 concentration (micro M) 0

========== ROOT STRUCTURE ==========

DEFAULT NUMBER OF ROWS IN ROOT MAP FILE = 1150

DEFAULT NUMBER OF COLS IN ROOT MAP FILE = 326

USE DEFAULT ROOT MAP DIMENSIONS? 1 = YES, 0 = NO 1

Default ROOT MAP FILE is RR1150pin12mapvs25.txt

Use default? 1 = YES, 0 = NO 1

INPUT SIZE OF EACH PIXEL (recommend 2 microns)? 2

REAL ROOT has been selected

Default CELL NO. FILE is rootmapcellno1150.txt

Use default? 1 = YES, 0 = NO: 1

The MAXIMUM CELL NUMBER used is 1165

REAL ROOT has been selected

Default PIN3 MAP is: RR1150pin3mapvs26.txt

Use default? 1 = YES, 0 = NO 1

REAL ROOT has been selected

Default PIN4 MAP is: RR1150pin4mapvs25.txt

Use default? 1 = YES, 0 = NO: 1

REAL ROOT has been selected

Default PIN7 MAP is: RR1150pin7mapvs25.txt

Use default? 1 = YES, 0 = NO 1

REAL ROOT has been selected

Default AUX1 MAP is: RR1150aux1mapvs10b.txt

Use default? 1 = YES, 0 = NO 1

REAL ROOT has been selected

Default LAX2 MAP is: RR1150lax2mapB.txt

Use default? 1 = YES, 0 = NO 1

REAL ROOT has been selected

Default LAX3 MAP is: RR1150lax3mapB.txt

Use default? 1 = YES, 0 = NO 1

Number of active Grid Points = 283816

========== START OF ITERATION # 1 out of 1 ==========

RUN NUMBER WT200 ITERATION # 1 out of 1

ROOT MODELLING TIME IS NOW =200

RUN NUMBER WT200 ITERATION # 1 out of 1

ROOT MODELLING TIME IS NOW =300

Results from MATLAB® 'Auxin profile and Image' program, using WT200 data from above.

Concentrations at GP9s peripheral to the root (ACTIVE) are set to medium concentration to highlight the root border but not counted in the root concentration results

Rootcount of GPs within the root = 281245

Auxin results:

Average root concentration = **0.7229**

The top 3 maximum auxin concentrations and their GP coordinates and cell numbers

i1 =167

j1 = 932

max1 =8.3893

max1cell =101

i2 = 167

j2 =933

max2 = 8.3653

max2cell =101

i3 = 167

j3 =934

max3 = 8.3409

max3cell = 101

APPENDIX 2: ETHYLENE, CYTOKININ AND AUXIN CROSSTALK

App 2.1 Annotated schematic of ethylene, cytokinin and auxin crosstalk.

Figure Ap 2.1 shows a more detailed schematic of auxin, cytokinin, ethylene and gene expression crosstalk, including some downstream components of the pathways. Explanations of the annotations are on the pages following.

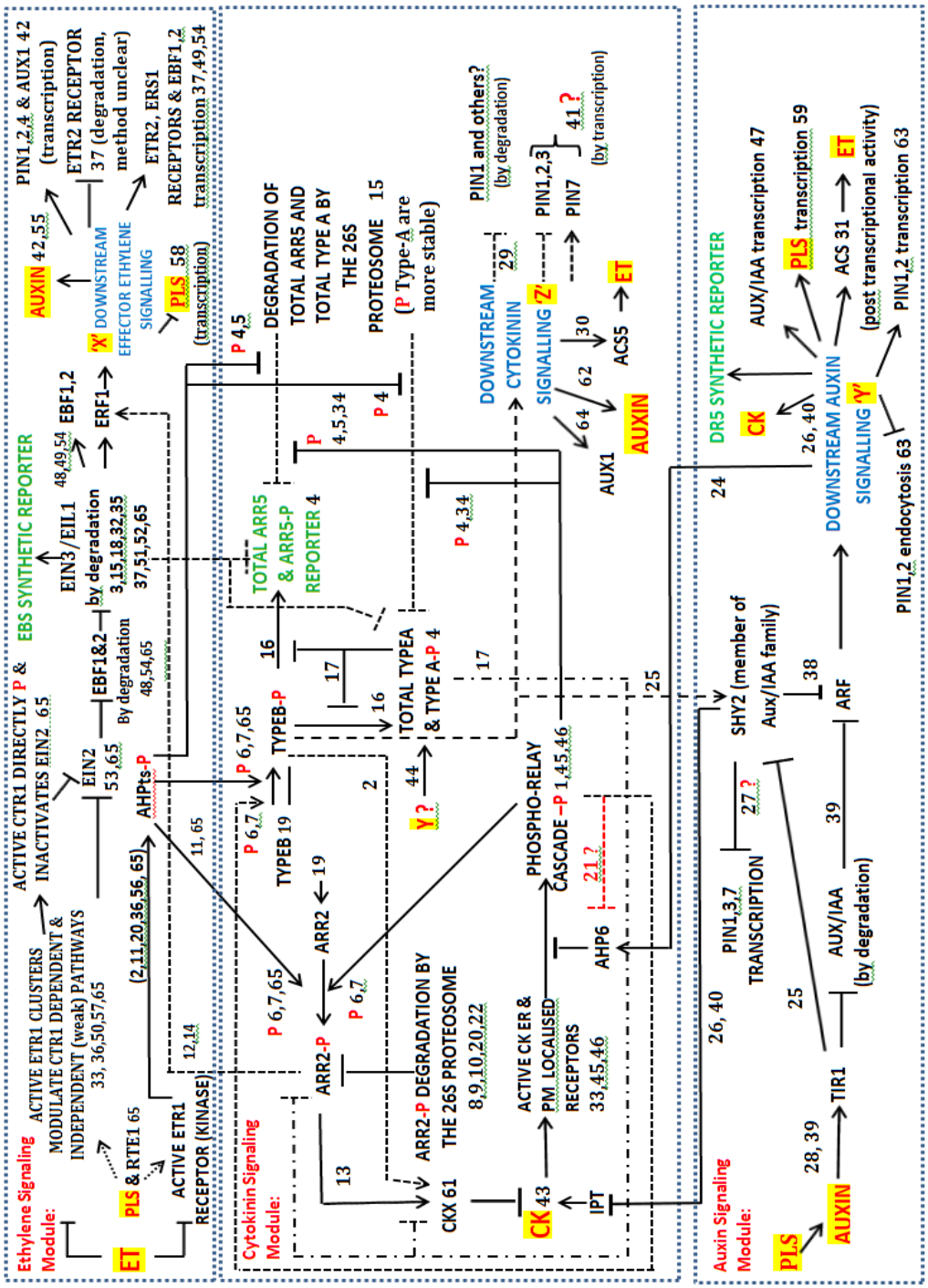

Figure Ap 2.1: Schematic of Ethylene, cytokinin and auxin crosstalk
(**P**, phosphorylation; **X**, downstream ET signalling; **Y**, downstream auxin signalling; **Z**, downstream CK signalling)

Network diagram annotations:

1. Phospho-relays form part of the CK signalling pathway (Fig 2, El-Showk *et al*., 2013; pg 1, Hass *et al*., 2004)
2. There is evidence of phospho-relays acting in the ethylene pathway (Hass *et al*., 2004; Yoo *et al*., 2008; Scharein *et al*., 2008; Bisson and Groth, 2010; Shakeel *et al*., 2013). However, it is now thought that the phospho-relay in Yoo is to do with ethylene biosynthesis (pg. 13, Shakeel *et al*., 2013). The proposed phospho-relay in Hass involves ETR1 kinase activity and AHPs activating CK signalling (see App 2.3 below for notes on the three proposed ethylene pathways).
3. EIN3 binds *ARR5, 7, 15* promoters and suppresses their expression (pg 8, El-Showk *et al*., 2013; abstract and pg 8, Fig 6 and 9, Shi *et al*., 2012)
4. Cytokinin induced phosphorylation stabilizes a subset of Type-A ARRs by reducing their rate of degradation (pg 3, El-Showk *et al*., 2013; Kim *et al*., 2012 ; Keiber and Schaller 2014). ARR5,6,7 were stabilised with increased half-lives by the application of cytokinin, however ARR4 and 9 showed no increase in half-life with cytokinin application (pg 5, To *et al*., 2007). Phosphorylation is required for Type-A stabilisation (pg 5&7, To *et al*., 2007) and for ARR5 activation and function (pg 2, To *et al*., 2007). Some but not all Type-As are degraded by the proteasome (pg 1, Kurepa *et al*., 2013; abstract, To *et al*., 2007). Type-As negatively regulate signalling by interaction with other pathway components, rather than competing with AHPs for phosphoryls (pg 4, To *et al*., 2007). Certain Type-Bs are necessary for cytokinin application to stabilise ARR5; therefore some Type-Bs possibly act to up-regulate elements involved in ARR5 stabilisation (pg 5, To *et al*., 2007).
5. Exogenous cytokinin treatment strongly stabilized the Type-A ARR5, 7,15 proteins (pg 9 &13, Shi *et al*., 2012).
6. Phosphorylation of Type-Bs enables DNA binding and activation of their transactivation function (pg 3, El-Showk *et al*., 2013; pg 2, Kim *et al*., 2012). In particular, phosphorylation of ARR2 plays an important role in its function (pg 4, Hass *et al*., 2004), and HPt proteins (histidine phospho transferases) possibly play a role in ETR1 initiated phosphorylation of

ARR2 by a two-component phospho-relay system (pg 10, Hass *et al*., 2004). Also see section App 2.3 below on ethylene signalling where direct interaction between ETR1 and AHPs is discussed and it is suggested that ETR1 (which has a kinase function) directly phosphorylates AHPs.

7. Phosphorylation of Type-B's is essential for their transactivation activity (Kim *et al*., 2012).
8. ARR2 is temporarily activated by CK application and subsequent phosphorylation and then rapidly degraded (by the 26S proteasome), while other Type-B ARRs are not (abstract, Fig 1, pg 2,3 & 4, Kim *et al*., 2012). Degradation of ARR2 is increased in constitutively phosphorylated forms such as $ARR2^{D80E}$ (pg 5, Kim *et al*., 2012). ARR2 degradation requires CK induced phosphorylation since in an ARR2 mutant (which prevents phosphorylation) and in CK receptor mutants, no degradation was observed (pg 2 & 5, Kim *et al*., 2012). ARR1 showed rapid degradation but the rate was not influenced by cytokinin application while ARR10,12,18 remained constant during cytokinin application (pg 2, Kim *et al*., 2012). ARR1,10,12,18 did not show electrophoretic mobility shifts on cytokinin application (pg 2 & 4, Fig 1, Kim *et al*., 2012).
9. Since other Type-B's (1, 10, 12, 18) showed no CK induced phosphorylation or CK induced degradation, ARR2 could be different in this property from other Type-B's (Kim *et al*., 2012).
10. *ARR6* (Type A) is a direct ARR2 target and is induced within 30mins of CK application; however with prolonged application this induction decreased rapidly (Kim *et al*., 2012), possibly indicating ARR2-P degradation.
11. ETR1 (a kinase) is an upstream regulator of ARR2 phosphorylation (pg 4, Hass *et al*., 2004). An ETR1 initiated phospho-relay possibly regulates ARR2 activity (pg 1 & 2, Hass *et al*., 2004; pg 2, Kushwah *et al*., 2011; pg 3, Gupta and Rashotte, 2012; pg 13, Shi *et al*., 2012). Interaction between ETR1 and AHP phospho-transfer protein has been demonstrated (Scharein *et al*., 2008), suggesting a CTR1 independent pathway in ethylene signalling. See further information on ethylene signalling pathways in section App 2.3 below.

12. ARR2 binds the *ERF1* promoter and up-regulates *ERF1* (pg 3, Fig 2C, Hass *et al*., 2004) therefore the ethylene pathway can still be activated independently of CTR1 by an ETR1 initiated phospho-relay mediated by ARR2 (pg 10,11 Hass *et al*., 2004).
13. Microarray analysis indicates that ARR2 up-regulates *CK oxidase* expression (pg 7, Hass *et al*., 2004).
14. Over-expressed constitutively active ARR2 displayed the ET triple response in the absence of ET biosynthesis (by AVG application) (pg 4, Hass *et al*., 2004).
15. ACC (ethylene) induced ARR5 degradation appears to be dependent on the 26S proteasome pathway since the ARR5 signal all but disappears after 12hr of ACC application but is stabilized by simultaneous application of ACC and the proteasome inhibitor MG132 (pg 10 and Fig 9B, Shi *et al*., 2012). ACC reduces ARR5 accumulation by both degradation and down-regulating transcription (Fig 9 A&B, Shi *et al*., 2012), presumably through the action of *EIN3*. Stabilization of ARR5 by CK does not appear to require new protein synthesis since ARR5 stabilization occurred with simultaneous treatment with CK and a protein synthesis inhibitor (Fig 3C, To *et al*., 2007).
16. Type-B ARRs up-regulate Type-A expression (pg 3, El-Showk *et al*., 2013; pg 3 & 4 Gupta and Rashotte, 2012). Certain Type-Bs possibly activate transcription of elements which are required for the stabilisation of Type-As by phosphorylation (pg 10, To *et al*., 2007).
17. Phosphorylation of the type-A ARRs acts to stabilize them, whereas phosphorylation of the type-B ARRs enables them to bind to DNA and initiate transcription of downstream targets, including the type-A ARRs (Figure Ap 2.2; pg 3, El-Showk *et al*., 2013).

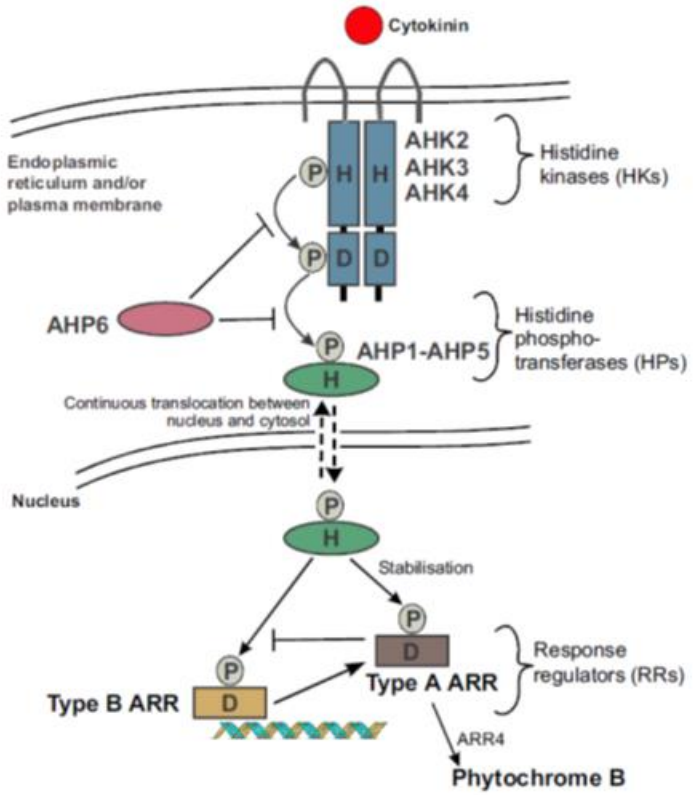

Figure Ap 2.2: Cytokinin signalling pathway
(El-Showk *et al*., 2013)

Type-A ARRs negatively regulate cytokinin signalling by suppressing Type-B activity (Fig 2, El-Showk *et al*., 2013). This suppression possibly occurs by 2 mechanisms, either by competing with AHPs for phosphorylation or by the phosphorylated Type-A ARRs interacting with regulatory proteins (pg 17, Keiber and Schaller 2014; pg 4, Gupta and Rashotte, 2012). It was concluded that the negative regulation is by Type-A interaction with regulatory proteins (pg 2, To *et al*., 2007). ARR4,5,6,7,9 all negatively regulate the cytokinin response (pg 5, To *et al*., 2007). The possibility of reverse phosphorylation flux was also discussed (pg 9, To *et al*., 2007), involving AHK4 (which has kinase and phosphatase capability depending on whether it binds cytokinin) and possibly Type-A ARRs. This might explain the negative regulation of cytokinin signalling by Type-A ARRs; however, this is not included in the network diagram.

18. *EIN3* over expression suppresses the up-regulation of *ARR5* by CK (BA) application (Fig 6c, Shi *et al*., 2012).
19. Transcription of Type-B ARRs is not induced by CK (Kakimoto, 2003; pg 2, Gupta and Rashotte, 2012).
20. The transactivation activity of ARR2 is reduced by ACC application in cell free protoplast systems but is increased by ACC application in seedlings, as measured by using an ERF1:GUS reporter (Fig 2C, 5D, pg 9 & 10 discussion section, Hass *et al*., 2004), possibly due to faster ARR2 phosphorylation and degradation in cell free systems?
21. CK signalling down-regulates the level of *AHP6* transcript (Fig 4B & pg 6, Mahonen *et al*., 2006). However, CK down-regulation of *AHP6* does not occur if auxin transport is inhibited by NPA suggesting that this response is mediated by auxin transport and PIN rather than directly (pg 4, Bishopp *et al*., 2011a).
22. Excluding ARR2, CK application has little effect on the rate of Type-B degradation (pg 16, Keiber and Schaller 2014).
23. ARR1 (type-B) is shown to directly up-regulate *CKX4* (pg 3, Taniguchi *et al*., 2007). *CKX4* is expressed highly and specifically in the root cap (pg 11, Werner *et al*., 2003).
24. Auxin promotes transcription of *AHP6* (pg 4, Bishopp *et al*., 2011a; Fig 3, El-Showk *et al*., 2013) which inhibits cytokinin signalling (Bishopp *et al*., 2011a).
25. Auxin mediates the degradation of *SHY2*, and cytokinin activated ARR1 directly binds and up-regulates *SHY2* transcription (abstract and pg 3 & 5, Dello Ioio *et al*., 2008). ARR12 up-regulates *SHY2* (Fig 3, El-Showk *et al*., 2013).
26. SHY2 inhibits IPT enzymes for cytokinin synthesis (pg 5, Fig 2, Gupta and Rashotte, 2012; pg 5, Dello Ioio *et al*., 2008).
27. SHY2 inhibits *PIN* expression (pg 5, Fig 2, Gupta and Rashotte, 2012 review referencing Dello Ioio). Cytokinin activated SHY2 inhibits *PIN1,3 and 7* transcription mediated through the AHK3 cytokinin receptor and the Type-B ARR1 cytokinin response regulator (pg 3, 4 & Fig 2J, Dello Ioio *et al*., 2008). CK treatment inhibits *PIN2 and 4* but it does not show significant inhibition of *PIN1,3 and 7* (Fig 6B, Persinova *et al*., 2009). CK

signalling inhibits *PIN1,2,3 and 4* but promotes *PIN7*. The responses to CK vary in time and dynamics and can be influenced by ET signalling, which promotes, to varying degrees, *PIN1,2 and 4* but appears to have no effect on *PIN3 and 7* (pg 4, Ruzicka *et al*., 2009). CK promotes *PIN7* expression and promotes the localisation of PIN1 and 7 to the plasma membrane (pg 7, Bishopp *et al*., 2011a; Bishopp *et al*., 2011b). There appears to be some contradictions (refer to notes 27, 29 and 41) on CK effects on PIN levels and these are commented upon (pg 6 in Zhang *et al*., 2011 and pg 7 in El-Showk *et al*., 2013).

28. Auxin and ethylene signalling pathways (Muday *et al*., 2012).
29. Cytokinin signalling mediated by ARR2 and ARR12 results in degradation of PIN1 by endocytic trafficking from the plasma membrane to the lytic vacuoles (pg 7, El-Showk *et al*., 2013; abstract, Marhavy *et al*., 2011). Type-A response regulators are involved in the negative regulation of PIN1,3 and 4 and this regulation takes place at a post-transcriptional level, not through SHY2 regulation of *PIN* expression. This data was derived using 0.5mm root tip samples including mainly the meristematic zone (pg 6, Zhang *et al*., 2011). There appears to be some contradictions (refer to notes 27, 29 and 41) on CK effects on PIN levels which are commented upon (pg 6 in Zhang *et al*., 2011 and pg 7 in El-Showk *et al*., 2013).
30. Cytokinin acts to increase *ACS* transcription and stability, and so ethylene biosynthesis (pg 7, Fig 4, El-Showk *et al*., 2013; pg 13, Shi *et al*., 2012).
31. Auxin acts to increase transcription of *ACS* and so ethylene biosynthesis (pg 7, El-Showk *et al*., 2013; pg 6, Zhao, 2010).
32. *ctr1* null mutants show continued accumulation of EIN3 with prolonged ET application, suggesting the possibility of an additional ethylene signalling pathway through ARR2 (pg 10 &11, Hass *et al*., 2004; Fig 1F and pg 2, Guo and Ecker, 2003). Alternatively, EIN3 could continue to accumulate since degradation of EIN2 (and therefore EIN3) in part relies on the availability of active CTR1 to complex with newly synthesised receptors (without bound ET) to initiate EIN2 degradation (Fig 1, pg 2 &

4, Zhao and Guo, 2011). Also see point 35 and App 2.3 below on ethylene signalling pathways.

33. Cytokinin receptors are ER localised (pg 2, El-Showk *et al*., 2013). Ethylene receptors are also ER localised (pg1, Hass *et al*., 2004) and the ligands bind tightly with a half-life of bound ethylene receptors of 10hrs (pg7, Chen *et al*., 2007). Therefore, there likely needs to be a mechanism to quickly down-regulate ethylene signalling in response to a changing environment, such as ligand-bound ethylene receptor degradation. Even though the ligand bound receptors are in fact largely inactive they need replacing with unbound receptors to enable the pathway to sense changes in ethylene concentrations (pg 7, Chen *et al*., 2007). Note that there are potentially 2 (or 3) ethylene signalling pathways that are CTR1 dependent and independent (see notes 36, 37) that need to be balanced. Degradation of the receptor will also release ethylene. The half-lives of the receptors range from 30mins to 12hrs (pg7, Chen *et al*., 2007), possibly depending on receptor type. See App 2.2 below for more ethylene receptor information.
34. Cytokinin signalling regulates the stability and activation of type-A ARRs by phosphorylation. Phosphorylation of ARR5, 7 (type-As) has been shown to activate their negative regulatory role in cytokinin signalling (pg 4, Gupta and Rashotte, 2012).
35. As noted in (32), it has been suggested that there is possibly an additional ethylene signalling pathway which by-passes CTR1 since EIN3 continues to accumulate when ethylene is applied in the *ctr1* null, demonstrating a possibly residual ethylene response in the *ctr1* mutant (pg 2, Guo and Ecker, 2003); however this residual response might not involve ARR2 since, while ARR2 binds the *ERF1* promoter and up-regulates *ERF1*, *EIN3* is upstream of *ERF1* therefore *ERF1* up-regulation by ARR2 does not explain the accumulation of EIN3 unless there is a feedback loop. Also see App 2.3 below on ethylene signalling pathways.
36. The proposed ethylene signalling pathway (Fig 2, Yoo *et al*., 2009) shows 2 phospho relay cascades, the one in which active CTR1 effectively results in degradation of downstream components with no

ethylene signalling, and the alternative cascade for inactive CTR1, which stabilises downstream ethylene signalling components and activates ethylene signalling but acts independently of EIN2 (Fig 2, Yoo *et al*., 2009). This is disputed (pg 5, Zhao and Guo, 2011) and it is argued that this latter phospho-relay pathway is involved in ethylene biosynthesis and NOT ethylene signalling and so it is no longer thought to be part of the ethylene signalling pathways (see notes in App 2.2 and 2.3 below on ethylene receptors and 3 possible signalling pathways).

37. Ethylene self regulates the ethylene signal by controlling the accumulation of EIN3. This is done by ethylene induced degradation and turnover of ETR2 (pg 7, Chen *et al*., 2007) and up-regulation of the transcript of the ETR2 and ERS1 receptors (pg 2 & 4, Zhao and Guo, 2011; abstract and Fig 3, Chen *et al*., 2007). Note the non-linear response of ETR1 levels to ethylene (Fig 3, Chen *et al*., 2007). Chen *et al*. (2007) also conclude (pg 7), that ETR2 degradation is caused by conformation change due to ethylene binding not to ethylene signalling. However this is not necessarily the case since there is also a CTR1 independent ethylene signalling pathway which could up-regulate elements required for ETR2 degradation in the *ctr1* mutant; however (pg 6, Chen *et al*., 2007), ETR2 degradation still occurs when protein synthesis was inhibited which possibly contradicts this latter explanation and supports degradation of ethylene bound ETR2 due to conformational change. EIN3 normally has a high turnover rate but is stabilised by ethylene application and could therefore accumulate with harmful effects. New ETR2 proteins may complex with CTR1 but not be immediately bound by ethylene (resulting in active CTR1) so promoting EIN3 degradation (pg 4, Zhao and Guo, 2011). See also App 2.3 below on ethylene signalling pathways.

38. *SHY2* (a member of the *Aux/IAA* family of genes degraded by auxin) inactivates ARF auxin response transcription factors through dimerization (pg 1, Dello Ioio *et al*., 2008).

39. When the concentration of auxin in the cell is low, the Aux/IAA (auxin/indole-3-acetic acid) proteins heterodimerize with the ARF (AUXIN RESPONSEFACTOR) transcription factors, repressing the transcription

of the auxin-response genes. At high auxin concentrations, auxin binds to the TIR1 (TRANSPORT INHIBITOR RESPONSE 1) receptor, stimulating the interaction of the Aux/IAAs proteins with the SCFTIR1 ubiquitin-ligase complex (SKP1, CDC53/CULLIN, F-box), thus promoting their degradation by the 26S proteasome. The consequent reduction in levels of Aux/IAA proteins releases the ARFs from their inhibition, inducing the expression of auxin-responsive genes (Fig 1, Moubayidin *et al*., 2009).

40. *IPT5* is up-regulated by auxin, mediated by SHY2 (pg 5, Dello Ioio *et al*., 2008).
41. Cytokinin treatment down-regulates *PIN1,2,3* and up-regulates PIN7 expression, based on *promoter::GFP* reporters (pg 4 & Fig 3, Ruzicka *et al*., 2009). *PIN7* is upregulated by exogenous CK (pg 14, Hwang *et al*., 2012). Other results show that CK application reduces the transcript of all *PIN1,3,7* mediated through ARR1 (Fig 2J, Dello Ioio *et al*., 2008). Consider that the Ruzicka results might be also mediated through SHY2. There appears to be some contradictions (refer to notes 27, 29 and 41) on CK effects on PIN levels which are commented upon (pg 6 in Zhang *et al*., 2011and pg 7 in El-Showk *et al*., 2013.
42. Ethylene upregulates auxin biosynthesis, transcription of *PIN1,2,4* and *AUX1* after varying treatment times, but appeared to have no effect on *PIN7* (pg 7 &10 and SI, Ruzicka *et al*., 2007).
43. It may also be necessary to consider transport of cytokinin in the phloem (shoot to root) and xylem (Bishopp *et al*., 2011b), possibly with differential synthesis, conversion and transport of iP and Z type cytokinins. iP appears to be the predominant type synthesised in the root (pg 6, Nordstrom *et al*., 2004).
44. Auxin directly up-regulates Type-A *ARR7,15* transcription in early development in the basal cell of the hypophysis (Fig 3t, u Muller and Sheen, 2008).
45. AHK cytokinin receptors are ER and plasma membrane localised and initiate a phospho-relay cascade (Fig 1, Hwang *et al*., 2012) and have different ligand binding affinities (pg 7, Hwang *et al*., 2012); AHK4 has an

intrinsic phosphatase activity in the absence of ligand binding (pg 7, Hwang *et al*., 2012)

46. Plasma membrane associated cytokinin independent CKI1 (not activated by cytokinin) possesses constitutive kinase activity and when over-expressed can activate the cytokinin signalling pathway (pg 5, Hwang *et al*., 2012).
47. *Aux/IAA* (an auxin signalling inhibitor) transcription is promoted by downstream auxin signalling (pg 3, Moubayidin *et al*., 2009).
48. There is a negative feedback loop which controls the level of EIN3 (preventing harmful accumulation) and controls homeostasis in ethylene signalling. Ethylene signalling promotes *EIN2* which promotes the degradation of EBF2 (&1). EBF2 (&1) promotes the degradation of EIN3. In fact in the *ein2* mutant no EIN3 or EIL1 is detectable. Therefore ethylene signalling results in the accumulation of EIN3, which directly binds to the promoter of *EBF2*. The increase in EBF2 in turn increases the rate of degradation of EIN3 to control EIN3 accumulation (pg 4, Zhao and Guo, 2011). Note EBF2 has the predominant role in controlling EIN3 in conditions of high ethylene (pg4, Zhao and Guo, 2011).
49. Ethylene induces the expression of *EBF1 and 2* enhancing the degradation of EIN3. So a negative feedback loop exists in the ethylene signalling pathway (pg 3, Yoo *et al*., 2009).
50. Evidence exists for an intermediate state of the ETR1 receptor between on and off ethylene signalling (pg 4, Yoo *et al*., 2009).
51. The primary nuclear event in ethylene signalling is the stabilisation of the key transcription factor EIN3, which is otherwise constantly degraded, (pg 4, Yoo *et al*., 2009) which allows a fast upregulation of ethylene response genes (within 1 hr).
52. Activation of the ethylene pathway requires the accumulation of EIN3. This is achieved by a switch between two phospho-relay pathways, from the CTR1-active pathway (when ethylene is not present) which promotes EIN3 degradation to the CTR1-inactive pathway (when ethylene is present) that promotes EIN3 stability (pg 5, Yoo *et al*., 2009). The results from Yoo *et al*., 2009 need to be questioned since the second pathway is

now thought to be involved in ethylene biosynthesis and not ethylene signalling. See section App 2.3 below on ethylene signalling pathways.

53. EIN2 is stabilised (by a reduction in degradation by the EIN2 targeting proteins ETP1/2) by ethylene application (pg 1, Zhao and Guo, 2011). See also section App 2.3 below on ethylene signalling pathways.
54. Ethylene application downgrades EBF1 & 2 by degradation (or lack of stabilisation) but also upregulates transcription of *EBF2* through EIN3, and to a lesser extent *EBF1* (see note 48 and pg 4, Zhao and Guo, 2011).
55. Ethylene induces the expression of *WEI2* and *WEI7* which encode subunits of the rate limiting enzyme for the synthesis of tryptophan which is involved in auxin biosynthesis (pg 2, Ruzicka *et al*., 2007).
56. In the absence of ethylene, CTR1 is activated and directly phosphorylates and inactivates EIN2 which inactivates ethylene signalling. When ET binds the receptors, CTR1 is inactivated, EIN2 dephosphorylated and cleaved with the C-terminus migrating to the nucleus to act as a transcription factor and directly or indirectly activating *EIN3* transcription and initiating ET downstream ethylene signalling (pg 2, Shakeel *et al*., 2013). See section App 2.3 below on ethylene signalling.
57. The 5 ethylene receptors are classified into 2 families and form homodimers (although in yeast they have been shown to form heterodimers) at the ER membrane which can form higher level heteromeric clusters (pg 3, Shakeel *et al*., 2013). See more information on ethylene receptors in section App 2.2 below.
58. Ethylene signalling negatively regulates *PLS* transcription (pg 10, Chilley *et al*., 2006).
59. *PLS* transcription is upregulated within 30 mins by the application of auxin (pg 5, Casson *et al*., 2002).
60. PLS promotes auxin biosynthesis (pg 5, Fig 4B, Chilley *et al*., 2006).
61. Different *CKX (1-7)* are expressed in different tissues at different stages of development (Fig 11, Werner *et al*., 2003; Fig 1, Werner *et al*., 2006)
62. CK promotes auxin biosynthesis in the root tip (abstract, Jones *et al*., 2010).

63. Auxin promotes *PIN1,2* transcription (Blilou *et al*., 2005) and inhibits PIN1,2 endocytosis from the plasma membrane into the cytosol (Paciorek *et al*., 2005).
64. Cytokinin inhibits *AUX1* expression (Street *et al*., 2016).
65. See sections App 2.2 and 2.3 below on ethylene receptors and ethylene signalling pathways.

App 2.2 Ethylene receptor complexes

1. There are 5 ET receptors belonging to 2 subfamilies (pg 1 and Fig 2, Yoo *et al*., 2009) predominantly residing in the ER
2. Among the five *Arabidopsis* ethylene receptors, ETR1 and ERS1 in subfamily I contain highly conserved signature motifs for HK (histidine kinase) and have a predominant role in ethylene perception in a redundant manner (pg 3, Yoo *et al*., 2009)
3. All of the ethylene receptors share a modular structure composed of an N-terminal transmembrane domain responsible for ethylene binding, a GAF domain involved in protein–protein interactions between different receptor types, and a C-terminal domain required for the interaction with the downstream components of the pathway (pg 1, Merchante *et al*., 2013).
4. Receptors form homo-dimers capable of binding ethylene (and hetero dimers in yeast) and higher order clusters of homo-dimers can form between receptors (Fig 1 and pg 3, Merchante *et al*., 2013). All combinations between receptor dimers are possible (pg 4, Yoo *et al*., 2009).
5. Receptors have been shown capable of forming multi-meric clusters (pg 4, Yoo *et al*., 2009)
6. The formation of heteromeric receptor clusters contributes to the broad range of ethylene responsiveness (abstract, Mayerhofer *et al*., 2012)
7. The receptors are not functionally equivalent and act synergistically for full receptor activity (pg 4, Yoo *et al*., 2009)

8. The receptor dimers form a complex with CTR1 and these complexes form clusters, with CTR1 mediated crosstalk between receptor clusters (abstract, Mayerhofer *et al*., 2012)
9. CTR1 is part of the ethylene receptor complexes and mediates convergent signalling output from multiple ethylene receptors (pg 4, Yoo *et al*., 2009)
10. In the absence of ET, the receptors are activated and activate CTR1 which suppresses downstream ET signalling (pg1 and Fig 2, Yoo *et al*., 2009; pg 2, Mayerhofer *et al*., 2012)
11. There is evidence for an intermediate state between 'on' and off' for the receptors (pg 4, Yoo *et al*., 2009)
12. A copper ion cofactor is required for high affinity binding of ET to the receptors (abstract, Rodriguez *et al*., 1999; pg 1, Mayerhofer *et al*., 2012). PLS binds the copper ion and promotes receptor binding while RAN1 is involved in copper transport (Mudge *et al*., 2017 (submitted)).
13. Two *etr1* mutants are discussed in this work:
    a. *etr1-1* gain-of-function mutant, with high receptor activity, a low sensitivity to ethylene and low downstream ethylene signalling.
    b. *etr1-7* loss-of-function mutant with low receptor activity and high downstream ethylene signalling.
14. Root length phenotypes (Chilley *et al*., 2006) show root lengths in ascending order approximately :
    a. *ctr1* mutant
    b. pls mutant
    c. PLSox/*ctr1* (PLSox results in slight rescue of *ctr1*)
    d. WT and *pls etr1-1* double mutant
    e. PLSox and ein-2 and *etr1-1* (*etr1-1* is effectively insensitive to ET)

App 2.3 Ethylene signalling pathways

App 2.3.1 The Canonical CTR1 dependent pathway:

1. Without ET, the active ethylene receptors activate CTR1 (which homo-dimerises when activated) which phosphorylates and inactivates EIN2, which physically interacts with the kinase domain of the receptors at the ER membrane (Fig 1, Merchante *et al*., 2013)
2. The activated CTR1 kinase dimers engage in interactions that might enable crosstalk between ethylene receptor clusters (pg 3, Merchante *et al*., 2013).
3. The exact receptor output is still unknown (pg 3, Merchante *et al*., 2013)
4. With ET application, receptors are inactivated and CTR1 is inactivated which prevents the phosphorylation of EIN2. EIN2 is then cleaved and the C-terminus migrates to the nucleus to regulate transcriptional activity (Fig 1, Merchante *et al*., 2013; pg 1, Yi and Guo, 2013).
5. Note that *ein2* mutants have no observed ethylene response (pg 3, Merchante *et al*., 2013). This could imply that all ethylene signalling is routed through EIN2, whether CTR1 dependent or not.
6. On ET application EIN2 accumulates (ET application inhibits the degradation of EIN2 by ETP1/2 F-box proteins and also downregulates ETP1/2). EIN2 is required for the stabilisation of the short-lived downstream components EIN3/EIL1 master transcription factors, which are targeted for degradation by EBF1/2 (also downregulated in the presence of ET) in the absence of ET (pg 4, Merchante *et al*., 2013).
7. EIN2 and EIN3 are tightly regulated by degradation in the absence of ethylene (pg 4, Merchante *et al*., 2013)
8. ETR1 has an autokinase activity which is suggested to be stimulated by ET application (pg 11, Hall *et al*., 2012) to facilitate the ethylene response. This is disputed (pg 1 & 3, Merchante *et al*., 2013) and ET application is said to inhibit the autokinase activity of the receptors and support the interaction of ETR1 and EIN2 (pg 5, Bisson and Groth, 2010).
9. The kinase activity of ETR1 could be an important link between ETR1 in the ethylene signalling pathway and the AHPs in the CK signalling

pathway. Note that (pg 1, Hass *et al*., 2004) it is suggested that ARR2 transcriptional activity (in the CK pathway) is regulated by an ETR1 initiated phospho-relay, with ARR2 effectively acting downstream of ETR1.

10. RTE1 is a negative regulator of ethylene responses which co-localises at the ER membrane with the receptors (and also is found in the Golgi) and acts by specifically activating ETR1 by promoting transition from its inactive state (in the presence of ET) to its active state (pg 3, Merchante *et al*., 2013).
11. PLS and CTR1 act to negatively regulate ethylene signalling and do not act in a simple linear pathway (Chilley *et al*., 2006). PLS promotes the binding of the copper ion to ETR1 and so the activation of ETR1 (Mudge *et al*., 2017 (submitted)).

App 2.3.2 The CTR1 independent pathway:

1. There is evidence of a separate (but weak) CTR1-independent ethylene signalling pathway which acts in the same direction as the main receptor signalling, and is suppressed by the application of ethylene (discussion section, Qui *et al*., 2012) as follows:
    a. *ctr1* mutants show the constitutive ethylene response, but are still somewhat responsive to ethylene
    b. The constitutive ethylene response is stronger in multiple ethylene receptor mutants than in the *ctr1* mutant.
    c. The constitutive ethylene response is stronger in mutants of EBF1/2 (which mediate EIN3/EIL1 degradation) than in *ctr1*
    d. The expression of the ETR1 N-terminus (*etr1* $^{1\text{-}349}$) could produce the ethylene receptor signalling output to suppress the constitutive ethylene response in *ctr1*
    e. RTE1 overexpression with the ‘ETR1 N-terminus’ (*etr1* $^{1\text{-}349}$ encodes the truncated ETR1 lacking the C-terminus) suppressed the constitutive ethylene response of the *ctr1* mutant. Also the ETR1 N-terminus did not suppress the constitutive ethylene response of *ctr1* in the *rte1-2* loss of function mutant.

2. The above suggests that there is a CTR1-independent ethylene signalling pathway mediated by the N-terminal of ETR1 which also involves RTE1 (discussion section, Qui *et al*., 2012).
3. Also RTE1 physically associates with ETR1 (discussion section, Qui *et al*., 2012).
4. The ETR1 C-terminus may largely inhibit ETR1 N-terminus signalling in the full length ETR1 or block the receptor cooperation essential for N-terminal signalling. CTR1 kinase activity could also block the inhibition by the ETR1 C-terminus and promote ETR1 N-terminal signalling (discussion section, Qui *et al*., 2012).
5. Possibly PLS, like RTE1, also acts in the CTR1 independent pathway, since the *ctr1* mutant does not fully suppress the PLSox phenotype (pg 11, Chilley *et al*., 2006)

App 2.3.3 ETR1 phospho-relay ethylene signalling pathway:

The support for the existence of this pathway is:

1. The ethylene receptors interact with AHP phospho-transfer proteins (pg 11, Kakimoto *et al*., 2003; abstract and discussion, Scharein *et al*., 2008; pg 10, Shakeel *et al*., 2013)
2. The affiliation of ETR1 for AHPs is phospho-dependent (pg 3, Scharein *et al*., 2008; pg 10, Shakeel *et al*., 2013)
3. *Arabidopsis* response regulator 2 (ARR2) acts as a signalling component functioning downstream of ETR1 in ethylene signal transduction (abstract, Hass *et al*., 2004).
4. ETR1 is an upstream regulator of ARR2 phosphorylation (pg 4, Hass *et al*., 2004).

The binding of ethylene stimulates the auto-phosphorylation of ETR1 (pg 11, Hall *et al*., 2012), although this remains unresolved (pg 1 & 3 Merchante *et al*., 2013). Also it has been demonstrated that auto-phosphorylation of ETR1 is decreased by ethylene application and in turn supports ETR1 affinity for EIN2 (pg 5, Bisson and Groth, 2010); but see additional comments on this (pg 11, Hall *et al*., 2012).

APPENDIX 3: RUNNING THE IMPROVED CYTOKININ MODEL (WT743)

(USER INPUTS IN RED)

==ROOT MODELLING PROGRAM vs29d WITH CK MODIFICATIOND FOR WT743==

Input the RUN NUMBER: WT743

Input the time step and simulation time:

The time step (second)= 100

The simulation Time(secs)= 30000

Input real root switch, 0 for rectangular root, 1 for real root: = 1

Input # data output sets/simulation time (recommend 1): = 1

SET MAX # OF DATA DUMPS ALLOWED (to restrict file size): = 5

This uses up to 300 MB of storage Is this OK? 0 = NO, 1 = YES: = 1

Input COMBINED PIN12347 START [ARRAY] ? NO = 0, YES = 1: 0

For RECOVERY ITERATIONS combined auxlax array must be input

Input COMBINED AUX1,LAX2,3 START [ARRAY] ? NO = 0, YES = 1: 0

AUTO RECOVERY BY AUXLAX OR PIN RE-SETS NO = 0, YES = 1: 0

SET START AUX1 concentration (& synthesis set=0) NO = 0, YES = 1: 1

SET START LAX2 concentrations NO = 0, YES = 1: 1

SET START LAX3 concentration NO = 0, YES = 1: 1

SET START PIN3 concentrations? NO = 0, YES = 1: 1

SET START PIN4 concentrations? NO = 0, YES = 1: 1

SET START PIN7 concentrations? NO = 0, YES = 1: 1

HORMONE FEEDING? Input 0 for NO or 1 for YES: 0

========== VALUE OF PARAMETERS ==========

Input START LEVEL 4 (MAX) PIN3 concentration (micro M) 0

Input START LEVEL 3 PIN3 concentration (micro M) 1

Input START LEVEL 2 PIN3 concentration (micro M) .25

Input START LEVEL 1 (MIN) PIN3 concentration (micro M) .06

Input START LEVEL 4 (MAX) PIN4 concentration (micro M) 0
Input START LEVEL 3 PIN4 concentration (micro M) .5
Input START LEVEL 2 PIN4 concentration (micro M) .1
Input START LEVEL 1 (MIN) PIN4 concentration (micro M) .02

Input START LEVEL 4 (MAX) PIN7 concentration (micro M) 0
Input START LEVEL 3 PIN7 concentration (micro M) 1
Input START LEVEL 2 PIN7 concentration (micro M) .25
Input START LEVEL 1 (MIN) PIN7 concentrations (micro M) .06

Input START LEVEL 15 (MAX) AUX1p concentration (micro M) 0
Input START LEVEL 14 AUX1p concentration (micro M) 0
Input START LEVEL 13 AUX1p concentration (micro M) 0
Input START LEVEL 12 AUX1p concentration (micro M) 0
Input START LEVEL 11 AUX1p concentration (micro M) 0
Input START LEVEL 10 AUX1p concentration (micro M) 0
Input START LEVEL 9 AUX1p concentration (micro M) 0
Input START LEVEL 8 AUX1p concentration (micro M) 0
Input START LEVEL 7 AUX1p concentration (micro M) 0
Input START LEVEL 6 AUX1p concentration (micro M) 0
Input START LEVEL 5 AUX1p concentration (micro M) 0
Input START LEVEL 4 AUX1p concentration (micro M) 0
Input START LEVEL 3 AUX1p concentration (micro M) 2.25
Input START LEVEL 2 AUX1p concentration (micro M) 1
Input START LEVEL 1 (MIN) AUX1p concentration (micro M) .75

Input START LEVEL 8 (MAX) LAX2 concentration (micro M) 0
Input START LEVEL 7 LAX2 concentration (micro M) 0
Input START LEVEL 6 LAX2 concentration (micro M) 0
Input START LEVEL 5 LAX2 concentration (micro M) 0
Input START LEVEL 4 LAX2 concentration (micro M) 0
Input START LEVEL 3 LAX2 concentration (micro M) .75
Input START LEVEL 2 LAX2 concentration (micro M) 0
Input START LEVEL 1 (MIN) LAX2 concentration (micro M) 0

Input START LEVEL 4 (MAX) LAX3 concentration (micro M) 0
Input START LEVEL 3 LAX3 concentration (micro M) 1.75
Input START LEVEL 2 LAX3 concentration (micro M) 0
Input START LEVEL 1 (MIN) LAX3 concentration (micro M) 0

Selected Parameters set in Value of Parameters for Fig: WT743

==========

k18a = 0.5, k18 = 10, k18c = 1, k18d = 10, k18e = 100

k10a = 5, k12a = 0.02, k1a = 0, k6 = 0, k6a = 3, k4 = 20

k2a = 1.25 k2b = 0.01, k2c = 0.02, k16 = 0.3, k16a = 1, k19 = 1

k11 = 4, k32b = 1, k3 = 0.001, k12d1 = 0.1, k12a = 0.02

PIN12 POLARITY: level 1 = 1; Level 2 = 5; Level 3 = 20

CK diffusion rate = 220

AUX1 level 4 = 0, Level 3 = 2.25, Level 2 = 1, Level 1 = 0.75

LAX2 level 4 = 0, Level 3 = 0.75, Level 2 = 0, Level 1 = 0

LAX3 level 4 = 0, Level 3 = 1.75, Level 2 = 0, Level 1 = 0

PIN3 level 4 = 0, Level 3 = 1, Level 2 = 0.25, Level 1 = 0.06

PIN4 level 4 = 0, Level 3 = 0.5, Level 2 = 0.1, Level 1 = 0.02

PIN7 level 4 = 0, Level 3 = 1, Level 2 = 0.25, Level 1 = 0.06

==========ROOT STRUCTURE ==========

DEFAULT NUMBER OF ROWS IN ROOT MAP FILE = 1150

DEFAULT NUMBER OF COLS IN ROOT MAP FILE = 326

USE DEFAULT ROOT MAP DIMENSIONS? 1 = YES, 0 = NO 1

Default ROOT MAP FILE is RR1150pin12mapvs26CKmods.txt

Use default? 1 = YES, 0 = NO 1

INPUT SIZE OF EACH PIXEL (recommend 2 microns)? 2

REAL ROOT has been selected

Default CELL NO. FILE is rootmapcellno1150.txt

Use default? 1 = YES, 0 = NO: 1

The MAXIMUM CELL NO. used is 1165

REAL ROOT has been selected

Default PIN3 MAP is: RR1150pin3mapvs26.txt

Use default? 1 = YES, 0 = NO 1

REAL ROOT has been selected

Default PIN4 MAP is: RR1150pin4mapvs25.txt

Use default? 1 = YES, 0 = NO: 1

REAL ROOT has been selected

Default PIN7 MAP is: RR1150pin7mapvs25.txt

Use default? 1 = YES, 0 = NO 1

REAL ROOT has been selected

Default AUX1 MAP is: RR1150aux1mapvsCKmods2.txt

Use default? 1 = YES, 0 = NO 1

REAL ROOT has been selected

Default LAX2 MAP is: RR1150lax2mapB.txt

Use default? 1 = YES, 0 = NO 1

REAL ROOT has been selected

Default LAX3 MAP is: RR1150lax3mapB.txt

Use default? 1 = YES, 0 = NO 1

Number of active Grid Points = 283816

==========START OF ITERATION # 1 out of 1 ==========

Selected parameters set in Model.h for Fig: WT743 c01 = 0.1; CK border = 0.04

==========

RUN NUMBER WT743 ITERATION # 1 out of 1

ROOT MODELLING TIME IS NOW =200

BIBLIOGRAPHY

Adamowski M, Friml J. 2015. PIN-dependent auxin transport: action, regulation, and evolution. *Plant Cell* 27*:* 20–32.

Aida M, Beis D, Heidstra R, Willemsen V, Blilou I, Galinha C, Nussaume L, Noh YS, Amasino R, Scheres B. 2004. The *PLETHORA* genes mediate patterning of the Arabidopsis root stem cell niche. *Cell* 119: 109-120.

Antoniadi J, Placková L, Simonovik B, Dolezal K, Turnbull C, Ljung K, Novák O. 2015. Cell-Type-Specific Cytokinin Distribution within the Arabidopsis Primary Root Apex. *Plant Cell* 27: 1955-67

Band L, Fozard J, Godin C, Jensen O, Pridmore T, Bennett M, King J. 2012. Multiscale Systems Analysis of Root Growth and Development: Modeling Beyond the Network and Cellular Scales. *The Plant Cell* 24: 3892–3906.

Band LR, Wells DM, Fozard JA, Ghetiu T, French AP, Pound MP, Wilson MH, Yu L, Li W, Hijazi HI et al. 2014. Systems analysis of auxin transport in the Arabidopsis root apex. *The Plant Cell* 26: 862–875.

Barbosa I, Zourelidou M, Willige B, Weller B, Schwechheimer C. 2014. D6 PROTEIN KINASE activates auxin transport-dependent growth and PIN-FORMED phosphorylation at the plasma membrane. *Developmental Cell* 29: 674–685.

Bargmann BO, Vanneste S, Krouk G, Nawy T, Efroni I, Shani E, Choe G, Friml J, Bergmann DC, Estelle M, Birnbaum KD. 2013. A map of cell type-specific auxin responses. *Molecular Systems Biology* 9: 688.

Beemster GTS, Baskin IS. 1998. Analysis of cell division and elongation underlying the developmental acceleration of root growth in Arabidopsis thaliana. *Plant Physiology* 116: 1515–1526.

Bishopp A, Help H, El-Showk S, Weijers D, Scheres B, Friml J, Benkova E, Mahonen AP, Helariutta Y. 2011a. A mutually inhibitory interaction between auxin and cytokinin specifies vascular pattern in roots. *Current Biology* 21: 917–926.

Bishopp A, Lehesranta S, Vaten V, Help H, El-Showk E, Scheres B, Helariutta K, Mahonen AP, Sakakibara H, Helariutta Y. 2011b. Phloem-transported cytokinin regulates polar auxin transport and maintains vascular pattern in the root meristem. *Current Biology* 21: 927–932.

Bisson MMA, Groth G. 2010. New insight in ethylene signaling: autokinase activity of ETR1 modulates the interaction of receptors and EIN2. *Mol Plant* 3: 882-889.

Blilou I, Xu1 J, Wildwater M, Willemsen V, Paponov I, Friml J, Heidstra R, Aida M, Palme K, Scheres B. 2005. The PIN auxin efflux facilitator network controls growth and patterning in Arabidopsis roots. *Nature* 433: 39–44.

Brunoud G, Wells DM, Oliva M, Larrieu A, Mirabet V, Burrow AH, Beeckman T, Kepinski S, Traas J, Bennett MJ, Vernoux T. 2012. A novel sensor to map auxin response and distribution at high spatio-temporal resolution. *Nature* 482: 103–106.

Cancel JD, Larsen PB, 2002. Loss-of-function mutations in the ethylene receptor ETR1 causes enhanced sensitivity and exaggerated response to ethylene in Arabidopsis. *Plant Physiol* 129: 1557–1567

Casson SA, Chilley PM, Topping JF, Evans IM, Souter MA, Lindsey K. 2002. The *POLARIS* gene of Arabidopsis encodes a predicted peptide required for correct root growth and leaf vascular patterning. *The Plant Cell* 14: 1705–1721.

Chae H.S. Faure F. Kieber JJ. 2003. The eto1, eto2 and eto3 mutations and cytokinin treatment increase ethylene biosynthesis in Arabidopsis by increasing the stability of the ACS protein*. Plant Cell* 15: 545–559.

Chandler JW. 2009. Auxin as compère in plant hormone crosstalk. *Planta* 231: 1–12.

Chapman EJ, Estelle M. 2009. Mechanism of auxin-regulated gene expression in plants. *Annual Review of Genetics* 43: 265–285.

Chatfield JM, Armstrong DJ. 1986. Regulation of Cytokinin Oxidase Activity in Callus Tissues of Phaseolus vulgaris L. cv Great Northern. *Plant Physiol.* 80: 493-499.

Chen YF, Shakeel SN, Bowers J, Zhao XC, Etheridge N, Schaller GE. 2007. Ligand-induced degradation of the ethylene receptor ETR2 through a proteasome-dependent pathway in Arabidopsis. *J. Biol. Chem*. 282: 24752–24758.

Chickarmane V, Roeder AH, Tarr PT, Cunha A, Tobin C, Meyerowitz EM. 2010. Computational morphodynamics: a modeling framework to understand plant growth. *Annual Review of Plant Biology* 61: 65–87.

Chilley PM, Casson SA, Tarkowski P, Hawkins N, Wang KL, Hussey PJ, Beale M, Ecker JR, Sandberg GK, Lindsey K. 2006. The POLARIS peptide of Arabidopsis regulates auxin transport and root growth via effects on ethylene signaling. *The Plant Cell* 18: 3058–3072.

Cho M, Lee SH, Cho HT. 2007. P-glycoprotein4 displays auxin efflux transporter-like action in Arabidopsis root hair cells and tobacco cells. *Plant Cell* 19: 3930–3943.

Cho M, Cho HT. 2012. The function of ABCB transporters in auxin transport. *Plant Signal. Behav.* 8, pii: e22990.

Cho H, Ryu H, Rho S, Hill K, Smith S, Audenaert D, Park J, Han S, Beeckman, T, Bennett MJ et al. 2014. A secreted peptide acts on BIN2-mediated

phosphorylation of ARFs to potentiate auxin response during lateral root development. *Nature Cell Biology* 16: 66–76.

Cieslak M, Runions A, Prusinkiewicz P. 2015. Auxin-driven patterning with unidirectional fluxes. *Journal of Experimental Botany* 66: 5085-5102.

Clark NM, de Luis Balaguer MA, Sozzani R. 2014. Experimental data and computational modeling link auxin gradient and development in the Arabidopsis root. *Frontiers in Plant Science* 5: 328.

De Rybel B, Adibi M, Breda AS, Wendrich JR, Smit ME, Novák O, Yamaguchi N, Yoshida S, Van Isterdael G, Palovaara J et al. 2014. Integration of growth and patterning during vascular tissue formation in Arabidopsis. *Science* 345: 1255215.

Del Bianco M, Giustini L, Sabatini S. 2013. Spatiotemporal changes in the role of cytokinin during root development. *New Phytologist* 199: 324-338.

Dello Ioio R, Linhares FS, Scacchi E, Casamitjana-Martinez E, Heidstra R, Costantino P, Sabatini S. 2007. Cytokinins determine Arabidopsis root meristem size by controlling cell differentiation. *Curr Biol* 17: 678–682

Dello Ioio R, Nakamura K, Moubayidin L, Perilli S, Taniguchi M, Morita MT, Aoyama T, Costantino P, Sabatini S. 2008. A genetic framework for the control of cell division and differentiation in the root meristem. *Science* 322: 1380–1384

Depuydt S, Hardtke CS. 2011. Hormone signalling crosstalk in plant growth regulation. *Current Biology* 21: R365-R373.

Dharmasiri S, Swarup R, Mockaitis K, Dharmasiri N, Singh SK, Kowalchyk M, Marchant A, Mills S, Sandberg G, Bennett MJ, Estelle M. 2006. AXR4 is required for localization of the auxin influx facilitator AUX1. *Science* 312: 1218–1220.

Diaz J, Alvarez-Buylla E. 2006. A model of the ethylene signalling pathway and its gene response in Arabidopsis thaliana: pathway cross-talk and noise-filtering properties. *Chaos* 16: 023112, 01–16.

Dolan L, Janmaat K, Willemsen V, Linstead P, Poethig S, Roberts K, Scheres B. 1993. Cellular organisation of the *Arabidopsis thaliana* root. *Development* 119: 71–84.

Drisch R, Stahl S. 2015. Function and regulation of transcription factors involved in root apical meristem and stem cell maintenance. *Frontiers in Plant Science* DOI: 10.3389/fpls.2015.00505

Dubrovsky JG, Napsucialy-Mendivil S, Duclercq J, Cheng Y, Shishkova S, Ivanchenko MG, Friml J, Murphy AS, Benková E. 2011. Auxin minimum defines a developmental window for lateral root initiation. *New Phytologist* 191: 970–983.

Eklof S, Åstot C, Blackwell J, Moritz T, Olsson O, Sandberg G. 1997. Auxin–cytokinin interactions in transgenic tobacco. *Plant and Cell Physiology* 38: 225–235.

El-Showk S, Ruonala R, Helariutta Y. 2013. Crossing paths: cytokinin signaling and crosstalk. *Development* 140: 1373-1383

Evans ML, Ishikawa H, Estelle MA. 1994. Responses of Arabidopsis roots to auxin studied with high temporal resolution: comparison of wild-type and auxin response mutants. *Planta* 194: 215–222.

Fàbregas N, Formosa-Jordan P, Confraria A, Siligato R, Alonso JM, Swarup R, Bennett MJ, Mähönen AP, Caño-Delgado AI, Ibañes M. 2015. Auxin influx carriers control vascular patterning and xylem differentiation in Arabidopsis thaliana. *PLoS Genet.* 11:e1005183.

Forzani C, Aichinger E, Sornay E, Willemsen V, Laux T, Dewitte W, Murray JAH. 2014. WOX5 Suppresses CYCLIN D Activity to Establish Quiescence at the Center of the Root Stem Cell Niche. *Current Biology* 24: 1939–1944

Friml J, Benkova E, Blilou I, Wisniewska J, Hamann T, Ljung K, Woody S, Sandberg G, Scheres B, Jürgens G, Palme K. 2002. AtPIN4 mediates sink-driven auxin gradients and root patterning in Arabidopsis. *Cell* 108: 661–673.

Friml J, Benkova E, Mayer U, Palme K, Muster G. 2003. Automated whole mount localisation techniques for plant seedlings. *Plant* J 34: 115–124

Garay-Arroyo A, Sanchez M, Garcıa-Ponce B, Azpeitia E, Alvarez-Buylla ER. 2012. Hormone Symphony During Root Growth and Development. *Developmental Dynamics* 241: 1867-1885

Geisler M, Blakeslee JJ, Bouchard R, Lee OR, Vincenzetti V, Bandyopadhyay A, Titapiwatanakun B, Peer WA, Bailly A, Richards EL et al. 2005. Cellular efflux of auxin catalyzed by the Arabidopsis MDR/PGP transporter AtPGP1. *Plant Journal* 44: 179-194.

Geisler M, Murphy AS. 2006. The ABC of auxin transport: The role of p-glycoproteins in plant development. *Febs Letters* 580: 1094-1102.

Geldner N, Friml J, Stierhof YD, Jurgens G, Palme K. 2001. Auxin transport inhibitors block PIN1 cycling and vesicle trafficking. *Nature* 413: 425–428.

Grieneisen VA, Xu J, Marée AFM, Hogeweg P, Scheres B. 2007. Auxin transport is sufficient to generate a maximum and gradient guiding root growth. *Nature* 449: 1008–1013.

Guo H, Ecker JR. 2003. Plant responses to ethylene gas are mediated by SCF(EBF1/EBF2)-dependent proteolysis of EIN3 transcription factor. *Cell* 115: 667–677.

Gupta S, Rashotte AM. 2012. Down-stream components of cytokinin signaling and the role of cytokinin throughout the plant. *Plant Cell Rep* 31: 801–812.

Hall BP, Shakeel SN, Amir M, Haq NU, Qu X, Schaller G. 2012. Histidine kinase activity of the ethylene receptor ETR1 facilitates the ethylene response in Arabidopsis. *Plant Physiol*, 159: 682-695.

Hass C, Lohrmann J, Albrecht V, Sweere U, Hummel F, Yoo S, Hwang I, Zhu T, Schafer E, Kudla J, Harter KT. 2004. The response regulator 2 mediates ethylene signaling and hormone signal integration in Arabidopsis. *The EMBO Journal* 23: 3290–3302

Helariutta Y, Fukaki H, Wysocka-Diller J, Nakajima K, Jung J, Sena G, Hauser M-T, Benfey P. 2000. The *SHORT-ROOT* Gene Controls Radial Patterning of the *Arabidopsis* Root through Radial Signaling. *Cell* 101: 555–567.

Hill K, Porco S, Lobet G, Zappala S, Mooney S, Draye X, Bennett MJ. 2013. Root systems biology: integrative modeling across scales, from gene regulatory networks to the rhizosphere. *Plant Physiology* 163: 1487–1503.

Hirose N, Makita N, Kojima M, Kamada-Nobusada T, Sakakibara H. 2007. Overexpression of a Type-A Response Regulator Alters Rice Morphology and Cytokinin Metabolism. *Plant Cell Physiol*. 48(3): 523–539

Hwang I, Sheen J. 2001. Two-component circuitry in Arabidopsis cytokinin signal transduction. *Nature* 413: 383-389.

Hwang I, Sheen J, Müller B. 2012. Cytokinin signalling networks. *Annu. Rev. Plant Biol.* 63: 353-380.

Ikeda Y, Men S, Fischer U, Stepanova AN, Alonso JM, Ljung K, Grebe M. 2009. Local auxin biosynthesis modulates gradient directed planar polarity in Arabidopsis. *Nature Cell Biology* 11: 731-738.

Ishida T, Adachi S, Yoshimura M, Shimizu K, Umeda M, Sugimoto K. 2010. Auxin modulates the transition from the mitotic cycle to the endocycle in Arabidopsis. *Development* 137: 63–71.

Jones AR, Kramer EM, Knox K, Swarup R, Bennett MJ, Lazarus CM, Leyser HMO, Grierson CS. 2008. Auxin transport through non-hair cells sustains root-hair development. *Nature Cell Biology* 11: 78–84.

Jones B, Gunneras SA, Petersson SV, Tarkowski P, Graham N, May S, Dolezal K, Sandberg G, Ljung K. 2010. Cytokinin regulation of auxin synthesis in arabidopsis involves a homeostatic feedback loop regulated via auxin and cytokinin signal transduction. *The Plant Cell* 22: 2956–2969.

Kakimoto T. 2003. Perception and signal transduction of cytokinins. *Annu. Rev. Plant Biol*. 54: 605–27.

Kieber J, Schaller G. 2014. Cytokinins. The Arabidopsis Book.

Kim K, Ryu H, Cho Y, Scacchi E, Sabatini S, Hwang I. 2012. Cytokinin-facilitated proteolysis of ARABIDOPSIS RESPONSE REGULATOR attenuates signaling output in two component circuitry. *The Plant Journal* 69: 934–945

Kleine-Vehn J, Dhonukshe P, Swarup R, Bennett M, Friml J. 2006. subcellular Trafficking of the Arabidopsis Auxin Influx Carrier AUX1 Uses a Novel Pathway Distinct from PIN1. *The Plant Cell* 18: 3171-3181

Kleine-Vehn J, Langowskia L, Wiśniewska J, Dhonukshe P, Brewer PB, Friml J. 2008. Cellular and molecular requirements for polar PIN targeting and transcytosis in plants. *Mol. Plant* 1*:*1056-1066.

Kramer EM. 2004. PIN and AUX/LAX proteins: their role in auxin accumulation. *Trends in Plant Science* 9: 578–582.

Kramer EM, Frazer NL, Baskin TI. 2007. Measurement of diffusion within the cell wall in living roots of Arabidopsis thaliana. *J. Exp. Bot.* 58: 3005–3015.

Kramer EM, Rutschow HL, Mabie SS. 2011. AuxV: A database of auxin transport velocities. *Trends in Plant Science* 16: 461–463.

Krupinski P, Jonsson H. 2010. Modeling Auxin-regulated Development. *Cold Spring Harbor Perspectives in Biology* 2: a001560.

Kurepa J, Li Y, Smalle JA. 2013. Proteasome-dependent proteolysis has a critical role in fine-tuning the feedback inhibition of cytokinin signaling. *Plant Signaling & Behavior* 8: 3.

Kushwah S, Jones AM, Laxmi A. 2011. Cytokinin Interplay with Ethylene, Auxin, and Glucose Signaling Controls Arabidopsis Seedling Root Directional Growth. *Plant Physiology*, 156: 1851–1866.

Laskowski M, Biller S, Stanley K, Kajstura T, Prusty R. 2006. Expression profiling of auxin-treated Arabidopsis roots: toward a molecular analysis of lateral root emergence. *Plant and Cell Physiology* 47: 788–792.

Laskowski M, Grieneisen VA, Hofhuis H, ten Hove CA, Hogeweg P, Maree AFM, Scheres B. 2008. Root System Architecture from Coupling Cell Shape to Auxin Transport. *PLoS Biology*, 6.

Lavenus J, Guyomarc'h S, Laplaze L. 2016. PIN transcriptional regulation shapes root system architecture. Trends in Plant Science *21*: 175-177.

Liao C-Y, Smet W, Brunoud G, Yoshida S, Vernoux T, Weijers D. 2015. Reporters for sensitive and quantitative measurement of auxin response. *Nature Methods* 12: 207–210.

Lin Z, Zhong S, Grierson D. 2009. Recent advances in ethylene research. *J Exp Bot* 60: 3311–3336.

Liu JL, Mehdi S, Topping J, Tarkowski P, Lindsey K. 2010. Modelling and experimental analysis of hormonal crosstalk in Arabidopsis. *Molecular Systems Biology* 6: 373.

Liu JL, Mehdi S, Topping J, Friml J, Lindsey K. 2013. Interaction of PLS and PIN and hormonal crosstalk in Arabidopsis root development. *Frontiers in Plant Science* 4: 75.

Liu J, Rowe J, Lindsey K. 2014. Hormonal crosstalk for root development: a combined experimental and modeling perspective. *Frontiers in Plant Science* 5:116.

Liu J, Moore S, Chen C, Lindsey K. 2017. Crosstalk complexities between auxin, cytokinin and ethylene in *Arabidopsis* root development: from experiments to systems modelling, and back again. *Molecular Plant* 10: 1480-1496.

Ljung K, Bhalerao RP, Sandberg G. 2001. Sites and homeostatic control of auxin biosynthesis in Arabidopsis during vegetative growth. *Plant J* 28: 465-474.

Ljung K. 2013. Auxin metabolism and homeostasis during plant development. *Development* 140: 943–950.

Long Y, Scheres B, Blilou I. 2015. The logic of communication: roles for mobile transcription factors in plants. *Journal of Experimental Botany*: 66, 1133–1144.

Mahonen AP, Bishopp A, Higuchi M, Nieminen K, Kinoshita K, Tormakangas K, Ikeda Y, Oka A, Kakimoto T, Helariutta Y. 2006. Cytokinin Signaling and Its Inhibitor AHP6 Regulate Cell Fate During Vascular Development. *Science* 311: 94.

Mahonen AP, ten Tusscher K, Siligato R, Smetana O, Díaz-Trivino S, Salojarvi J, Wachsman G, Prasad K, Heidstra R, Scheres B. 2014. PLETHORA gradient formation mechanism separates auxin responses. *Nature* 515: 125–129.

Marhavy P, Bielach A, Abas L, Abuzeineh A, Duclercq J, Tanaka H, Parezova M, Petrasek J, Friml J, Kleine-Vehn J, Benkova E. 2011. Cytokinin modulates endocytic trafficking of PIN1 auxin efflux carrier to control plant organogenesis. *Dev. Cell* 24: 796–804

Martin-Rejano EM, Camacho-Cristoval JJ, Herrera-Rodriguez MB, Rexach J, Navarro-Gochicoa MT, Gonzales-Fontes A. 2011. Auxin and ethylene are involved in the responses of root system architecture to low boron supply in Arabidopsis. *Physiologia Plantarum* 142: 170-178.

Mayerhofer H, Panneerselvam S, Mueller-Dieckmann J. 2012. Protein Kinase Domain of CTR1 from Arabidopsis thaliana Promotes Ethylene Receptor Cross Talk. *J. Mol. Biol.* 415: 768–779

Mellor N, Bishopp A. 2014. The innermost secrets of root development. *Science* 345: 622-623.

Mellor N, Péret B, Porco S, Sairanen I, Ljung K, Bennett MJ, King JR. 2015. Modelling of Arabidopsis LAX3 expression suggests auxin homeostasis. *J Theor Biol 366*: 57–70.

Mellor N, Bennett MJ, King JR. 2016. GH3-mediated auxin conjugation can result in either transient or oscillatory transcriptional auxin responses. *Bull Math Biol. 78*: 210-34.

Mellor N, Banda L, Pencík A, Novák O, Rashed A, Holman T, Wilson M, Voß U, Bishopp A, King J, Ljung K, Bennett M, Owen M. 2016b. Dynamic regulation of auxin oxidase and conjugating enzymes AtDAO1 and GH3 modulates auxin homeostasis. *PNAS* 113: 11022-11027.

Merchante C, Alonso JM, Stepanova AN. 2013. Ethylene signaling: simple ligand, complex regulation. *Current Opinion in Plant Biology*, 16: 554–560.

Mintz-Oron S, Meir S, Malitsky S, Ruppin E, Aharoni A, Shlomi T. 2012. Reconstruction of Arabidopsis metabolic network models accounting for subcellular compartmentalization and tissue specificity. *Proceedings of the National Academy of Sciences, USA* 109: 339–344.

Mironova VV, Omelyanchuk NA, Yosiphon G, Fadeev SI, Kolchanov NA, Mjolsness E, Likhoshvai VA. 2010. A plausible mechanism for auxin patterning along the developing root. *BMC Systems Biology* 4: 98.

Mironova VV, Omelyanchuk NA, Novoselova ES, Doroshkov AV, Kazantsev FV, Kochetov AV, Kolchanov NA, Mjolsness E, Likhoshvai VA. 2012. Combined in silico/in vivo analysis of mechanisms providing for root apical meristem self-organization and maintenance. *Annals of Botany* 110: 349–360.

Miyawaki K, Matsumoto-Kitano M, Kakimoto K. 2004. Expression of cytokinin biosynthetic isopentenyltransferase genes in Arabidopsis: tissue specificity and regulation by auxin, cytokinin, and nitrate. *The Plant Journal* 37: 128–138.

Mockaitis K, Estelle M. 2008. Auxin receptors and plant development: A new signaling paradigm. *Annu. Rev. Cell Dev. Biol.* 24: 55–80.

Moore S, Zhang X, Mudge A, Rowe JH, Topping JF, Liu J, Lindsey K. 2015a. Spatiotemporal modelling of hormonal crosstalk explains the level and patterning of hormones and gene expression in Arabidopsis thaliana wildtype and mutant roots. *New Phytologist* 207: 1110–1122.

Moore S, Zhang X, Liu J, Lindsey K. 2015b. Some fundamental aspects of modeling auxin patterning in the context of auxin-ethylene-cytokinin crosstalk. *Plant Signaling & Behavior*: 10:10 e1056424.

Moore S, Zhang X, Liu J, Lindsey K. 2015c. Modelling Plant Hormone Gradients. *eLS*. DOI: 10.1002/9780470015902.a0023733

Moore S, Liu J, Zhang X, Lindsey K. 2017. A recovery principle provides insight into auxin pattern control in the Arabidopsis root. *Scientific Reports* 7: 430004

Moubayidin L, Di-Mambro R, Sabatini S. 2009. Cytokinin–auxin crosstalk. *Trends in Plant Science* 14: 10.

Moubayidin L, Perilli S, Dello Ioio R, Di Mambro R, Costantino P, Sabatini S. 2010. The rate of cell differentiation controls the Arabidopsis root meristem growth phase. *Curr. Biol.* 20:1138–43.

Muday GK, Rahman A, Binder BM. 2012. Auxin and ethylene: collaborators or competitors? *Trends in Plant Science* 17: 181-196.

Mudge A, Mehdi S, Foster AW, Orosa-Puente B, Shen W, Lear S, Tomlinson C, Cobb SL, Sadanandom A, Topping JF, Robinson NJ, Lindsey K. 2017. A peptide that regulates metallation of the *Arabidopsis* ethylene receptor. *Science* (submitted).

Muller A, Guan C, Galweiler L, Tanzler P, Huijser P, Marchant A, Parry G, Bennett M, Wisman E, Palme K. 1998. AtPIN2 defines a locus of Arabidopsis for root gravitropism control. *EMBO J* 17: 6903–6911.

Muller B, Sheen J. 2008. Cytokinin and auxin interaction in root stem-cell specification during early embryogenesis Advances in cytokinin signaling. *Nature* 19: 1094-1097.

Muraro D, Byrne H, King J, Voß U, Kieber J, Bennett M. 2011. The influence of cytokinin-auxin cross-regulation on cell-fate determination in Arabidopsis thaliana root development. *Journal of Theoretical Biology* 283: 152–167

Muraro D, Mellor N, Pound MP, Help H, Lucas M, Chopard J, Byrne HM, Godin C, Hodgman TC, King JR, et al. 2014. Integration of hormonal signaling networks and mobile microRNAs is required for vascular patterning in Arabidopsis roots. *Proceedings of the National Academy of Sciences, USA* 111: 857–862.

Nishimura C, Ohashi Y, Sato S, Kato T, Tabata S, Ueguchi C. 2004. Histidine kinase homologs that act as cytokinin receptors possess overlapping functions in the regulation of shoot and root growth in Arabidopsis. *Plant Cell* 16: 1365–1377.

Nordstrom A, Tarkowski P, Tarkowska D, Norbaek R, Åstot C, Dolezal K, Sandberg G. 2004. Auxin regulation of cytokinin biosynthesis in Arabidopsis thaliana: a factor of potential importance for auxin–cytokinin-regulated development. *Proceedings of the National Academy of Sciences, USA* 101: 8039–8044.

Omelyanchuk NA, Kovrizhnykh VV, Oshchepkova EA, Pasternak T, Palme K, Mironova VV. 2016. A detailed expression map of the PIN1 auxin transporter in Arabidopsis thaliana root. *BMC Plant Biology* 16: (Suppl 1), 5.

Overvoorde P, Fukaki H, Beeckman T. 2010. auxin Control of Root Development *Perspectives in Biology*: 2

Paciorek T, Zazimalova E, Ruthardt N, Petrásek J, Stierhof Y-D, Kleine-Vehn J. Morris DA, Emans N, Jürgens G, Geldner N, Friml J. 2005. Auxin inhibits endocytosis and promotes its own efflux from cells. *Nature* 435: 1251–1256.

Peret B, Swarup K, Ferguson A, Seth M, Yang Y, Dhondt S, James N, Casimiro I, Perry P, Syed A. et al. 2012. AUX/LAX genes encode a family of auxin influx transporters that perform distinct functions during Arabidopsis development. *Plant cell* 24: 2874–2885.

Peret B, Middleton AM, French AP, Larrieu A, Bishopp A, Njo M, Wells DM, Porco S, Mellor N, Band LR, et al. 2013. Sequential induction of auxin efflux and influx carriers regulates lateral root emergence. *Mol Syst Biol* 9: 699.

Pernisova M, Klıma P, Horak J, Valkova M, Malbeck J, Soucek P, Reichman P, Hoyerova K, Dubova J, Friml J, Zazímalova E, Hejatkoa J. 2009. Cytokinins modulate auxin-induced organogenesis in plants via regulation of the auxin efflux. *Proc Natl Acad Sci USA* 106: 3609–3614.

Petersson SV, Johansson AI, Kowalczyk M, Makoveychuk A, Wang JY, Moritz T, Grebe M, Benfey PN, Sandberg G, Ljung K. 2009. An auxin gradient and maximum in the Arabidopsis root apex shown by high-resolution cell-specific analysis of IAA distribution and synthesis. *Plant Cell* 21: 1659–1668.

Petrásek J, Friml J. 2009. Auxin transport routes in plant development. *Development* 136: 2675-2688.

Petrášek J, Mravec J, Bouchard R, Blakeslee JJ, Abas M, Seifertová D, Wiśniewska J, Tadele Z, Kubeš M, et al. 2006. PIN proteins perform a rate-limiting function in cellular auxin efflux. *Science* 312: 914–918.

Qiu L, Xie F, Yu J, Wen C. 2012. RTE1 is Essential to ETR1 N-terminal signaling. *Plant Physiology* 159: 1263–1276.

Robert HS, Grunewald W, Sauer M, Cannoot B, Soriano M, Swarup R, Weijers D, Bennett M, Boutilier K, Friml J. 2015. Plant embryogenesis requires AUX/LAX-mediated auxin influx. *Development* 142: 702–11.

Rodrıguez FI, Esch JJ, Hall AE, Binder BM, Schaller GE, Bleecker AB. 1999. A Copper Cofactor for the Ethylene Receptor ETR1 from Arabidopsis. *Science* 283: 996-998.

Rowe JH, Topping JF, Liu J, Lindsey K. 2016. Abscisic acid regulates root growth under osmotic stress conditions via an interacting hormonal network with cytokinin, ethylene and auxin. *New Phytologist* doi: 10.1111/nph.13882.

Rutschow HL, Baskin TI, Kramer EM. 2011. Regulation of solute flux through plasmodesmata in the root meristem. *Plant Physiology* 155:1817-1826.

Rutschow HL, Baskin TI, Kramer EM. 2014. The carrier AUXIN RESISTANT (AUX1) dominates auxin flux into Arabidopsis protoplasts. *New Phytologist* 204: 536-544.

Ruzicka K, Ljung K, Vanneste S, Podhorska R, Beeckman T, Friml J, Benkova E. 2007. Ethylene regulates root growth through effects on auxin biosynthesis and transport-dependent auxin distribution. *The Plant Cell* 19: 2197–2212.

Ruzicka K, Simásková M, Duclercq J, Petrásek J, Zazímalová E, Simon S, Friml J, Van Montagu MC, Benková E. 2009. Cytokinin regulates root meristem activity via modulation of the polar auxin transport. *Proceedings of the National Academy of Sciences, USA* 106: 4284–4289.

Sabatini S, Sabatini S, Beis D, Wolkenfelt H, Murfett J, Guilfoyle T, Malamy J, Benfey P, Leyser O, Bechtold N, et al. 1999. An auxin-dependent distal organizer of pattern and polarity in the *Arabidopsis* root. *Cell* 99: 463-472.

Santner A and Estelle M. 2009. Recent advances and emerging trends in plant hormone signalling. *Nature* 459: 1071-1078.

Sarkar AK, Luijten M, Miyashima S, Lenhard M, Hashimoto T, Nakkajima K, Scheres B, Heidstra R, Laux T. 2007. Conserved factors regulate signalling in *Arabidopsis thaliana* shoot and root stem cell organizers. *Nature* 446: 811-814.

Scharein B, Voet-van-Vormizeele J, Harter K, Groth G. 2008. Ethylene signaling: Identification of a putative ETR1–AHP1 phosphorelay complex by fluorescence spectroscopy. *Analytical Biochemistry* 377: 72–76.

Shakeel SN, Wang X, Binder BM, Schaller GE. 2013. Mechanisms of signal transduction by ethylene: overlapping and non overlapping signalling roles in a receptor family. *AoB Plants* 5.

Shi Y, Tian S, Hou L, Huang X, Zhang X, Guo H, Yang S. 2012. Ethylene signaling negatively regulates freezing tolerance by repressing expression of CBF and type-A ARR genes in Arabidopsis. *The Plant Cell* 24: 2578–2595

Skoog F, Miller CO. 1957. Chemical regulation of growth and organ formation in plant tissue cultured in vitro. *Symp Soc Exp Biol*. 11:118-30

Stepanova AN, Jun J, Likhacheva AV, Alonso JM. 2007. Multilevel interactions between ethylene and auxin in Arabidopsis roots. *The Plant Cell* 19: 2169–2185.

Street IH, Mathews DE, Yamburkenko MV, Sorooshzadeh A, John RT, Swarup R, Bennett MJ, Kieber JJ, Schaller GE. 2016. Cytokinin acts through the auxin influx carrier AUX1 to regulate cell elongation in the root. *Development*.

Suttle JC. 1988. Effect of ethylene treatment on polar IAA transport, net IAA uptake and specific binding of N-1-naphthylphthalamicacid in tissues and microsomes isolated from etiolated pea epicotyls. *Plant Physiology* 88: 795–799.

Swarup R, Friml J, Marchant A, Ljung K, Sandberg G, Palme K, Bennett MJ. 2001. Localization of the auxin permease AUX1 suggests two functionally distinct hormone transport pathways operate in the Arabidopsis root apex. *Genes and Development* 15: 2648–2653

Swarup R, Kramer EM, Perry P, Knox K, Leyser HM, Haseloff J, Beemster GT, Bhalerao R, Bennett MJ. 2005. Root gravitropism requires lateral root cap and epidermal cells for transport and response to a mobile auxin signal. *Nature Cell Biology* 7: 1057-1065.

Swarup R, Perry P, Hagenbeek D, Van Der Straeten D, Beemster GT, Sandberg G, Bhalerao R, Ljung K, Bennett MJ. 2007. Ethylene upregulates auxin biosynthesis in Arabidopsis seedlings to enhance inhibition of root cell elongation. *The Plant Cell* 19: 2186–2196.

Swarup K, Benková E, Swarup R, Casimiro I, Péret B, Yang Y, Parry G, Nielsen E, De Smet I, Vanneste S, et al. 2008. The auxin influx carrier LAX3 promotes lateral root emergence. *Nature Cell Biology* 10: 946-954.

Swarup R, Peret B. 2012. AUX/LAX family of auxin influx carriers-an overview. *Front Plant Sci.* 3: 225.

Taiz L, Zeiger E. 2010. *Plant Physiology 5th ed.* Sunderland: Sinauer Assoicates Inc.

Taniguchi M, Sasaki N, Tsuge T, Aoyama T, Oka A. 2007. ARR1 directly activates cytokinin response genes that encode proteins with diverse regulatory functions. *Plant Cell Physiol*. 48: 263-277.

Tanimoto M, Roberts K, Dolan L. 1995. Ethylene is a positive regulator of root-hair development in Arabidopsis thaliana. Plant J 8: 943–948.

Tivendale ND, Ross JJ, Cohen JD. 2014. The shifting paradigms of auxin biosynthesis. *Trends in Plant Science* 19: 44-51.

To JP, Haberer G, Ferreira FJ, Deruere J, Mason MG, Schaller GE, Alonso JM, Ecker JR, Kieber JJ. 2004. Type-A Arabidopsis response regulators are partially redundant negative regulators of cytokinin signaling. *The Plant Cell* 16: 658–671.

To JPC, Derue J, Maxwell BB, Morris VF, Hutchison CE, Ferreira FJ, Schaller GE, Kieber JJ. 2007. Cytokinin Regulates Type-A Arabidopsis Response Regulator Activity and Protein Stability via Two-Component Phosphorelay. *The Plant Cell* 19: 3901–3914.

Ugartechea-Chirino Y, Swarup R, Swarup K, Peret B, Whitworth M, Bennett M, Bougourd S. 2010. The AUX1 LAX family of auxin influx carriers is required for the establishment of embryonic root cell organization in Arabidopsis thaliana. *Annals of botany* 105: 277–289.

van Berkel K, de Boer RJ, Scheres B, ten Tusscher K. 2013. Polar auxin transport: models and mechanisms. *Development* 140: 2253–2268.

Vanneste S, Friml J. 2009. Auxin: A trigger for change in plant development. *Cell* 136: 1005-1016.

Vanstraelen M, Benkova E. 2012. Hormonal interactions in the regulation of plant development. *Annual Review of Cell and Developmental Biology* 28: 463–487.

Vernoux T, Brunoud G, Farcot E, Morin V, Van den Daele H, Legrand J, Oliva M, Das P, Larrieu A, Wells D, Guedon Y, Armitage L, Picard F, Guyomarc'h S, Cellier C, Parry G, Koumproglou R, Doonan JH, Estelle M, Godin C, Kepinski S, Bennett M, De Veylder L, Traas J. 2011. The auxin signalling network translates dynamic input into robust patterning at the shoot apex. *Molecular Systems Biology* 7: 508.

Vogel JP, Woeste KE, Theologis A, Kieber JJ. 1998. Recessive and dominant mutations in the ethylene biosynthetic gene ACS5 of Arabidopsis confer cytokinin insensitivity and ethylene overproduction, respectively. Proc Natl Acad Sci USA 95: 4766–4771.

Wabnik K, Kleine-Vehn J, Balla J, Sauer M, Naramoto S, Reinöhl V, Merks RMH, Govaerts W, Friml J. 2010. Emergence of tissue polarization from synergy of intracellular and extracellular auxin signaling. *Molecular Systems Biology* 6: 447.

Wang KL, Li H, Ecker JR. 2002. Ethylene biosynthesis and signaling networks. Plant Cell 14 (suppl.): S131–S151.

Wang H-Z, Yang K-Z, Zou J-J, Zhu L-L, Xie ZD, Morita MT, Tasaka M, Friml J, Grotewold E, Beeckman T. 2015. Transcriptional regulation of PIN genes by FOUR LIPS and MYB88 during Arabidopsis root gravitropism. *Nat. Commun*. 6: 8822.

Weller B, Zourelidoua M, Frank L, Barbosa I, Fastner A, Richter S, Jürgens G, Hammes U, Schwechheimer C. 2017. Dynamic PIN-FORMED auxin efflux carrier phosphorylation at the plasma membrane controls auxin efflux-dependent growth. *PNAS*: E887–E896

Werner T, Motyka V, Laucou V, Smets R. van Onckelen H, Schmülling T. 2003. Cytokinin-deficient transgenic Arabidopsis plants show multiple developmental alterations indicating opposite functions of cytokinins in the regulation of shoot and root meristem activity. *The Plant Cell* 15: 2532–2550.

Werner T, Kollmer I, Bartrina I, Holst K, Schmulling T. 2006. New Insights into the Biology of Cytokinin Degradation. *Plant Biol*. 8: 371–381

Weyers DBW, Paeterson NW. 2001. Plant hormones and the control of physiological processes. *New Phytolologist* 152: 375-407.

Wisniewska J, Xu J, Seifertova D, Brewer P, Ruzicka K, Blilou I, Rouquie D, Benkova E, Scheres B, Friml J. 2006. Polar PIN localization directs auxin flow in plants. *Science* 312: 883

Woodward AW, Bartel B. 2005. Auxin: regulation, action, and interaction. *Annals of Botany* 95: 707–735.

Xuan W, Band LR, Kumpf RP, VanDamme D, Parizot B, DeRop G, Opdenacker D, Moller BK, Skorzinski N, Njo MF, et al. 2016. Cyclic programmed cell death

stimulates hormone signalling and root development in Arabidopsis. *Science* 351: 384–38.

Yang H, Murphy A. 2009. Functional expression and characterization of Arabidopsis ABCB, AUX 1 and PIN auxin transporters in Schizosaccharomyces pombe. *The Plant Journal* 59: 179-191.

Yi J, Guo H. 2013. EIN2 cleavage bridges the Gap in Ethylene Signaling. *Molecular Plant* 6: 11–14.

Yoo S, Cho Y, Tena G, Xiong Y, Sheen J. 2008. Dual control of nuclear EIN3 by bifurcate MAPK cascades in C2H4 signaling. *Nature* 451.

Yoo S, Cho Y, Sheen J. 2009. Emerging connections in the ethylene signaling network. *Trends in Plant Science* 14: 270-279

Zazimalova E, Murphy AS, Yang H, Hoyerova K, Hosek P. 2010. Auxin transporters—why so many? *Cold Spring Harbor Perspectives in Biology* 2, a001552.

Zhang J, Nodzynski T, Pencík A, Rolcík J, Friml J. 2010. PIN phosphorylation is sufficient to mediate PIN polarity and direct auxin transport. *PNAS* 107: 918-922.

Zhang W, To JPC, Cheng C, Schaller EG, Kieber JJ. 2011. Type-A response regulators are required for proper root apical meristem function through the post-transcriptional regulation of PIN auxin efflux carriers. *Plant J.* 68: 1–10.

Zhang H, Zhou C. 2013. Signal transduction in leaf senescence. *Plant Molecular Biology*. 82: 539–545.

Zhao Y. 2010. Auxin biosynthesis and its role in plant development. *Annual Review of Plant Biology* 61: 49–64.

Zhao Q, Guo H. 2011. Paradigms and Paradox in the Ethylene Signaling Pathway and Interaction Network. *Molecular Plant* 4: 626–634.

Zourelidou M, Absmanner B, Weller B, Barbosa I, Willige B, Fastner A, Streit V, Port S, Colcombet J, van Bentem S, Hirt H, Kuster B, Schulze W, Hammes U, Schwechheimer C. 2014. Auxin efflux by PIN-FORMED proteins is activated by two different protein kinases, D6 PROTEIN KINASE and PINOID. *eLife* DOI: 10.7554/eLife.02860

M, Absmanner B, Weller B, Barbosa I, Willige B, Fastner A, Streit V, Port S, Colcombet J, van Bentem S, Hirt H, Kuster B, Schulze W, Hammes U, Schwechheimer C. 2014. Auxin efflux by PIN-FORMED proteins is activated by two different protein kinases, D6 PROTEIN KINASE and PINOID. *eLife* DOI: 10.7554/eLife.02860

Zürcher E, Tavor-Deslex D, Lituiev D, Enkerli K, Tarr PT, Müller B. 2013. A Robust and Sensitive Synthetic Sensor to Monitor the Transcriptional Output of the Cytokinin Signaling Network in Planta. *Plant Physiology* 161: 1066–1075

Zürcher E, Liu J, di Donato M, Geisler M, Müller B. 2016. Plant development regulated by cytokinin sinks. *Science* 353: 1027-1030